



APPENDIX H7.2

Spencer Gulf modelling assessments (280 ML/day desalination plant)

Spencer Gulf Modelling Assessments (280 ML/Day Desalination Plant) Final Report

R.B17994.001.07.Assessments.doc
October 2010



Spencer Gulf Modelling Assessments (280 ML/day Desalination Plant) Final Report

Prepared For: BHP Billiton

Prepared By: BMT WBM Pty Ltd (Member of the BMT group of companies)

Offices

*Brisbane
Denver
Mackay
Melbourne
Newcastle
Perth
Sydney
Vancouver*

CONTENTS

Contents		i
1	INTRODUCTION	1-1
2	COMPUTATIONAL FLUID DYNAMICS: DETAILED DIFFUSER SIMULATION	2-1
2.1	Computational Fluid Dynamics	2-2
2.2	OpenFOAM	2-2
2.3	CFD Model Setup	2-3
2.3.1	Equations	2-3
2.3.2	Turbulence Model	2-4
2.3.3	Domain and Mesh	2-4
2.3.4	Boundary Conditions	2-7
2.3.5	Initial Conditions	2-8
2.4	Validation	2-8
2.4.1	Comparison with Roberts Predictions	2-9
2.4.2	Comparison with CORMIX	2-11
2.4.3	Comparison with Field Measurements	2-12
2.4.3.1	<i>Potential for Re-entrainment</i>	2-12
2.4.3.2	<i>Comparison with Roberts 97</i>	2-14
2.4.4	Summary	2-14
2.5	Preliminary Simulations	2-14
2.5.1	Zero Background Current DEIS Configuration	2-15
2.5.2	Alternative Configurations – Steady State Simulations	2-16
2.5.3	Transient Dodge Tide ALT2 Configuration	2-22
2.6	Final Suite of CFD Simulations	2-23
2.6.1	Revised Diffuser Geometry	2-24
2.6.2	CFD Simulations Performed	2-26
2.7	Summary	2-26
3	HIGH RESOLUTION SCENARIO ASSESSMENTS	3-1
3.1	Model Grid and Bathymetry	3-1
3.2	Simulations	3-1

3.3	Simulation Period	3-1
3.4	Initial Conditions	3-1
3.5	Boundary Conditions	3-4
3.6	Nearfield and Hydrodynamic Model Linkage	3-5
3.6.1	Literature Linkage Techniques	3-6
3.6.2	Applicability to the Current Study	3-7
3.6.2.1	<i>Salt Mass Conservation</i>	3-7
3.6.2.2	<i>Controllable Linkage with Near Field Predictions</i>	3-8
3.6.2.3	<i>Controllable Dynamic Response to Tidal Forcing</i>	3-9
3.6.2.4	<i>Hydrodynamic Model Grid Independence</i>	3-9
3.6.2.5	<i>Hydrodynamic Model Timestep Independence</i>	3-10
3.6.3	Summary of Techniques	3-10
3.6.4	Adopted Linkage Technique	3-11
3.6.4.1	<i>Methodology Overview</i>	3-11
3.6.4.2	<i>CFD Plume Dilution Extraction</i>	3-19
3.6.4.3	<i>Outfall Flow Distribution</i>	3-21
3.6.4.4	<i>Sensitivity Analysis – Direct Insertion</i>	3-22
3.6.4.5	<i>Sensitivity Analysis – Single and Multiline Pre-Dilution</i>	3-28
3.7	Simulation Results	3-36
3.7.1	Control Points	3-36
3.7.2	Curtain	3-42
3.7.3	Dilution Contour Maps and Timeseries	3-47
3.7.4	Rate of Change of Salinity	3-61
4	LONG TERM SIMULATIONS	4-1
4.1	Model Schematisation	4-1
4.1.1	Modelling Platform	4-1
4.1.2	Model Grid and Bathymetry	4-1
4.1.3	Simulation Period	4-3
4.1.4	Initial Conditions	4-3
4.1.5	Model Forcing	4-3
4.1.6	Desalination Input	4-4
4.2	Model Validation	4-7
4.2.1	Salt Ejection	4-7
4.2.2	Salinity and Temperature Variation	4-8
4.2.3	Tidal Amplification and Modulation	4-10
4.3	Assessments	4-14
4.3.1	Simulations	4-14

4.3.2	Model Interrogation	4-14
4.3.3	Results	4-15
4.3.3.1	<i>Timeseries Results</i>	4-15
4.3.3.2	<i>Spatially Integrated Results</i>	4-24
5	CLIMATE CHANGE SIMULATIONS	5-1
5.1	Model Schematisation	5-1
5.2	Climate Change Parameterisation	5-1
5.2.1	Overview	5-1
5.2.2	Meteorological Forcing Modulation	5-1
5.2.2.1	<i>Air Temperature and Rainfall</i>	5-2
5.2.2.2	<i>Other Meteorological Data</i>	5-5
5.2.2.3	<i>Longwave Radiation</i>	5-6
5.2.3	Open Boundary Forcing Modulation	5-6
5.2.4	Summary	5-7
5.3	Simulations	5-13
5.4	Results	5-13
6	DISSOLVED OXYGEN SIMULATIONS	6-1
6.1	Model Setup	6-1
6.1.1	Simulation Period	6-1
6.1.2	Initial Conditions	6-2
6.1.2.1	<i>Salinity</i>	6-2
6.1.2.2	<i>Temperature</i>	6-2
6.1.2.3	<i>Dissolved Oxygen</i>	6-2
6.1.2.4	<i>Model Spin Up</i>	6-3
6.1.3	Boundary Conditions	6-3
6.1.3.1	<i>Return Water</i>	6-3
6.1.3.2	<i>Atmospheric Forcing</i>	6-4
6.1.4	CAEDYM Configuration	6-4
6.2	Model Execution	6-6
6.3	Results	6-6
6.3.1	Bottom Sheets	6-7
6.3.2	Mid Depth Sheets	6-8
6.3.3	Profiles	6-9
6.3.3.1	<i>100 Metres Northeast</i>	6-9
6.3.3.2	<i>100 Metres Southwest</i>	6-10
6.3.3.3	<i>500 Metres Northeast</i>	6-11

6.3.3.4	<i>500 Metres Southwest</i>	6-12
6.3.4	Curtain	6-13
7	UPWELLING POTENTIAL	7-1
7.1	Background	7-1
7.2	Two-Dimensional Model	7-2
7.2.1	Model Domain	7-2
7.2.2	Vertical Resolution	7-2
7.2.3	Timestep	7-2
7.2.4	Longitudinal Resolution	7-2
7.2.5	Initial Condition	7-5
7.2.6	Wind Forcing	7-5
7.2.7	Tidal Forcing	7-5
7.2.8	Simulation Period	7-5
7.2.9	Results	7-5
7.3	Quasi Three-Dimensional Model	7-11
7.3.1	Results	7-11
7.4	Fully Three-Dimensional Model	7-14
7.4.1	Model Domain	7-14
7.4.2	Vertical Resolution	7-15
7.4.3	Longitudinal Resolution	7-15
7.4.4	Initial Condition	7-15
7.4.5	Wind Forcing	7-15
7.4.6	Tidal Forcing	7-16
7.4.7	Simulation Period	7-16
7.4.8	Results	7-16
	7.4.8.1 <i>Westerly Wind</i>	7-18
	7.4.8.2 <i>Northerly Wind</i>	7-19
	7.4.8.3 <i>North Westerly Wind</i>	7-20
7.5	Fully Three Dimensional Model – Tides Active	7-24
7.5.1	Model Domain	7-24
7.5.2	Vertical Resolution	7-24
7.5.3	Longitudinal Resolution	7-24
7.5.4	Initial Condition	7-24
7.5.5	Simulation Period	7-24
7.5.6	Wind Forcing	7-25
7.5.7	Tidal Forcing	7-25
7.5.8	Results	7-25

8	LARVAL ENTRAINMENT	8-1
8.1	ELCOM Simulations	8-1
8.1.1	Simulation Suite	8-1
8.1.2	Implementation of ELCOM Drifter Module	8-2
8.1.3	Simulation Durations	8-2
8.1.4	Temporal Release Pattern	8-2
8.1.5	Spatial Release Pattern	8-2
8.1.6	Vertical Migration	8-6
8.1.7	Larvae Counts	8-6
8.1.8	Outputs	8-6
8.2	Post Processing Techniques	8-7
8.2.1	ELCOM Inputs	8-7
8.2.2	User Defined Parameters	8-7
8.2.3	Outputs	8-15
8.2.3.1	<i>GIS Data</i>	8-15
8.2.3.2	<i>Numerical Data</i>	8-16
8.3	Results	8-16
8.3.1	GIS Data	8-16
8.3.1.1	<i>Larval Pathway Maps</i>	8-16
8.3.1.2	<i>Initial Locations of Entrained Larvae</i>	8-23
8.3.2	Numerical Outputs	8-28
8.4	Summary	8-30
9	REFERENCES	9-1

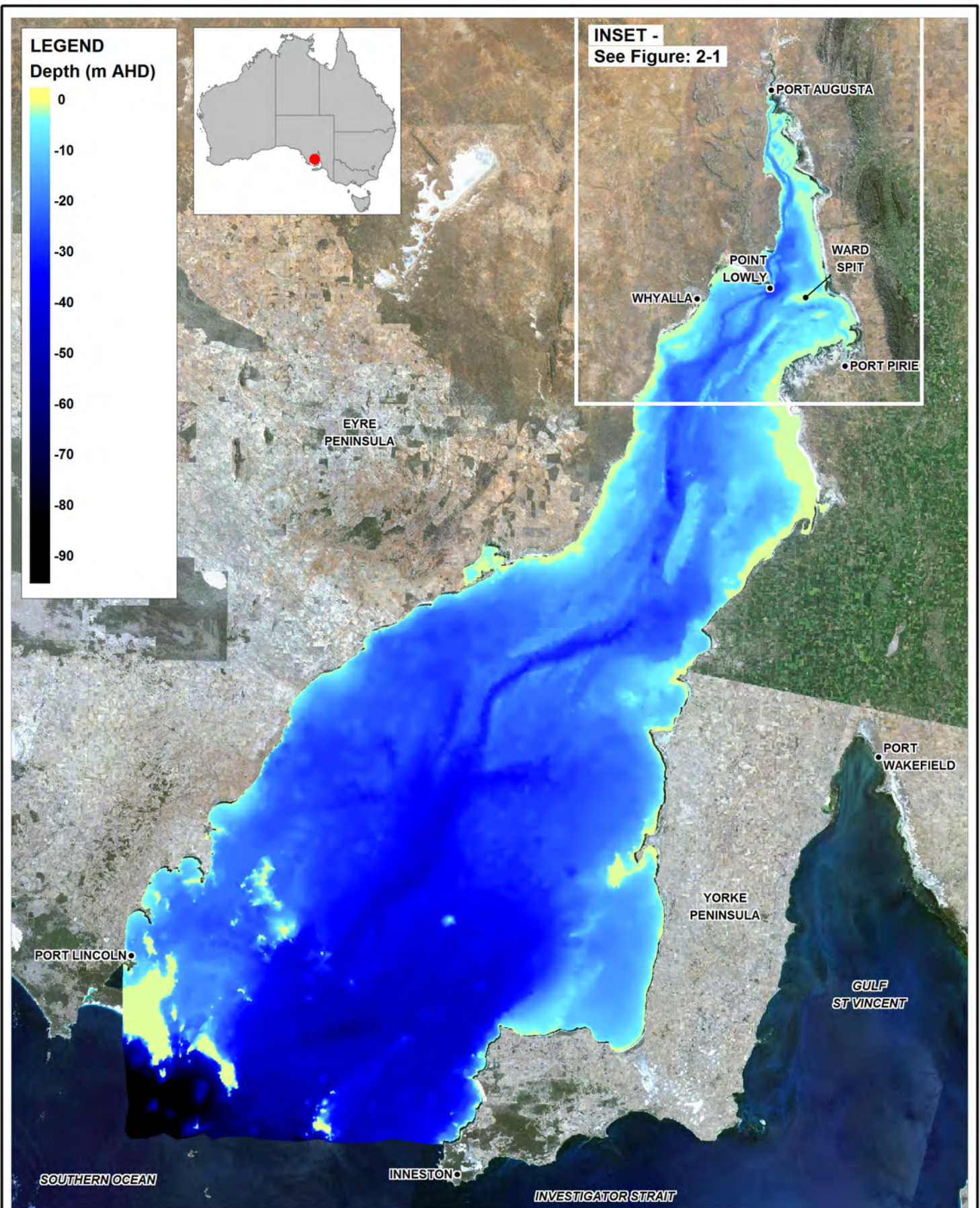
1 INTRODUCTION

BHP Billiton is proposing to expand its mining operations at Olympic Dam, South Australia. Part of this proposal includes construction and operation of a desalination plant at Point Lowly on the coastline of Spencer Gulf (Figure 1-1 and Figure 1-2). This plant would provide water to the proposed mine if approved.

BHP Billiton (2009) released the Olympic Dam Expansion Draft Environmental Impact Statement (hereafter DEIS) document with respect to the proposed expansion and desalination plant in May 2009. Part of this Draft EIS described numerical modelling undertaken to better understand the behaviour of return water discharged from the proposed desalination plant. BMT WBM and the Centre for Water Research (CWR) of the University of Western Australia undertook this numerical modelling on behalf of BHP Billiton, and details have been provided in a series of peer reviewed reports contained in the DEIS (see Appendices O11.2, O11.3 and O11.4). Similar studies have been undertaken in the Australian context, and the reader is referred to these contextually relevant studies for further information (Okely *et al.* 2007a, 2007b; SA Water 2008, 2009; DSE 2008).

Since the release of the DEIS, BHP Billiton has commissioned BMT WBM to upgrade modelling tools and approaches used in that study so that the quality of assessments is able to keep pace with industry best practise and to ensure the ongoing delivery of robust and rigorous modelling outcomes. This has included execution of a targeted and comprehensive supporting field data collection program in 2009. The resultant upgraded modelling tools and supporting field data are described in Appendix H5.2 of the Supplementary Environmental Impact Statement (hereafter SEIS).

This report presents the methodology and outcomes of a series of analyses that have used these upgraded modelling tools, approaches and techniques to support preparation of the SEIS. Each analysis is presented in a separate chapter, with linkages between assessments and techniques noted as required.

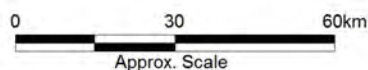


Title:
Spencer Gulf location and bathymetry

Figure:
1-1

Rev:
A

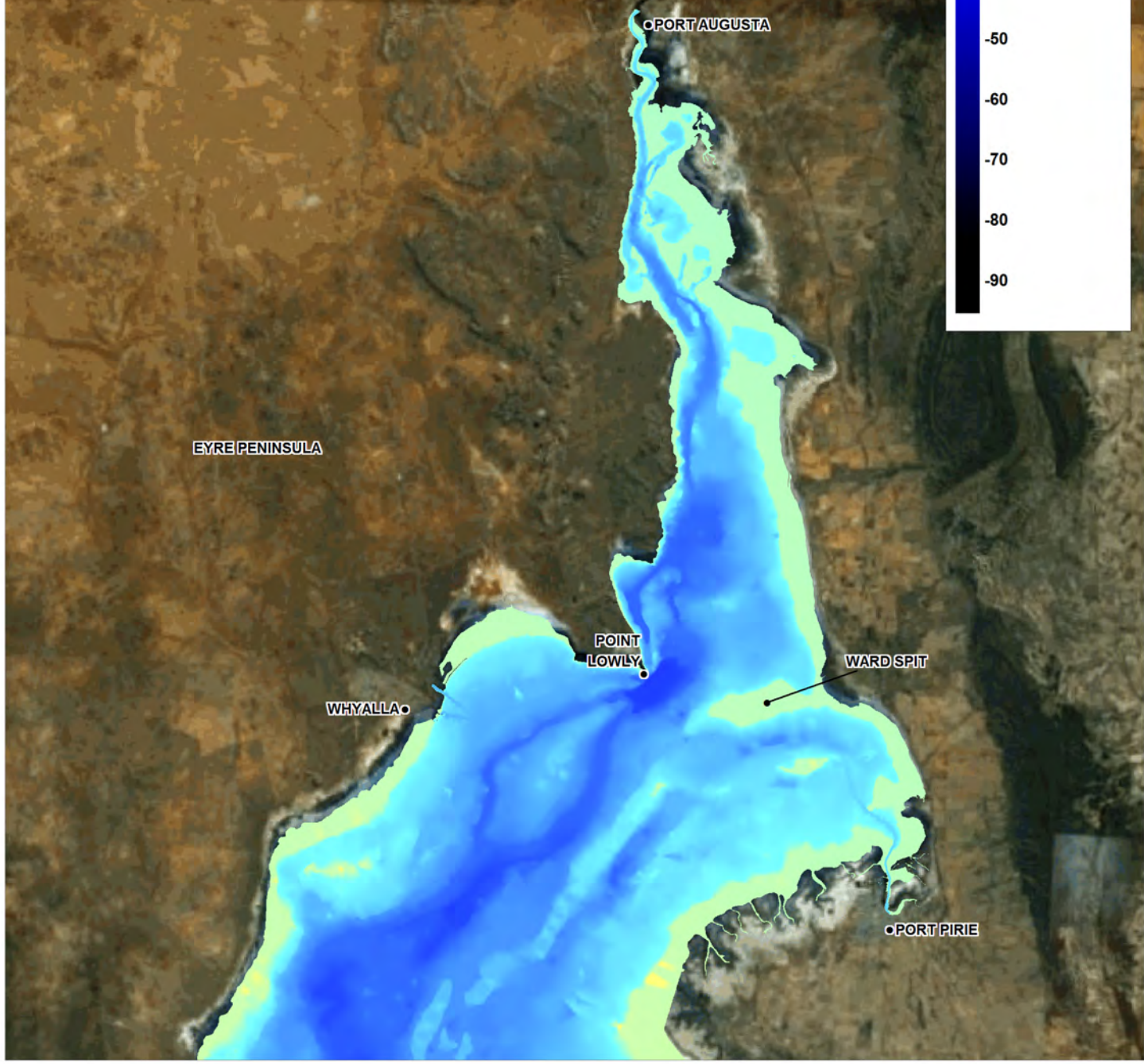
BMT WBM endeavours to ensure that the information provided in this map is correct at the time of publication. BMT WBM does not warrant, guarantee or make representations regarding the currency and accuracy of information contained in this map.



Filepath :



Image ©2009 Google™
 Data SIO, NOAA, U.S. Navy,
 NGA, GEBCO
 Image © 2010 DigitalGlobe
 Image NASA
 Image © 2010 Cnes/Spot Image

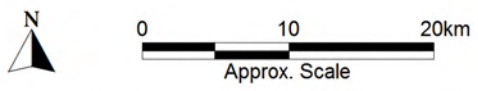


Title:
**Northern Spencer Gulf
 Location and Bathymetry**

Figure:
1-2

Rev:
A

BMT WBM endeavours to ensure that the information provided in this map is correct at the time of publication. BMT WBM does not warrant, guarantee or make representations regarding the currency and accuracy of information contained in this map.



Filepath :

2 COMPUTATIONAL FLUID DYNAMICS: DETAILED DIFFUSER SIMULATION

Following completion of a diffuser optimisation study (see Appendix H6.1), it was determined that more advanced tools were required to adequately support BHP Billiton in its design of the proposed return water diffuser arrangement. This section describes such a Computational Fluid Dynamics (CFD) tool and its application to the current study.

CFD modelling was applied to a range of diffuser configurations over the course of the study, including both linear and rosette style designs. Initially, a suite of linear diffusers was considered, and the design of these was determined with BHP Billiton (supported in part by information provided by BMT WBM, as reproduced in Appendix H6.1). The linear diffusers were typically 200 metres in length and had alternating side ports oriented at 60 degrees to the horizontal. This initial suite included diffuser designs that varied this general linear arrangement in a range of ways, focussing primarily on alterations to port diameter and spacing. BMT WBM did not contribute to detailed engineering design matters.

Following review of matters beyond the scope of this modelling study, BHP Billiton determined that rosette diffusers were to be simulated and included in the modelling study, rather than the linear arrangements considered initially. The general arrangement of these diffusers was provided by BHP Billiton to BMT WBM for CFD simulation, with BHP Billiton being responsible for detailed engineering design considerations. This rosette arrangement is shown schematically in Figure 2-1 (for one rosette unit). Some degree of optimisation of the rosette arrangement was undertaken using CFD analyses (including varying the central column elevation, for example), and a final design, including rosette spacing, was then determined by BHP Billiton for inclusion in the SEIS modelling described in this report.

The following sections describe the CFD tool, its validation to existing literature and its application to both the linear and rosette diffuser arrangements.

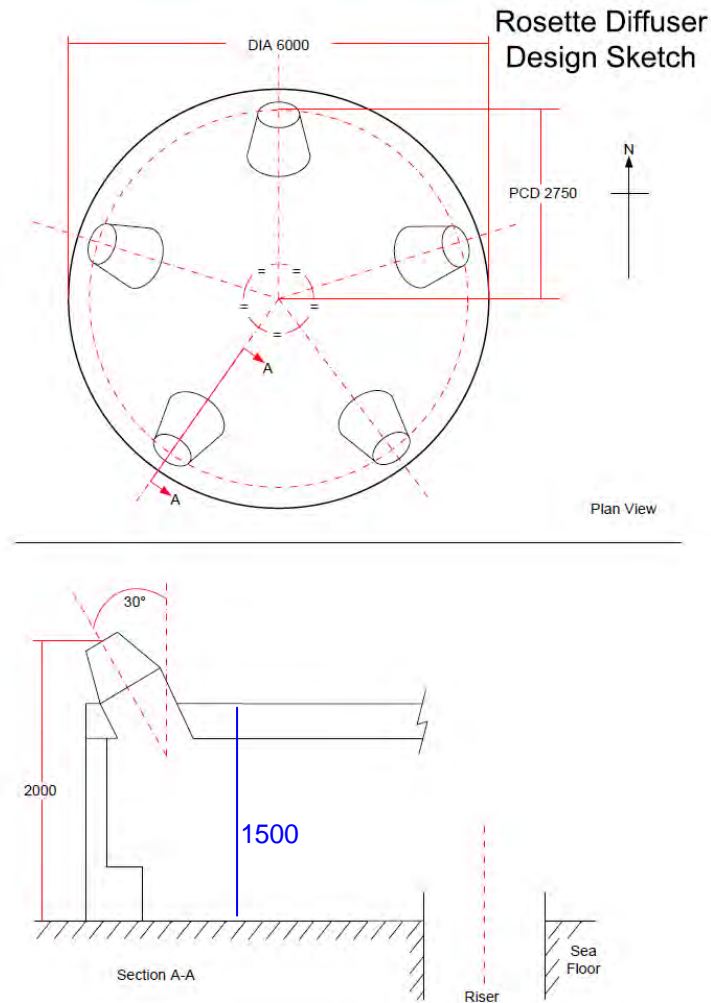


Figure 2-1 Rosette sketch supplied by BHP Billiton, annotated with additional dimensions estimated by BMT WBM (blue). Dimensions in millimetres.

2.1 Computational Fluid Dynamics

CFD has evolved over the last three decades to become a highly advanced and relied upon tool for studying fluid flows. Most available CFD packages offer the ability to:

- Solve on an arbitrary mesh constructed around specified geometry;
- Solve for compressible and incompressible fluid flows;
- Solve for steady state and transient problems; and
- Select from a wide selection of turbulence models.

The equations solved are typically a reduced set of the Navier-Stokes equations, depending on assumptions made regarding the flow.

2.2 OpenFOAM

There are a number of commercially available CFD packages, however there is an open source alternative, namely OpenFOAM, which offers many advantages. OpenFOAM (Open Field Operation

and Manipulation) is developed by Open CFD Ltd (based in the UK) and is used by Shell, Audi, and some Formula one motor racing teams. Three significant advantages of using OpenFOAM are:

- Transparency of code. The user is able to interrogate any aspect of the source code to determine exactly which equations are being used;
- Extension of code. The user is able to write tailored conditions, modify equations, and create new solvers for specific problems; and
- Parallel computation. As the software is licensed under a GNU license, a multi-CPU computer cluster may be used to solve large problems without incurring significant license fees. This can translate to significant increases in run speeds for complex models.

BMT WBM has been using OpenFOAM for a significant portion of its CFD work for many years. Projects include reacting chemistry in smelting furnaces, coal dust combustion and explosion modelling, RAAF engine test bunker airflow modelling, tidal turbine hydrodynamics, and other diffuser outfall models.

2.3 CFD Model Setup

2.3.1 Equations

The equations solved in this application of OpenFOAM are listed below, where α (also referred to as alpha in subsequent text, figures and illustrations) is the mixing fraction of outfall fluid of density ρ_1 to background fluid of density ρ_2 (it is the reciprocal of dilution), ϕ is the mass flux vector, U the mean velocity vector, ν_t the turbulent contribution to kinematic viscosity, and p_d a modified pressure field.

$$\nabla \cdot [\phi \alpha] - \nabla^2 \left[\left(D + \frac{\nu_t}{Sc_t} \right) \alpha \right] = 0$$

$$\rho = \alpha \rho_1 + (1 - \alpha) \rho_2$$

$$\phi = \rho U$$

$$\nabla \cdot [\phi U] - \nabla^2 [\mu_{eff} U] - \nabla U \cdot \nabla \mu_{eff} = -(gh \nabla \rho + p_d)$$

$$p_d = p - \rho gh$$

$$\mu_{eff} = \rho \nu_{eff} = \rho (\nu + \nu_t)$$

The model constants are listed in Table 2-1. Note that the molecular diffusion constant, D , is very small compared to the turbulence induced mass diffusion (ν_t / Sc_t) throughout the majority of the model domain.

Table 2-1 Model constants

Parameter	Description	Value
D	Molecular diffusion constant for salt in water	$2e-9 \text{ m}^2\text{s}^{-1}$
Sc_t	Turbulent Schmidt number	0.71
ν	Laminar kinematic viscosity	$1e-6 \text{ m}^2\text{s}^{-1}$
g	Gravity vector	$(0 \ 0 \ -9.81) \text{ ms}^{-2}$

2.3.2 Turbulence Model

The turbulent contribution to the viscosity ν_t is calculated by a turbulence model which estimates the energy and length scales of the random fluctuations in the flow field. This variable influences the rate of dispersion/diffusion of the plume, in terms of both momentum and brine concentration. As the Reynolds numbers of the plumes are of the order of 1,000,000 both of the k- ϵ or k- ω turbulence models were appropriate choices. The k- ω model was selected due to its greater stability and reduced sensitivity to initial conditions. Standard model constants were used.

2.3.3 Domain and Mesh

The model domain for this study was a Cartesian box aligned with the diffuser (or series of rosettes), spanning 160 m either side of the centre of the diffuser alignment in both directions (i.e. producing a 320 m wide domain). The top surface of the model was the $z = 0$ mAHD plane and the bottom surface was fitted to digital elevation model (DEM) data from the ELCOM model (which is derived from BHP Billiton survey data and other supplementary data sets). Models with varying tide levels were not run as it was considered unlikely that this would have a significant bearing on the primary output of the CFD effort.

Approximately cubic cells were required within the immediate vicinity of the diffuser for the successful operation of an automatic mesh generation tool designed to refine the mesh around the risers (see below). These were initialised at a 0.5 m edge length before refinement. However, to use 0.5 m cells in the remainder of the domain would produce a 5 million cell mesh even before diffuser/rosette refinement, so a grading system was adopted such that the horizontal spacing of cells was increased in steps to 4 metres in outer regions of the domain, which is acceptable since the vertical component of the flow at those locations is not significant. Figure 2-2 provides an illustration of this refinement.

Following initialisation as above, the mesh was then automatically and iteratively refined around the diffuser risers as shown in Figure 2-3 (for a linear diffuser – the refinement technique was also applied to rosettes). This process refined the mesh down to ~15 mm cells immediately adjacent to the riser exits.

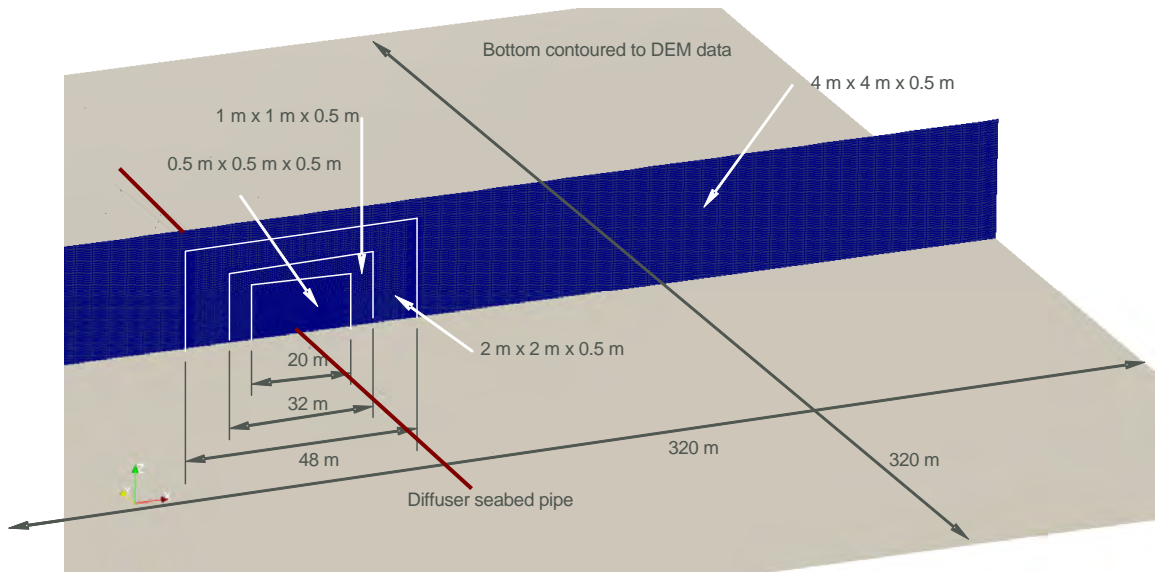


Figure 2-2 Domain and initial mesh

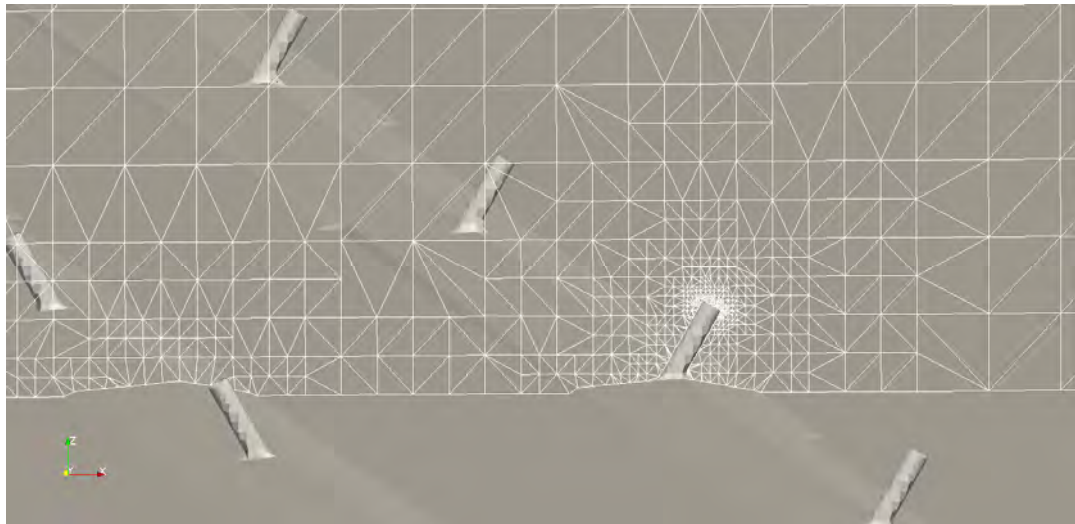


Figure 2-3 Refined riser mesh

Accurately calculating the evolution of the predicted plumes is clearly the most critical aspect of the CFD work. This requires a fine mesh around the boundaries of the plumes where spatial gradients in velocity, density and concentration (α) are high) to appropriately resolve plume morphology and mixing. However, utilising such a fine mesh through the entire model domain is not tractable and locating the plume to selectively provide this high resolution for each simulation in advance (where plume position responds to applied boundary conditions) is clearly not possible. As such, the automatic mesh refinement tool described above was adapted for iterative and dynamically responsive application within the CFD solutions. Specifically, for each simulation, a first pass solution was computed, then the mesh automatically refined in the regions where spatial gradients exceeded a pre-defined threshold. This refinement process was repeated until predictions converged. Figure 2-4 shows a cross section of a mesh (coloured by velocity) through an example riser at each stage of an illustrative mesh refinement process.

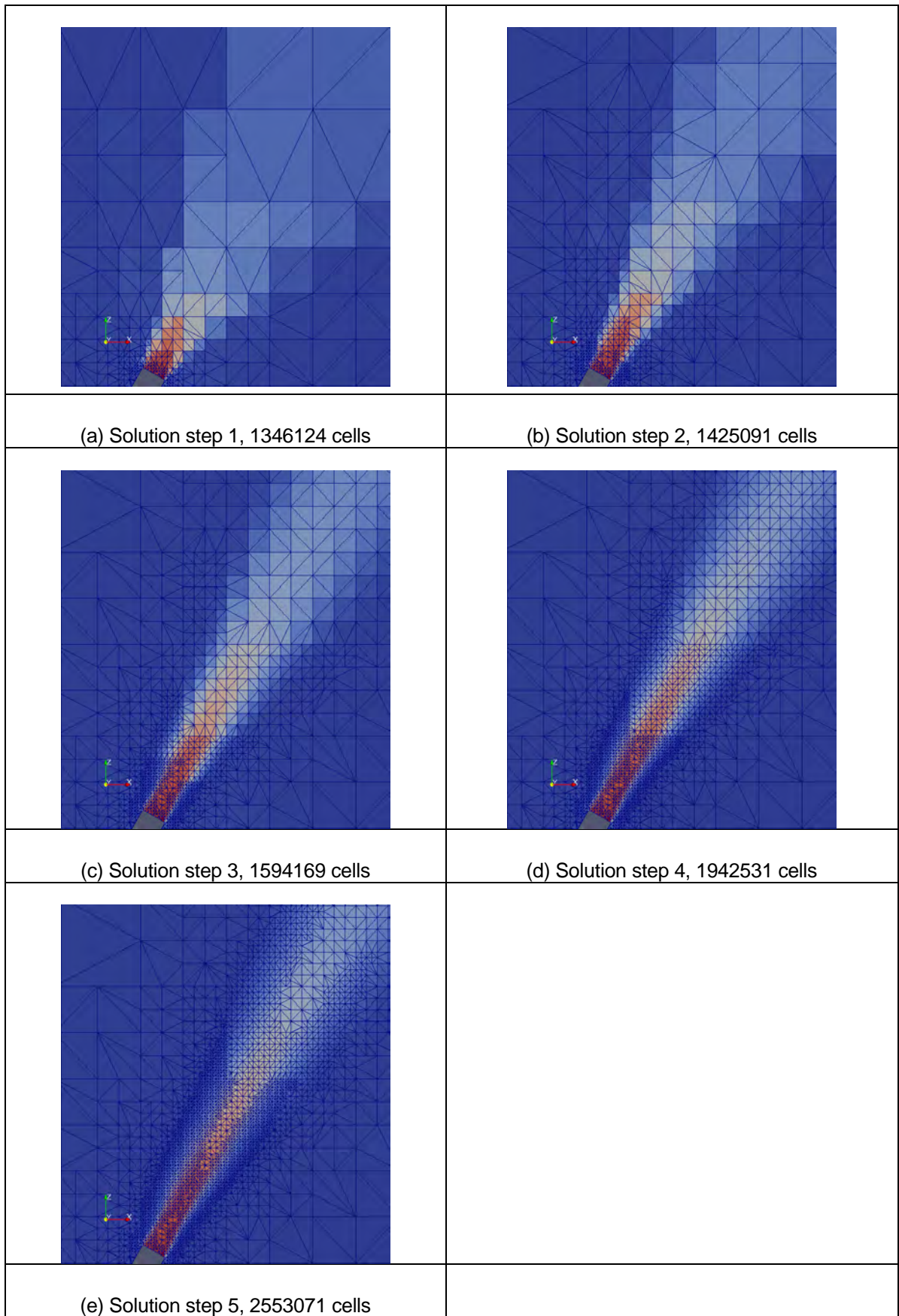


Figure 2-4 Adaptive mesh refinement

2.3.4 Boundary Conditions

The bottom surface of the model (including risers where appropriate) was defined as a wall (velocity = 0 vector), against which standard wall functions were used in the turbulence model. The top surface of the model was defined as a 'slip wall' which has no friction but constrains the flow to be parallel to the surface. The remaining field variables were defined as zero-gradient against the top and bottom boundaries. The change in model depth with tide cycle was not taken into account in the CFD model.

For the studies involving zero background velocity, the four vertical boundaries of the model were defined to be 'zero gradient' in all variables except for alpha (which is the tracer capturing dilution), and thus they allowed inflow and outflow such that total volume flux in and out of the domain was conserved. The boundary condition for alpha was such that any inflows on the model boundaries were defined as being zero in alpha, and outflows were defined as zero-gradient.

For the studies involving non-zero background velocities, the two vertical boundaries with influx were constrained to have a specified velocity profile (magnitude and direction) as a function of depth, as extracted from either the calibrated ELCOM model (see Appendix H5.2) or targeted ADCP data, as appropriate. The other two vertical boundaries were unconstrained in velocity except that total volume flux was conserved. Again the boundary condition for alpha was such that any inflows on the model boundaries were defined as zero in alpha, and outflows were defined as zero-gradient. The remaining variables were defined as zero gradient.

The background velocity profiles for all simulations were obtained by calculating a depth averaged velocity from either the ELCOM model or ADCP data collected specifically for this study (see Appendix H5.2), as appropriate, and ranking these from maximum flood through to maximum ebb flow. The profiles were obtained from three complete neap and spring tides cycles from 24 April to 6 June 2009 corresponding to a subset of the model validation period presented in Appendix H5.2. Velocity profiles were then selected to represent 10%, 30%, 50%, 70%, and 90% flood flow based on time, and similar for ebb flow. Note that the percentiles represent percent of time not exceeded – i.e. 10% represents a small flow velocity and 90% a large flow velocity. Figure 2-5 below illustrates 50% ebb and flood profiles chosen as an example.

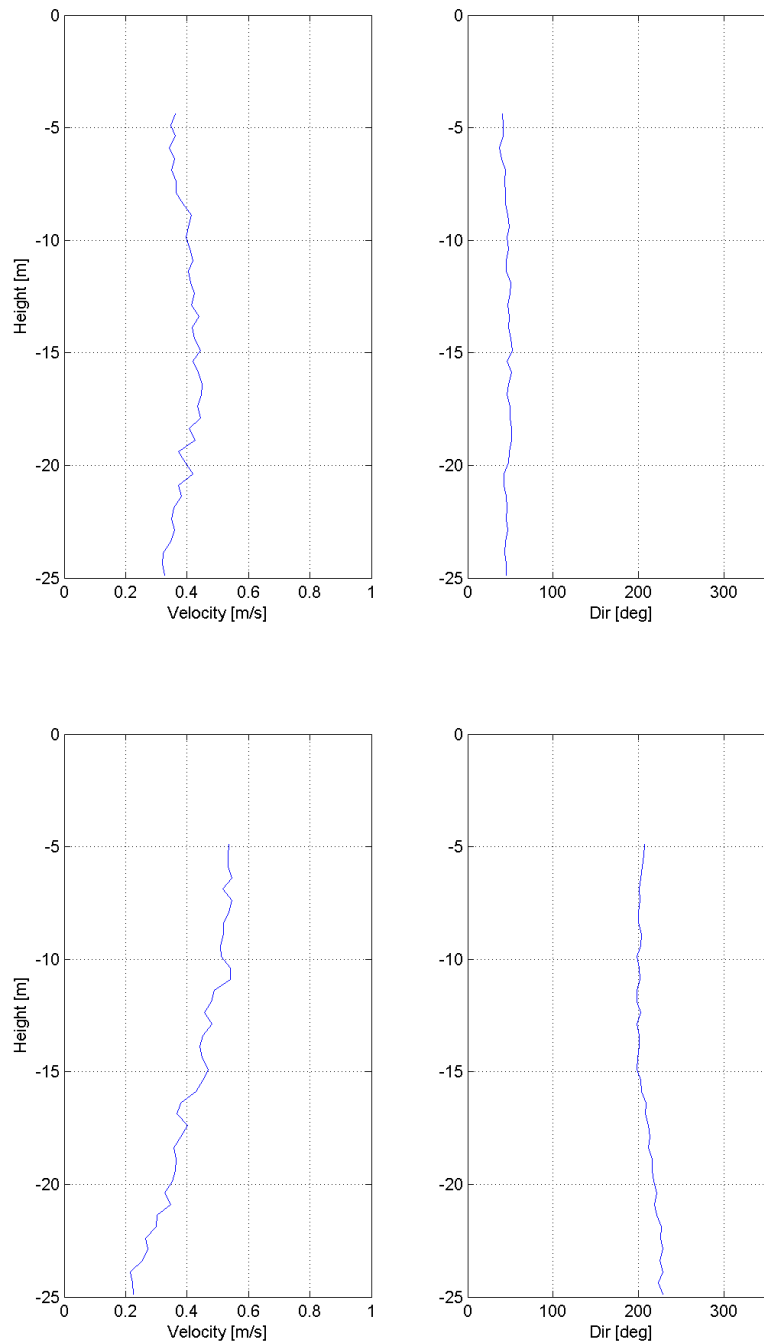


Figure 2-5 Representative 50% flood flow profile (top) and 50% ebb flow profile (bottom) from ADCP data

2.3.5 Initial Conditions

For steady state runs initial conditions are not particularly relevant.

2.4 Validation

The primary goal for the CFD modelling was to provide best estimates for outfall dilutions in the near vicinity of the diffuser for subsequent seeding of the ELCOM models (see discussion in Section 3.6 of

this report). As such, the CFD predictions were benchmarked to previous studies (where possible) to ensure prediction robustness.

At present, three commonly used tools for estimating the behaviour of single negatively buoyant outfall plumes are those developed by Roberts *et al.* (1997), Roberts and Toms (1987) (which were both experimental studies) and the CORMIX model. For simplicity, the former two studies are referred to herein as Roberts 97 and Roberts 87, respectively. It has been documented in the literature that Roberts 97 predicts greater dilution ratios than Roberts 87 for the same jet-densimetric Froude number by some margin, with some supporting instrument-based explanation for same. In contrast to these Roberts studies, however, it is noted that extensive experimental data that accounts for multiport dense plume overlap and outfall re-entrainment is not known to BMT WBM at this point. This has, in part, provided the motivation to apply computational fluid dynamics to the proposed multiport diffusers (and rosettes) in this study, following validation of the CFD predictions against simpler single port historical results.

To do so, the CFD predictions were sequentially compared with the Roberts experiments, CORMIX predictions and field measurements. These comparisons are presented below.

2.4.1 Comparison with Roberts Predictions

Given the above, it was deemed appropriate to compare CFD predictions with Roberts 97 and Roberts 87. Specifically, a CFD simulation was constructed to replicate (at the same physical scale) a Roberts 97 experimental configuration with a densimetric Froude number of 27.6. It is noted, however, that not all the information required to exactly replicate this experiment setup was published, so some assumptions were required regarding tank configuration in the CFD model. Table 2-2 below summarises the parameters used for the steady state comparison.

Table 2-2 CFD validation case parameters

Parameter	Description	Value
ρ_1	Outfall density	1015.7 kgm ⁻³
ρ_2	Background density	998.2 kgm ⁻³
d	Port diameter	4.07 mm
Q (single port)	Flow rate	0.0095 Ls ⁻¹

The resulting plume, after adaptive mesh refinement, is shown in Figure 2-6 a) and b). The figure has been annotated to illustrate the relevant results that were extracted for comparison with Roberts 97.

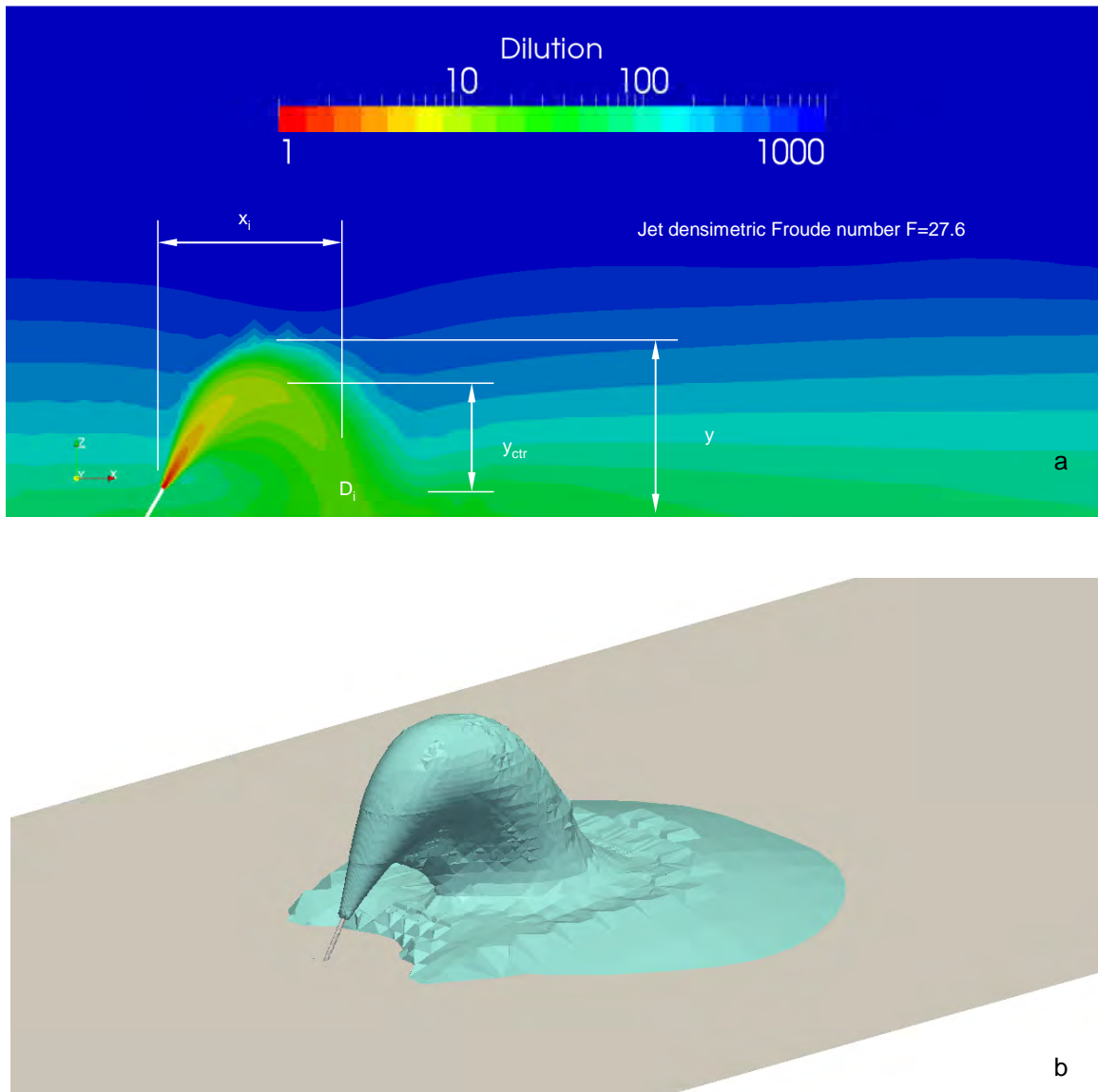


Figure 2-6 CFD validation case (a) plume cross-section and (b) 50:1 dilution iso-surface

The CFD results (with Roberts 87 and Roberts 97 predictions) are presented in Table 2-3. Impact point dilution D_i (on plume centreline) is normalised with respect to jet densimetric Froude number F , and plume throw to impact point x_i and height y (upper visual extent) are normalised with respect to the product of port diameter d and F .

Table 2-3 CFD validation case results

Parameter	Roberts 97	Roberts 87	CFD
D_i/F	1.6	1.03	0.98
x_i/dF	2.4	-	2.05
y/dF	2.2	2.08	1.85

It is apparent in Table 2-3 that the CFD results match well with those of Roberts 87, given that the issue of primary importance is that of dilution at impact. Importantly, Roberts 97 predicts both plume

heights and throws greater than the CFD (and Roberts 87), and this results (non-linearly) in a greater dilution prediction by Roberts 97 compared to CFD.

2.4.2 Comparison with CORMIX

Further insight into the above was obtained by introducing a range of small background velocities, U_x , to the CFD simulations and comparing the predictions with those of CORMIX for the same configuration and range of ambient currents. A representative cross-section of the CFD prediction is provided in Figure 2-7, with $U_x = 0.02 \text{ ms}^{-1}$.

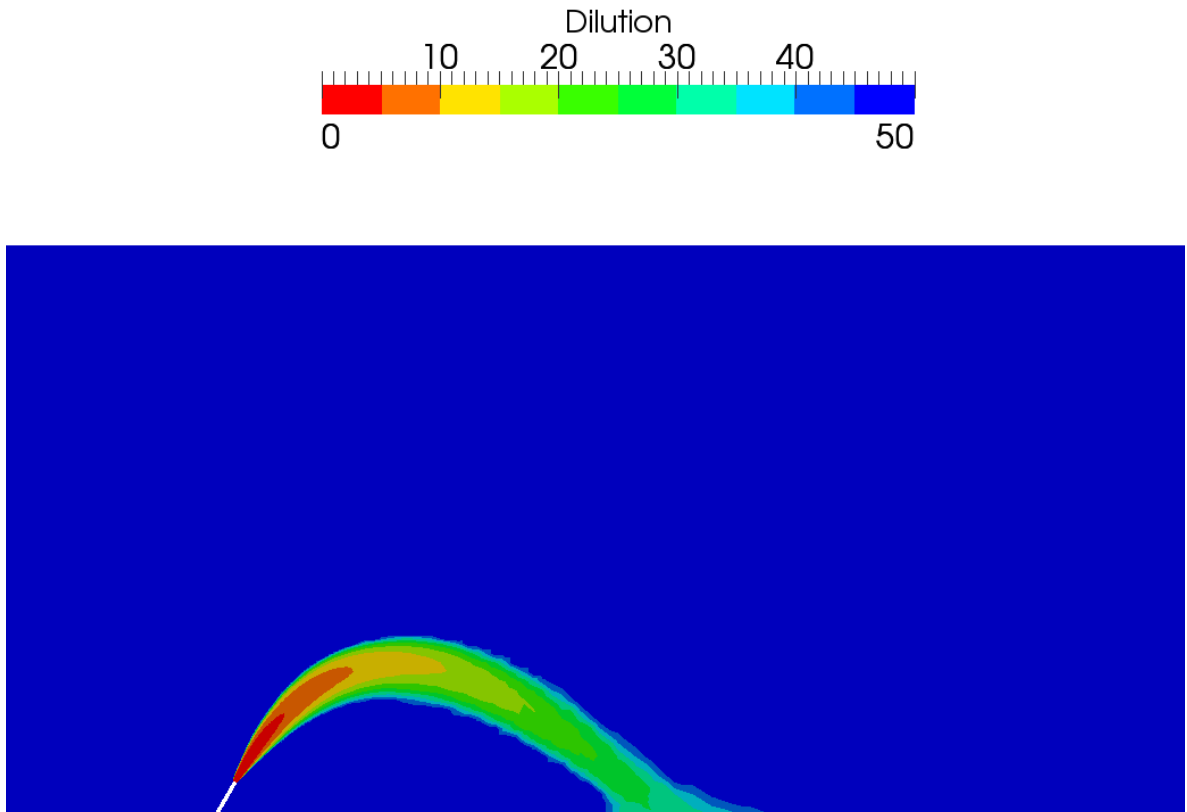


Figure 2-7 CFD simulation of CORMIX configuration. Note the different colour scale to Figure 2-6, with re-entrainment being less obvious in this figure as a result.

Comparative CFD and CORMIX results are provided in

Table 2-4 (only $U_x = 0.02 \text{ ms}^{-1}$) and Figure 2-8 (all background velocities considered). Note that the CORMIX predictions and the CFD results plot the height of the plume centreline, y_{ctr} , whereas Roberts 1997 refers to the uppermost reach of the plume, y .

Table 2-4 CFD validation to CORMIX results, $U_x = 0.02 \text{ ms}^{-1}$

Parameter	CORMIX	CFD
$Y_{ctr} (m)$	0.12	0.12
$D_i [-]$	33.4	32
$x_i (m)$	0.35	0.38

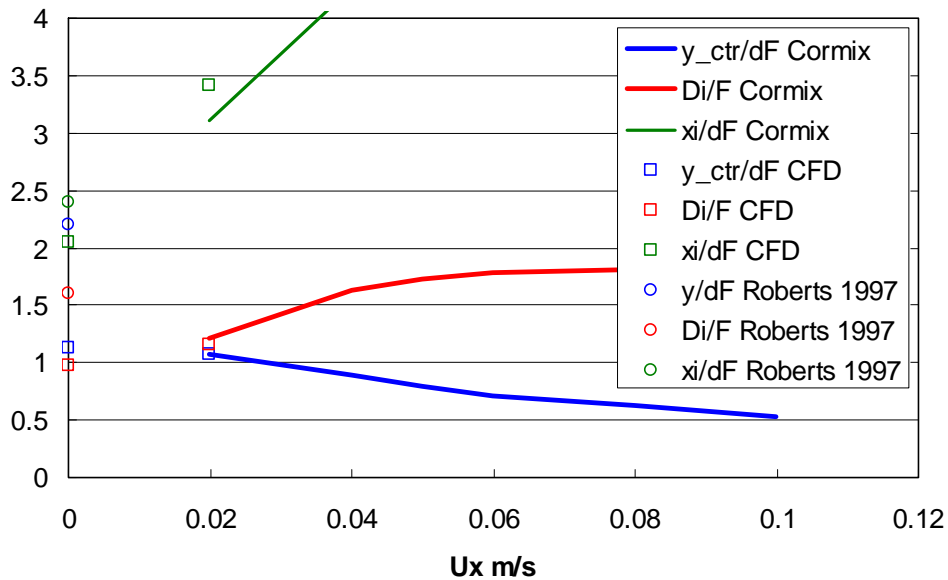


Figure 2-8 CFD validation against CORMIX

The CFD results for $U_x = 0.02 \text{ ms}^{-1}$ agree very well with those of CORMIX, and even though CORMIX cannot always easily be used at zero background velocity, the CFD results for $U_x = 0.0 \text{ ms}^{-1}$ appear sensibly projected with respect to the CORMIX results describing non-zero current conditions.

2.4.3 Comparison with Field Measurements

2.4.3.1 Potential for Re-entrainment

A key outcome of the CFD validation study has been the prevalence of re-entrainment of discharged brine for some configurations, especially those associated with diffusers that provide lower plume throws and heights. An example of such is shown in Figure 2-9. Re-entrainment is clearly evident through the stagnant bottom layer of mixed brine that is several metres thick and smothers the diffuser. Commensurate reductions in impact dilution are thus expected, and the extent to which this process has been accounted for in the laboratory experiments of Roberts 97 is unclear.

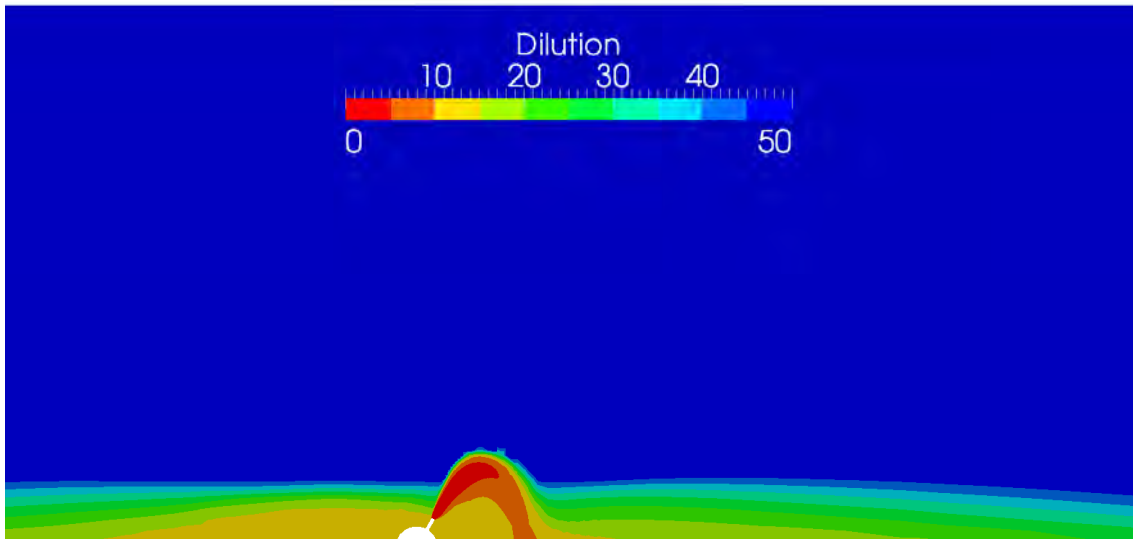


Figure 2-9 Example CFD simulation showing re-entrainment

To illustrate this effect in a ‘real world’ situation, below is presented field measurements ([www.watercorporation.com.au/ files/CockburnSoundFieldStudy.pdf](http://www.watercorporation.com.au/files/CockburnSoundFieldStudy.pdf) page 26) of the Cockburn Sound diffuser. The figure shows time (not space) evolution of rhodamine, salinity and temperature from vertical profiles taken near the diffuser line (i.e. where the plumes are actively mixing with ambient water and potentially exposed to re-entrainment). The original report caption has been maintained for clarity.

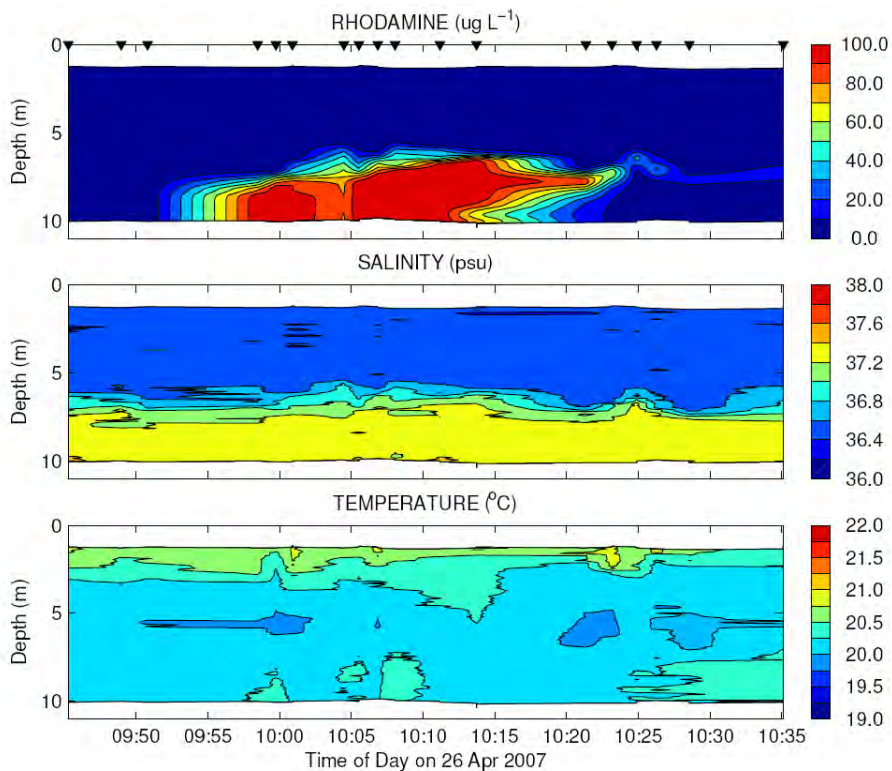


Figure 2-10 Time contour of profile data collected at diffuser during dye release on 26 Apr: rhodamine concentration (top panel), salinity (middle panel) and temperature (bottom panel).

Source: [www.watercorporation.com.au/ files/CockburnSoundFieldStudy.pdf](http://www.watercorporation.com.au/files/CockburnSoundFieldStudy.pdf) page 26

The second panel in the figure is remarkably similar to the CFD cross section in Figure 2-9 (albeit on a time abscissa) and demonstrates that the salinity layer due to the accumulated brine is approximately 3 to 4 metres thick. Importantly, the diffuser ports are 1 metre from the sea bed. As a result, there is potential for re-entrainment of previously discharged brine in this situation, consistent with CFD predictions.

2.4.3.2 Comparison with Roberts 97

Marti *et al.* (2010) measured end of near field dilutions at the above Cockburn Sound site under three separate discharge regimes. The only regime that had a densimetric Froude number greater than 20 (i.e. where Roberts 97 is thought to be applicable) had an ambient current of approximately 5 cms^{-1} . The predictions of Roberts 97 were compared to the CWR measurements for this case and it was found that the observations matched Roberts 97 well.

This is an interesting result as Roberts 87 claims that under such conditions with non-zero background currents (with ambient Froude numbers of about 0.5) dilutions should be significantly influenced (and increased) by ambient conditions. Despite this, the Marti *et al.* (2010) measurements *match* the Roberts 97 predictions well (for end of near field dilutions). It is not easy to discern precisely the mechanism(s) for this, but for example, it is possible that the expected dilution increases due to the action of background currents counterbalanced expected dilution reductions due to re-entrainment suggested by measurements presented in Figure 2-10 and CFD modelling.

2.4.4 Summary

In summary, we have shown that Roberts 87, CORMIX (with small background velocities) and CFD predictions (importantly with using commonly accepted model parameters for turbulent mixing) are all very close for near-zero current conditions, and that Roberts 97 predicts greater dilutions than this suite of approaches. This then provides confidence in using the CFD modelling approach in the current study, and, if anything shows that the CFD predictions are conservative with respect to the Roberts 97 (which has recently been applied as part of other desalination plant impact assessments). Application of CFD also has the major advantage over other approaches in that it can handle the complex plume interactions expected to characterise multiport linear and rosette diffusers under a range of non-zero tidal current conditions. Such applications are described in subsequent sections.

2.5 Preliminary Simulations

In order to provide a feel for the range and variability of CFD predictions under complex (i.e. multiport and re-entraining) conditions, a suite of preliminary steady state solutions were computed for a variety of linear diffuser configurations (including the DEIS diffuser) and background velocities. These simulations preceded the final suite of simulations pertaining to the ultimate rosette diffuser design and flow rate specified by BHP Billiton (see Section 2.6). The following sub sections provide some insight into the evolution of the exploratory path taken in this regard, with some presentation of salient results. The final CFD simulations used to seed the ELCOM model for the SEIS assessments are described in Section 2.6. The relevant results and seeding process are described in Section 3.6.

2.5.1 Zero Background Current DEIS Configuration

Subsequent to the validation process described above, the first results obtained were those for the DEIS configuration at $4.3 \text{ m}^3\text{s}^{-1}$ and zero background velocity, as shown in Figure 2-11 and Figure 2-12. In this configuration the exit velocity from the ports throws the plume less than 6 m into the water column, and this, combined with the presence of the other ports produced a 'puddle' around the diffuser. This demonstrates the need to account for plume overlap and interaction in the current study.

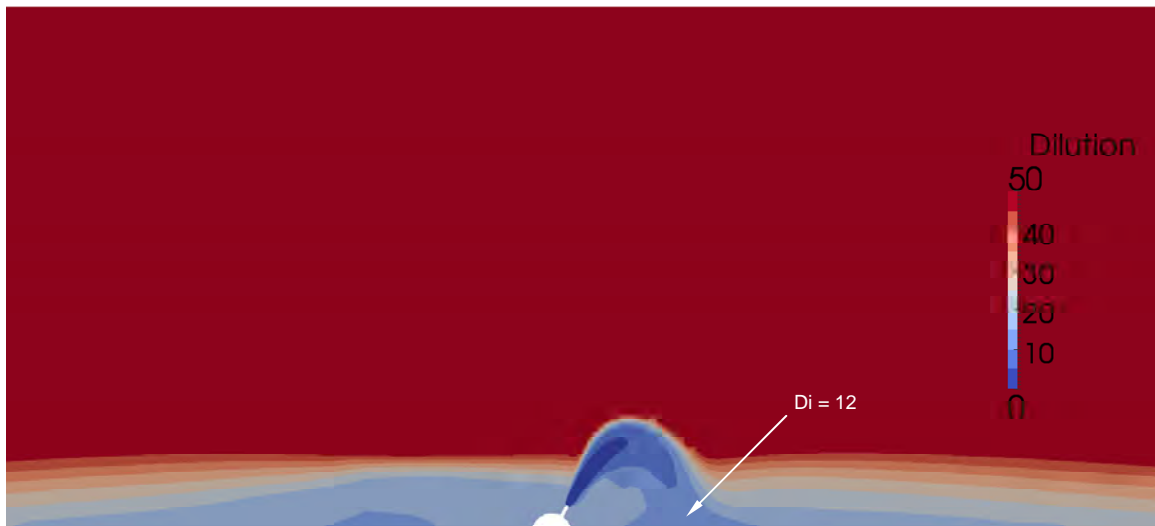


Figure 2-11 DEIS $4.3 \text{ m}^3\text{s}^{-1}$ return water flow rate zero background velocity, plume cross-section. Lower dilutions to the left of the figure originate from adjacent ports that are out of the plane of the port shown.

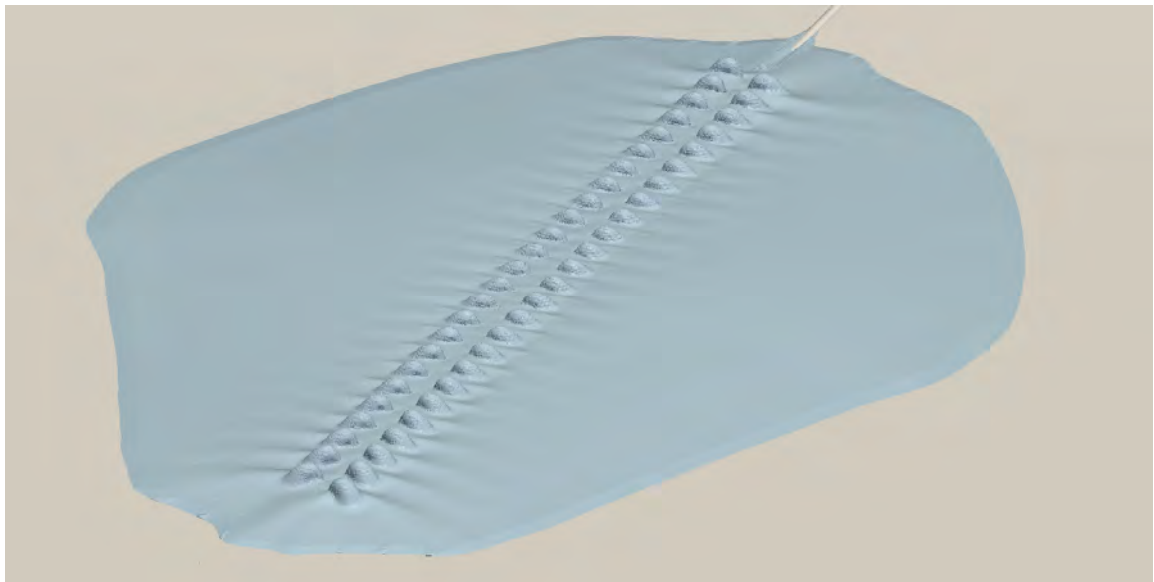


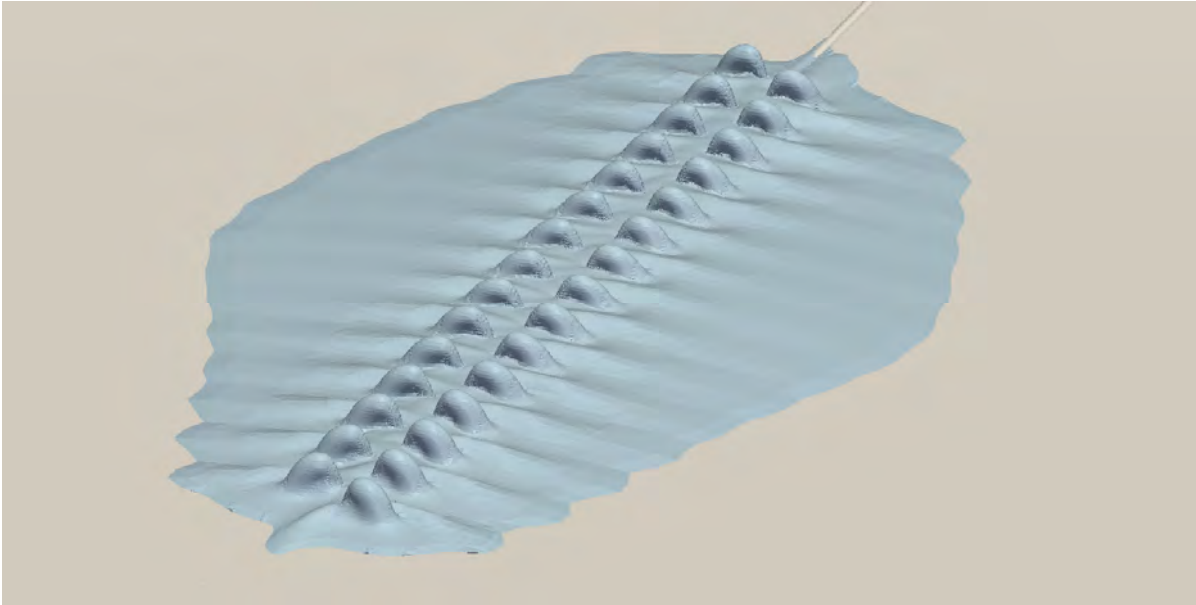
Figure 2-12 DEIS $4.3 \text{ m}^3\text{s}^{-1}$ return water flow rate zero background velocity, 45 to 1 dilution iso-surface

2.5.2 Alternative Configurations – Steady State Simulations

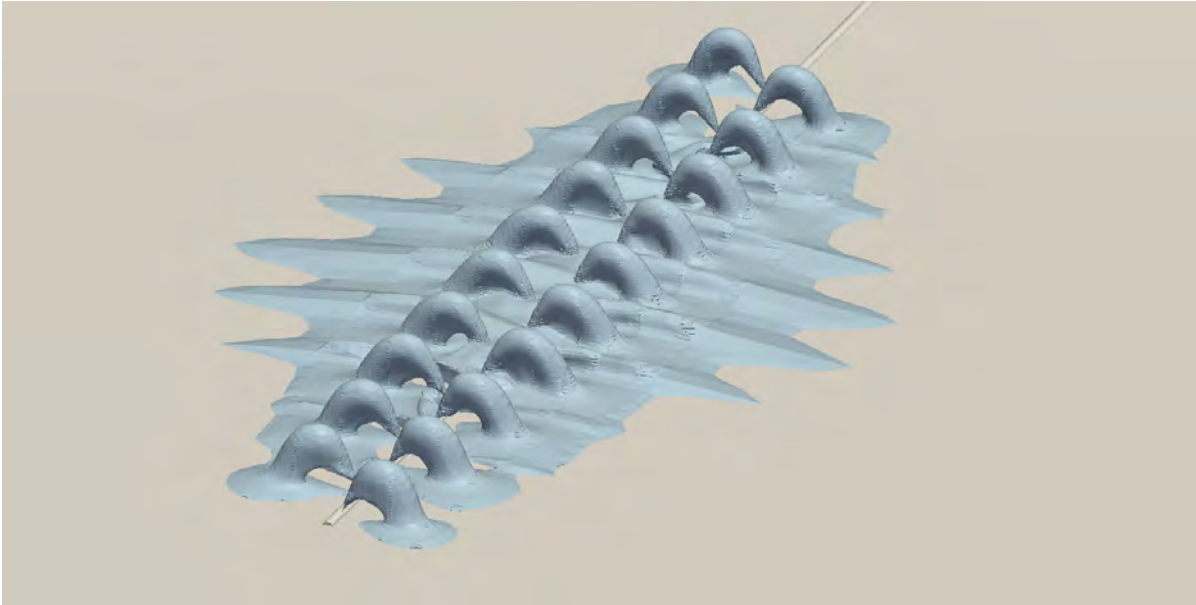
The above result prompted simulation of a range of selected combinations of port diameter and number within the linear diffuser arrangement. These are listed in Table 2-5 as ALT1, ALT2, ALT3 and ALT4. These designs comprised the initial suite of linear diffusers mentioned previously. Figure 2-13 (a – d) illustrates the zero background velocity plume that formed for each of these configurations, as 45:1 iso-surfaces. As can be seen, using fewer and smaller ports to increase the port exit velocity has the plumes reaching higher into the water column and better dilutions are achieved (as expected). In Table 2-5 again note that the percentiles represent percent of time not exceeded – i.e. 10% represents a small flow velocity and 90% a large flow velocity. Table 2-6 summarises the results for these configurations at zero background velocity. Note that the term D_{100} refers to the minimum dilution seen on a vertical cross-section, parallel to the diffuser, 100 m from the diffuser centreline.

Table 2-5 Steady state solutions computed. Q is total flow rate

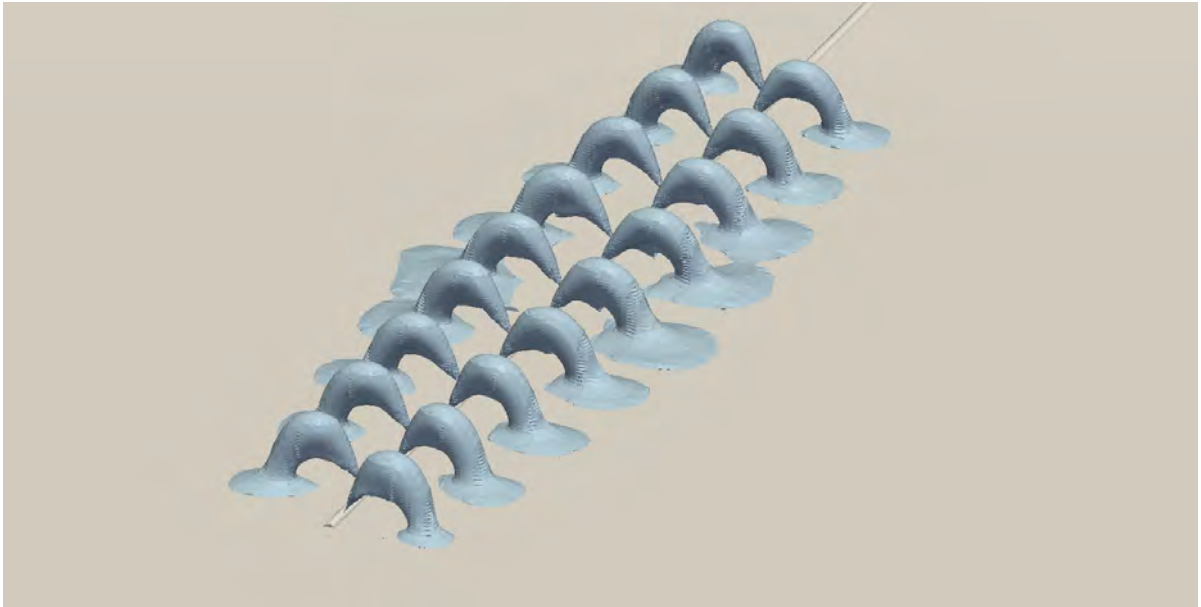
Name	d [mm]	N ports	Q m^3s^{-1}	Ebb 90%	Ebb 70%	Ebb 50%	Ebb 30%	Ebb 10%	Zero Vel	Flood 10%	Flood 30%	Flood 50%	Flood 70%	Flood 90%
DEIS	175	50	4.3	✓	✓	✓	✓	✓	✓	✓	✓	✓	✓	✓
ALT1	150	30	3.1						✓					
ALT2	150	20	3.1	✓	✓	✓	✓	✓	✓	✓	✓	✓	✓	✓
ALT3	140	18	3.1						✓					
ALT4	150	14	3.1						✓					



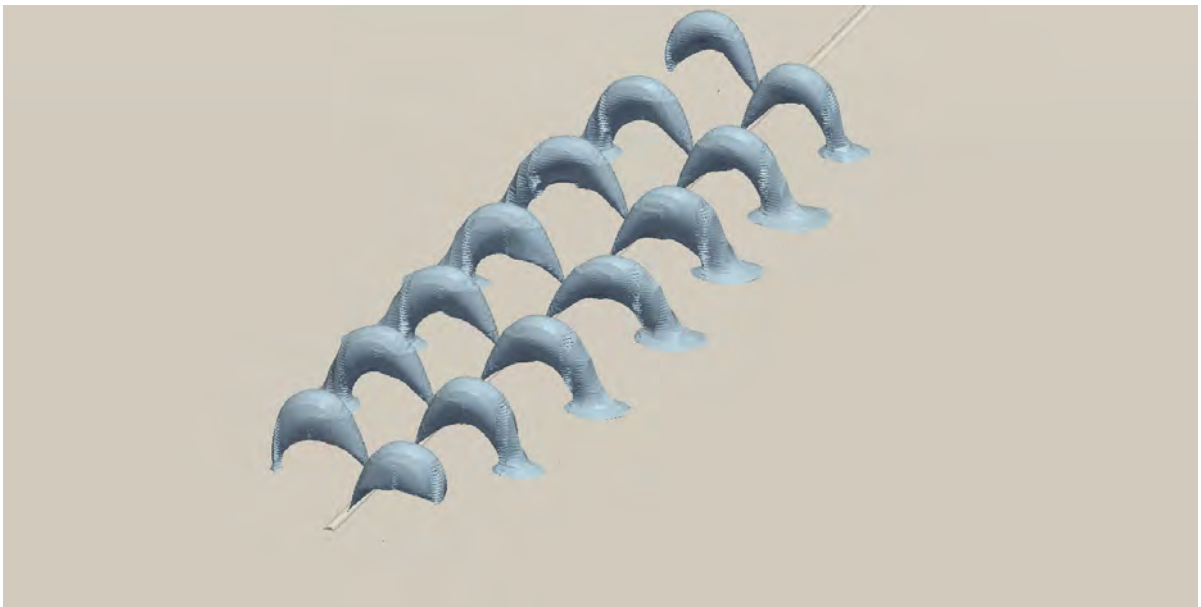
(a) ALT1



(b) ALT2



(c) ALT3



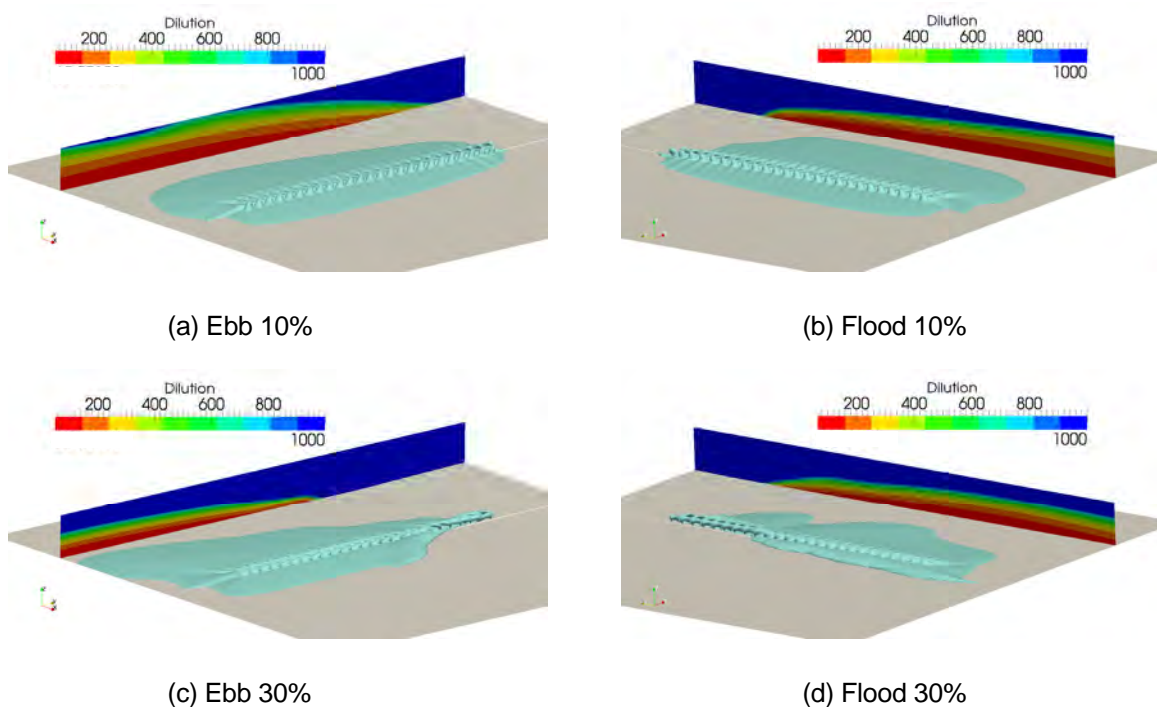
(d) ALT4

Figure 2-13 Alternative configurations $3.1 \text{ m}^3\text{s}^{-1}$ return water flow rate zero background velocity, 45:1 dilution iso-surface. Plume overlap does occur (not shown) at dilutions greater than 45:1 where the plumes above appear not to interact in the figure.

Table 2-6 Alternative and DEIS configurations zero background velocity, dilution results

Name	d [mm]	N ports	Q m ³ s ⁻¹	Exit Vel ms ⁻¹	D _i	D ₁₀₀
DEIS	175	50	4.3	3.6	12	53
ALT1	150	30	3.1	5.9	21	67
ALT2	150	20	3.1	8.9	27	70
ALT3	140	18	3.1	10.9	31	83
ALT4	150	14	3.1	12.5	39	87

Following execution of the zero current simulations, a suite of ambient (non-zero) current scenarios were investigated firstly for the original DEIS configuration and flow rate. Figure 2-14 shows the 45:1 dilution iso-surfaces and 100 m curtains for the DEIS configuration at 4.3 m³s⁻¹ with a range of (steady state) tidal flows. Percentages refer to tidal current velocity percentiles. Note that in each case the colour bar has been scaled from the minimum dilution seen on the 100 m curtain to an upper limit of 1000:1, and that the actual currents speeds for 50% ebb and flood, for example, are not necessarily equal and opposite.



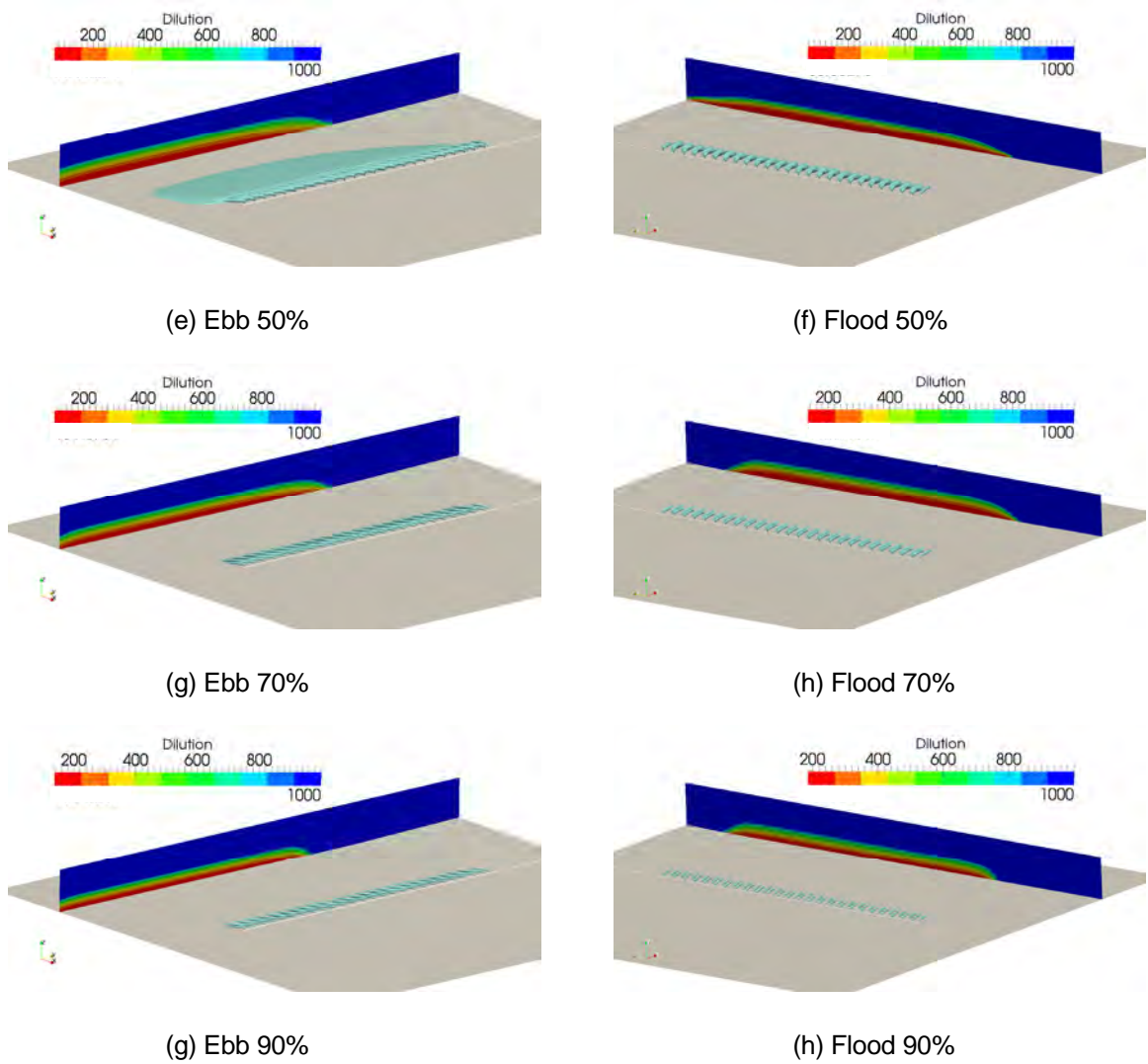
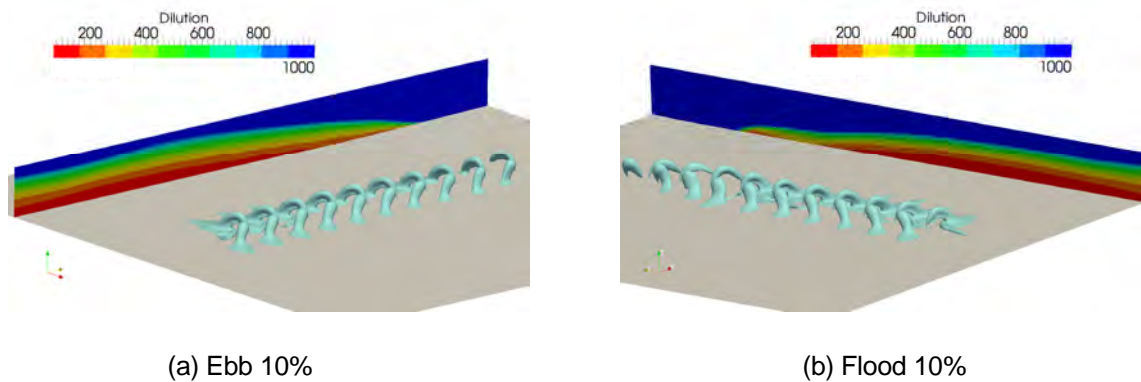


Figure 2-14 DEIS 4.3 m³s⁻¹ return water flow rate 45:1 dilution iso-surfaces and 100 m curtains at ebb and flood tides

Following review of the above results, a similar suite of simulations were conducted relative to the ALT2 configuration. Figure 2-15 shows the 45:1 dilution iso-surfaces and 100 m curtains for the ALT2 configuration at 3.1 m³s⁻¹ with tidal flow.



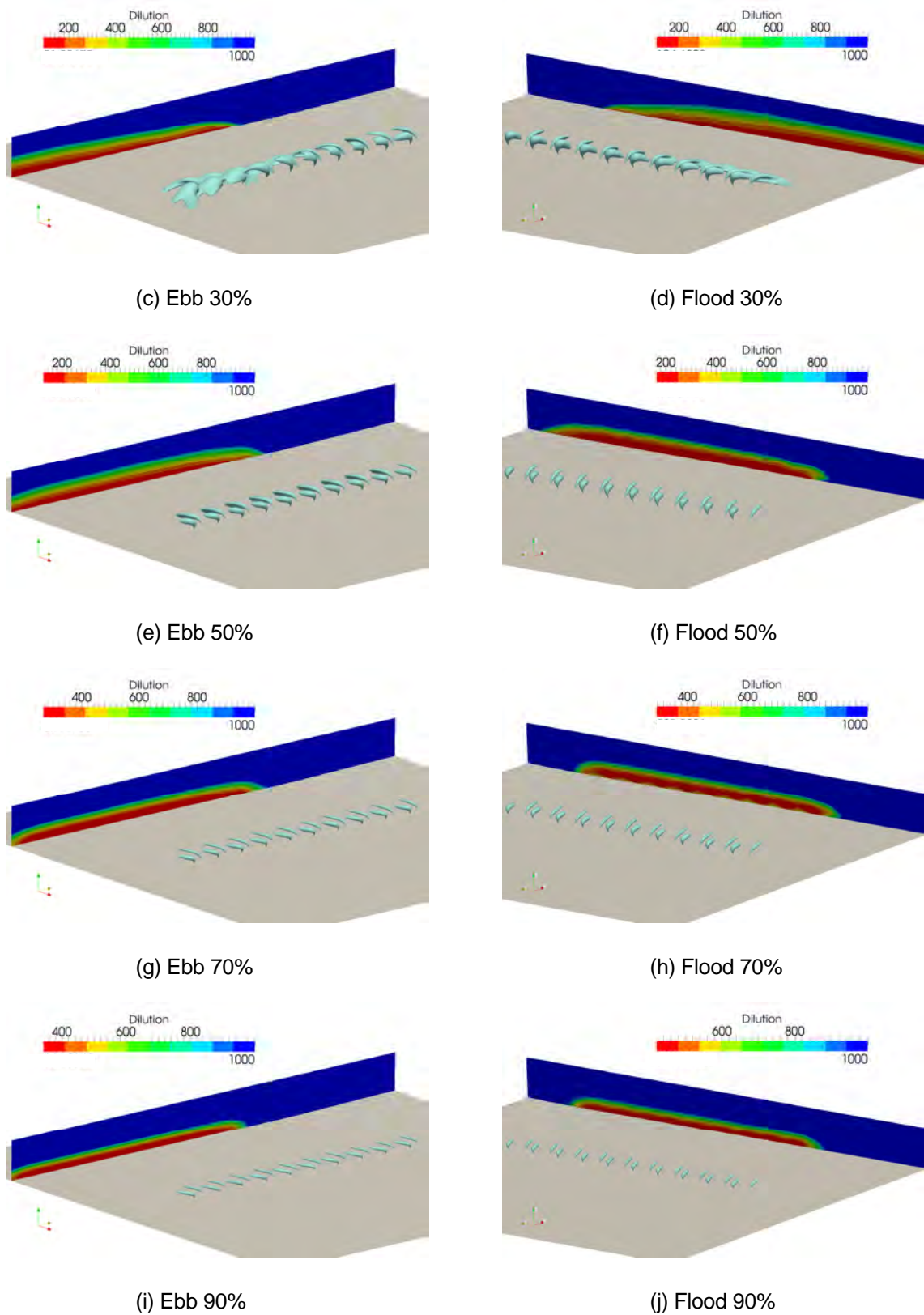


Figure 2-15 ALT2 configuration of $3.1 \text{ m}^3\text{s}^{-1}$ return water flow rate 45:1 dilution iso-surfaces and 100 m curtains at ebb and flood tides

2.5.3 Transient Dodge Tide ALT2 Configuration

A transient simulation of the ALT2 configuration at $3.1 \text{ m}^3\text{s}^{-1}$ return water flow rate was run for a period of 12 hrs over a selected dodge tide. This simulation was not intended to reproduce any particular dodge tide or to provide direct comparison with ELCOM results (the two are not comparable due to differences in scale and physics – see Section 3.6), but rather, to provide some indication of the likely transient dynamics of the selected diffuser. The transient results were not used for seeding ELCOM simulations, and this is discussed further in Section 3.6.

Instead of steady state values, velocity data (from ELCOM) as a function of depth and time was applied on the model boundaries. Model boundary faces with influx used outfall concentrations as output by ELCOM. The depth averaged velocity as a function of time is shown in Figure 2-16. Here 'x' denotes the direction transverse to the diffuser, in an approximately NE direction, and 'y' denotes the direction parallel to the diffuser, in an approximately NW direction.

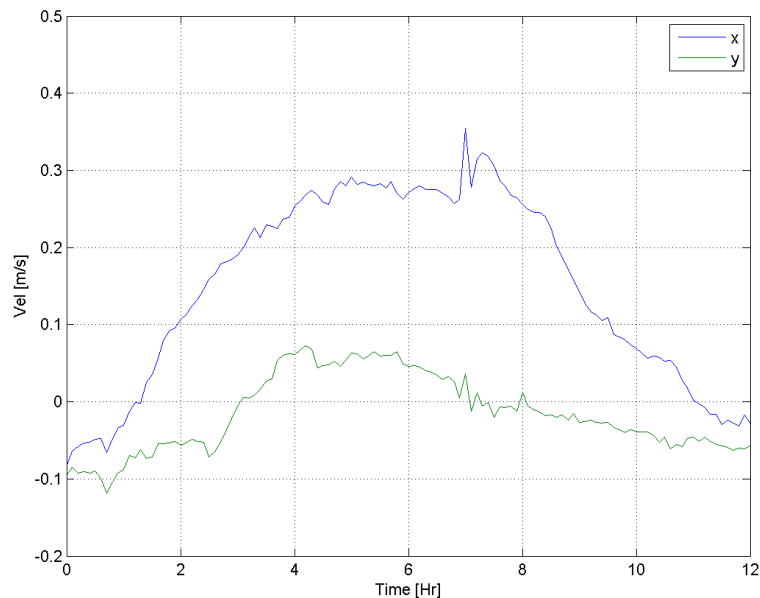


Figure 2-16 Depth-averaged velocity time series corresponding to the ELCOM velocity profiles during a transient dodge tide

Figure 2-17 below shows the first hour of the results (10 min intervals) using the 45:1 dilution iso-surfaces and transverse curtains of dilution. The complex nature of the plumes and their interactions is evident.

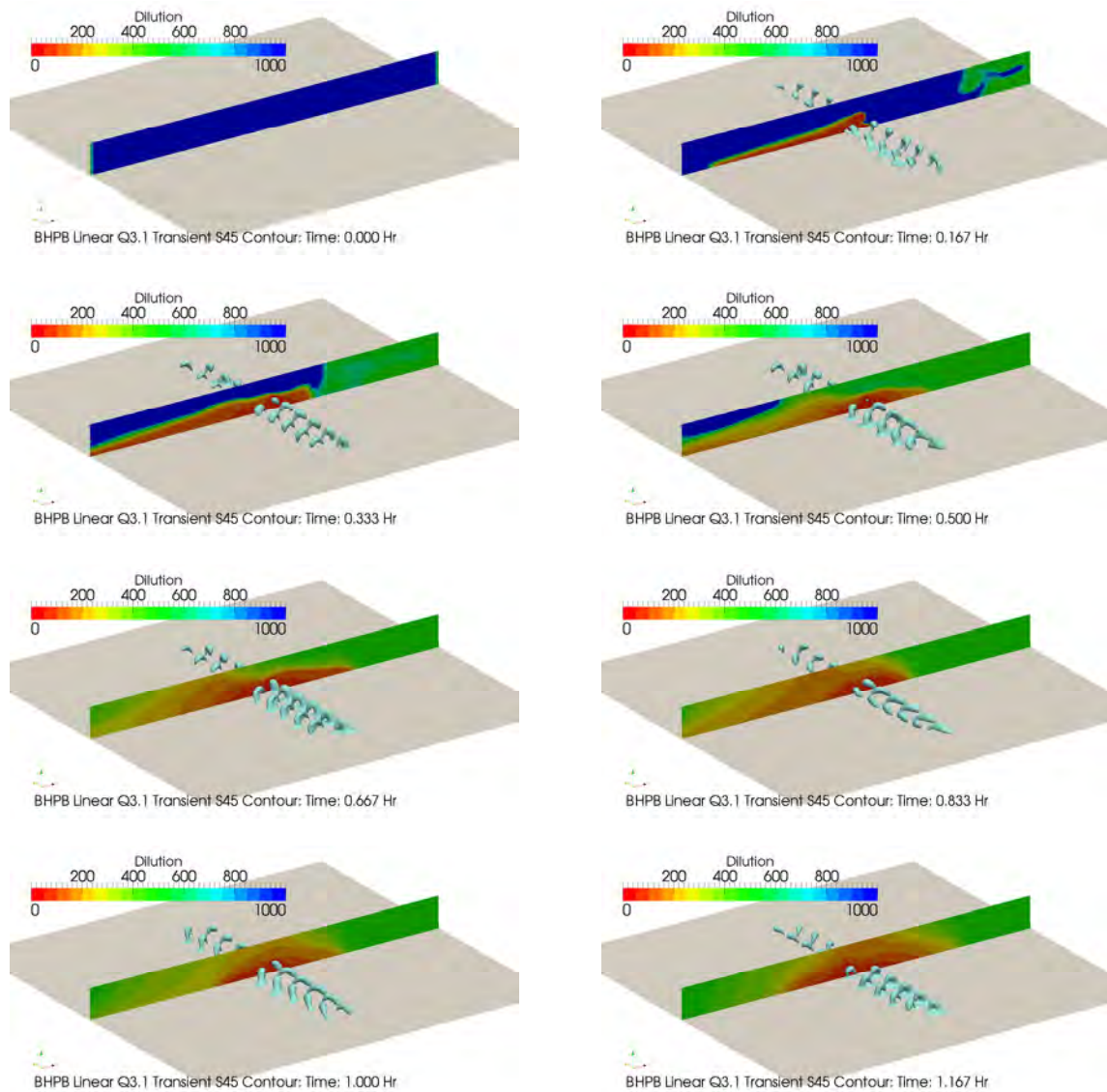


Figure 2-17 Transient dodge tide – first hour

2.6 Final Suite of CFD Simulations

Following execution, examination and discussion of the above simulations (and others not reported here) with BHP Billiton over the range of steady state and transient simulations, BMT WBM was directed to simulate a rosette diffuser design 200 metres further offshore than previous modelling studies had considered. In addition, BMT WBM was instructed to simulate the maximum and long term average return water flow rates of $4.3 \text{ m}^3\text{s}^{-1}$ and $3.6 \text{ m}^3\text{s}^{-1}$ for the current study.

The differences between the work presented previously and the results presented forthwith are:

- Change of diffuser geometry to four (4) rosettes each with five (5) ports. The rosettes are spaced at 50 m intervals along the alignment that the original linear diffuser would have taken; and
- Revised diffuser location to 200 m further offshore along the original linear diffuser alignment (and change flood and ebb velocity profiles corresponding to the revised diffuser location, as sourced from the ELCOM model).

The remainder of the methodology, i.e. the finite volume equation set, fluid densities, turbulent Schmidt number, turbulence model and iterative mesh refinement schemes remain unchanged from those previously presented.

2.6.1 Revised Diffuser Geometry

Figure 2-18 below presents an approximated rosette design, as supplied by BHP Billiton. BMT WBM subsequently used 1500 mm for the height of the top of the rosette (above sea floor), without the risers. Figure 2-19 shows the CFD mesh created around the rosette geometry, including ports.

The rosettes were specified to have five 175 mm ports, and four rosettes were simulated and located at 25, 75, 125 and 175 m along the previous diffuser alignment (i.e. evenly and symmetrically spaced), but displaced 200 m further offshore (along its own line).

Figure 2-20 shows typical resulting plumes from the rosette configuration, and demonstrates the complex nature of the plume dynamics.

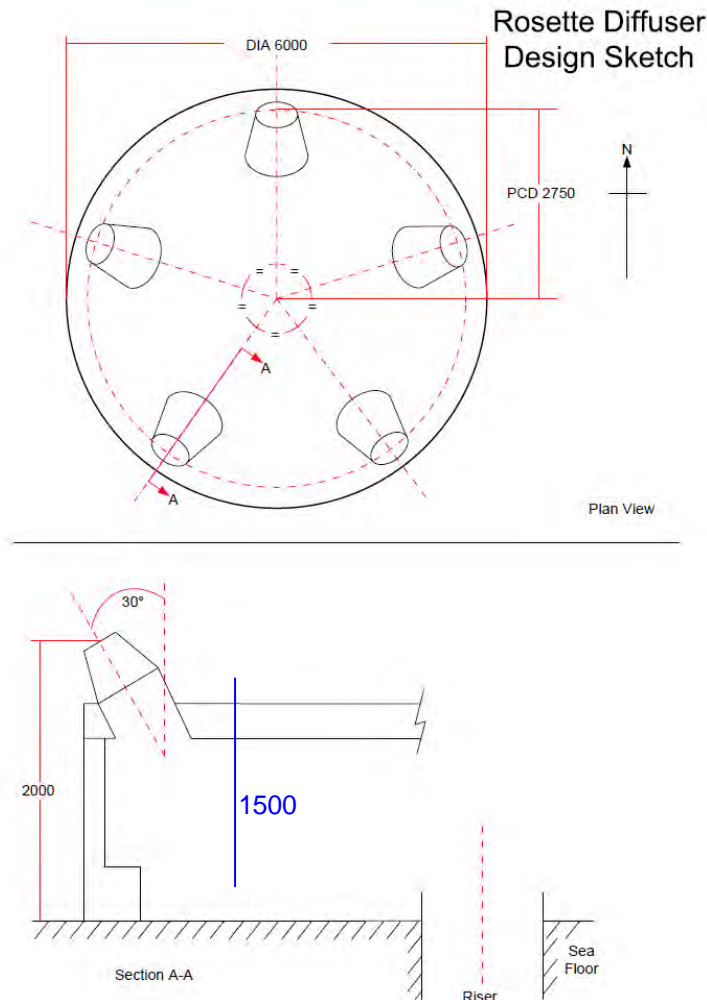


Figure 2-18 Rosette sketch supplied by BHP Billiton, annotated with additional dimensions estimated by BMT WBM (blue)

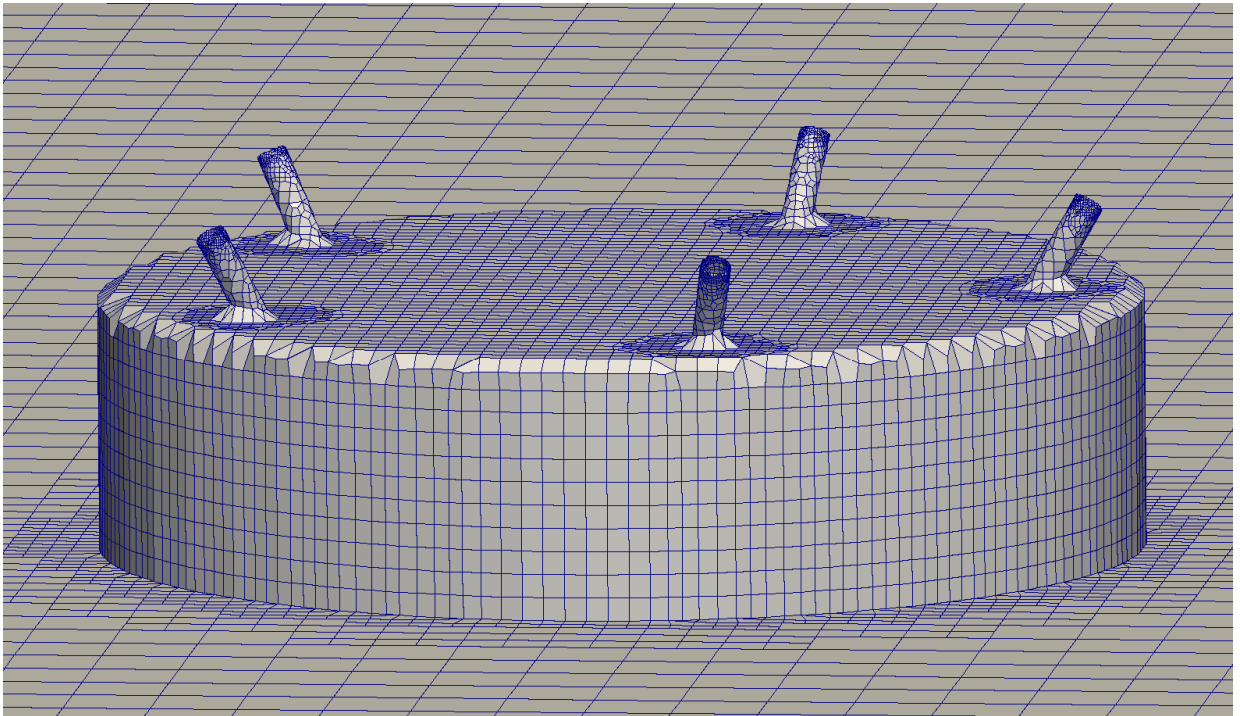


Figure 2-19 Meshed rosette, 175 mm ports

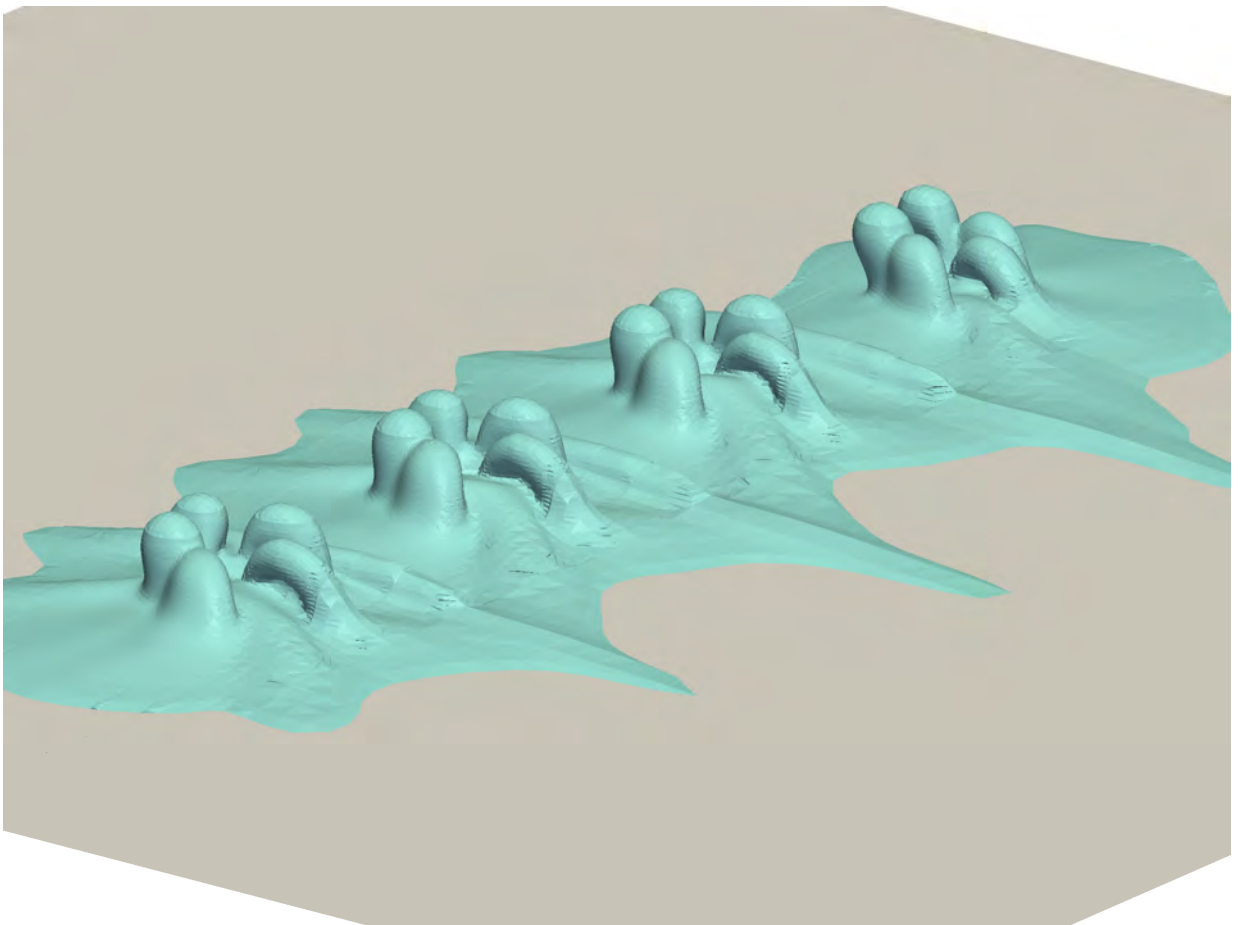


Figure 2-20 Rosette plumes, 10th percentile flood tide, 50:1 dilution iso-surface

2.6.2 CFD Simulations Performed

Steady state solutions were computed for the zero background current, and the 10th, 30th, 50th, 70th and 90th percentiles for ebb and flood tides, for both 4.3 m³s⁻¹ (peak) discharge and 3.6 m³s⁻¹ (long term average) discharge rates, totalling 22 solutions. Velocity depth averaged profiles for the new revised location were used, as extracted from the calibrated ELCOM model. These results, and the application to the ELCOM model, are described in Section 3.6.

2.7 Summary

In this section:

- CFD framework and predictions have been benchmarked against other tools and literature, with good agreement reached with the majority of historical approaches;
- CFD has also been shown to provide at least qualitative agreement with recent field measurements, particularly with reference to the development of an ambient background vertical salinity structure. This agreement provides independent evidence to suggest that re-entrainment of brine is possible in multiport diffusers, and should be taken into account in subsequent modelling studies;
- Effects of plume overlap and outfall re-entrainment were also found to be significant, especially with respect to low-throw linear diffusers and rosette arrangements;
- CFD has been applied to calculate the evolution of negatively buoyant plumes from multiport linear and rosette diffusers over a range of steady state (and one transient) tidal flow conditions and a range of discharge flow rates; and
- The performance of the Draft EIS configuration diffuser was assessed in detail and an improved rosette design and location for the Supplementary EIS was determined by BHP Billiton.

Finally, as empirical correlations based on experimental data are only available for single port diffusers, and as we have found the effects of plume overlap and outfall re-entrainment on plume dispersion to be significant, we believe this establishes the use of CFD as best-practice for calculation of near field dilutions around multiport diffusers of this nature.

3 HIGH RESOLUTION SCENARIO ASSESSMENTS

Tools presented in the previous section were used to describe the detailed characteristics of discharge plumes in the near field zone across a range of diffuser configurations. They were also used to support selection of a rosette diffuser arrangement for consideration in the SEIS modelling studies. The assessments presented in this section aim to characterise the transport and dispersion of brine at larger scales, taking into consideration the temporal and spatial variability of the hydrodynamic flow field as a combination of the tidal and atmospheric forcing experienced in Spencer Gulf. The validated model of Spencer Gulf presented in Appendix H5.2 (hereafter high resolution model) was used as the basis for the simulations.

3.1 Model Grid and Bathymetry

The high resolution model used in the simulations had the same set-up as the validated model previously reported (Appendix H5.2). The model domain was discretised using a non-uniform grid in both vertical and horizontal directions with the model bathymetry extracted from the DEM presented in Appendix H5.2. This grid was designed to provide higher resolution in the vicinity of Point Lowly (where the horizontal grid resolution was 40 m) and Northern Spencer Gulf. Horizontal grid resolution was progressively decreased from Point Lowly to 300 m at Port Augusta and to 5 km near the southern end of the domain. The detail of the domain at the location of the proposed outfall is presented in Figure 3-1. A non-uniform grid size was used in the vertical direction with a resolution of 1.30 m at the seabed level at the proposed diffuser location, modified by bathymetry. The resulting mesh consisted of 228 by 293 by 31 cells with a total of 244,755 maximum wet cells. A 24 s time step was chosen to ensure model stability and manageable run times.

3.2 Simulations

Two high resolution simulations were performed, these being with and without the proposed desalination plant discharge. Amongst other things, the simulation without the proposed discharge (the 'baseline' simulation) was used to provide a basis for comparison and to support generation of appropriate inflow boundary conditions for the simulation that included the proposed brine discharge (see Section 3.6).

3.3 Simulation Period

Simulations were performed for a period of one 1 year between 1st of November 2007 and 1st of November 2008.

3.4 Initial Conditions

Initial conditions for the model required the initialisation of background scalar fields with the long term influence of the proposed desalination plant discharge. To this end, simulations were produced for a three year time period in a low resolution ELCOM model (see Section 4) with and without the inclusion of the proposed desalination plant discharge. The resultant scalar fields were then interpolated from the low resolution model to form the initial scalar fields in the high resolution model. This methodology ensured manageable run times and inclusion of long term influences within the

high resolution simulations. The different scalar fields for simulations including the proposed desalination plant discharge are presented in Figure 3-2 to Figure 3-5. The same field preparation technique was used for simulations without the proposed desalination plant discharge.

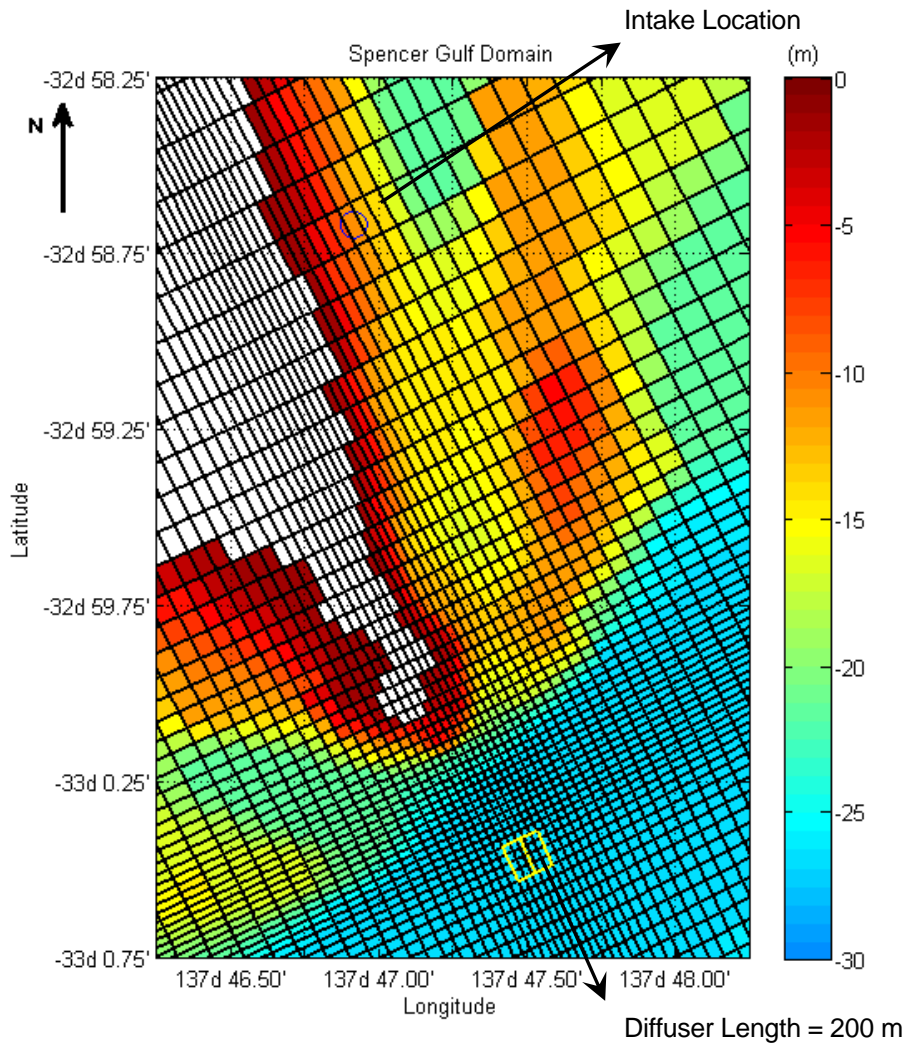


Figure 3-1 High resolution model grid and bathymetry at the location of the proposed intake and outfall. The area within the yellow rectangle defines the location of the boundary condition cells representing the outfall. The vertical datum is metres AHD.

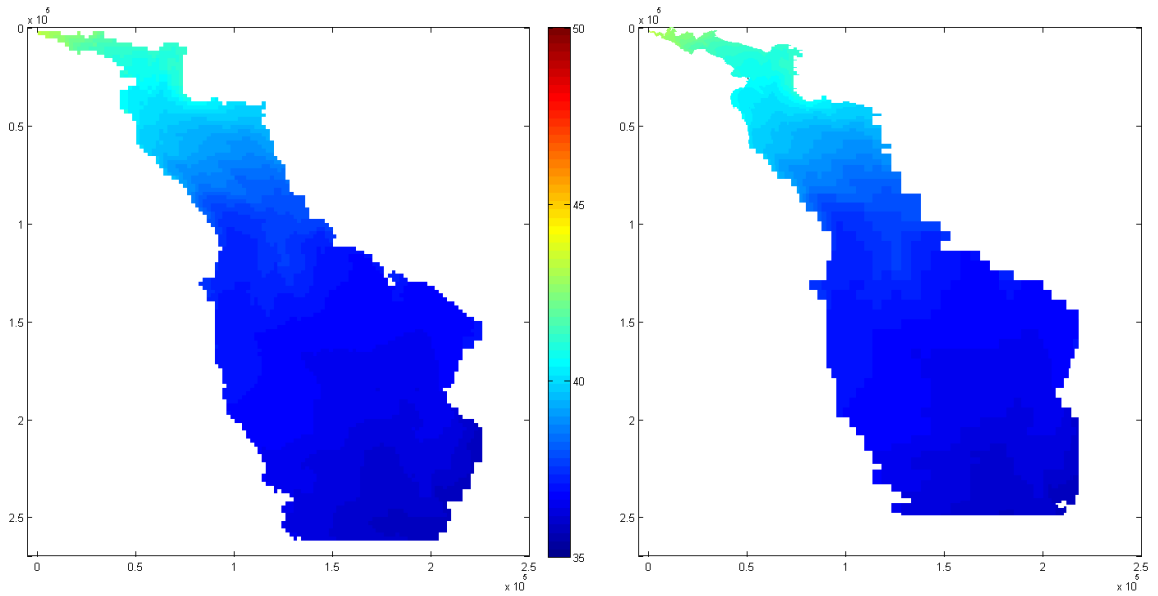


Figure 3-2 Results of the initial depth averaged salinity field interpolation from low (left) to high (right) resolution model - 1st of November 2007. Horizontal scale is given in metres and the grid is rotated 64 degrees anti clockwise from North. high resolution model cells are 5km wide near the open boundary, and are 2km wide at the same location in the low resolution model

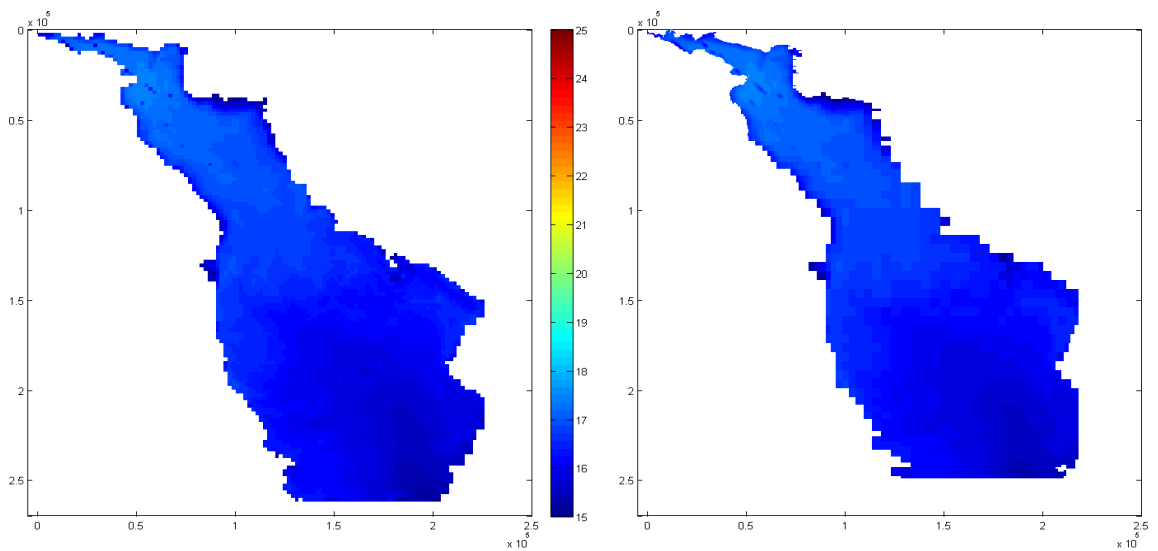


Figure 3-3 Results of the initial depth averaged temperature field interpolation from low (left) to high (right) resolution model - 1st of November 2007. Horizontal scale is given in metres and the grid is rotated 64 degrees anti clockwise from North.

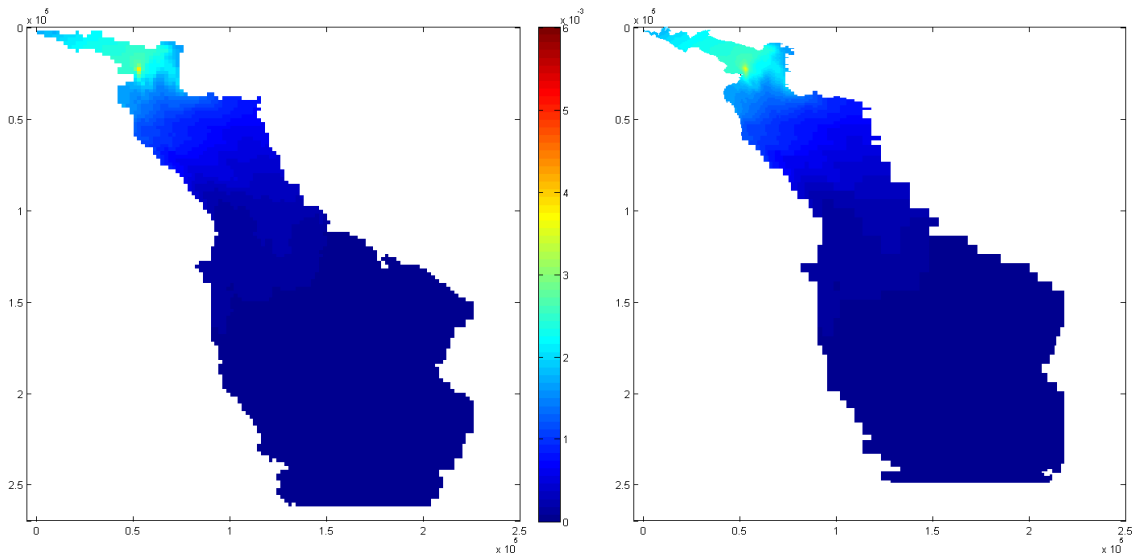


Figure 3-4 Results of the initial depth averaged tracer (equivalent to inverse of dilution) field interpolation from low (left) to high (right) resolution model - 1st of November 2007. Horizontal scale is given in metres and the grid is rotated 64 degrees anti clockwise from North.

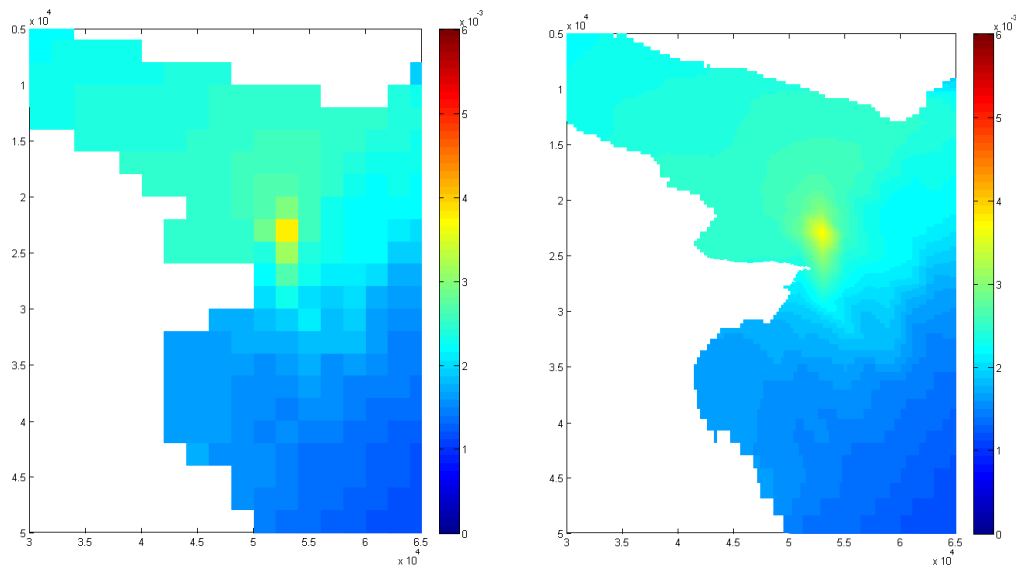


Figure 3-5 Zoom of the initial depth averaged tracer (inverse of dilution) interpolation result presented in Figure 3-4 with detail in the vicinity of the proposed outfall. Horizontal scale is given in metres and the grid is rotated 64 degrees anti clockwise from North.

3.5 Boundary Conditions

The boundary conditions for the two high resolution simulations were common and are presented in Appendix H5.2 of the SEIS. The reader is referred to this document for further details, however these boundary conditions are summarised as follows:

- Meteorological:

- Hourly meteorological forcing from the Weather Research Forecast model, on an approximate 15 km by 15 km grid. The forcing includes air temperature, relative humidity, solar radiation, incoming long wave radiation, wind speed and wind direction;
- Daily rainfall from the Bureau of Meteorology SILO database;
- Open Boundary:
 - Hourly water surface elevations at the open boundaries from the combination of a BMT ARGOSS global tidal model with the mean water levels from HYCOM data assimilation model;
 - Daily and vertically varying water salinity and temperature from the HYCOM data assimilation model;
- Other:
 - Same salinities and temperatures assumed in the DEIS for salt lake inflow north of Port Augusta and for the power station at Port Augusta.

For the simulation including the proposed desalination plant discharge, the boundary flow was assumed to originate from the seabed. The flow was distributed over five to 25 cells according to the diluted discharge flow rate (see Section 3.6). The locations of these cells are illustrated in Figure 3-1. Details of the desalination plant discharge are summarised as follows:

- outfall flow rate: $Q_o = 4.3 \text{ m}^3\text{s}^{-1}$;
- outfall salinity: $S_o = 75$;
- outfall temperature: $T_o = T_i + 1$ (as specified by BHP Billiton) where T_i is the temperature at the intake (see below); and
- intake flow rate: $Q_i = 7.52 \text{ m}^3\text{s}^{-1}$.

The above parameters were used to produce the required model boundary conditions as described in Section 3.6.

3.6 Nearfield and Hydrodynamic Model Linkage

The manner in which near field predictions of brine dilution (e.g. from a designated near field model such as the BMT WBM CFD model) are linked with hydrodynamic models that examine broader scale advection and dispersive processes (e.g. ELCOM in the current study) is critical to the robust execution of dispersion studies such as this. Fundamentally, a problem of integration arises because plume dynamics occur on the scale of 0.01 – 10 metres, whereas numerical grids used in hydrodynamic models typically have horizontal scales of 50 – 100 metres (and sometimes greater). The initial dilution of brine is thus a sub-grid scale process for the hydrodynamic model. In addition to differences in scale, there are differences in the physics involved: the initial plume dispersion involves large vertical accelerations, whereas the hydrodynamic processes do not (i.e. they are inherently hydrostatic). Hence the equation sets between the nearfield and hydrodynamic models are not the same, and requiring that one replicate the physics of the other under this constraint is problematic.

Given the above, the way in which small-scale plume dynamics and hydrodynamic models are linked can have a significant influence on the spatial distribution of subsequent hydrodynamic model dilution predictions, at least in the direct vicinity of the diffuser. Given our experience in this regard, and the

variety of techniques currently being applied to this end, significant attention has been paid to the development of a robust linkage in the current study.

As such, descriptions of some different linkage techniques reported in the literature are reviewed below. In addition, their advantages and disadvantages and applicability to the current study (against a set of study specific criteria) are assessed. This assessment is then used to derive and describe a tailored linkage method appropriate for the current study and associated modelling assessments.

3.6.1 Literature Linkage Techniques

There are three main categories of linkage techniques (or combinations thereof) that have been adopted in the literature that are relevant to the current works, these being:

- Direct brine insertion;
- Pre-diluted brine insertion; and
- Flux approximation.

Direct brine insertion delivers the 'point of discharge' brine flow rate and salinity (i.e. as leaving the desalination facility prior to delivery to a diffuser) directly to the hydrodynamic model. In the current case, this would mean injecting a computational cell (or suite of cells) in the high resolution ELCOM model with a flow rate of $4.3 \text{ m}^3\text{s}^{-1}$ and salinity of 75 gL^{-1} . If this injection was set to occur over more than one cell, then the flow rate to each cell would be divided by the number of cells selected. This direct injection method has been applied as part of the Port Stanvac modelling assessments (SA Water, 2009) where the injection cells were set to be those encompassing a water depth of ten metres along the diffuser alignment.

Rather than delivering brine concentrate to a hydrodynamic model, the pre-diluted insertion method delivers a brine flow that has been altered in an attempt to capture the dilution delivered by the selected diffuser arrangement. This method acknowledges the fact that the near field dynamics (especially mixing) are not captured by hydrodynamic models (due to the spatial scale and physics mismatch described above), but that hydrodynamic models will 'see' inflows that have already been subjected to dilution as a result of the action of a diffuser. Thus, the pre-dilution method explicitly acknowledges that this detailed dilution behaviour is beyond the simulation capability of hydrodynamic models. As such, this linkage technique forces the hydrodynamic model with an inflow boundary condition informed by a (separate) near field model. In essence, this linkage technique draws directly on complementary near field modelling and employs near field results to force hydrodynamic models with appropriately resolved and matched inflow boundary conditions (noting that introduction of pre-diluted water requires a separate extraction to balance mass overall).

As a hypothetical example, if near field modelling of a particular outfall has shown that typical plume dilutions might be 50:1 at some distance downstream of a diffuser, then the pre-dilution insertion technique will insert a flow 51 times greater than the brine concentrate flow rate, and at a correspondingly reduced salinity that conserves mass. This salinity will be computed using estimates (measured or modelled) of ambient background salinity in combination with the known brine concentrate salinity. A similar pre-dilution and extraction technique was successfully applied for the Cockburn Sound modelling studies (Okely *et al.* 2007b, Section 2.6). Marti *et al.* (2010) reported excellent agreement between modelled and subsequently measured salinities and brine dilutions at

the Cockburn Sound facility, having used this pre-dilution technique as the linkage approach in the supporting modelling studies.

The final linkage method is the flux approximation and, rather than taking a physically based approach or considering near field modelling studies, it assumes that the rate of change of salinity in a hydrodynamic model injection cell (that contains the diffuser) is a function of the cell salinity (S), undiluted brine salinity (S_{brine}) and flow rate (q_{brine}), and the volume of the selected hydrodynamic model injection cell (V), such that:

$$\frac{\partial S}{\partial t} = (S_{brine} - S) \frac{q_{brine}}{V} \quad (1)$$

This technique has been applied by Kaempf *et al.* (2009), for example.

3.6.2 Applicability to the Current Study

We have reviewed these three techniques in order to assess which (if any) are best suited to the current study. To do so, we have adopted the following assessment criteria, in order of importance for this study:

- 1 Salt mass conservation (which is essential for any such study);
- 2 Controllable and defensible linkage of hydrodynamic inflow boundary condition with near field dilution predictions;
- 3 Controllable dynamic hydrodynamic model response to the influence of tidal forcing on near field dilution performance;
- 4 Hydrodynamic model grid independence; and
- 5 Hydrodynamic model timestep independence.

3.6.2.1 Salt Mass Conservation

Salt mass conservation is critical to the credible application of any linkage technique. The direct insertion and pre-dilution insertion techniques ensure both. The former achieves this by virtue of injecting exactly the pre-diffuser flow rate and salinity to the hydrodynamic model (i.e. $S_{brine} \times q_{brine}$ in the nomenclature from equation 1) so conserves salt by definition (assuming intake processes are included elsewhere). The latter acknowledges that the pre-dilution approach introduces additional salt mass and so sets up appropriate compensatory extractions to exactly conserve mass (Okely *et al.* 2007b, Section 2.6).

The flux approximation modulates local salinity without addition of water (unless other equations are deployed to do so). Equation (1) above can be re-written as the rate of change of salt mass as (assuming that V , the numerical cell volume is constant)

$$\frac{\partial(VS)}{\partial t} = (S_{brine} - S)q_{brine} \quad (2)$$

Equation (2) shows that the rate of change (i.e. pseudo-introduction) of total salt mass (VS) is less than $S_{brine} \times q_{brine}$ (by subtraction of an always positive S from S_b), and as such it is unclear as to

whether salt mass is actually conserved in terms of its delivery from the desalination plant. Further investigation and testing would be required to more robustly assess this outcome, and it is possible (although not immediately obvious) that on consideration of the full set of governing equations (including potentially source and sink volume fluxes), the system is indeed delivering the correct salt mass.

3.6.2.2 Controllable Linkage with Near Field Predictions

The defensible and direct linkage with near field dilution predictions was critical to this study, for the primary reason that some sensitive receptors are within close proximity to the proposed diffuser, but outside the nearfield model domain (and one that could be tractably and realistically simulated within the CFD framework). As such, the hydrodynamic model developed and employed (i.e. the high resolution ELCOM model) was required to provide robust dilution estimates as close to the diffuser (or rosette) as practicably possible. This in turn required that the near field modelling be used to its full potential in controllably forcing the hydrodynamic model in undertaking broader scale assessments. In particular, it was necessary to ensure that the hydrodynamic model was given as little latitude as possible to auto-determine the boundary condition flows (and hence dilutions and salinities) at the site of the diffuser for subsequent advection and dispersion through its domain. In other words, maximal control over the flow, dilution and salinity at the hydrodynamic boundary insertion location(s) was required in this modelling study to minimise uncertainty and avoid unnecessary conservatism in dilution predictions at sensitive receptors relatively close to the diffuser.

The direct injection method does not appear to readily allow for controllable linkage of near field and hydrodynamic models to the extent required in this study, as far as BMT WBM is aware. For example, in the Port Stanvac modelling study (SA Water 2009) it is our understanding that brine was directly inserted (i.e. not pre-diluted) to the hydrodynamic model over a range of cells both horizontally and vertically. As there is no explicit pre-dilution technique applied in the model, the only dilution available is numerical. Specifically, the collapse (reported to be in one timestep) and associated mixing of the vertically inserted brine concentrate within the hydrodynamic model set the effective insertion flow dilution and salinity at bed level for subsequent advection and dispersion at depth. Thus, it is our understanding that this boundary condition was thus not entirely controlled with reference to the near field modelling.

Notwithstanding the above, SA Water (2009) does provide an analysis of the relationship between some hydrodynamic dilutions and those predicted by near field modelling at selected distances from the diffuser. A relationship between a median hydrodynamic model dilution and near field model dilutions was described, and showed that the hydrodynamic model was conservative in its predictions.

The pre-dilution method does make an attempt to link near field and hydrodynamic models with a degree of control. It does so by delivering diluted brine (with the dilution determined by a near field model) directly to the hydrodynamic model. A constant pre-dilution was adopted by Okely *et al.* (2007b), which is most likely in response to the relatively uniform tidal/wind driven currents (hence near field performance) in Cockburn Sound. The initial pre-dilution is often based on background (baseline) salinities.

The flux approximation method takes no account of near field modelling, so is unrelated to any near field modelling predictions.

3.6.2.3 *Controllable Dynamic Response to Tidal Forcing*

A similarly important requirement for the current study was to be able to dynamically vary, in a controlled fashion, the hydrodynamic model boundary condition for flow, dilution and salinity, primarily to capture variations in the performance of diffuser dilution as a result of varying tidal current magnitudes. This was needed to ensure maintenance of a defensible and physically based linkage between the near and hydrodynamic models over the wide range of tidal conditions experienced at Point Lowly.

The direct insertion method does not appear to support such control, and (although possible) it is not clear to BMT WBM how the initial numerical dilution and/or subsequent collapse-driven mixing could controllably vary the resultant dilution as a function of current speed, and match the dilutions to near field dilution predictions.

The pre-dilution method, in the cases BMT WBM has encountered to date, has been implemented using a constant (temporally invariant) pre-dilution, so has not, so far, allowed for dynamic alteration of injected dilutions.

The flux approximation method takes no account of near field modelling so does not have the ability to deliver a controlled time variant flow, dilution and salinity that is tied to near field modelling studies.

3.6.2.4 *Hydrodynamic Model Grid Independence*

It was important for the current study to deploy a method of injection that was as independent as possible of the hydrodynamic grid. This was required to ensure that grid related numerical artefacts were minimised or eliminated entirely, primarily to reduce associated predictive uncertainties. In addition, it was considered important to be able to apply the same methodology to different hydrodynamic models (or model configurations) and facilitate consistency of prediction without needing to retrospectively alter a grid dependent injection method to suit.

The direct insertion method is grid dependent to the extent that the initial numerical dilution that occurs when the brine concentrate is injected into the model varies with varying model grid size. This then may have potential implications for subsequent prediction of dilutions – the starting dilution varies with grid size as the same brine concentrate is spread over varying initialisation volumes as grid size changes. This variation applies in the horizontal and vertical, and the effect becomes more pronounced as the incremental brine concentrate volume becomes smaller relative to the volume of the initialisation cells (i.e. lower flow rates or model timesteps – see Section 3.6.2.5).

The pre-dilution insertion technique is also somewhat susceptible to grid dependence, but to a lesser extent than the direct insertion method. This is because the pre-dilution volumes (for a given brine concentrate flow rate) are generally much larger than the concentrate flow rate itself (by a factor of the dilutions achieved by a diffuser), so form a greater proportion of the injection cell volumes within a given timestep. Notwithstanding this, however, both the direct and pre-dilution techniques mix inserted brine with some volume of background water that (potentially) has already felt the influence of previously discharged brine. The extent to which this mixing occurs is different in the two techniques by a factor related to the performance of the near field diffuser.

For example, if the proposed Point Lowly desalination plant brine was inserted into a strip of high resolution ELCOM bottom cells totalling 200 m (L) by 40 m (W) by 1.3 m (H) in dimension, and at the worst dilution predicted by the near field CFD model (43:1), then (in the absence in advective influxes) it would take three numerical timesteps to completely fill the cells with the pre-diluted brine that characterises zero current conditions at Point Lowly (with that injected brine mixing at each timestep with ambient waters that already feel the effect of prior discharges). In other words, the dominant signature of the detailed near field CFD simulations takes approximately minute to establish itself in the model domain under this scenario, with minimal numerical dilution occurring, and mixing with background conditions also included. The direct injection method would, however, take 43 times as long to reach this point, with numerical dilution playing an initially important role.

The flux approximation method is grid dependent as the injection cell volume (V) appears explicitly in the flux equation (equation 1). For example, as the injection cell volume reduces, the rate of change of salinity in that cell (and hence the predicted salinity) increases.

3.6.2.5 Hydrodynamic Model Timestep Independence

Finally, it was important for the current study to deploy a method of injection that was as independent of the hydrodynamic model timestep as possible. This was again required to ensure that model related numerical artefacts were minimised or eliminated entirely, and so reducing associated predictive uncertainties. In addition, it was considered important to be able to apply the same methodology to different hydrodynamic models and facilitate consistency of prediction without needing to retrospectively alter injection methods.

The direct injection method is timestep dependent in that it numerically mixes a given volume of brine concentrate (V_c) within a suite of pre-selected cells, where V_c is computed as (Δt is the model timestep):

$$V_c = q_{brine} \Delta t \quad (3)$$

A doubling in timestep, for example, would result in a doubling of the volume of brine concentrate injected into the suite of insertion cells, and a doubling of the resultant initial brine concentration computed by the hydrodynamic model by virtue of numerical dilution, advection aside and assuming zero brine background conditions.

The pre-dilution technique is less susceptible to changes in model timestep, for similar reasons as described in Section 3.6.2.4. Specifically, this method will 'fill' the insertion cells with diluted brine (representing diffuser performance) at a rate greater than the direct injection method. This increased rate is at least equal to the worst dilution predicted by near field modelling.

The flux approximation method employs a rate of change approach to salinity in a receiving cell, so it is possible (although unclear) that this method is timestep dependent.

3.6.3 Summary of Techniques

Having considered a range of hydrodynamic model brine insertion methods presented in previous studies and the literature, we were able to summarise their applicability to the current study and determine an appropriate method to support ongoing modelling, targeted to the conditions at Point

Lowly. Table 3-1 summarises our assessment of the suitability of each of the three methods against the above criteria, as applied to needs and setting of Point Lowly. It is emphasised that this assessment is not intended to be absolute for all modelling studies, but that it is very specifically tailored to the needs of the current BHP Billiton study. For example, the modelling reported in SA Water (2009) has been shown to be well suited for that application and BMT WBM's assessment is not intended to reflect an evaluation of that modelling in that setting, but rather, to determine how well suited that approach might be to Point Lowly, with its very specific needs regarding the proximity of sensitive receptors to the proposed diffuser site.

Table 3-1 Insertion method comparison

Criteria	Direct Injection	Pre-Dilution	Flux Approximation
<i>Salt mass conservation</i>	✓	✓	?
<i>Controllable boundary condition physically linked to near field modelling</i>	?	Partial	✗
<i>Controllable dynamic response of boundary condition to tidal current speed</i>	?	Possible, but not previously implemented	✗
<i>Grid independence</i>	✗	Partial	✗
<i>Timestep independence</i>	✗	Partial	?

Given the above, it was our assessment that the only reasonable choice of methods to be applied at Point Lowly is between direct injection and pre-dilution. It was also evident that there is a clear point of trade off between these two preferable approaches in terms of this study's second highest priority assessment criteria (i.e. delivering controllable insertion boundary conditions to the hydrodynamic model): direct injection does not readily provide this capability (but does not require mass removal) and pre-dilution does (but requires mass removal). As discussed previously, the ability to link to nearfield model predictions has a high priority in the current study given the proximity of some sensitive receptors to the diffuser alignment, with travel distances to these receptors being short, but outside the near field (CFD) model domain.

Notwithstanding the above, it also became clear that none of these techniques were able to fully satisfy all criteria. As such, a new technique, based heavily on the best suited technique of pre-dilution (for reasons described above, and again as related to Point Lowly only) was developed for this study. This new methodology is described in the following section, and in short represents an upgrade of the Okely *et al.* (2007b) method by allowing for, amongst other things, tidally driven dynamic alteration to pre-dilution calculations.

3.6.4 Adopted Linkage Technique

3.6.4.1 Methodology Overview

Given the above, and the specific requirements of the current study as captured in the assessment criteria listed in the previous section, BMT WBM developed an injection method (i.e. linkage technique) that preserves discharged salt mass whilst ensuring delivery of flows, salinities and dilutions to the ELCOM models that directly reflect near field (CFD) modelling predictions across a range of background tidal conditions. It is our view that this represents the state-of-the-art in this

respect, in particular as there is a clear, defensible link between the near-field dilution and the implementation of the hydrodynamic model boundary conditions, and this was important at Point Lowly.

A schematic of this method is given in Figure 3-6. A step-by-step description of this injection method is given below.

- Step 1.** Depth-averaged velocities for ebb and flood tides were obtained from the velocity profiles modelled at the proposed diffuser location (Figure 3-1). These profiles were obtained for three complete neap and spring tides cycles from 24 April to 6 June 2009 corresponding to a subset of the model validation period (SEIS Appendix H5.2).
- Step 2.** Cumulative distributions of depth-averaged velocity magnitudes for each of the tidal phases were obtained (Figure 3-7). A total of 14,640 profiles were used to produce the velocity distribution.
- Step 3.** Vertical profiles representative of the 10th, 30th, 50th, 70th, and 90th depth-averaged velocity magnitude percentiles were extracted from the timeseries to be used as background ambient conditions for nearfield CFD simulations (representative profiles of the 50th percentile are presented in Section 2). The selection of the representative profile was based on the five profiles for which depth-averaged magnitudes most closely matched the selected percentiles (based on velocity magnitude alone).
- Step 4.** CFD simulations were performed for each of these representative profiles (Section 2) and dilutions computed. More detail is provided on this computation in Section 3.6.4.2.
- Step 5.** The CFD dilution predictions were collated into a 'lookup table' relating depth-averaged ambient velocities and plume dilution. An example for the tabulated dilutions is given in Figure 3-8, and it is noted that the adopted dilutions refer to the rosette outfall configuration described in Section 2.6.
- Step 6.** Baseline Spencer Gulf hydrodynamic simulations (i.e., without the inclusion of the proposed discharge) were processed for the provision of background depth-averaged velocities. An example of these velocities is given in Figure 3-9.
- Step 7.** Dilutions as a function of the modelled background velocities were obtained from the table produced in step 5 (i.e. Figure 3-8).
- Step 8.** Salinities and other scalar fields at the boundary cells representing the proposed diffuser were computed as a function of the dilutions obtained in step 7 (Figure 3-10). The fluid entrained in the plume was assumed to have scalar (i.e. temperature, salinity, and tracer concentration) characteristics of the depth-averaged scalars in the background (baseline) simulations. This assumption is consistent with the CFD prediction that plume travel paths reach higher parts of the water column (Section 2) and as such plumes entrain relatively unaffected background waters, once they are well clear of the bottom salinity layer (i.e. where CFD has shown re-entrainment to be significant). This has also been qualitatively confirmed by field experiments presented by Okely *et al.* (2007b).
- Step 9.** The final scalars and discharges used as boundary conditions were calculated as follows.
Given the following problem data:

 S_a - Ambient salinity (depth averaged salinity in the background simulation)

T_a - Ambient temperature (depth averaged salinity in the background simulation)

S_o - Salinity at diffuser nozzle (equals 75 gL^{-1})

T_o - Temperature at desalination intake (from background simulation)

C_o - Tracer concentration at diffuser nozzle (equals 1)

Q_o - Discharge at nozzle (equals $4.3 \text{ m}^3\text{s}^{-1}$)

D - Inverse of dilution at point of impact (given by the CFD look-up table)

The following quantities are used as boundary conditions in the model:

C - Tracer concentration at point of impact (equals $1/D$ for $C_o = 1$)

S - Salinity at point of impact

T - Temperature at point of impact

Q - Discharge at point of impact

In order to conserve the brine mass flux:

$$QC = \frac{Q}{D} = Q_o C_o = \text{const.}$$

Such that

$$Q = Q_o C_o D = Q_o D$$

Salinities (S) were computed as follows:

$$S = \frac{\frac{1}{D} S_a + S_o}{\frac{1}{D} + 1} = \frac{S_a + D S_o}{(1 + D)}$$

Temperatures (T) were assumed to increase by 1°C due to the desalination process (on advice from BHP Billiton), such that:

$$T = \frac{\frac{1}{D} T_a + (T_i + 1)}{\frac{1}{D} + 1} = \frac{T_a + D(T_i + 1)}{(1 + D)} = \frac{T_a + D(T_o)}{(1 + D)}$$

The assumed boundary conditions for tracer, temperature, and salinity in the model were given by D , T , and S , respectively. Of particular importance here is the derivation of tracer concentrations and salinities, which under this method, directly reflect the spatially and temporally variant performance of the diffuser under the full range of tidal current conditions.

It is noted that the scalar fields computed in this step (that use CFD dilutions and base case ELCOM scalars) are based on zero background concentration of previously discharged brine. However, it is also noted that the dilutions predicted by CFD (regardless of how these are incorporated into ELCOM) are conservative, as:

- CFD was shown to be conservative relative to Roberts 97 (by more than 10%); and
- CFD inherently includes the process of re-entrainment (from previously delivered brine that accumulates near the diffuser), and the resultant dilutions reflect this in a conservative manner, with our estimates showing that this could be in the order of 10-20% conservatism in dilution predictions.

In addition, and in terms of the injection method in ELCOM, subsequent sensitivity analyses (see above) have shown that the adopted 5 line injection method is conservative with respect to dilution (as compared to an analogous 1 line injection method), and at some sensitive receptors this can be up to 20% in terms of dilution predictions.

It is our opinion that the above provide a degree of conservatism to the scalar (and dilution) predictions computed in this step. Potentially offsetting this to some extent, however, is the necessary assumption that the pre-diluted brine mixes with unaffected background (baseline) water in delivering the brine-derived flux at each timestep. However, it is noted that ELCOM with the pre-dilution method, does account for this in a manner similar (but not the same) as a direct injection technique. Specifically, the pre-diluted brine flux, on injection, occupies (on average) one quarter to one third of the volume of the numerical cells receiving the injection, and as such each delivery does mix with ambient waters that potentially carry the influence of previously discharged brine. Specifically, the pre-dilution technique does not ignore background salinities – it includes them in a manner similar to that of the direct injection method. The difference, however, between this and the direct injection technique, is that the pre-dilution technique delivers a strong signature of the nearfield modelling predictions to the far field (hydrodynamic) model, which was of critical importance to this study (as reflected in the above selection criteria).

Step 10. As discussed above with reference to the work undertaken in Cockburn Sound (Okely *et al.* 2007b), a salt sink was introduced to remove excess entrained salt (generated via pre-dilution) and the required sink was distributed at specified bottom cells in the domain. The excess entrained salt ($\Delta(QS)$) is obtained by the following relationship:

$$\Delta(QS) = QS - Q_o S_o$$

with the variables as defined previously. Outflow boundary condition cells were set up such that $\Delta(QS)$ could be removed from the computational domain. These cells were specified in such a way that

- 1) they occupied a relatively broad area, such that the sink discharge would have minimal disruption to the local hydrodynamics. For example, under the lowest dilution regime (where background currents are small), the maximum velocity induced by the sink was 5 mms^{-1} ;

- 2) they were, however, within the general vicinity of the proposed outfall such that excess salt did not accumulate in the Northern Spencer Gulf; but
- 3) the outflow cells were specified at distance from the outfall (i.e. away from the deep basin where dilutions were relatively low) and at least 5 m above the seabed at the location of the outfall where rigid walls could be used as outflow boundary conditions, therefore ensuring the salinities at the outflow cells were similar in the simulation with and without the desalination plant discharge, such that the salt sink discharge could be accurately computed.

Final computation of the sink discharge (Q_d) was given by

$$Q_d = \frac{\Delta(QS)}{S_d}$$

where S_d was given by the average salinity at the outflow cells. The average used to compute S_d was weighted by the size of the outflow area corresponding to each particular outflow cell, and was variant in time with the background salinity.

The outflow cell locations for low and high resolution models are shown in Figure 3-11.

It is noted that at any time the magnitude of the salt sink discharge was proportional to the dilution, such that the maximum outflow rates occurred during spring tides, when the nearfield processes provided superior dilution and any velocities or other hydrodynamic effects associated with the sink were very much masked by highly energetic background flows through the convergence zone where the rosettes are proposed to be located. Also, the calculation aims at enforcing a salt balance.

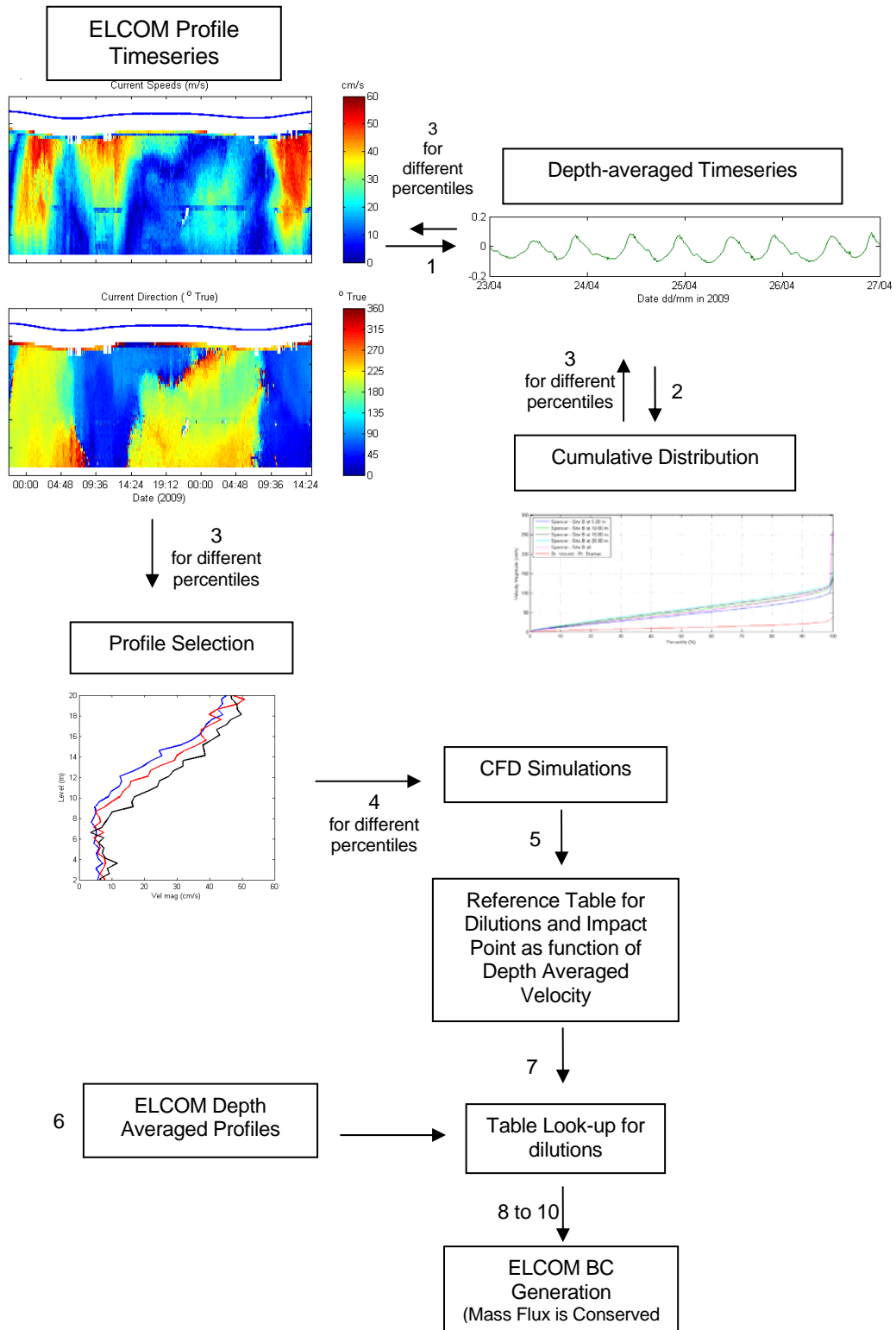


Figure 3-6 Schematic of the injection method

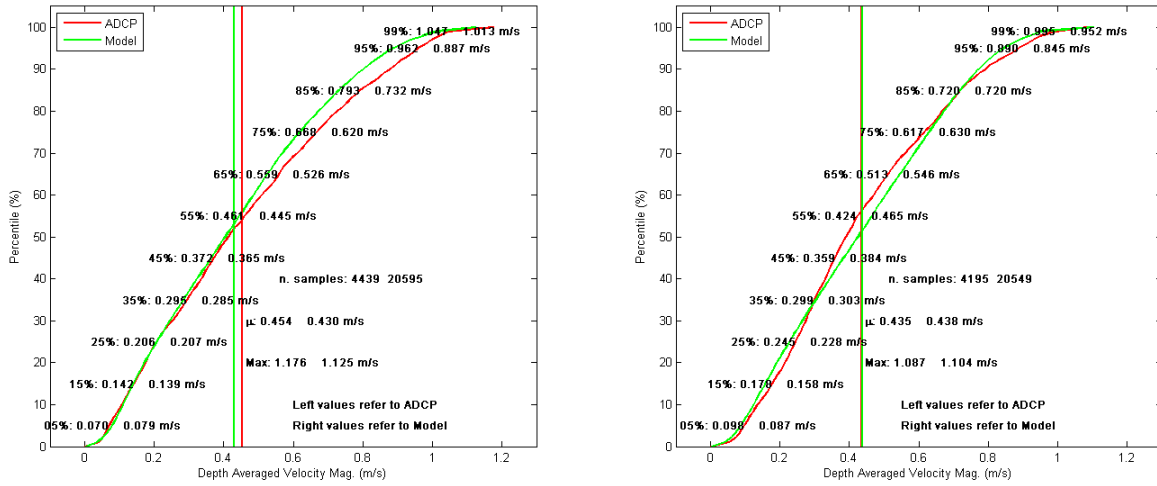


Figure 3-7 Cumulative distribution of the modelled depth-averaged ambient background velocity for ebb (left panel) and flood (right panel) tides (SEIS Appendix H5.2). Measured ADCP data at Site B3 (about 300 m onshore) is also shown for comparison.

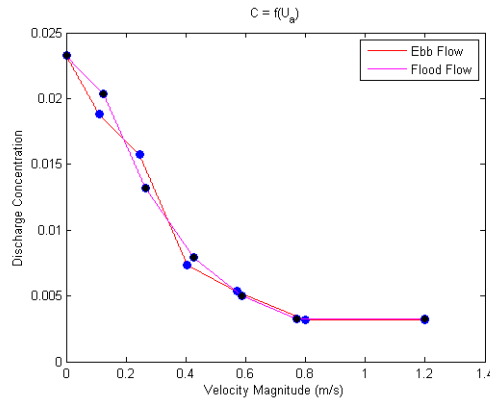


Figure 3-8 Dilutions as a function of depth-averaged ambient background velocity

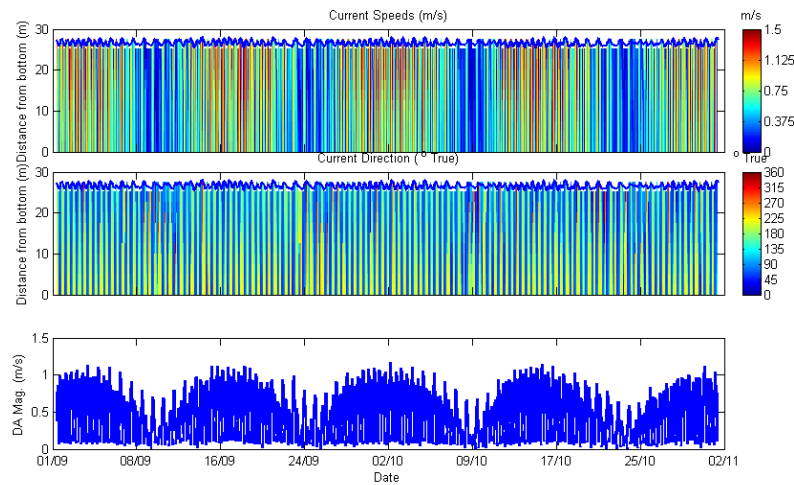


Figure 3-9 Modelled background velocity profiles and resulting depth-averaged time series used to obtain nearfield dilutions

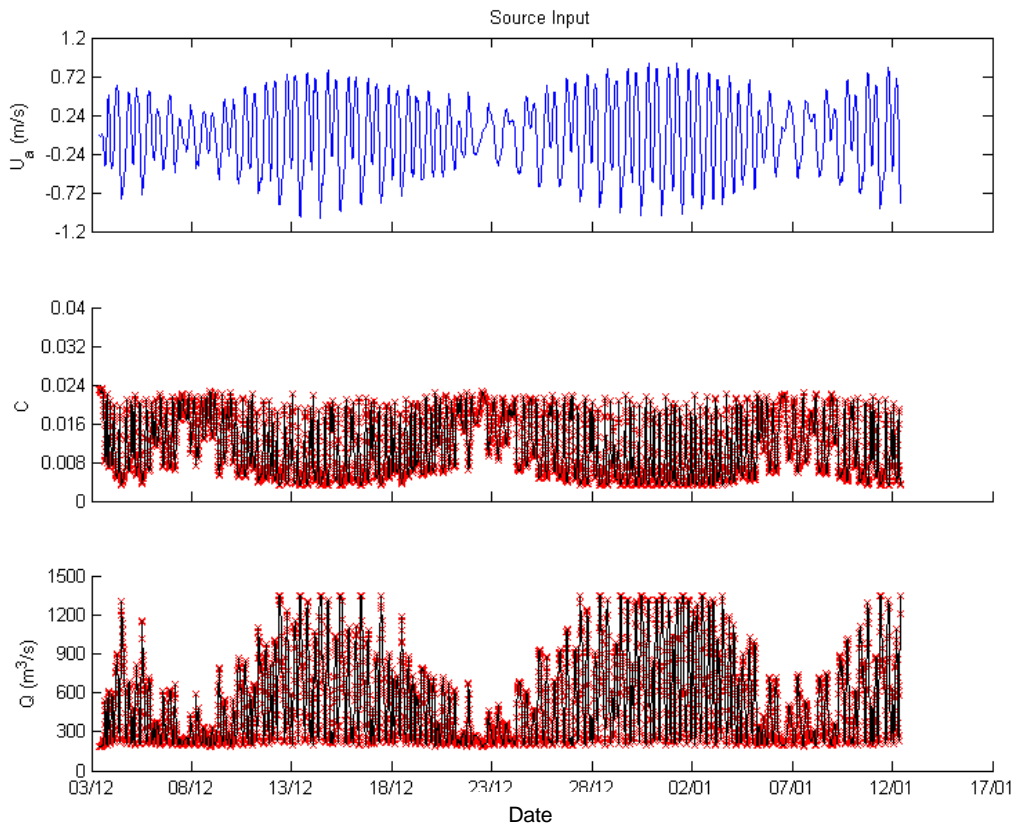


Figure 3-10 Example of Input boundary conditions for the proposed diffuser in the high resolution model. Top panel: depth averaged velocities (ebb is negative); middle panel: trace concentration used to compute dilutions (in relation to a concentration 1 at the diffuser nozzle); bottom panel: discharge rates.

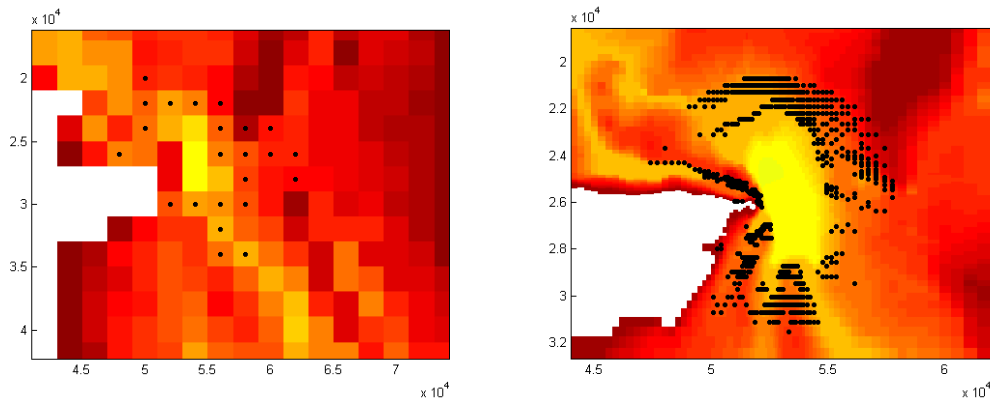


Figure 3-11 Salt sink locations (dots) for the low (left) and high resolution models (right). Colour scale indicates the bathymetry. Horizontal scale is given in metres and the grid is rotated 64 degrees anti clockwise from the North direction.

3.6.4.2 CFD Plume Dilution Extraction

Step 5 above called for interrogation of a lookup table of CFD predictions for plume dilution, where these dilutions were computed as a function of ambient current conditions. Given the importance of these dilutions in translating into broader scale dilution predictions, considerable effort was expended in developing a rigorous and consistent post processing technique to convert the three dimensional CFD predictions (as noted in Section 2.6.2) to a suite of representative insertion dilutions that varied with tidal current speed. This is described below.

The first method considered for extracting the relevant pre-dilutions from the CFD simulations for use in the mid and far field ELCOM models was selected to match simulation of a linear diffuser. Specifically, the lowest dilution observed on the sea floor anywhere in the domain that was 20 m or more (i.e. half an ELCOM grid cell width) removed from the diffuser line was selected as the ELCOM injection dilution. This was deemed acceptable given the relatively uniform distribution of discharged brine in the along-diffuser direction. This was found to be very slightly conservative in the case of a linear diffuser in that it yielded lower dilutions than a number of other plausible methods.

This approach, however, proved to be significantly conservative when applied to the rosette configuration specified by BHP Billiton, due primarily to the ‘plume groups’ associated with the design. These plume groups are illustrated in Figure 3-12 in which the lowest dilution 20 m away from the diffuser line (i.e. at the edge of the greyed box) is clearly not representative of a typical dilution around the 20 m perimeter.

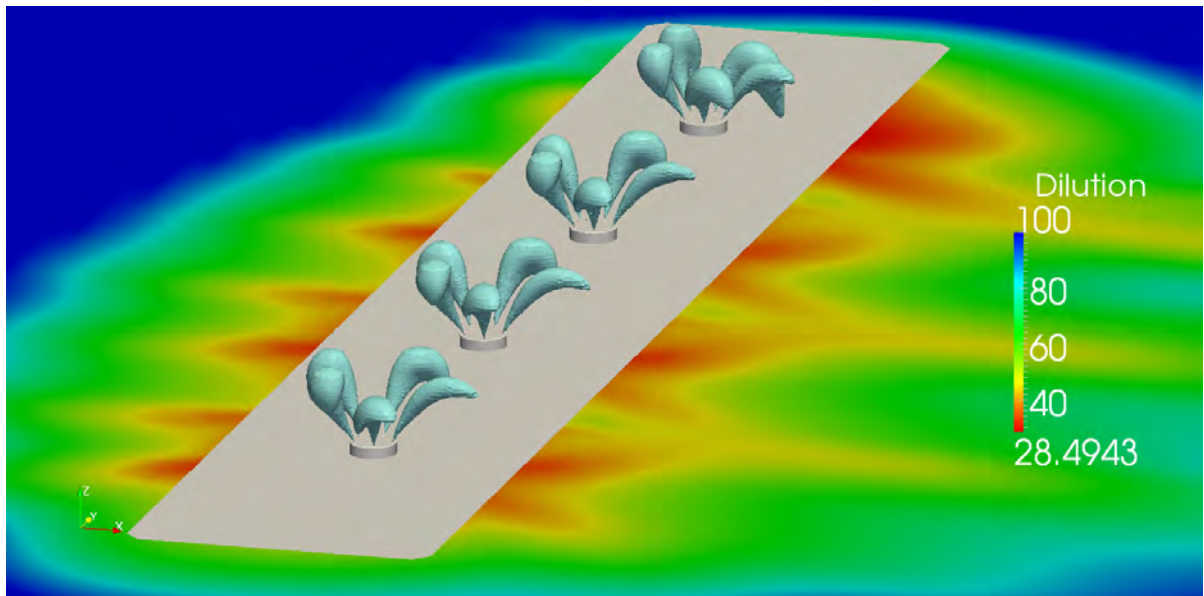


Figure 3-12 Plume groups and uneven dilution at 20 m from diffuser line, as predicted from the CFD modelling

To further illustrate this grouping effect, the figure below shows an example of dilutions at the 20 metre distance from a typical rosette diffuser arrangement, as extracted from a bank of preliminary CFD rosette simulations. The relatively large variation in dilution is evident as a function of lineal distance along the diffuser alignment. The location of the rosettes at 25, 75, 125, and 175 m is clear, with their signature being lower dilutions.

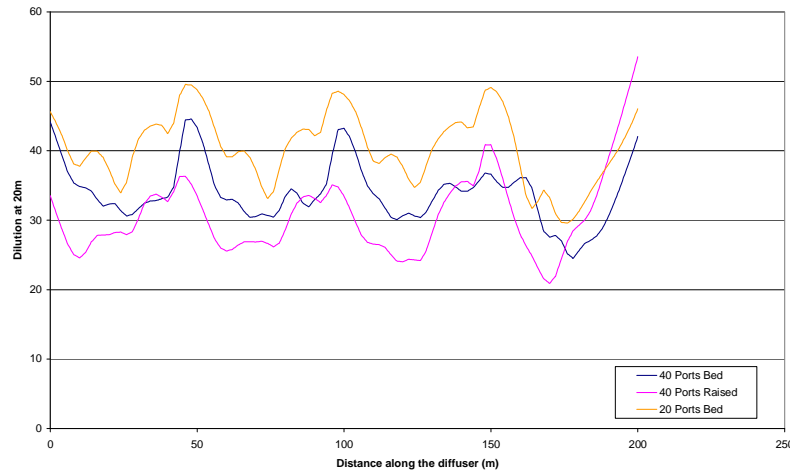


Figure 3-13 Typical dilutions at 20 metres downstream of the rosette diffuser

In contrast to this behaviour, the CFD solutions clearly show that the dilutions become more uniform about their average value before exiting the CFD model domain. To take account of this, and in acknowledgement that the axial variation in dilution under the rosette configuration was significant, a volume average technique was adopted to populate the CFD results lookup table referenced by ELCOM.

Figure 3-14 shows, as an example, the 50:1 dilution iso-surface for the 10th percentile flood tide for the 4.3 m³s⁻¹ discharge, in which merging of the groups of plumes from the rosettes is apparent. Also shown in this figure is a rod of 4 m width and height, and 200 m length, representing the volume selected for averaging. For each CFD solution, this rod was moved throughout the domain (but not inside of 20 m from the diffuser line) to find the location of lowest average dilution within the rod’s volume. The pre-dilution used in the ELCOM lookup table was this value. The rod length of 200 m is based on the diffuser length. The rod height of 4 m is based on both CFD and Roberts predictions for the downstream layer thickness. The rod width of 4 m is based on the largest cell width in the CFD mesh. A cross section of the same is shown in Figure 3-15. The resulting values for the pre-dilutions for all cases are listed in Table 3-2.

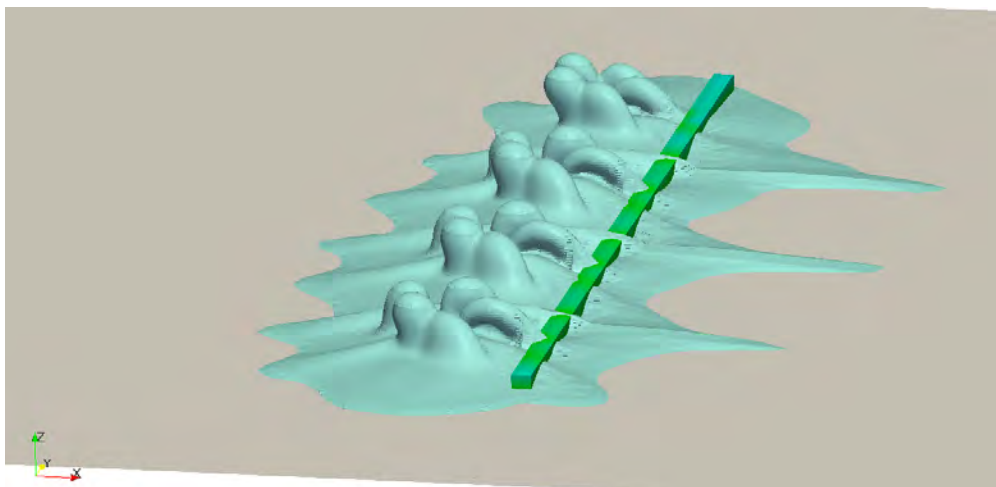


Figure 3-14 Volume averaged dilution method illustration, 10th percentile flood velocity with iso-surface

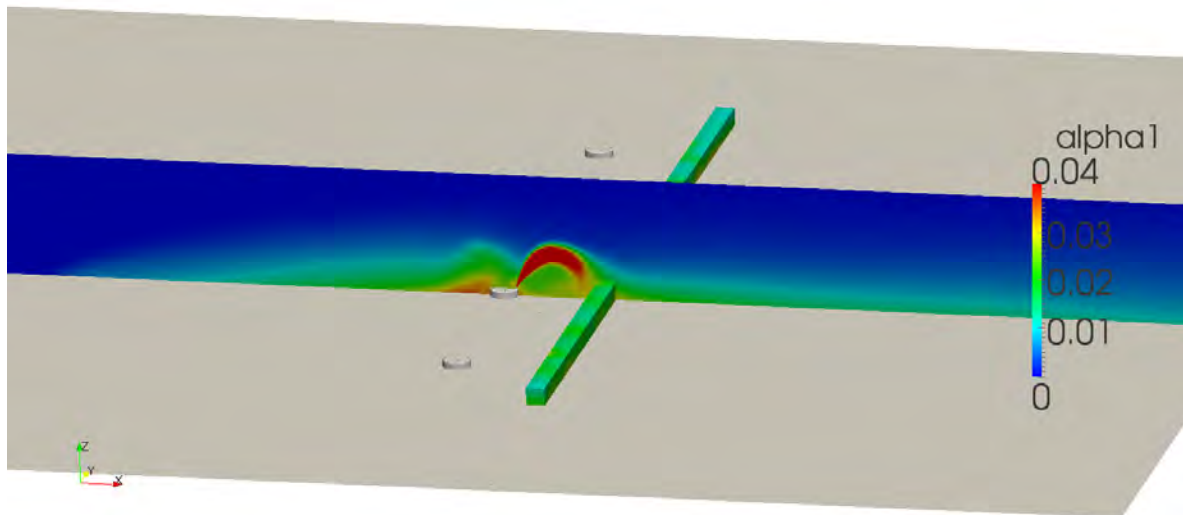


Figure 3-15 Volume averaged dilution method illustration, 10th percentile flood velocity with cross-section

Table 3-2 Computed pre-dilutions

Case	Discharge 4.28 m ³ s ⁻¹	Discharge 3.58 m ³ s ⁻¹
Zero background	43.0	43.3
Ebb 10 th percentile	53.2	56.0
Ebb 30 th percentile	63.6	64.4
Ebb 50 th percentile	136	144
Ebb 70 th percentile	187	200
Ebb 90 th percentile	314	335
Flood 10 th percentile	49.1	53.6
Flood 30 th percentile	75.8	76.7
Flood 50 th percentile	126	138
Flood 70 th percentile	199	221
Flood 90 th percentile	308	319

3.6.4.3 *Outfall Flow Distribution*

As a further step in improving the physical linkage between the near field and far field modelling predictions, the high resolution ELCOM model was configured to spread the diffuser inflow (as computed via the augmented pre-dilution method described above) across a cell stencil whose size varied temporally in response to varying plume dynamics and impact points, as resulting from tidal current speed variations. Specifically, the CFD modelling predicted that at low tidal current speeds plume impact points were typically within the 40 m ELCOM cell width at the diffuser location. As such, during neap tides and turns of the tides, when current velocities (and dilutions) were at a minimum, the boundary condition flow was distributed over only a row of five 40 m cells (i.e. 200 m in length) corresponding exactly to the location of the proposed outfall diffuser.

Conversely, with increased flow velocity, the CFD simulations showed that plume impact points were further from the diffuser line and as such the ELCOM insertion stencil was expanded dynamically to

accommodate this behaviour. In addition, these times of higher tidal current speeds coincided with higher plume dilutions, thus producing increased discharge rates using the adopted pre-dilution insertion technique. As such, increasing the ELCOM insertion stencil also assisted in maintaining model stability. The cells used to increase the stencil were located parallel to the diffuser line and were sited two grid-cell lines northwest and southeast of the diffuser line (Figure 3-1). For convenience the cells encompassing the diffuser line are called the central diffuser line and adjacent cells are called (north and south) side diffuser lines. The following flow distribution as a function of the brine dilution was assumed:

- $D < 58$: flow rate was distributed over the central diffuser line alone;
- $58 \leq D < 117$: flow rate was distributed over the central line and another side line in the side of tide flow direction;
- $117 \leq D < 175$: flow rate was distributed over the central line and two side lines in the side of tide flow direction;
- $175 \leq D < 234$: flow rate was distributed over the central line, the two side lines depending on tide flow direction, and the side line adjacent to the diffuser in the opposite side of the tide flow direction; and
- $D > 234$: all boundary cells were used.

3.6.4.4 Sensitivity Analysis – Direct Insertion

Having developed and adopted the linkage technique described above, a series of sensitivity tests were undertaken within the high resolution ELCOM modelling framework to assess the relative performance of the BMT WBM insertion technique compared to direct insertion, as applied to Point Lowly and the ELCOM schematisation (it is noted that ELCOM cannot deliver inflows away from boundary cells within its numerical scheme). Specifically, two simulations were executed with different injection techniques, namely:

- Direct injection; and
- New pre-dilution methodology.

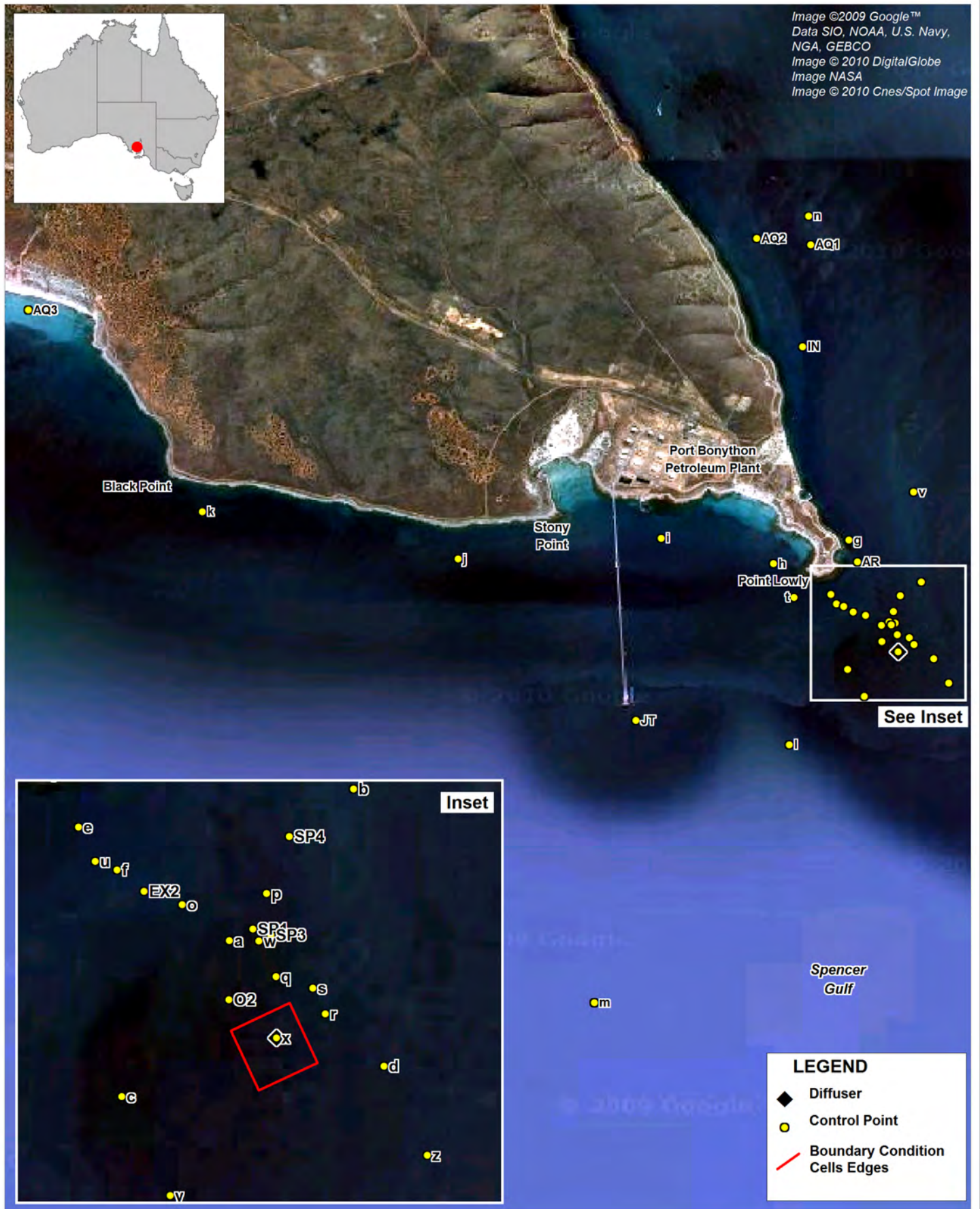
It is noted that the dilutions adopted in this analysis are only for the purposes of comparing injection methods, and do not relate to the dilutions handled in the rosette production runs results presented in Section 3.7. Further, these simulations were all executed for the Draft EIS diffuser location, which corresponds to site 'a' (Figure 3-16); site 'x' in the same figure shows the location of the production run rosette diffuser.

The direct injection method was implemented within ELCOM by directly delivering the brine concentrate at a salinity of 75 gL^{-1} and flow rate a $4.3 \text{ m}^3\text{s}^{-1}$, spread across the bottom cells covering the diffuser alignment (at site 'a'). The dimensions of all these cells were 40 m (L) by 40 m (W) by 1.3 m (H), where the height was the vertical thickness of the ELCOM layer modified locally by bathymetry. Direct injection of the brine concentrate to cells other than those in the bottom layer (as per SA Water 2009) is not allowed by ELCOM.

Comparisons were made between the two methods in terms of salinities and dilutions obtained at a sub-set of receptor locations as indicated in Figure 3-16. The simulations were run for 40 days

between 03 December 2008 and 12 January 2009, which included two representative dudge tides (see third page top left panel of Figure 3-17) The timeseries comparisons between the injection methods are presented in Figure 3-17 (which continues over three pages).

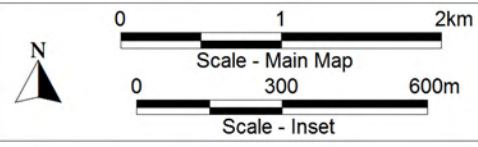
Image ©2009 Google™
 Data SIO, NOAA, U.S. Navy,
 NGA, GEBCO
 Image © 2010 DigitalGlobe
 Image NASA
 Image © 2010 Cnes/Spot Image



Title:
Location of control points

Figure: **3-16** Rev: **A**

BMT WBM endeavours to ensure that the information provided in this map is correct at the time of publication. BMT WBM does not warrant, guarantee or make representations regarding the currency and accuracy of information contained in this map.



Filepath :

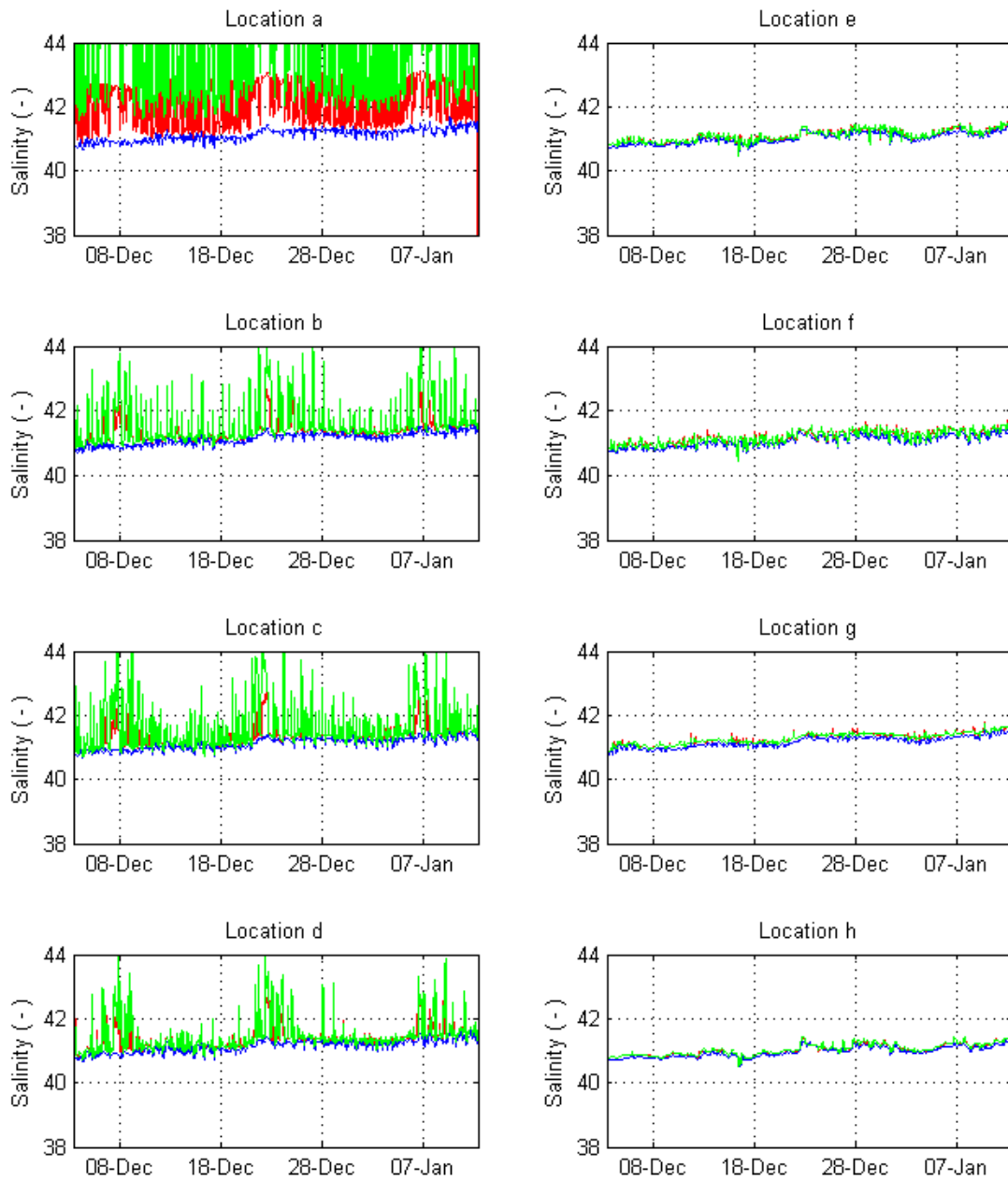


Figure 3-17 Comparisons of salinity at different receptor locations. Blue line shows the baseline (without diffuser) simulation results, red line shows the “adopted pre-dilution” injection method simulation results, and green line shows the direct injection method results.

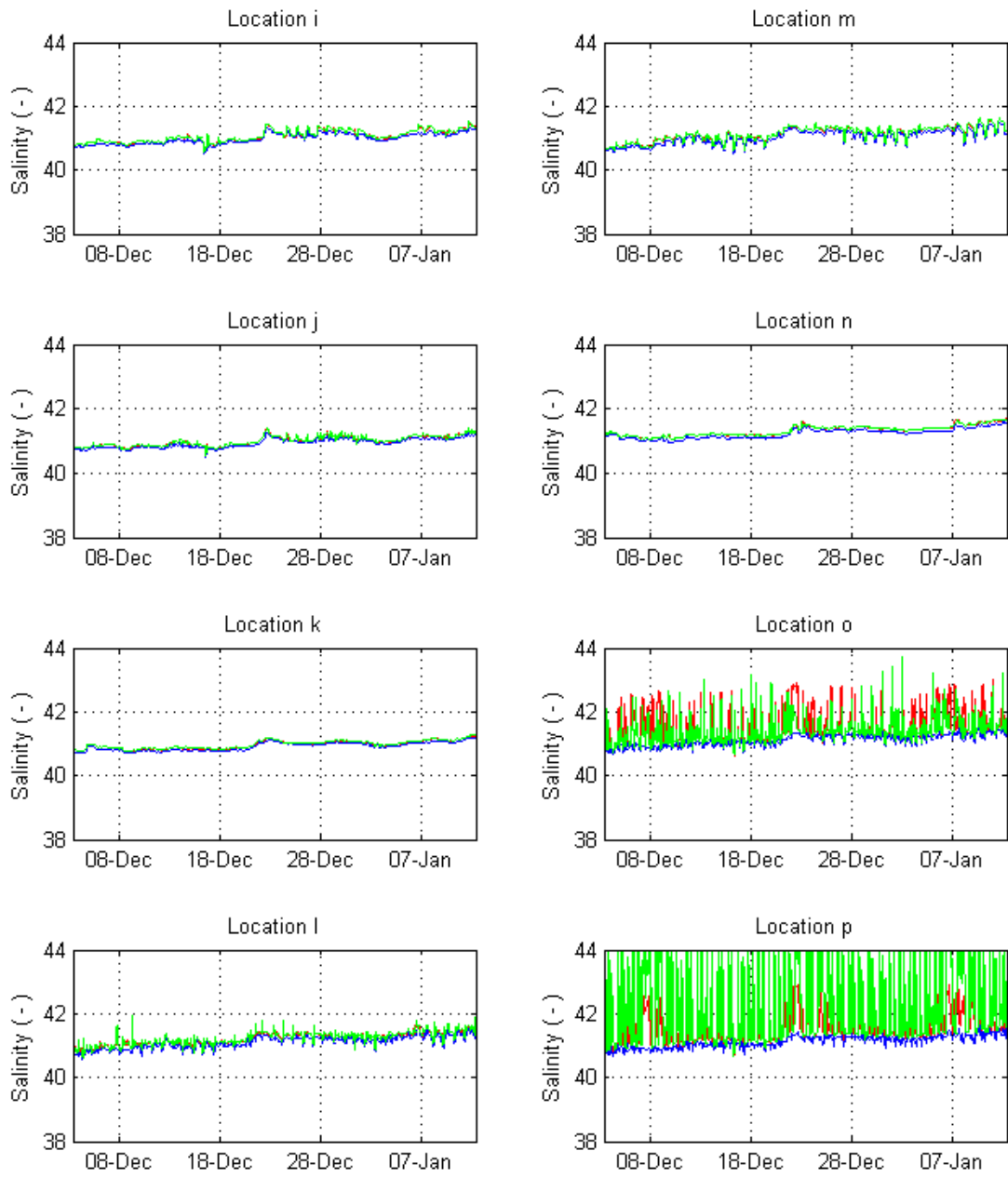


Figure 3-17 (continued)

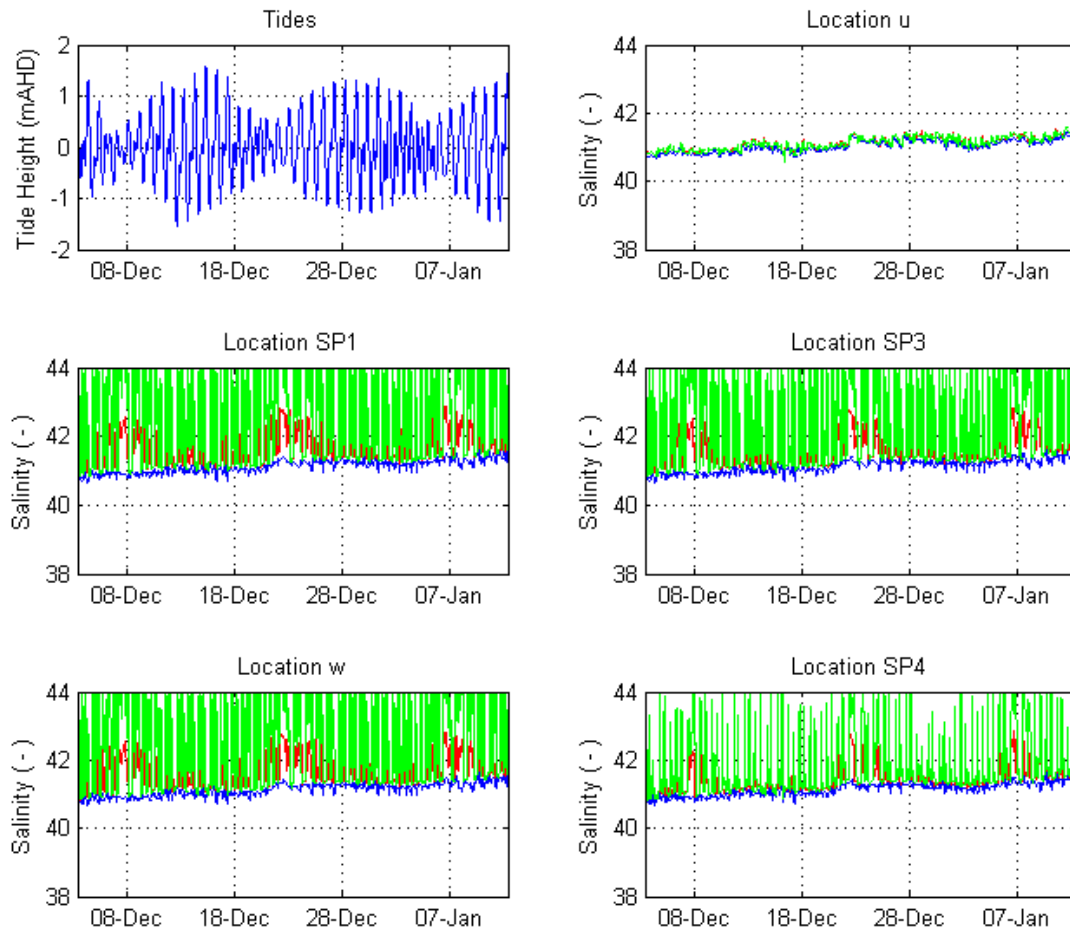


Figure 3-17 (continued)

It can be seen that a series of key sites proximate to the proposed diffuser (especially sites a, b, c, d, o and p, SP1, w, SP3, and SP4, with the SP sites being sponge gardens) exhibit very high salinities when the brine concentrate is introduced to the ELCOM model using the direct insertion technique (green lines). Importantly, the figure shows that these spiky salinities predicted by the direct insertion method at considerable distance from the diffuser can be greater than the maximum salinities predicted by the CFD model at plume impact point (the red line for site a essentially describes these maxima as site a is directly over the diffuser in these simulations). This physically unreasonable prediction is because the direct insertion method, as applied to ELCOM in the bottom layers (which is different to SA Water, 2009), does not reference the near field modelling results: numerical dilution across the injection cells is the only mechanism available for dilution of the brine concentrate prior to advection and dispersion further afield.

In addition to the above it is noted that sites b and c are approximately 600 m from the diffuser, which is considerably further than some key sensitive receptors. This distance is also well outside that able to be tractably simulated by CFD (especially in a dynamic sense) such that we cannot resort to CFD to examine dilutions at these locations. Rather, we are forced to rely on the high resolution ELCOM model to predict dilutions in and around this transitional zone that encompasses sensitive receptors. Such reliance further underscores the importance of appropriately and robustly defining controllable

brine discharge boundary conditions in dispersion modelling studies at Point Lowly - direct linkage to the near field modelling results is essential.

Finally, the figure shows that all sites relatively distant from the diffuser (i.e. in the order of several kilometres distant and/or at higher sea bed levels – e.g. sites e to n) present only minor differences in salinity with respect to the injection methods, indicating that at these distances and locations the two methods appear to converge. Notwithstanding this however, it is noted that these convergences are at sites where both methods indicate very small (and sometimes indistinguishable) differences in salinity due to the desalination discharge over the base case.

3.6.4.5 Sensitivity Analysis – Single and Multiline Pre-Dilution

Further to the above, additional sensitivity testing was undertaken to assess potential differences in prediction of the adopted multi-line pre-dilution insertion stencil (“adopted” or 5 lines pre-dilution) and a method that simply constrained the pre-diluted insertion to a single line of cells (1 line pre-dilution). The latter simulation was executed at an 8 second time step to maintain model stability. Both methods used the same simulation period, CFD lookup table and pre-dilution method, other than the insertion stencil.

The same suite of comparisons are presented above are shown in Figure 3-18 (which also extends over three pages).

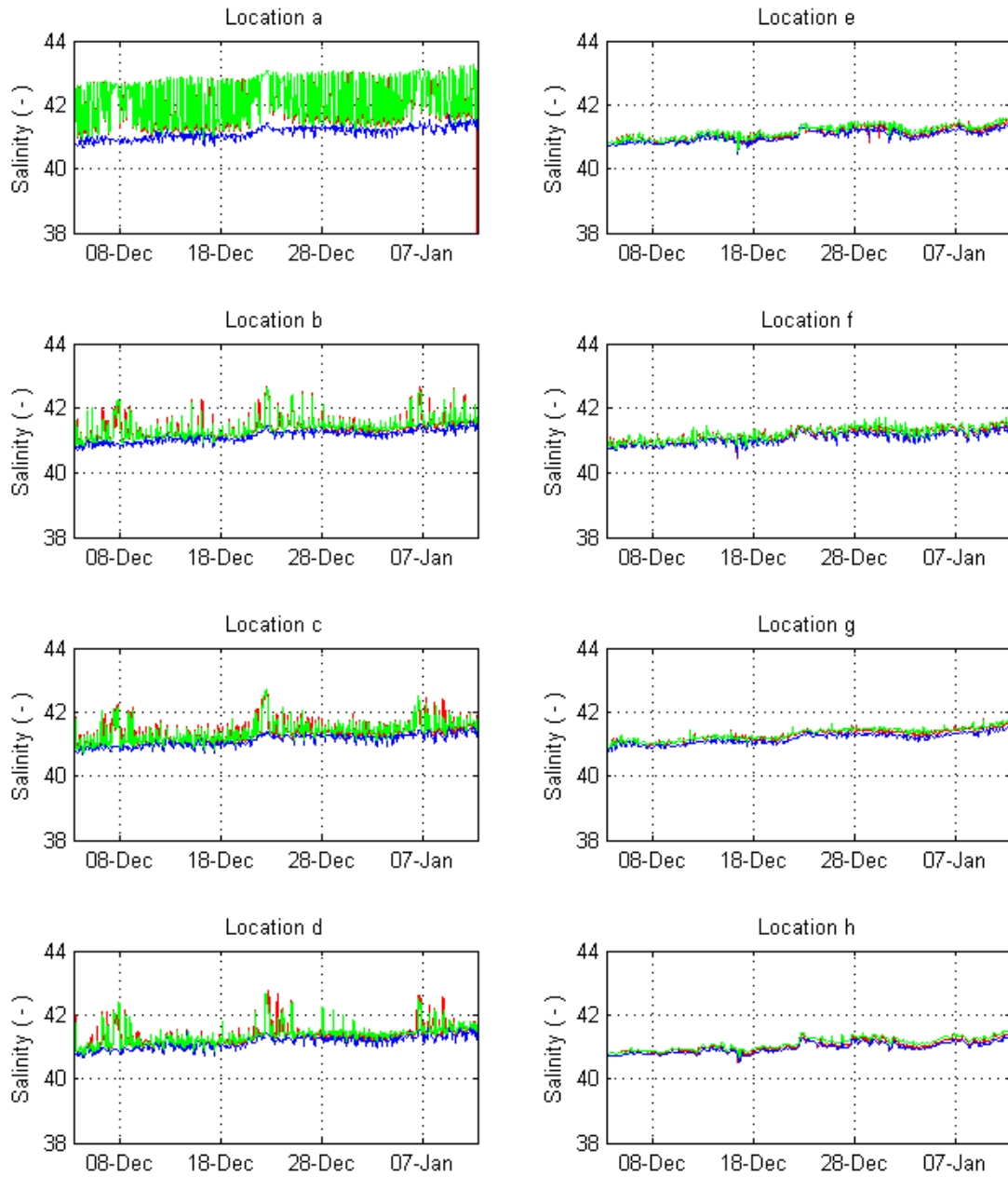


Figure 3-18 Comparisons of salinity at different receptor locations. Blue line shows the baseline (without diffuser) simulation results, red line shows the “adopted pre-dilution” injection method simulation results, and green line shows the “1 line pre-dilution” injection method results.

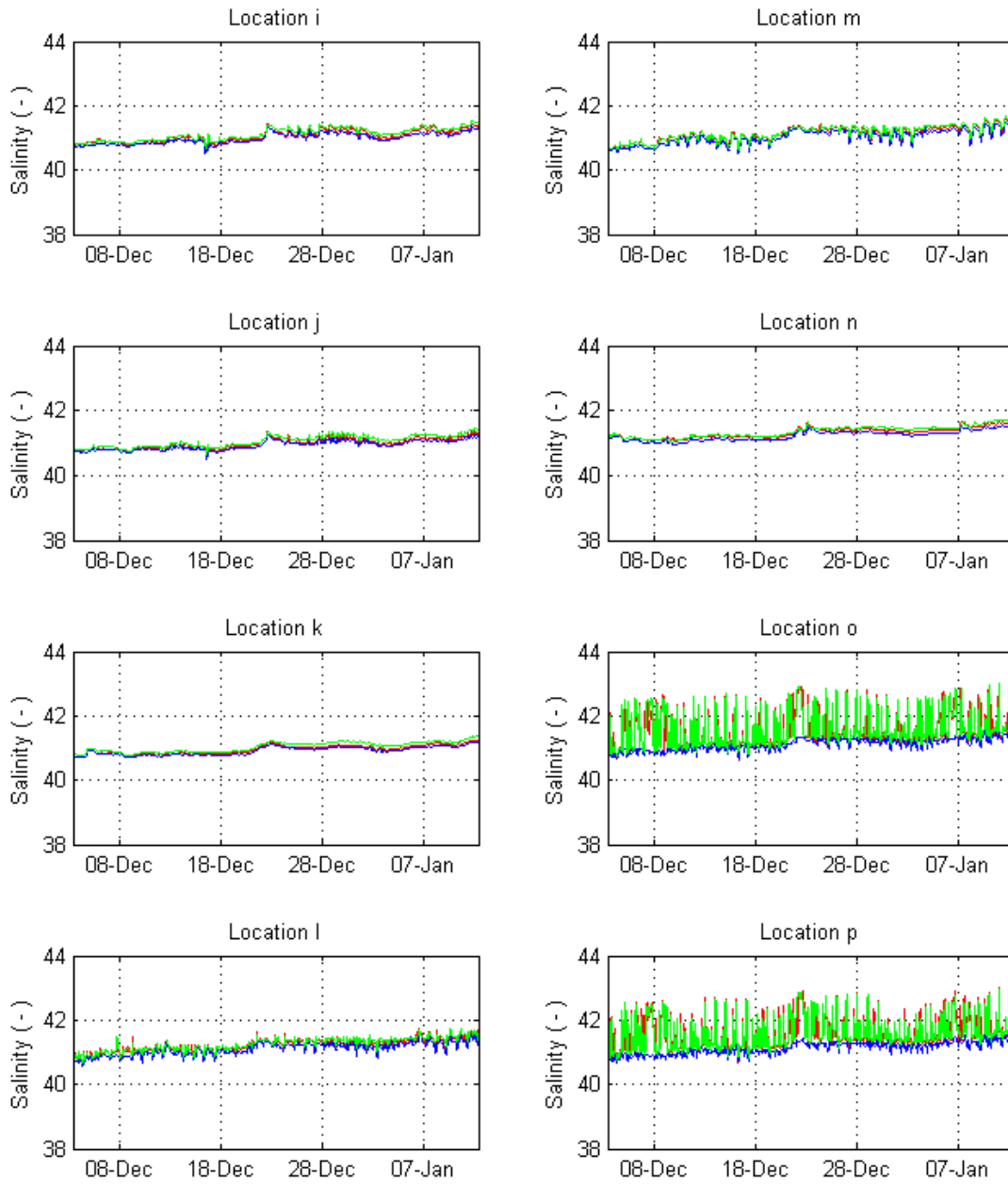


Figure 3-18 (continued)

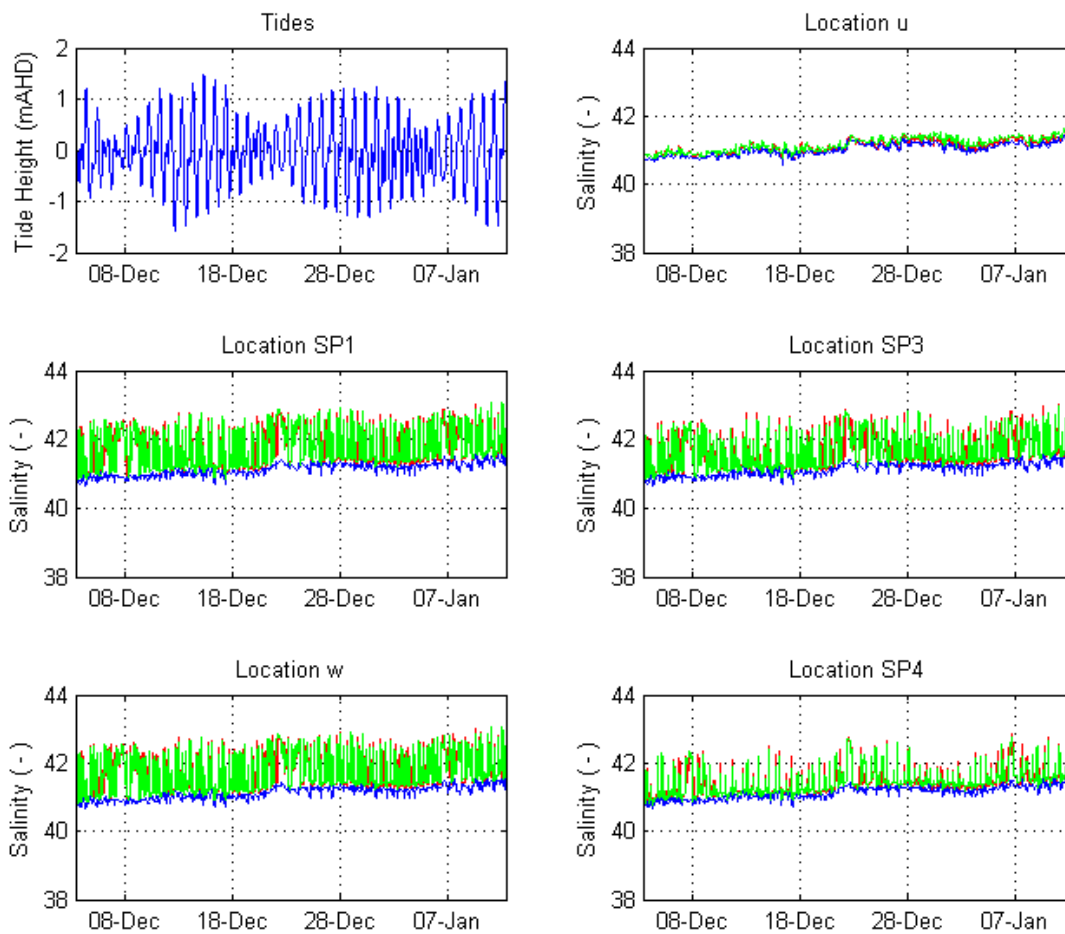


Figure 3-18 (continued)

The figure shows that the two techniques do not present any significant differences in salinity behaviour at any of the receptor sites, with the adopted (5 line) method generally indicating slightly larger salinities (i.e. more conservative). The small differences that are sometimes observed could easily be due to differences in driving hydrodynamics (as driven by the different injection methods) however this would require further investigation to be certain.

To more fully explore this correlation, and to provide some confidence estimates around subsequent ELCOM dilution predictions, percentile distributions of salinity have been prepared for a range of key locations at varying distances from the diffuser, as predicted by the 1 and 5 line methods. These data are presented in Figure 3-19 below (which also extends over three pages). The direct injection percentiles have also been included for reference.

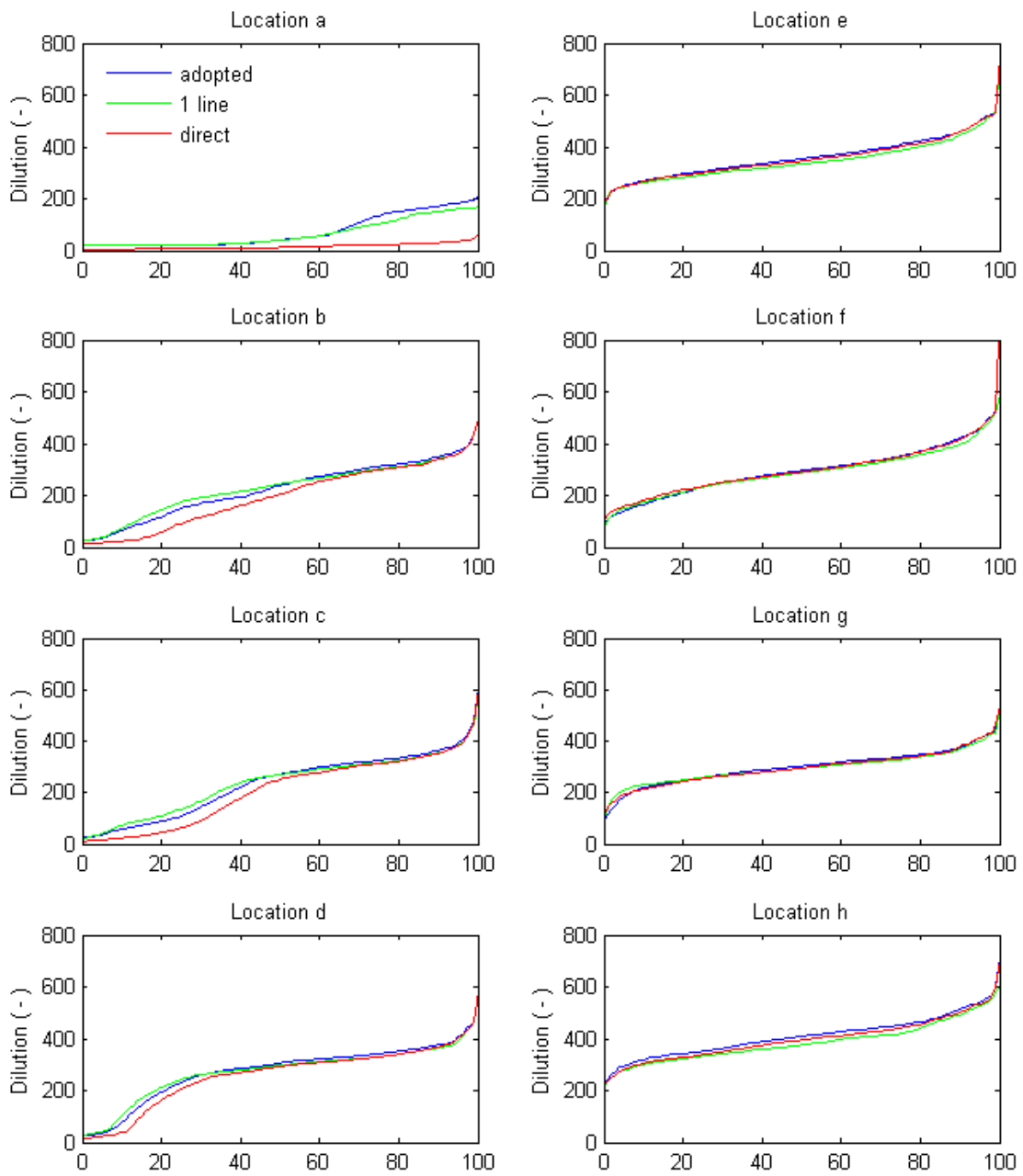


Figure 3-19 Comparisons of dilution percentile distributions at different receptor locations. Blue line shows the “adopted pre-dilution” injection method simulation results, the green line shows the “1 line pre-dilution” injection method results, and the red line shows “direct” injection method simulation results.

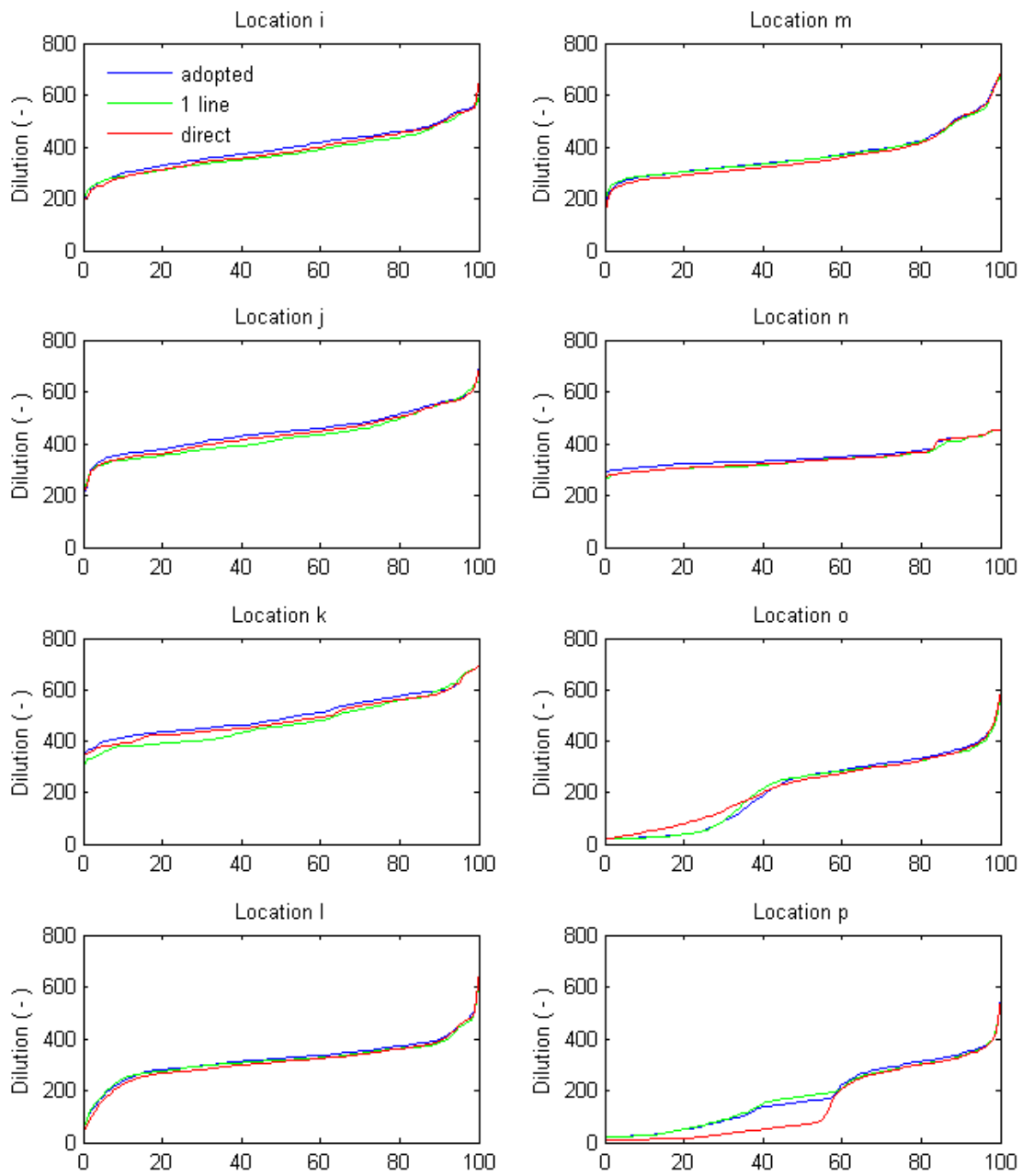


Figure 3-19 (continued)

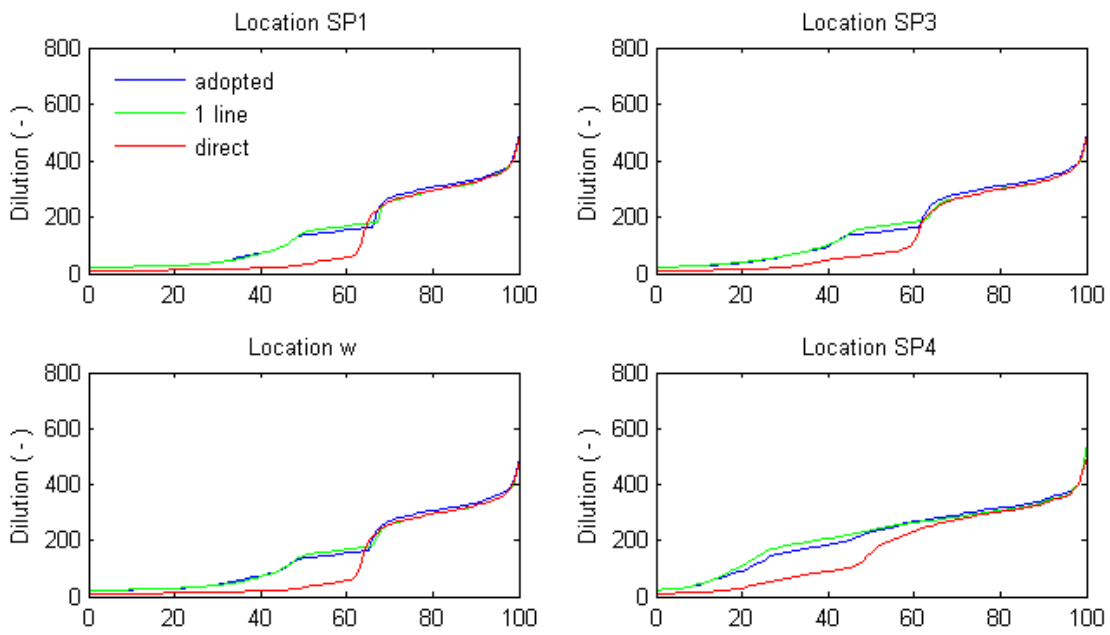


Figure 3-19 (continued)

Key statistics (i.e. dilution percentiles) are also provided in Table 3-3.

Table 3-3 Comparative Dilution Statistics – 1 and 5 Line Methods. These are not results of the optimised diffuser arrangements adopted in the SEIS production runs, so dilutions reported are not representative of the outcomes of this modelling study.

Site	0 th Percentile (Min.)		1 st Percentile		5 th Percentile		10 th Percentile		25 th Percentile		50 th Percentile	
	5 lines	1 line	5 lines	1 line	5 lines	1 line	5 lines	1 line	5 lines	1 line	5 lines	1 line
a	19	19	19	19	19	19	19	19	19	20	40	40
b	23	23	27	27	37	37	66	73	152	175	238	244
c	22	22	26	25	36	40	57	74	110	136	272	270
d	22	22	26	28	35	41	77	104	232	243	305	298
e	166	157	206	211	248	246	269	262	305	292	354	335
f	85	74	108	107	137	148	166	174	233	233	297	288
g	90	90	113	141	181	210	218	230	260	260	303	295
h	223	215	246	237	295	280	319	301	352	334	409	376
i	177	189	231	231	265	269	298	287	341	322	392	368
j	199	220	235	258	337	319	359	336	391	365	445	417
k	343	303	364	330	398	356	412	381	444	397	486	458
l	53	57	87	89	177	181	236	245	287	285	324	317
m	162	190	222	235	265	273	286	288	313	312	350	350
n	286	258	294	269	302	287	309	294	325	309	340	332
o	19	19	20	20	22	22	26	25	53	50	262	262
p	19	20	21	21	24	23	27	27	65	67	157	178
SP1	19	19	21	20	22	22	24	25	33	33	136	145
w	19	19	21	21	22	23	25	25	34	34	137	147
SP3	19	20	21	21	25	25	28	28	48	51	144	163
SP4	21	22	23	23	29	29	40	44	130	156	230	238
u ¹	137	126	153	170	185	194	213	216	274	266	332	317

¹Timeseries at site u in this instance was output at 20 minutes resolution, whilst other sites were output at 4 minutes resolution

In general, deep sensitive receptors (i.e., sites a, b, c, d, l, o, p, SP1, w, SP3, and SP4 – these include the sponge gardens) presented lower dilutions for the 5 lines method in relation to the 1 line pre-dilution injection method, particularly in the lower dilution range (i.e. below 85:1, shown in bold in Table 3-3). The figures and table show that under the 5 lines approach the predictions are mostly conservative. Specifically, it is estimated that the uncertainty of ELCOM predictions at these key sensitive receptors (given by the difference between 5 line and 1 line the two pre-dilution insertion approaches) is -20% to +3% relative to the 5 lines insertion method. Negative differences indicate lower dilutions predicted by the 5 lines method and therefore more conservative for the purposes of this assessment.

For shallow sensitive receptors (i.e. representative of the cuttlefish habitat), only minimum dilutions observed at sites e, g, and u presented dilutions lower or similar to the 85:1 target (again noting that these results do not apply to the SEIS production runs). In these locations the uncertainty was estimated to be -25% to +6%. Other receptors (e.g. sites h, i, j, k, n) always presented dilutions well above 85:1, such that uncertainties did not present concern with respect to the dilution estimates.

Even though the 5 lines approach was generally more conservative than the 1 line, the relevant uncertainties for sites relevant to this study were estimated as +3% in the deeper and relatively close

sensitive receptors (sponge gardens) and +6% in the cuttlefish habitats. These ranges should be noted when considering dilution predictions presented in the following sections.

Given the above, the two methods were deemed equivalent for the purposes of this assessment. The adaptive insertion stencil pre-dilution method was thus adopted in all assessments presented in this report as it facilitated higher runtime ratios.

3.7 Simulation Results

3.7.1 Control Points

Timeseries at different control points chosen by BHP Billiton are presented below. These points are largely consistent with the timeseries presented in the DEIS and also include complementary point sets. The locations of the different points are presented in Figure 3-16. The timeseries were output at a frequency of 4 minutes (except for points u and ex2 which were 20 minutes) and dilutions compared to (dilution) targets of 45:1, 70:1, and 85:1, as instructed by BHP Billiton.

Bottom salinities at control points for simulations with and without the proposed diffuser are presented in Figure 3-20 to Figure 3-22. The corresponding dilution statistics at the model bottom cells are presented in Table 3-4. The first two weeks were removed from the timeseries for analysis to avoid potential contamination due to warmup issues.

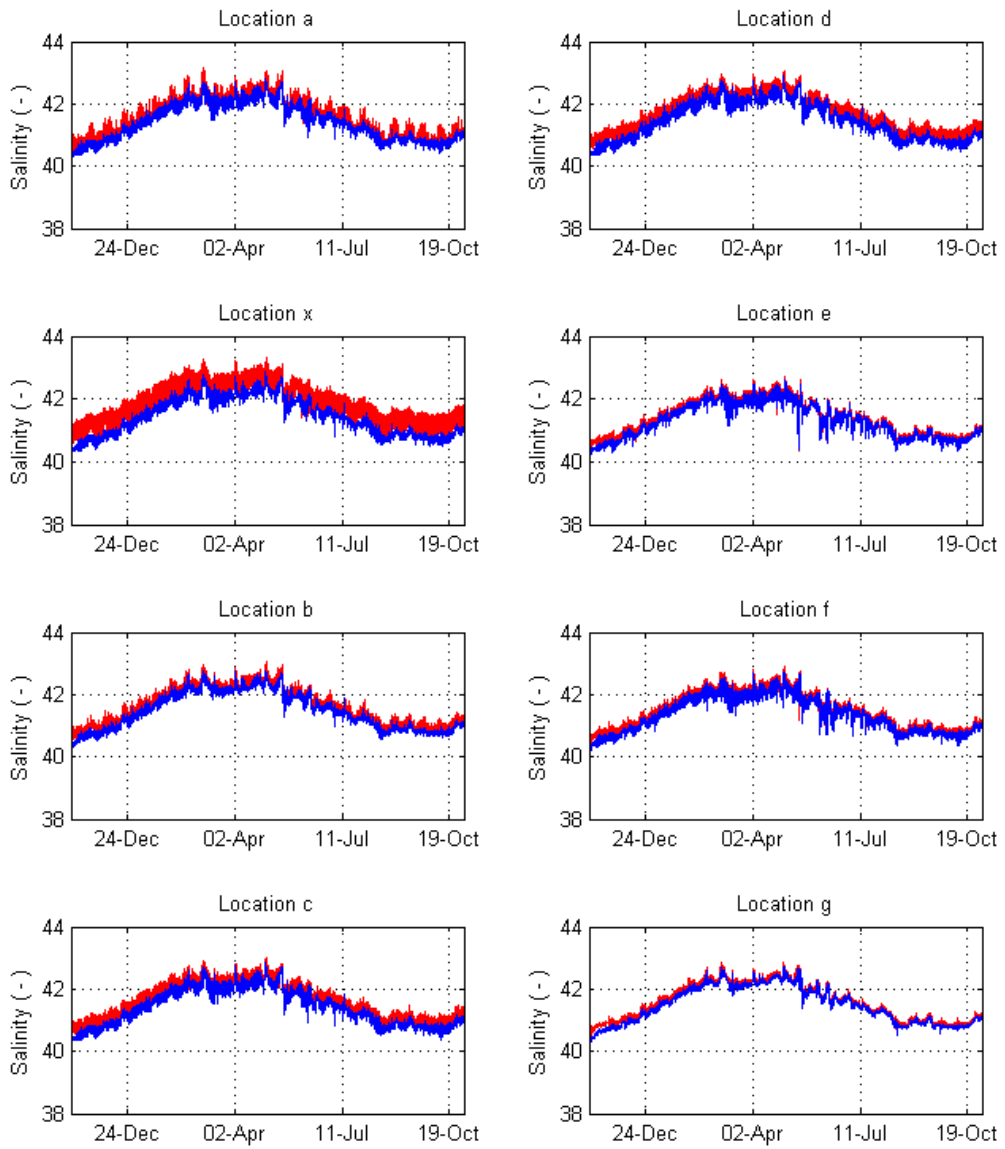


Figure 3-20 Salinities at the bottom for point a (discharge location), and a to g. Red: with proposed desalination outfall. Blue: baseline.

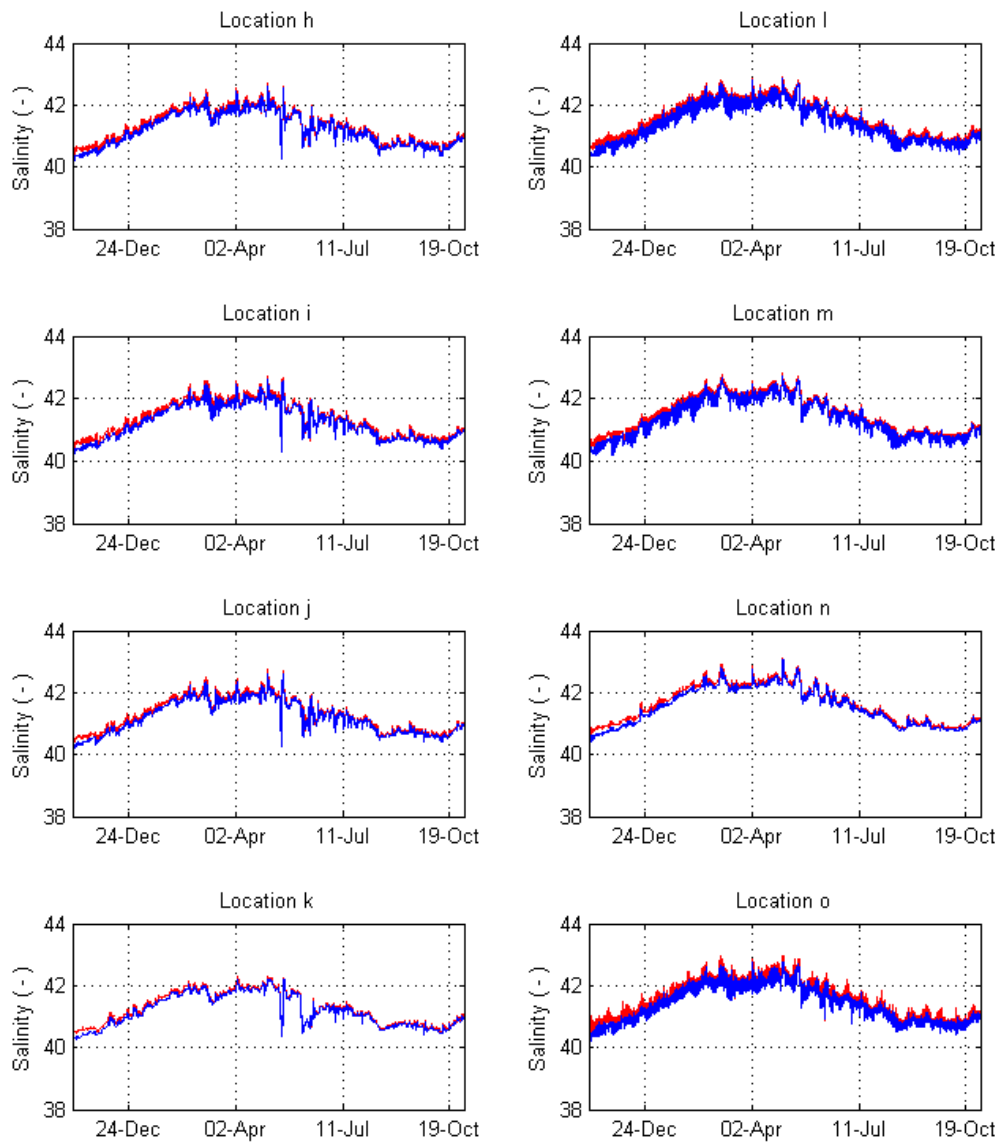


Figure 3-21 Salinities at the bottom for points h to o. Red: with proposed desalination outfall. Blue: baseline.

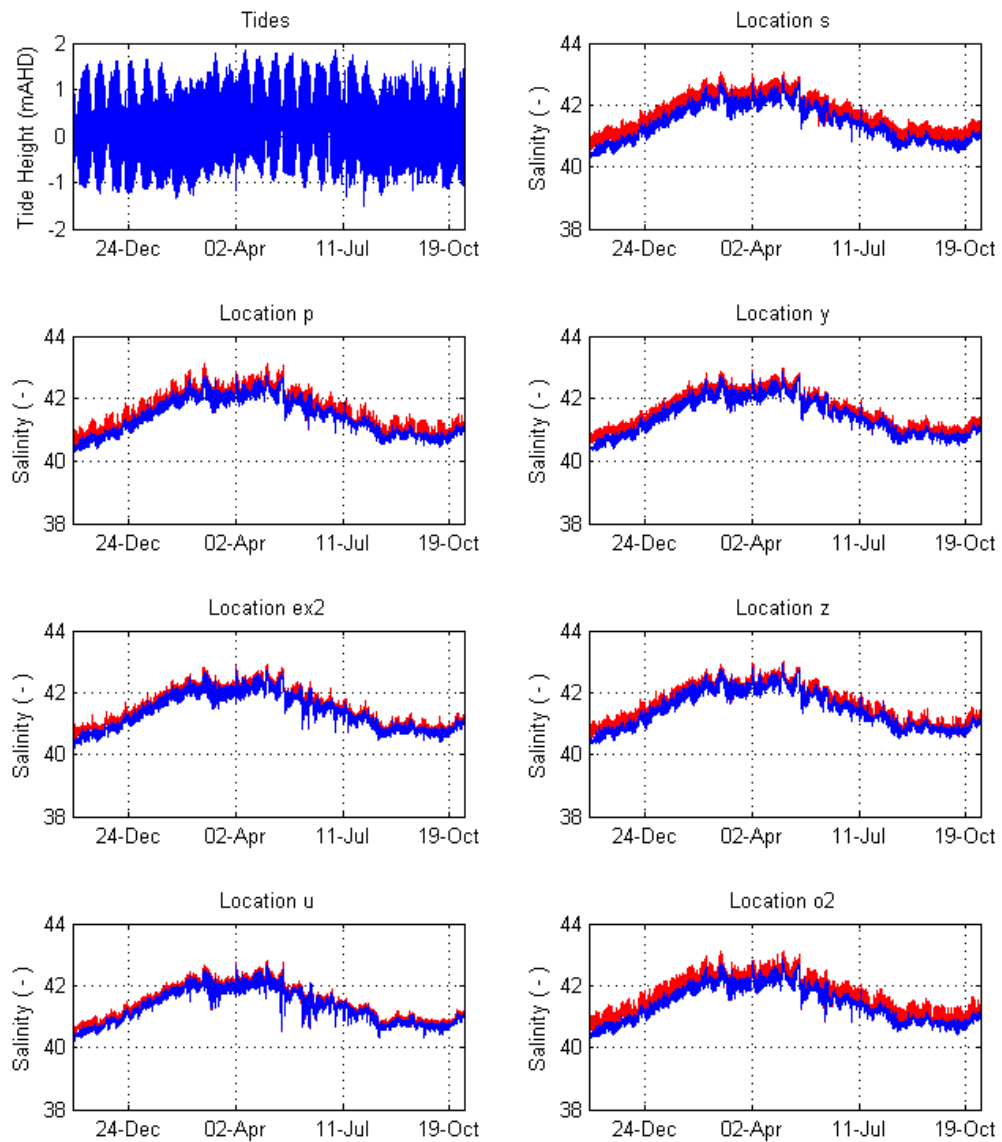


Figure 3-22 Salinities at the bottom for points p, ex2, u, s, y, z, and o2. Red: with proposed desalination outfall. Blue: baseline. Tides at Point Lowly are also presented in the top left panel.

Table 3-4 Dilution statistics obtained for time series at the control points. Numbers relating to dilution threshold breaches are bolded (based on 85:1 for percentiles).

Site	Percentiles									Occurrence of dilutions less than given dilutions					
	Min	1	5	10	25	50	75	90	95	<45 cnt	<45 pct	<70 cnt	<70 pct	<85 cnt	<85 pct
a	46	64	119	205	293	325	349	368	382	0	0	2371	1.9	3852	3
x	43	46	49	53	69	144	215	300	309	686	0.5	32598	25.7	41394	32.7
b	59	84	146	206	286	322	347	365	374	0	0	422	0.3	1311	1
c	59	83	104	121	180	288	335	363	378	0	0	142	0.1	1545	1.2
y	62	91	111	132	214	312	348	370	382	0	0	118	0.1	644	0.5
d	56	77	94	110	209	314	348	368	378	0	0	386	0.3	3204	2.5
z	59	77	107	162	288	330	358	376	386	0	0	389	0.3	2755	2.2
e	161	243	291	311	340	369	408	448	481	0	0	0	0	0	0
f	88	165	226	259	301	332	365	406	436	0	0	0	0	0	0
g	91	168	253	283	309	332	353	367	380	0	0	0	0	0	0
h	179	261	317	334	363	397	441	482	520	0	0	0	0	0	0
i	172	245	301	327	355	386	428	465	496	0	0	0	0	0	0
j	200	277	333	352	379	416	451	489	527	0	0	0	0	0	0
k	320	337	364	374	406	443	480	531	604	0	0	0	0	0	0
l	72	126	183	235	302	335	360	380	393	0	0	0	0	81	0.1
m	136	256	288	303	327	352	378	407	430	0	0	0	0	0	0
n	272	287	305	311	329	347	362	375	385	0	0	0	0	0	0
o	57	76	180	238	295	325	352	373	390	0	0	931	0.7	1612	1.3
o2	49	62	74.0	99.0	266	320	348	368	381	0	0	4503	3.6	10004	7.9
p	52	70	130	214	293	324	349	368	380	0	0	1285	1	3017	2.4
s	55	68	81.3	94.4	170	297	336	361	372	0	0	1931	1.5	8101	6.4
q	50	63	73.5	95	261	317	345	365	378	0	0	4386	3.5	10938	8.3
r	51	67	80.7	91.2	137	280	331	358	370	0	0	1923	1.5	9108	6.9
v	102	187	243	272	305	329	350	365	377	0	0	0	0	0	0
t	164	252	299	319	350	384	429	468	502	0	0	0	0	0	0
u*	107	201	258	286	320	352	388	429	458	0	0	0	0	0	0
ex2*	62	101	188	241	294	325	353	378	402	0	0	49	0.2	162	1
JT	86	145	222	267	308	338	364	400	426	0	0	0	0	0	0
AR	121	218	276	293	316	340	358	380	398	0	0	0	0	0	0
IN	177	269	296	307	324	344	359	372	384	0	0	0	0	0	0
AQ1	274	293	308	317	338	352	363	378	387	0	0	0	0	0	0
AQ2	239	293	308	317	339	353	364	379	392	0	0	0	0	0	0
AQ3	327	349	369	378	417	454	496	559	647	0	0	0	0	0	0
SP1	50	66	111	197	291	325	349	368	381	0	0	2083	1.6	4225	3.3
w	50	65	95	176	288	324	349	368	381	0	0	2460	1.9	5244	4.1
SP3	51	67	96	172	287	324	350	368	381	0	0	1802	1.4	4956	3.9
SP4	56	73	141	216	290	323	348	365	376	0	0	965	0.8	2352	1.9

*Statistics obtained from 20 minute output frequency

It is noted that some spikes in salinity are evident in Figure 3-20 to Figure 3-22. These spikes are particularly pronounced during a dodge tide spanning 17 May 2008, and could reflect the inherent salt ejection dynamics in the Northern Gulf, explored in Appendix H5.2 of the SEIS. The spikes occur both

in the baseline and the desalination plant scenario, and therefore are not related to the desalination discharge or injection technique. An animation of modelled bottom salinities can be found in the accompanying animation (Animation of Natural Salt Slugs) and it illustrates these dynamics in the Northern Gulf.

Salinities at three different levels in the water column (lower-most, 5, and 10 m from seabed) at points x (diffuser), y (approximately 450 m south), and s (approximately 100 m north) are presented in Figure 3-23. The model shows stronger salinity stratification at the diffuser location and very rapid loss of vertical structure with increased distance to the other sites. These results indicate that significant vertical mixing and associated dilution of the plume occurs within several hundred metres from the outfall, consistent with the CFD simulations

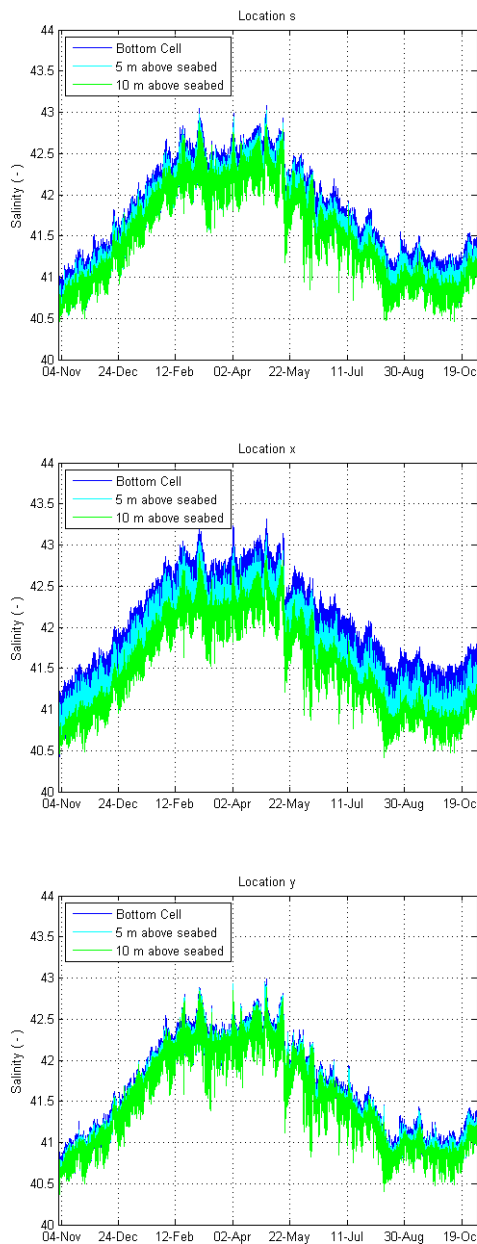


Figure 3-23 Salinities at the bottom for points s, x, and y

3.7.2 Curtain

Minimum dilutions on a vertical curtain running from inshore to offshore corresponding to points d to e (Figure 3-16) are presented in Table 3-5. Corresponding 1st and 10th percentile data are presented in Table 3-6 and Table 3-7, respectively. The longest durations that dilutions were continuously lower than the target dilutions are presented in Table 3-8 to Table 3-10.

Table 3-5 Minimum dilutions in a curtain from points d to e over the entire one year simulation. Dilutions lower than 85:1 are given in bold. Hatched cells represent land cells. k is the vertical cell index, and z is the cell elevation given in mAHD. Cell grid sizes varied between 40 and 65 m.

		Dilution								
		e	u	f	ex2	o	a	q	r	d
Distance Along the Path		0	59	178.2	282.1	405.2	584.9	764.0	950.7	1188.7
K = 31	z = 0.98	195	200	192	201	216	200	213	196	176
K = 30	z = -1.02	186	163	156	161	161	169	165	182	163
K = 29	z = -3.02	183	143	134	154	163	170	167	181	166
K = 28	z = -4.92	161	119	112	142	161	168	172	173	167
K = 27	z = -6.65		109	106.8	142	152	151	119	136	144
K = 26	z = -8.22		107	107	122	132	125	78	109	100
K = 25	z = -9.67			97	107	128	112	76	96	97
K = 24	z = -11.02			91	103	120	91	64	86	101
K = 23	z = -12.27			89	94	97	67	64	84	92
K = 22	z = -13.42			88	91	87	66	65	81	90
K = 21	z = -14.47				83	68	66	65	77	91
K = 20	z = -15.47				80	62	65	65	75	90
K = 19	z = -16.47				71	62	64	64	76	77
K = 18	z = -17.47				66	61	60	64	76	74
K = 17	z = -18.47				64	59	58	64	73	73
K = 16	z = -19.47				63	58	55	61	71	71
K = 15	z = -20.47				64	57	53	59	69	71
K = 14	z = -21.47				62	57	50	55	66	65
K = 13	z = -22.47				62	56	48	52	62	60
K = 12	z = -23.52					56	47	51	58	59
K = 11	z = -24.67					57	46	50	52	56
K = 10	z = -25.92						46	50	51	56

Table 3-6 1st percentile dilutions in a curtain from points d to e over the entire one year simulation. Dilutions lower than 85:1 are given in bold. Hatched cells represent land cells. k is the vertical cell index, and z is the cell elevation given in mAHD. Cell grid sizes varied between 40 and 65 m.

		Dilution								
		e	u	f	ex2	o	a	q	r	d
Distance Along the Path		0	59	178.2	282.1	405.2	584.9	764.0	950.7	1188.7
K = 31	z = 0.98	282	282	282	285	282	279	279	279	278
K = 30	z = -1.02	264	251	244	252	261	266	269	269	271
K = 29	z = -3.02	255	237	234	248	257	263	266	267	270
K = 28	z = -4.92	243	211	214	237	251	260	263	264	267
K = 27	z = -6.65		205	198	226	243	255	258	259	263
K = 26	z = -8.22		201	185	215	236	249	251	253	259
K = 25	z = -9.67			177	207	227	242	244	244	253
K = 24	z = -11.02			171	196	218	234	233	235	244
K = 23	z = -12.27			168	186	208	223	222	226	236
K = 22	z = -13.42			165	177	197	213	212	214	224
K = 21	z = -14.47				170	185	202	201	201	214
K = 20	z = -15.47				161	174	190	186	187	204
K = 19	z = -16.47				151	159	176	168	170	192
K = 18	z = -17.47				139	143	159	151	151	176
K = 17	z = -18.47				128	128	136	129	131	154
K = 16	z = -19.47				118	113	115	106	115	131
K = 15	z = -20.47				110	97	93	89	103	110
K = 14	z = -21.47				105	86	78	78	93	97
K = 13	z = -22.47				101	79	70	71	84	89
K = 12	z = -23.52					77	66	66	76	82
K = 11	z = -24.67					76	65	64	69	79
K = 10	z = -25.92						64	63	67	77

Table 3-7 10th percentile dilutions in a curtain from points d to e over the entire one year simulation. Dilutions lower than 85:1 are given in bold. Hatched cells represent land cells. k is the vertical cell index, and z is the cell elevation given in mAHD. Cell grid sizes varied between 40 and 65 m.

		Dilution								
		e	u	f	ex2	o	a	q	r	d
Distance Along the Path		0	59	178.2	282.1	405.2	584.9	764.0	950.7	1188.7
K = 31	z = 0.98	341	343	343	341	335	324	322	323	323
K = 30	z = -1.02	321	317	313	313	310	306	306	306	307
K = 29	z = -3.02	317	308	305	308	307	304	305	305	306
K = 28	z = -4.92	311	293	290	298	302	302	302	302	304
K = 27	z = -6.65		287	281	292	298	299	300	300	302
K = 26	z = -8.22		286	273	286	295	296	297	298	300
K = 25	z = -9.67			267	282	292	294	295	295	297
K = 24	z = -11.02			263	278	289	291	292	292	295
K = 23	z = -12.27			260	273	286	289	290	290	293
K = 22	z = -13.42			259	270	283	286	287	286	290
K = 21	z = -14.47				266	279	284	284	281	287
K = 20	z = -15.47				262	275	281	280	274	284
K = 19	z = -16.47				257	270	277	273	265	278
K = 18	z = -17.47				252	264	272	265	250	270
K = 17	z = -18.47				248	257	265	252	229	254
K = 16	z = -19.47				245	250	255	234	200	228
K = 15	z = -20.47				243	245	244	210	170	190
K = 14	z = -21.47				241	241	232	175	143	155
K = 13	z = -22.47				241	239	220	143	120	131
K = 12	z = -23.52					238	212	117	103	118
K = 11	z = -24.67					238	206	101	94	112
K = 10	z = -25.92						205	97	92	110

Table 3-8 Longest durations (minutes) that modelled dilutions in a curtain from points d to e were lower than 85:1 over the entire one year simulation. Hatched cells represent land cells. k is the vertical cell index, and z is the cell elevation given in mAHD. Cell grid sizes varied between 40 and 65 m.

		Longest durations that modelled dilutions were lower than in 85:1 (in minutes)								
		e	u	f	ex2	o	a	q	r	d
Distance Along the Path		0	59	178.2	282.1	405.2	584.9	764.0	950.7	1188.7
K = 31	z = 0.98	0	0	0	0	0	0	0	0	0
K = 30	z = -1.02	0	0	0	0	0	0	0	0	0
K = 29	z = -3.02	0	0	0	0	0	0	0	0	0
K = 28	z = -4.92	0	0	0	0	0	0	0	0	0
K = 27	z = -6.65		0	0	0	0	0	0	0	0
K = 26	z = -8.22		0	0	0	0	0	16	0	0
K = 25	z = -9.67			0	0	0	0	24	0	0
K = 24	z = -11.02			0	0	0	0	28	0	0
K = 23	z = -12.27			0	0	0	40	36	16	0
K = 22	z = -13.42			0	0	0	48	48	16	0
K = 21	z = -14.47				60	40	40	60	20	0
K = 20	z = -15.47				60	52	24	56	20	0
K = 19	z = -16.47				140	64	52	108	16	32
K = 18	z = -17.47				180	100	56	100	36	68
K = 17	z = -18.47				280	192	80	84	56	132
K = 16	z = -19.47				360	256	116	92	92	144
K = 15	z = -20.47				540	380	188	108	148	132
K = 14	z = -21.47				600	628	536	184	160	124
K = 13	z = -22.47				760	864	756	420	284	156
K = 12	z = -23.52					876	772	948	452	248
K = 11	z = -24.67					876	964	1296	668	404
K = 10	z = -25.92						964	1296	844	416

Table 3-9 Longest durations (minutes) that modelled dilutions in a curtain from points d to e were lower than 70:1 over the entire one year simulation. Hatched cells represent bottom cells. k is the vertical cell index, and z is the cell elevation given in mAHD. Cell grid sizes varied between 40 and 65 m.

		Longest durations that modelled dilutions were lower than 70:1 (in minutes)								
		e	u	f	ex2	o	a	q	r	d
Distance Along the Path		0	59	178.2	282.1	405.2	584.9	764.0	950.7	1188.7
K = 31	z = 0.98	0	0	0	0	0	0	0	0	0
K = 30	z = -1.02	0	0	0	0	0	0	0	0	0
K = 29	z = -3.02	0	0	0	0	0	0	0	0	0
K = 28	z = -4.92	0	0	0	0	0	0	0	0	0
K = 27	z = -6.65		0	0	0	0	0	0	0	0
K = 26	z = -8.22		0	0	0	0	0	0	0	0
K = 25	z = -9.67			0	0	0	0	0	0	0
K = 24	z = -11.02			0	0	0	0	16	0	0
K = 23	z = -12.27			0	0	0	20	24	0	0
K = 22	z = -13.42			0	0	0	28	28	0	0
K = 21	z = -14.47				0	12	16	28	0	0
K = 20	z = -15.47				0	40	16	28	0	0
K = 19	z = -16.47				0	48	20	28	0	0
K = 18	z = -17.47				100	56	24	32	0	0
K = 17	z = -18.47				140	64	24	32	0	0
K = 16	z = -19.47				160	88	24	32	0	0
K = 15	z = -20.47				180	148	76	68	12	0
K = 14	z = -21.47				200	232	240	88	20	24
K = 13	z = -22.47				220	512	472	188	92	52
K = 12	z = -23.52					732	520	352	268	56
K = 11	z = -24.67					784	660	412	272	140
K = 10	z = -25.92						668	424	400	152

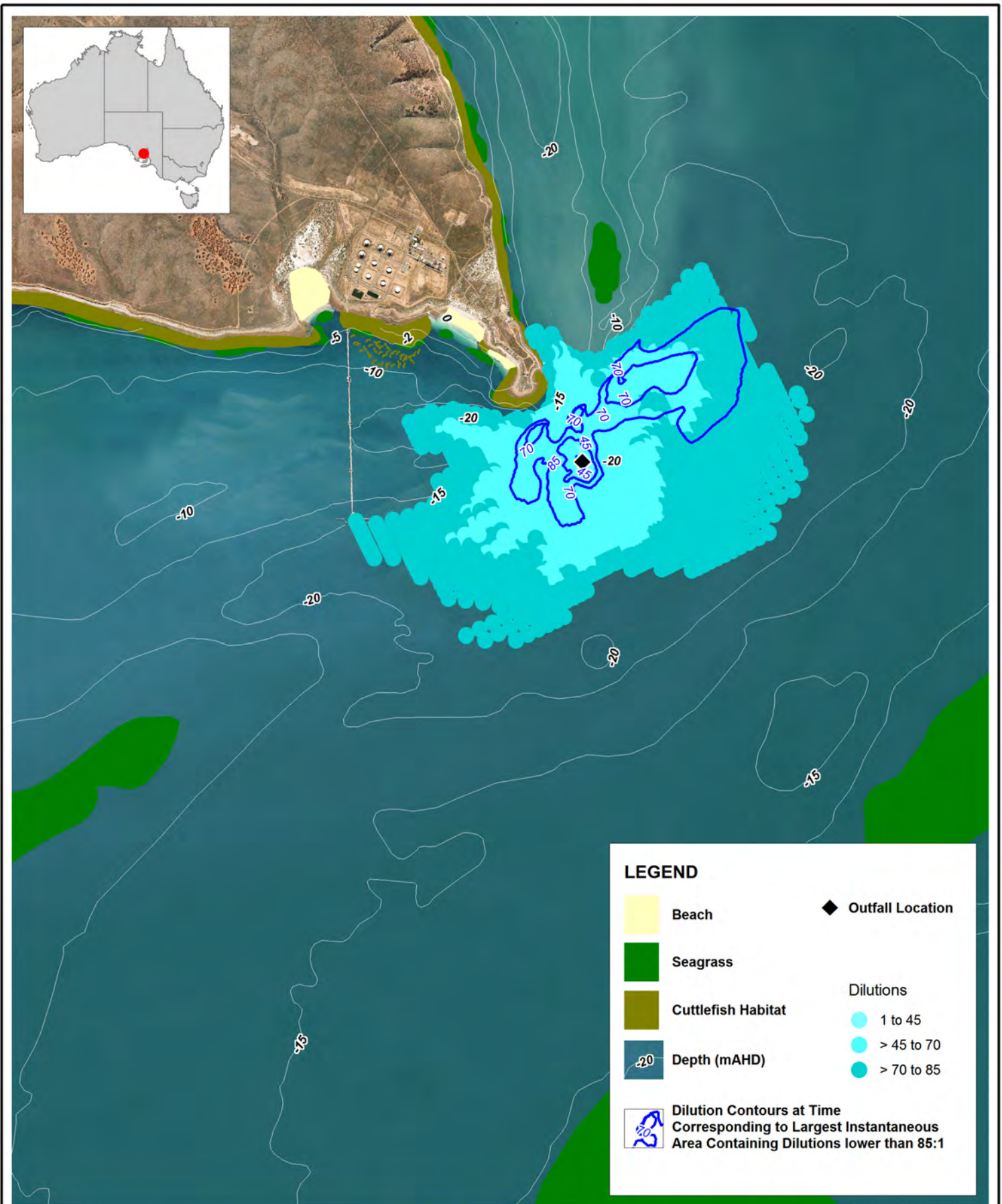
Table 3-10 Longest durations (minutes) that modelled dilutions in a curtain from points d to e were lower than 45:1 over the entire one year simulation. Hatched cells represent bottom cells. k is the vertical cell index, and z is the cell elevation given in mAHD. Cell grid sizes varied between 40 and 65 m.

		Longest durations that modelled dilutions were lower than 45:1 (in minutes)								
		e	u	f	ex2	o	a	q	r	d
Distance Along the Path		0	59	178.2	282.1	405.2	584.9	764.0	950.7	1188.7
K = 31	z = 0.98	0	0	0	0	0	0	0	0	0
K = 30	z = -1.02	0	0	0	0	0	0	0	0	0
K = 29	z = -3.02	0	0	0	0	0	0	0	0	0
K = 28	z = -4.92	0	0	0	0	0	0	0	0	0
K = 27	z = -6.65		0	0	0	0	0	0	0	0
K = 26	z = -8.22		0	0	0	0	0	0	0	0
K = 25	z = -9.67			0	0	0	0	0	0	0
K = 24	z = -11.02			0	0	0	0	0	0	0
K = 23	z = -12.27			0	0	0	0	0	0	0
K = 22	z = -13.42			0	0	0	0	0	0	0
K = 21	z = -14.47				0	0	0	0	0	0
K = 20	z = -15.47				0	0	0	0	0	0
K = 19	z = -16.47				0	0	0	0	0	0
K = 18	z = -17.47				0	0	0	0	0	0
K = 17	z = -18.47				0	0	0	0	0	0
K = 16	z = -19.47				0	0	0	0	0	0
K = 15	z = -20.47				0	0	0	0	0	0
K = 14	z = -21.47				0	0	0	0	0	0
K = 13	z = -22.47				0	0	0	0	0	0
K = 12	z = -23.52					0	0	0	0	0
K = 11	z = -24.67					0	0	0	0	0
K = 10	z = -25.92						0	0	0	0

3.7.3 Dilution Contour Maps and Timeseries

Dilution contour maps are presented for the 85:1, 70:1, and 45:1 dilution targets. These dilutions were expressed in terms of 0th, 1st, 10th, and 50th percentiles. They do not represent snapshots in time, but rather are cumulative maps of brine extents. These percentiles were calculated for each bottom cell of the model and represent the relative period in which dilutions remain below the given target. For example, the 0th percentile map represents the minimum dilution observed in each model computational cell over the entire one year simulation period and the 10th percentile map represents the dilution exceeded 90% of the time at each cell over the annual simulation period. These percentiles have then been grouped into contours reflecting the target dilutions, hence the presentation of dilution ranges in each maps legend.

The dilution maps are presented in Figure 3-24 to Figure 3-26 and, for comparison purposes, include the 45:1, 70:1 and 85:1 dilution contours at the snapshot in time for which the largest instantaneous area encompassing dilutions less than 85:1 occurs over the one year simulation period. The model predicts that the area corresponding to dilutions less than 85:1 is zero for the 50th percentile and above and as such these maps are not presented.



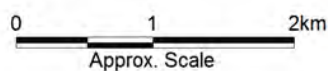
Title:
0th Percentile (minimum) dilution for 1 year simulation period

Figure:
3-24

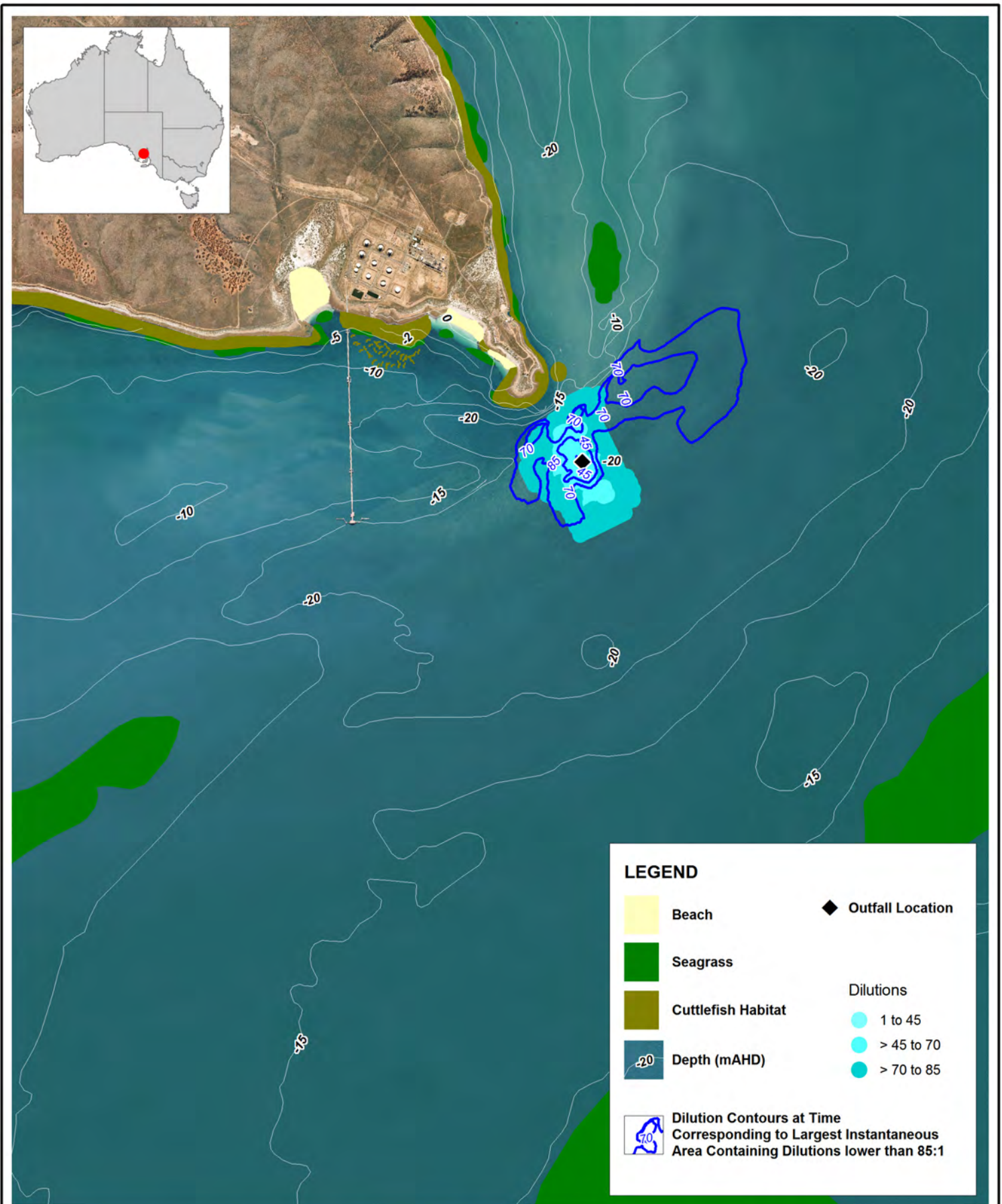
Rev:
A

BMT WBM endeavours to ensure that the information provided in this map is correct at the time of publication. It does not warrant, guarantee or make representations regarding the currency and accuracy of information contained in this map.

Air photo from Google Earth.



Filepath :



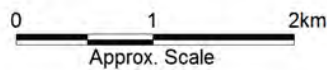
Title:
1st Percentile dilution for 1 year simulation period

Figure:
3-25

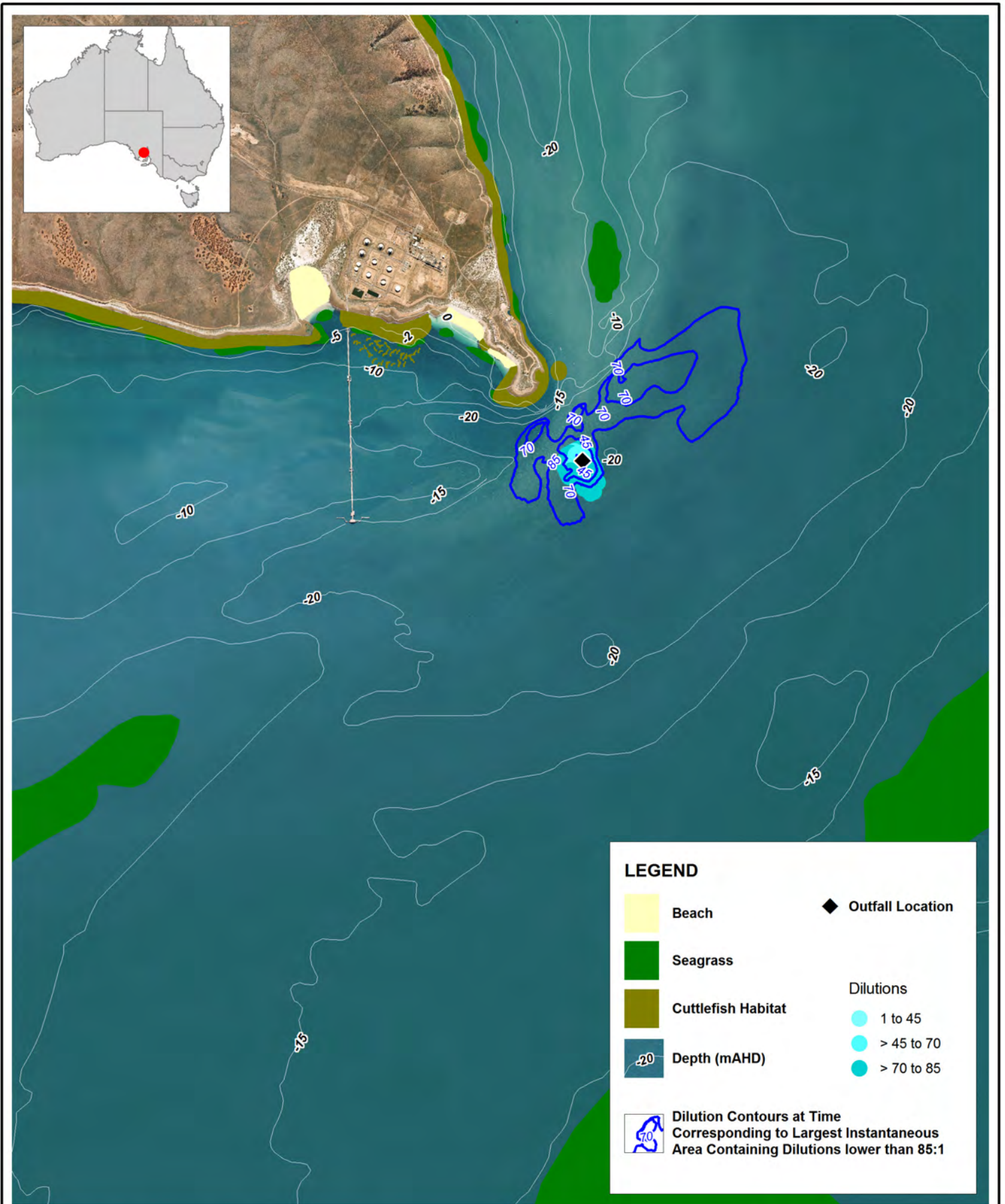
Rev:
A

BMT WBM endeavours to ensure that the information provided in this map is correct at the time of publication. It does not warrant, guarantee or make representations regarding the currency and accuracy of information contained in this map.

Air photo from Google Earth.



Filepath :



Title:
10th Percentile dilution for 1 year simulation period

Figure:
3-26

Rev:
A

BMT WBM endeavours to ensure that the information provided in this map is correct at the time of publication. It does not warrant, guarantee or make representations regarding the currency and accuracy of information contained in this map.

Air photo from Google Earth.



0 1 2km
 Approx. Scale



www.wbmpl.com.au

Filepath :

The areas (i.e. spatial extents) for each dilution target and percentile corresponding to the above maps are presented in Table 3-11, where it can be seen that, for the one year simulation period, the 1st percentile dilution areas for 70:1 and 85:1 targets are approximately one tenth of the corresponding 0th dilution percentile areas. This indicates that a footprint determined by 0th percentile dilutions is considerably larger than the corresponding 1st percentile area at Point Lowly. It is noted again that neither refer to instantaneous conditions, but are cumulative footprints over the entire year of simulation.

Table 3-11 Areas for the dilution target percentiles

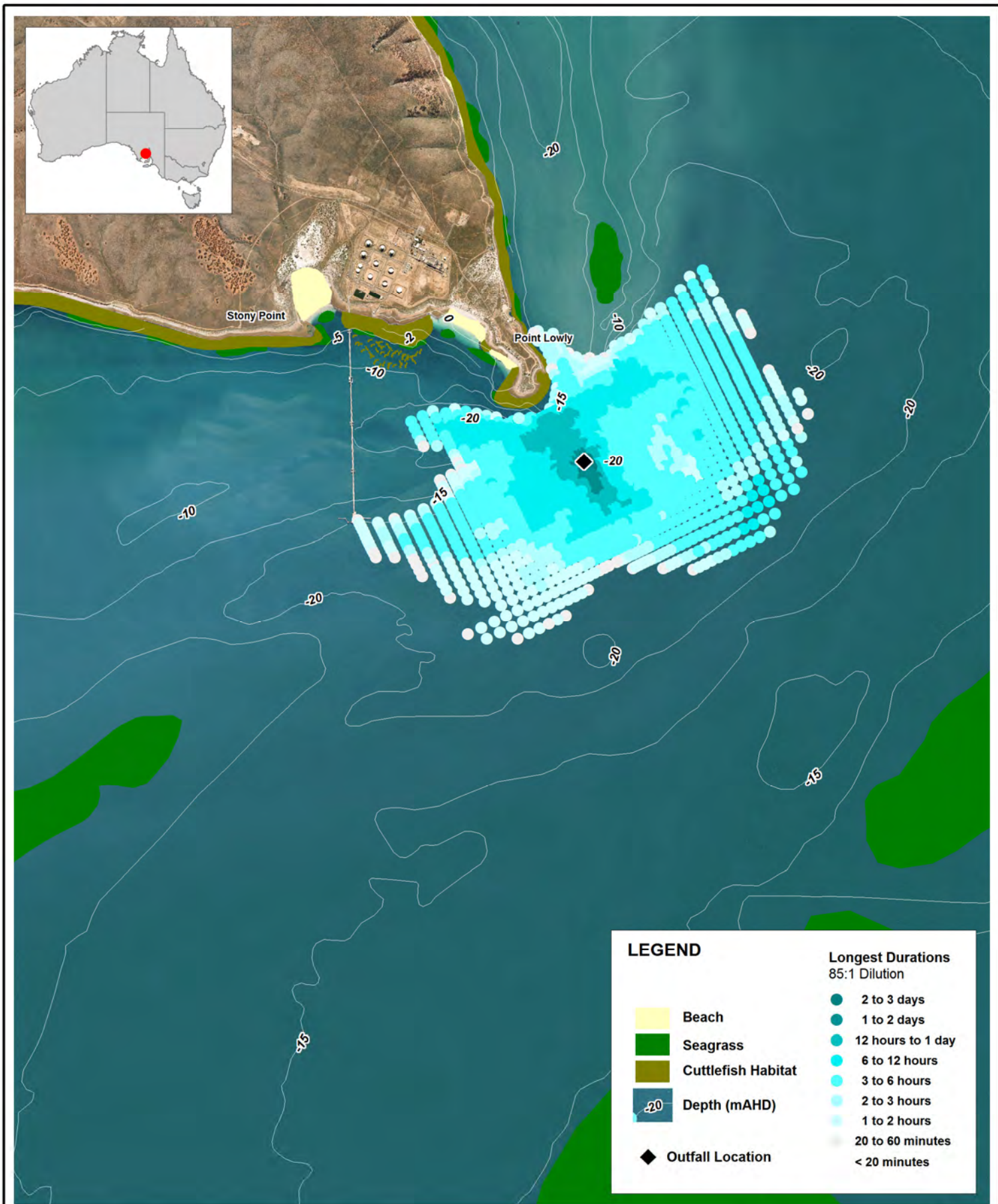
Percentile	Area < 45:1 Dilution (m ²)	Area < 70:1 Dilution (m ²)	Area < 85:1 Dilution (m ²)
0th	22,640	3,842,900	10,457,000
1st	0	314,700	1,064,500
10th	0	59,900	134,100
50th	0	0	0

It is also noted that the previous figures represent dilution maps slightly different in character from those presented in the DEIS, with this difference manifest primarily as a reduction in the spatial extents of low dilution zones. The differences are related to the following:

- a) The SEIS maps are produced over a one year period, whereas the DEIS maps were generated over a 40 day period;
- b) The SEIS maps include a spatially variant long term (background) tracer initial condition whereas the majority of the DEIS maps were produced with no long term (spin-up) influences included within the simulation framework. Where long term effects were included in the DEIS, it was only as a single (spatially invariant) number;
- c) The SEIS model (from which the maps and data were generated) was of a much higher temporal and spatial resolution (24 seconds and minimum 40 metres, respectively) compared to the DEIS 'mid field' model (8 minutes and 200 m, respectively). This results in much less numerical diffusion (see DEIS Appendices for a detailed explanation of this process) in the SEIS model than the DEIS model, and hence the more accurate and controlled transport of low dilution brine parcels; and
- d) The SEIS model was calibrated to a much higher standard (with extensive supporting targeted field data collection programs) than the DEIS model, to the extent that the SEIS model was able to better reproduce high (advective) currents, again leading to better representation of brine movement compared to the DEIS.

The SEIS model also used a sophisticated linkage to a supporting near field model (explained in detail in Section 3.6) superior to that used in the DEIS, thus providing a more realistic and defensible suite of predictions than previously presented.

In a process similar to that presented for the curtains in Table 3-8 to Table 3-10, longest duration that modelled dilutions were lower than the 85:1, 70:1, and 45:1 dilution targets were analysed, as related to the footprints presented above. These results were compiled into "longest duration" maps and are presented in Figure 3-27 to Figure 3-29. It is noted that the outputs for the bottom sheets were set at 20 minutes resolution, and that all data was produced from the full one year simulation.



Title:
Longest durations that dilutions were lower than 85:1 over 1 year period

Figure:
3-27

Rev:
A

BMT WBM endeavours to ensure that the information provided in this map is correct at the time of publication. It does not warrant, guarantee or make representations regarding the currency and accuracy of information contained in this map.

Air photo from Google Earth.

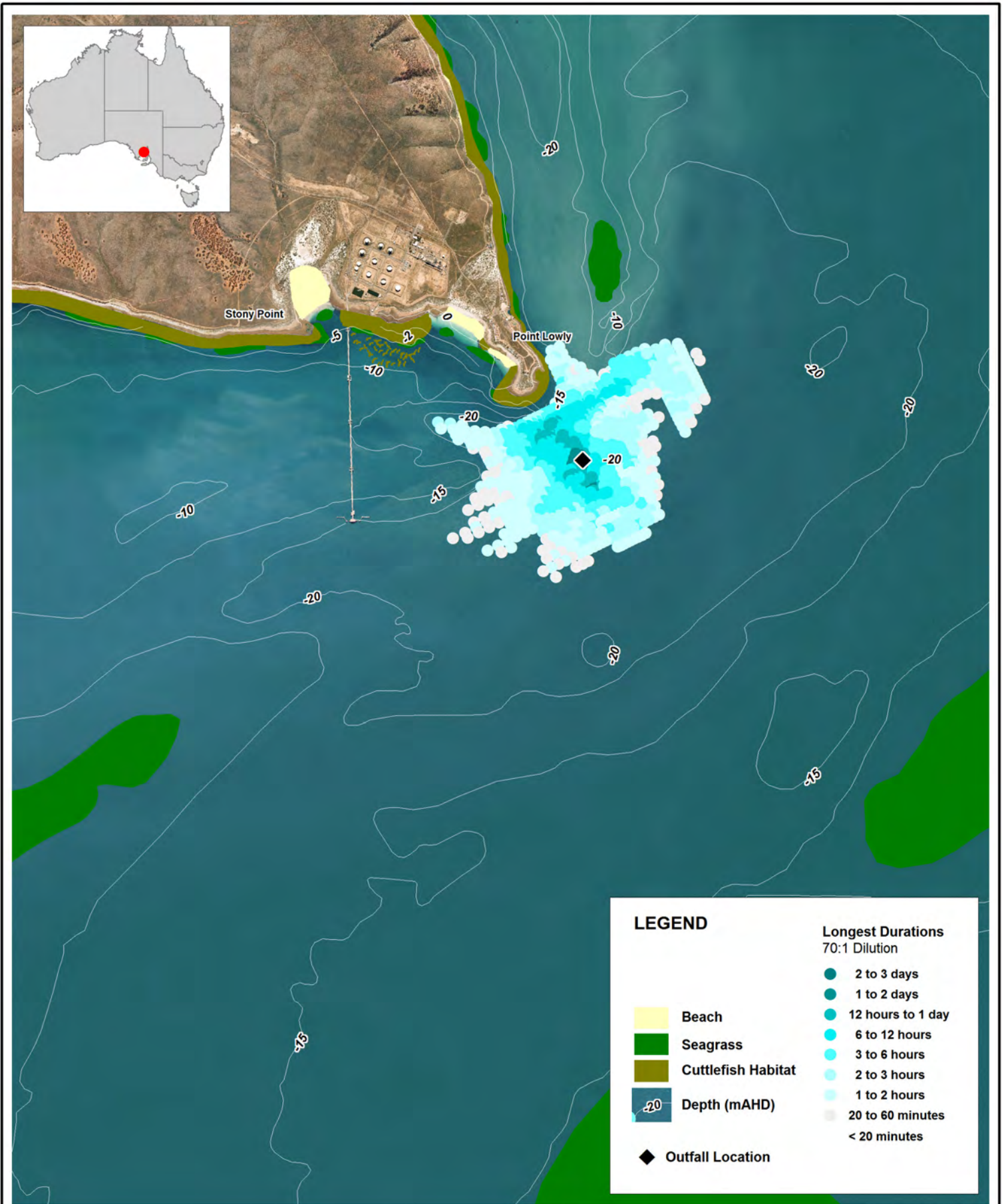


0 1 2km
 Approx. Scale



www.wbmpl.com.au

Filepath :



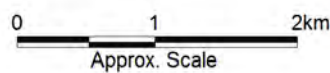
Title:
Longest durations that dilutions were lower than 70:1 over 1 year period

Figure:
3-28

Rev:
A

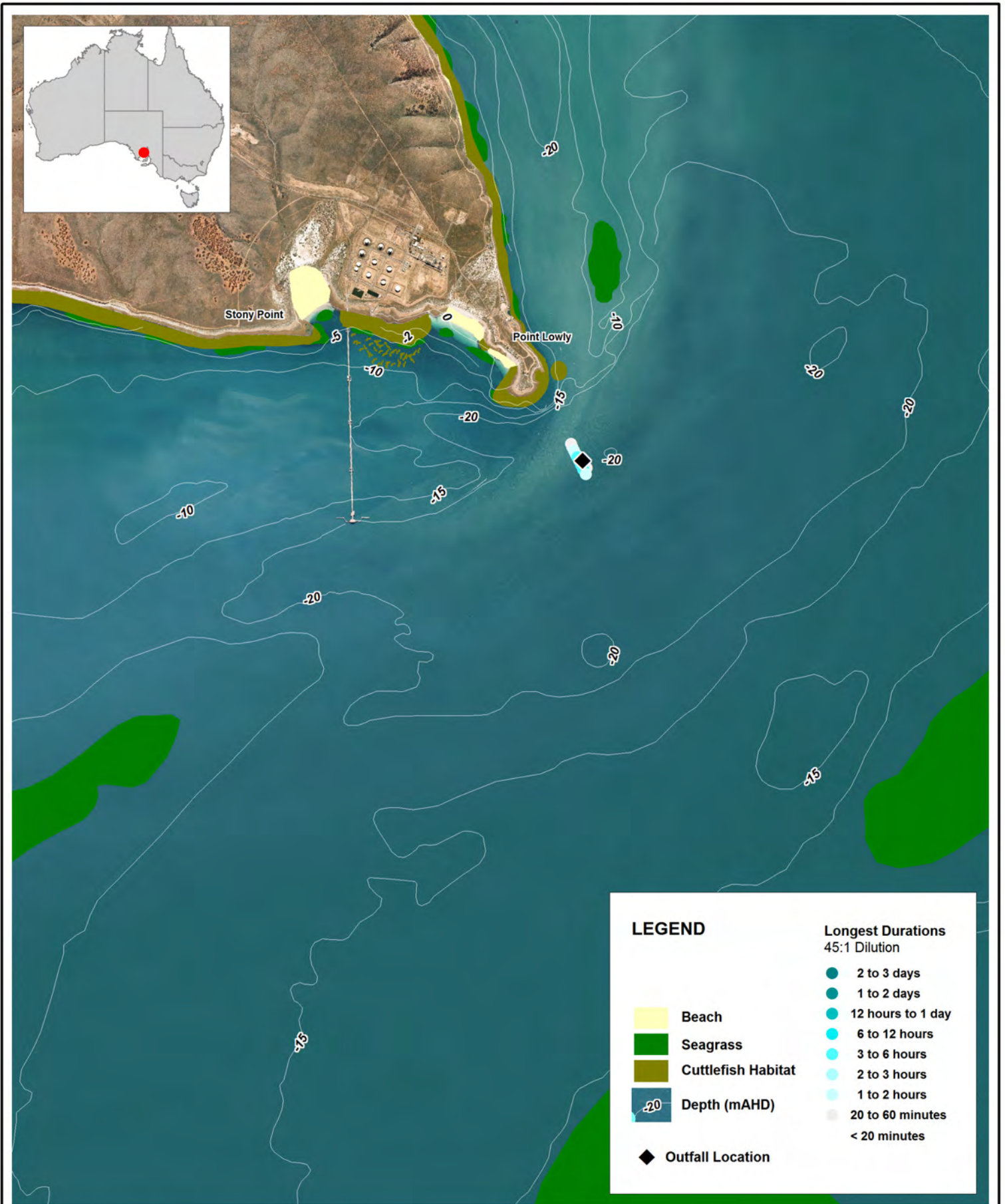
BMT WBM endeavours to ensure that the information provided in this map is correct at the time of publication. It does not warrant, guarantee or make representations regarding the currency and accuracy of information contained in this map.

Air photo from Google Earth.



www.wbmpl.com.au

Filepath :



Title:
Longest durations that dilutions were lower than 45:1 over 1 year period

Figure:
3-29

Rev:
A

BMT WBM endeavours to ensure that the information provided in this map is correct at the time of publication. It does not warrant, guarantee or make representations regarding the currency and accuracy of information contained in this map.

Air photo from Google Earth.



0 1 2km
 Approx. Scale

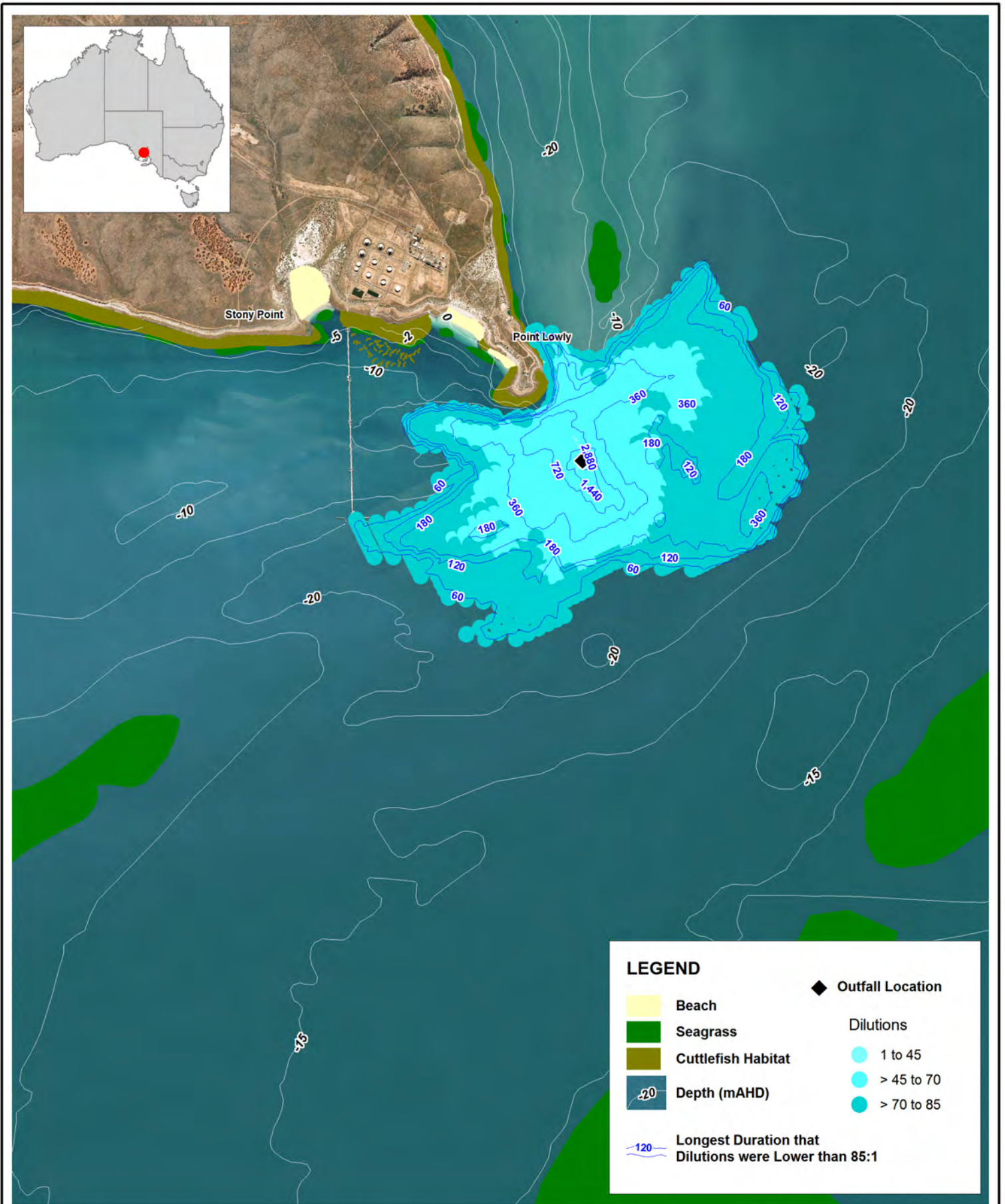


www.wbmpl.com.au

Filepath :

Consistent with previous footprint maps, Figure 3-27 to Figure 3-29 show that low dilutions were persistent for relatively longer times only in the immediate vicinity of the diffuser. Conversely, at the boundary of the minimum (0th percentile) dilution footprint, the longest duration of dilutions below the target were generally less than one hour.

In order to provide some context for the spatial extents of the 0th percentile dilution map, Figure 3-30 is a reproduction of Figure 3-24, but with the contours of longest duration of dilutions below the 85:1 target overlain (as derived from Figure 3-27). The figure shows that the durations decrease with increasing distance from the diffuser. For example, dilutions were lower than 85:1 for up to 12 hours at approximately 600 m from the diffuser, but were half this duration at approximately 1,400 m.



Title:
**0th Percentile dilution overlain with longest duration
 that dilutions were lower than 85:1 over 1 year period**

Figure:
3-30

Rev:
A

BMT WBM endeavours to ensure that the information provided in this map is correct at the time of publication. It does not warrant, guarantee or make representations regarding the currency and accuracy of information contained in this map.

Air photo from Google Earth.



0 1 2km
 Approx. Scale



www.wbmpl.com.au

Filepath :

Finally, Figure 3-31 presents timeseries of instantaneous bottom layer footprint areas under each dilution target over the entire year simulation. In all cases, the instantaneous footprint areas are very much less than the year long (cumulative) respective 0th percentile areas reported in Table 3-11.

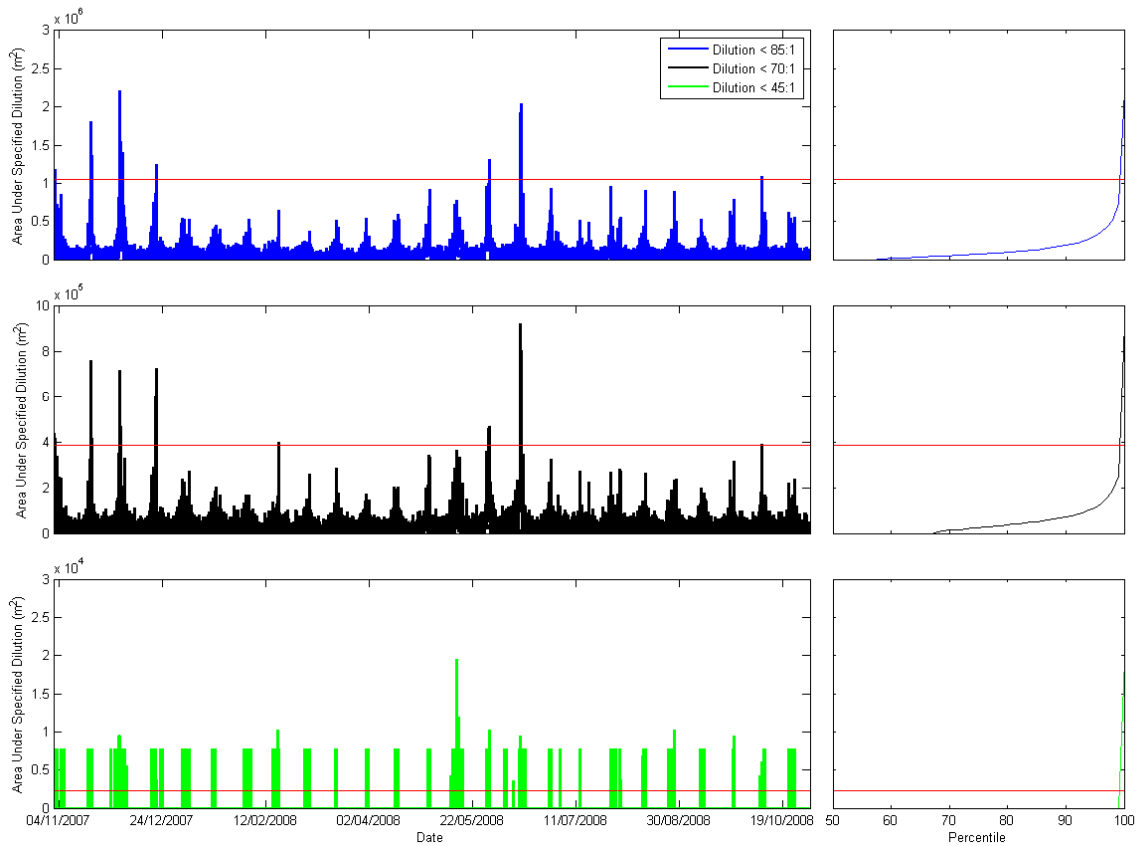


Figure 3-31 Time series for areas encompassing the dilution targets. Red line indicates an area equivalent to one tenth of the area of the 0th percentile dilution presented in Table 3-11.

As a means of assessing the likely brine footprint characteristics under persistently poor mixing conditions, a (hot-started) two-day simulation in which the wind stress was set to zero was executed for the period in which the plume area of dilution 85:1 was the largest across the entire one year simulation period. This occurred between 03 December and 05 December 2007 (see Figure 3-31). It is noted that (not surprisingly) these simulations coincided with a dodge tide period. The timeseries of the footprint areas for the different dilution targets across this two-day simulation period are presented in Figure 3-32 (these are analogous to the timeseries presented in Figure 3-31).

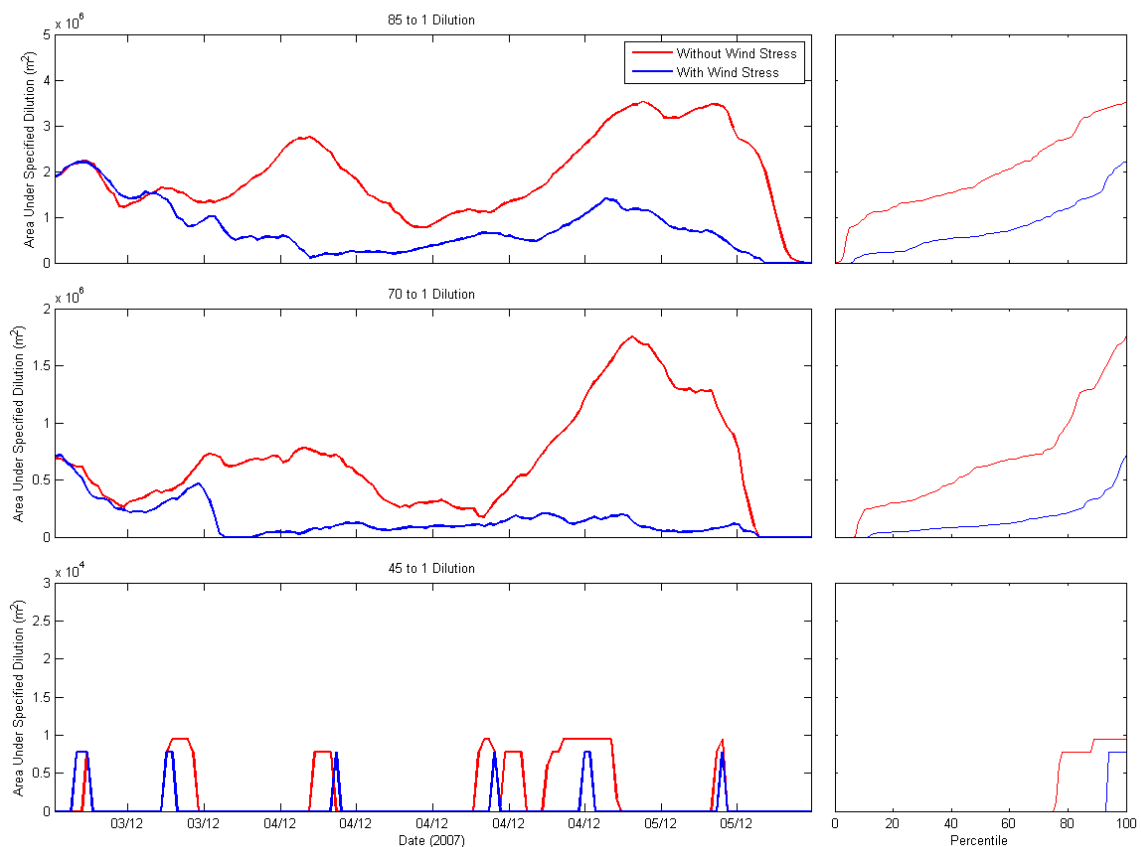


Figure 3-32 Time series for areas encompassing the dilution targets between 03 December and 05 December 2010 for cases with and without wind stress.

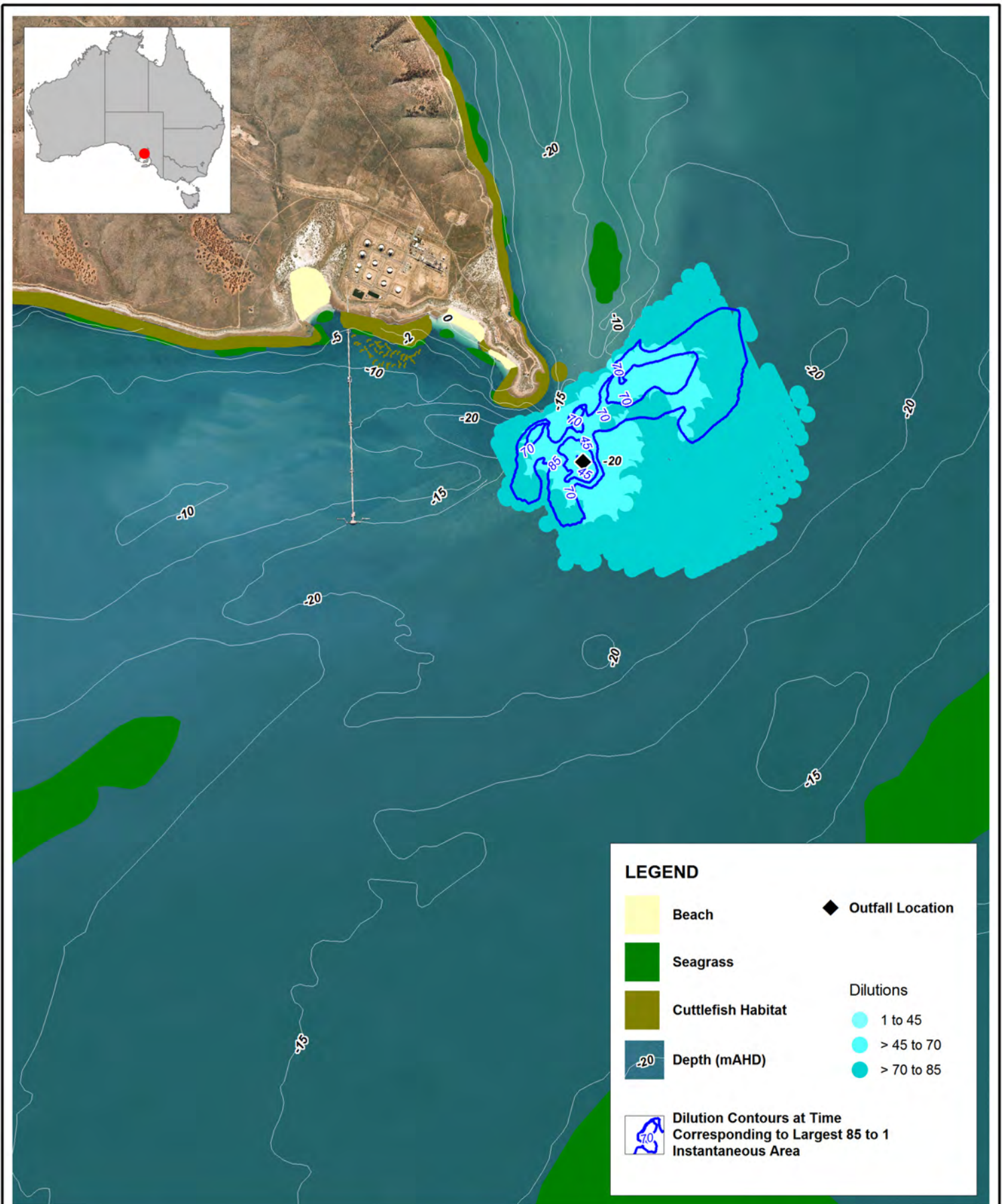
The figure reveals that the areas under a given dilution target are larger in the absence of wind. The areas defining dilutions lower than 45:1 are not significantly different from one case to another, as these were primarily controlled by the nearfield dilution. Contrastingly, the areas defining the higher dilutions appear more responsive to hydrodynamic forcing conditions (i.e. wind mixing), as expected.

The 0th percentile dilution footprint areas for the two-day simulations are provided in Figure 3-33 (with wind stress) and Figure 3-34 (without wind stress), with corresponding areal values provided in Table 3-12. For comparison purposes, the contour lines derived from the 0th percentile footprint in Figure 3-33 (with wind stress) have been overlain on the footprint map in Figure 3-34 (no wind stress).

Table 3-12 Areas for the 0th percentile dilution target over 2 days simulation period

Wind Stress	Area < 45:1 Dilution (m2)	Area < 70:1 Dilution (m2)	Area < 85:1 Dilution (m2)
Included	7,800	715,300	7,015,300
Not Included	9,400	1,758,000	8,444,400

With the exception of the 70:1 dilution target, footprint areas between the two simulations were of the same order of magnitude, albeit with different spatial distributions. With the exception of the 45:1 dilution target, the footprint areas obtained for the simulation without the inclusion of the wind stress were the same order of magnitude of the footprint areas obtained for the entire 1-year simulation.



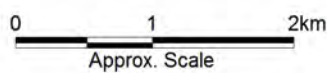
Title:
**0th Percentile (minimum) dilution map
 for the 2-day simulation period with wind stress**

Figure:
3-33

Rev:
A

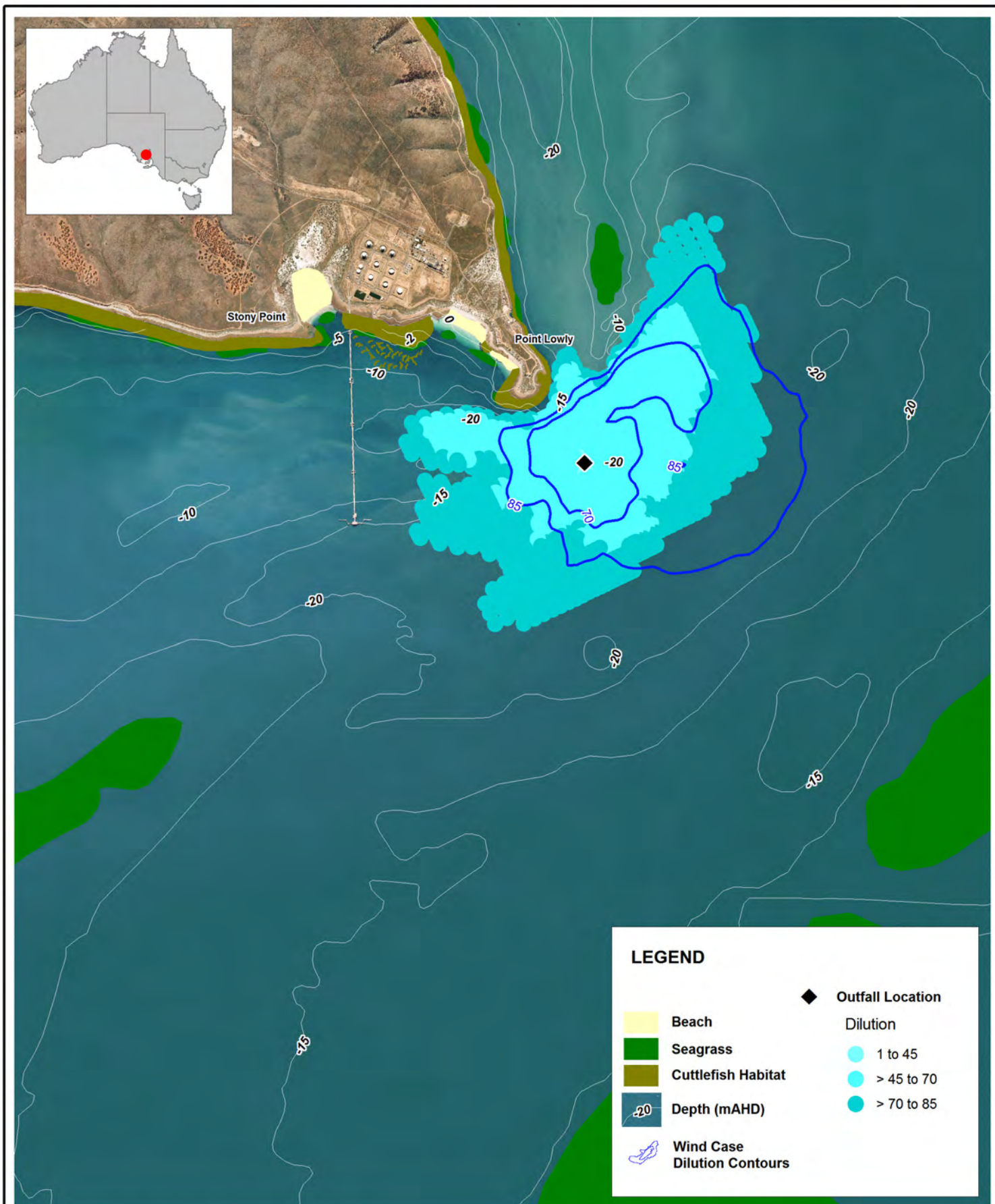
BMT WBM endeavours to ensure that the information provided in this map is correct at the time of publication. It does not warrant, guarantee or make representations regarding the currency and accuracy of information contained in this map.

Air photo from Google Earth.



www.wbmpl.com.au

Filepath :



Title:
**0th Percentile (minimum) dilution map
 for the 2-day simulation period without wind stress**

Figure:
3-34

Rev:
A

BMT WBM endeavours to ensure that the information provided in this map is correct at the time of publication. It does not warrant, guarantee or make representations regarding the currency and accuracy of information contained in this map.

Air photo from Google Earth.



0 1 2km
 Approx. Scale



Filepath :

3.7.4 Rate of Change of Salinity

Data collected as part of a targeted field monitoring program conducted to support this modelling study (Appendix H5.2) were interrogated to characterise the natural rate of change of salinity experienced near the proposed desalination plant discharge site (site a, or B3 in Appendix H5.2). These data, together with baseline and desalination model predictions of the same, are presented in Figure 3-35.

Analysis of the field data (which were appropriately re-sampled to ensure a tolerable noise to signal ratio) found that salinity changes of up to $0.8 \text{ gL}^{-1}\text{hr}^{-1}$ occur at this site naturally. Despite being over a different period to the 2009 measurements, the baseline model was able to reproduce the magnitudes of the rates of change measured at site a, as well as the modulation of this signal with respect to tidal forcing. Other model sites revealed similar baseline behaviour. To demonstrate this more clearly, the percentile distributions of the timeseries presented in Figure 3-35 are provided in Figure 3-36. The percentile distributions of the measurements and baseline predictions (top left panel) are similar in shape and extents, despite being over different time periods.

Figure 3-35 suggests that the inclusion of a desalination discharge increases the rate of change of salinity at some model sites, with this effect being most pronounced at or near the diffuser (sites x and a). This effect is much less pronounced at site u, which is representative of cuttlefish communities, with the panel corresponding to site u in Figure 3-36 showing very similar percentile distributions between the baseline and desalination simulations.

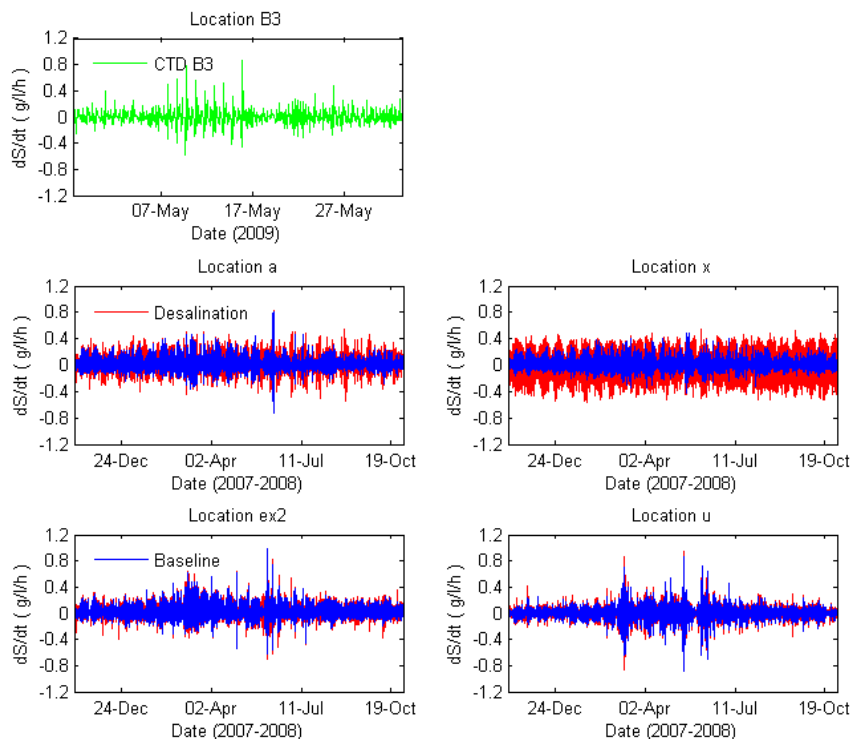


Figure 3-35 Time series of the rate of change of salinity at the bottom for points a, x, ex2, and u. Red: with proposed desalination outfall. Blue: baseline. Green shows the field measurements.

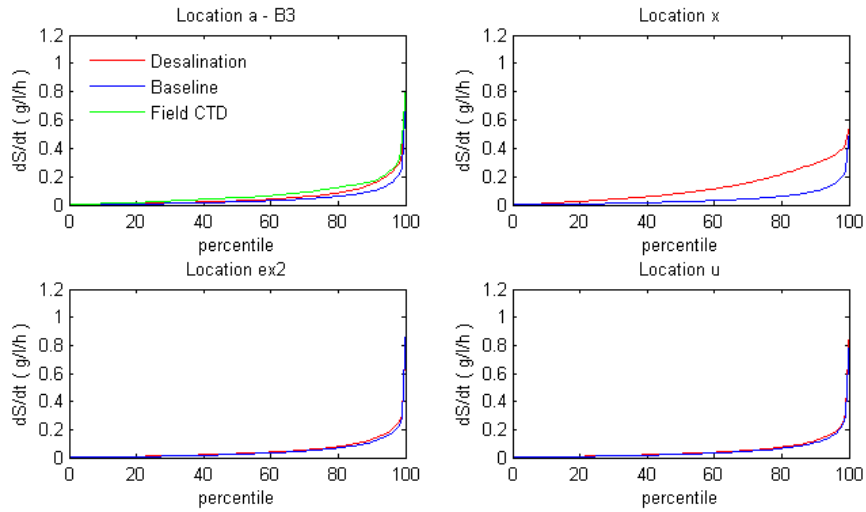


Figure 3-36 Percentile distribution of the rate of change of salinity at the bottom for points a, x, ex2, and u. Red: with proposed desalination outfall. Blue: baseline. Green shows the field measurements.

4 LONG TERM SIMULATIONS

In order to understand any long term influences of the proposed return water discharge on gulf wide processes, a lower resolution model was derived from both the previously described high resolution model and, in some ways, the DEIS low resolution model. In contrast to the high resolution model, the intent of the low resolution model was to provide indications of gross large scale and long term trends (primarily in salinity), and the likely response of these trends to climate change and desalination discharge at Point Lowly. This section describes the low resolution model and applies it to long term (no climate change) simulations.

It is noted for clarity that throughout this and following sections, 'Northern Spencer Gulf' refers to the portion of Spencer Gulf that is north of latitude 33 0.00' S.

4.1 Model Schematisation

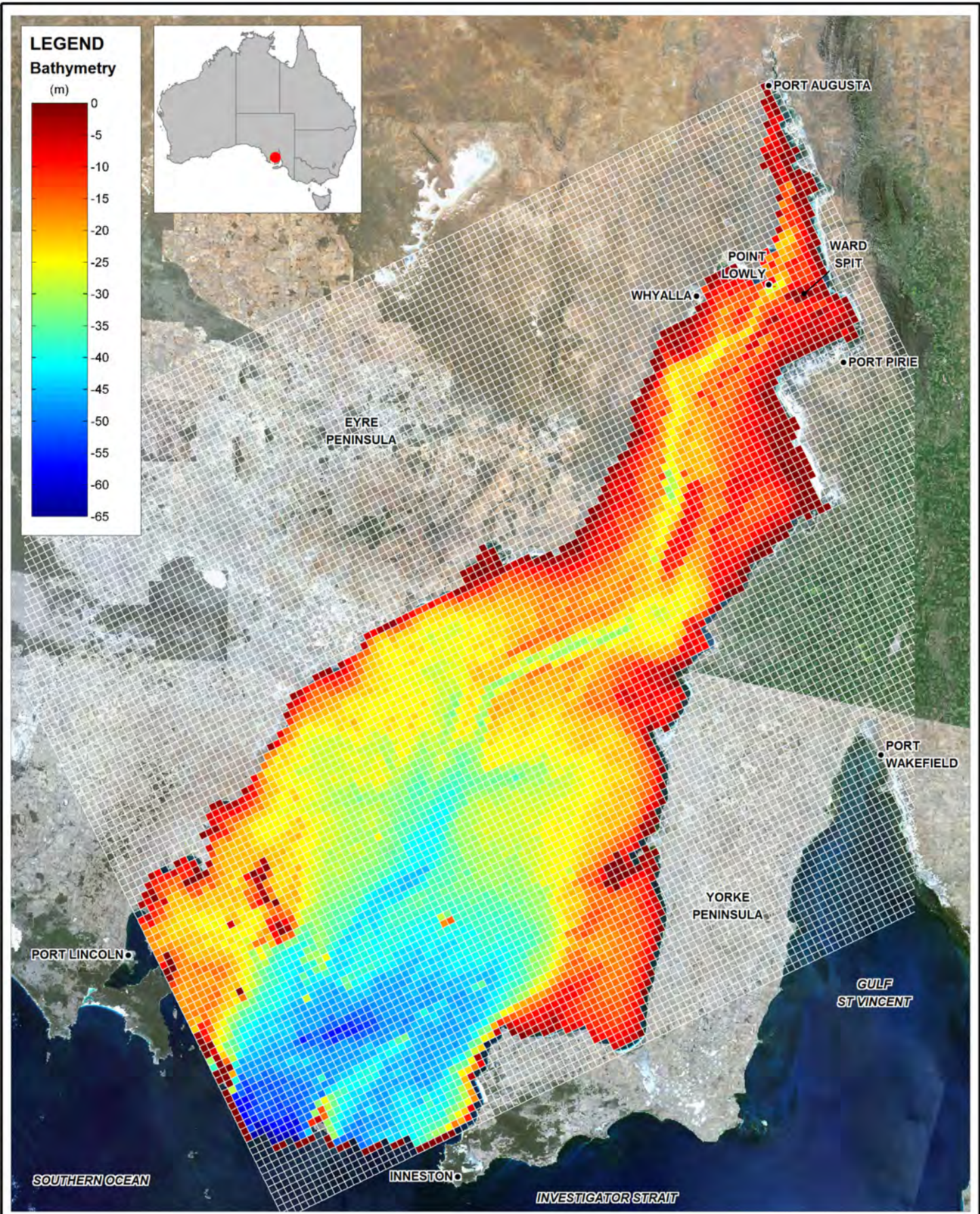
4.1.1 Modelling Platform

As per the DEIS, ELCOM was again used for these low resolution simulations.

4.1.2 Model Grid and Bathymetry

The model domain was designed to cover a similar area used in the high resolution model previously validated (SEIS Appendix H5.2) and the DEIS 'far field' model. As per the DEIS, the model domain was discretised using a uniform 2 km grid size in both horizontal directions and the model bathymetry was extracted from the Digital Elevation Model presented in (SEIS Appendix H5.2). At this 2 km resolution, the resultant bathymetry was largely unchanged from that used in the DEIS.

The horizontal grid superimposed on the model bathymetry is presented in Figure 4-1. A non-uniform grid size was used in the vertical direction (Figure 4-2). The resulting mesh consisted of 132 by 114 x 31 cells with a total of 106,060 maximum wet cells. An 1800 seconds time step was chosen to ensure model stability and model output compatible with the high resolution model.

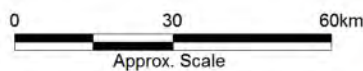


Title:
Low resolution model grid and bathymetry level referenced to Australian height datum (mAHD)

Figure:
4-1

Rev:
A

BMT WBM endeavours to ensure that the information provided in this map is correct at the time of publication. BMT WBM does not warrant, guarantee or make representations regarding the currency and accuracy of information contained in this map.



Filepath :

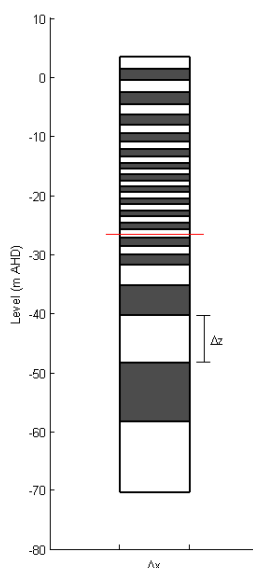


Figure 4-2 Vertical grid distribution. Red line indicates seabed level at the proposed diffuser location

4.1.3 Simulation Period

Simulations were performed from November 2004 to November 2072. November was chosen as the starting month as this corresponds to generally low salinities in the gulf following baroclinic salt ejection.

4.1.4 Initial Conditions

Similarly to the high resolution model presented in the SEIS Appendix H5.2, salinity and temperature data collected on 1-2 November 1983 by Dr. Rick Nunes-Vaz (Nunes 1985) and HYCOM data at the open boundary were used to provide model initial conditions.

4.1.5 Model Forcing

The low resolution model adopted the same original forcing data used in the high resolution model previously validated (SEIS Appendix H5.2). This forcing included:

- The salt lake inflows in the northern boundary of the domain;
- The inflows and outflows associated with the Port Augusta Power Station;
- Hourly water surface elevations at the open boundary conditions as derived from the combination of global tide model with mean surface elevations obtained from a global data assimilation model. These data spanned only 2004 to 2008 so were extended over the 70 year simulations using harmonic analyses (see below);
- Daily temperature, and salinity at the open boundary conditions as derived from a global data assimilation model;

- Hourly and approximately 15 km (square grid) spatial resolution meteorological forcing (air temperature, solar radiation, net long wave radiation, relative humidity, wind speed and wind direction) as derived from the Weather Research Forecast model; and
- Daily rainfall derived from the Bureau of Meteorology SILO database.

The open boundary conditions were imposed in the South and South Eastern ends of the rotated domain (Figure 4-1).

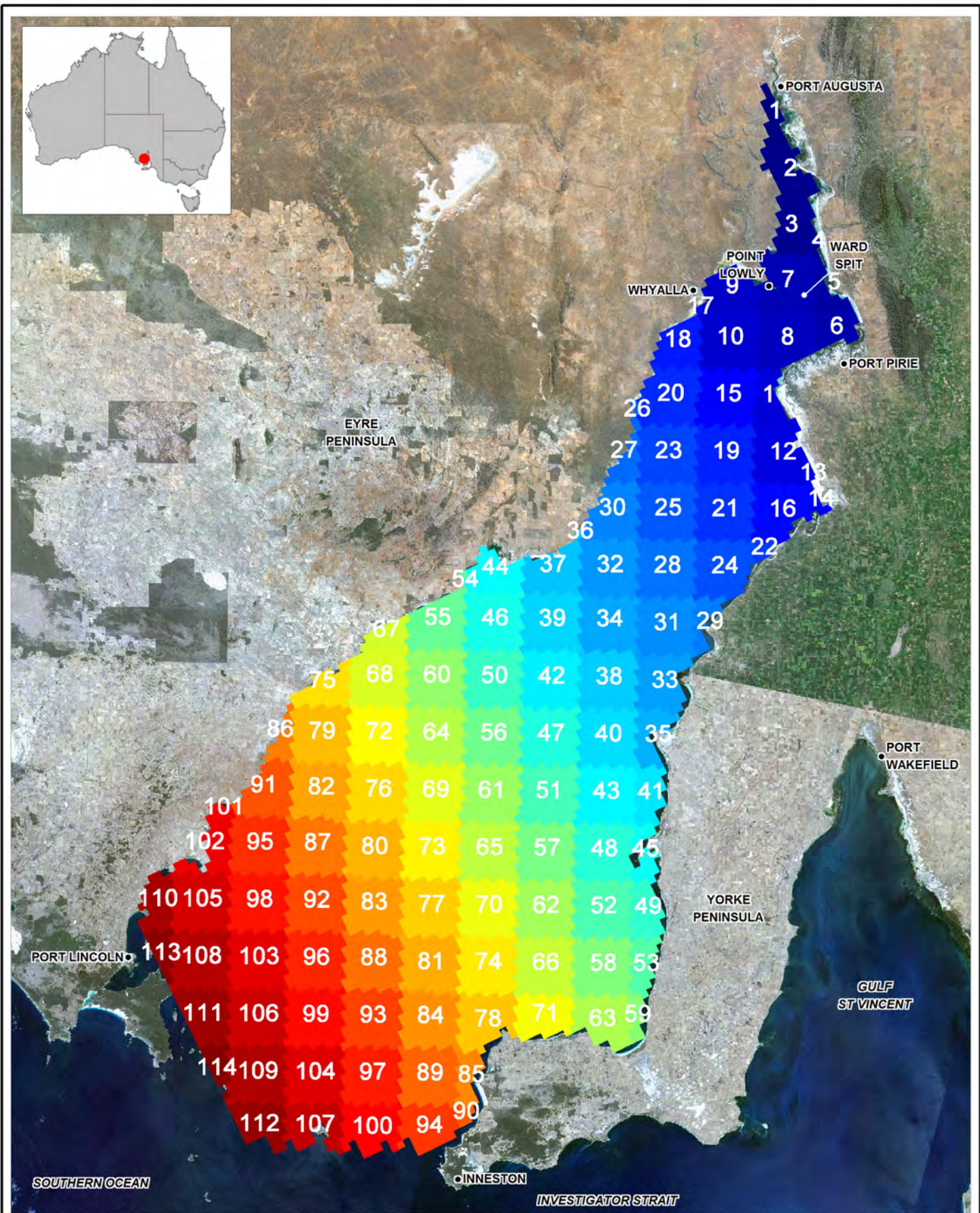
The meteorological forcing distribution at the free surface is shown in Figure 4-3 and the forcing at selected boundary condition sets from Figure 4-3 are provided in Figure 4-4. The data is plotted at daily resolution for clarity and reveals the strong latitudinal variability, particularly in the relative humidity and air temperature that are the drivers for increased summer evaporation rates in the Northern Gulf.

The meteorological data forcing and open boundary data sets were repeated (unchanged) to span the desired simulation period. Climate change analyses altered both of these systematically (see Section 0). To avoid discontinuities, tidal boundary data for the simulation period was reconstructed from harmonic analysis of the 2004-2008 data using 68 harmonic constituents. The residuals between the raw tidal data and the harmonic components of the 2004-2008 period were then added to the harmonic components in a similar fashion of the meteorological and scalar data at the open boundaries. Discussion of the 2004-2008 data is presented with the climate change forcing parameterisation in Section 5.2.

4.1.6 Desalination Input

When required, the long term average desalination discharge rate ($3.6 \text{ m}^3\text{s}^{-1}$) was used in these simulations, at the instruction of BHP Billiton.

The brine injection technique described in Section 3.6.4 for the high resolution model was also applied to the current simulations. The only difference was that depth averaged velocities used to enter the CFD lookup table of dilutions were not sourced directly from the low resolution model. This is because velocities from the low resolution model at the location of the proposed discharge were consistently lower than velocities computed with the high resolution model. This occurred because the 2 km grid was too coarse to describe the fine scale and non-uniform features in the flow convergence zone through “The Rip” (i.e. the diffuser site). As such, linear scalings between depth-averaged velocity magnitudes in the low and high resolution models were developed for both ebb and flood tides (Figure 4-5), and the scaling was then applied to the dynamically extracted low resolution model velocities before looking up dilutions from the CFD results.

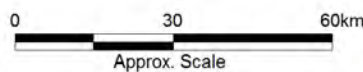


Title: **Spatial distribution of the surface boundary forcing**
 Colour code indicates area of influence of each boundary condition and has no implicit quantitative meaning.

Figure:
4-3

Rev:
A

BMT WBM endeavours to ensure that the information provided in this map is correct at the time of publication. BMT WBM does not warrant, guarantee or make representations regarding the currency and accuracy of information contained in this map.



Filepath :

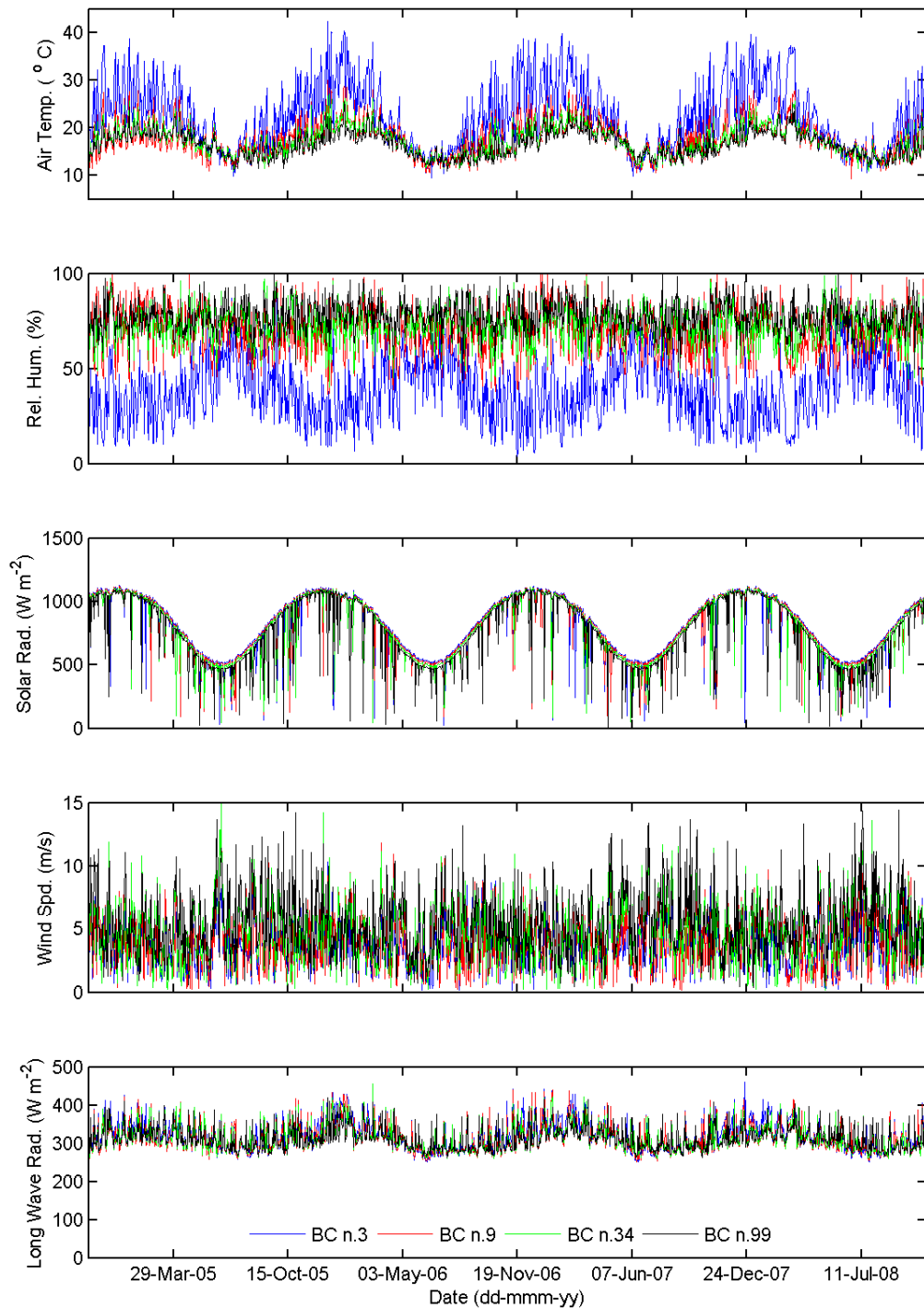


Figure 4-4 Forcing at selected surface boundary condition sets. Boundary condition numbers correlate with the values shown in Figure 4-3. Strong north-south variation in key atmospheric data sets is clear.

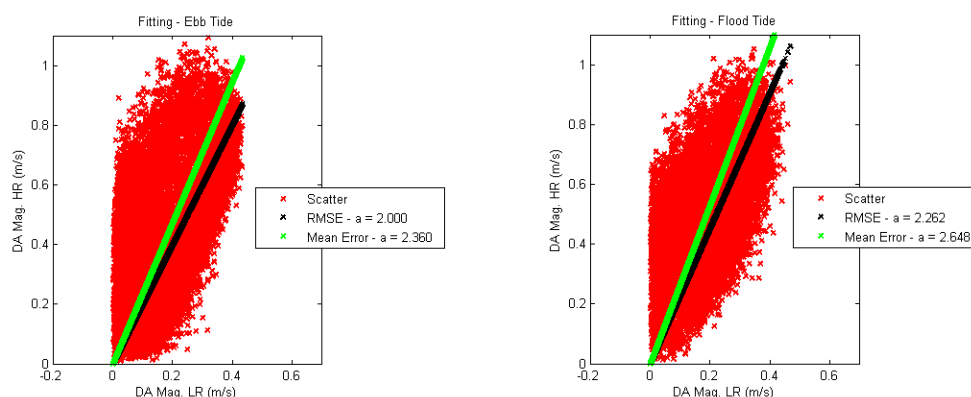


Figure 4-5 Velocity scaling between low and high resolution models at the proposed outfall location

4.2 Model Validation

Prior to executing any production simulations, the model was validated to appropriate data sets and prior model predictions. Importantly, this validation focused on demonstrating the reliable performance of the low resolution model with respect to key broad scale and long term hydrodynamic features, consistent with the subsequent intended model use and application. In particular, the processes of relevance (and those considered during the validation stage) included the salt ejection mechanism, broadscale tide amplification, and latitudinal and seasonal gradients of temperature and salinity. This level of validation is commensurate with the description of the features of broad scale processes in Spencer Gulf and has been set to match the intended model use as described above.

4.2.1 Salt Ejection

The mechanisms responsible for salt dynamics in Spencer Gulf have been extensively described in the high resolution model validation report (SEIS Appendix H5.2) and Appendices of the DEIS. The ability of the low resolution model to reproduce these dynamics is illustrated in Figure 4-6 and Table 4-1. Figure 4-6 shows very clearly the consistency between the salt fluxes given by the low and high resolution models, which were based in the same high temporal and spatial resolution forcing, indicating that both models are equivalent when used to assess the broad scale features in Spencer Gulf. Specifically, both reproduce the tendency for salt accumulation in summer and salt ejection in winter. The figure also provides the equivalent timeseries from the DEIS 'far field' model, and again this is consistent with predictions from the current low resolution model. It is noted that the data in Figure 4-6 was filtered by a moving average as detailed in the Appendix H5.2 of the SEIS, such that the patterns of accumulation and ejection could be revealed, while data presented in Table 4-1 was produced from the unfiltered timeseries.

Annual salt budgets indicated a difference of less than approximately 3% between high and low resolution models, with very similar incoming and outgoing tidal fluxes (Table 4-1). For the 2004-2005 year, the low resolution model predicted a small tendency for salt accumulation in the Gulf, which was reversed for the average of the 2004-2008 period as shown in the high resolution model results (Table 4-1). These results indicate that both modelling approaches produce a near-zero net salt flux in the gulf with equivalent seasonal dynamics at these spatial and temporal scales.

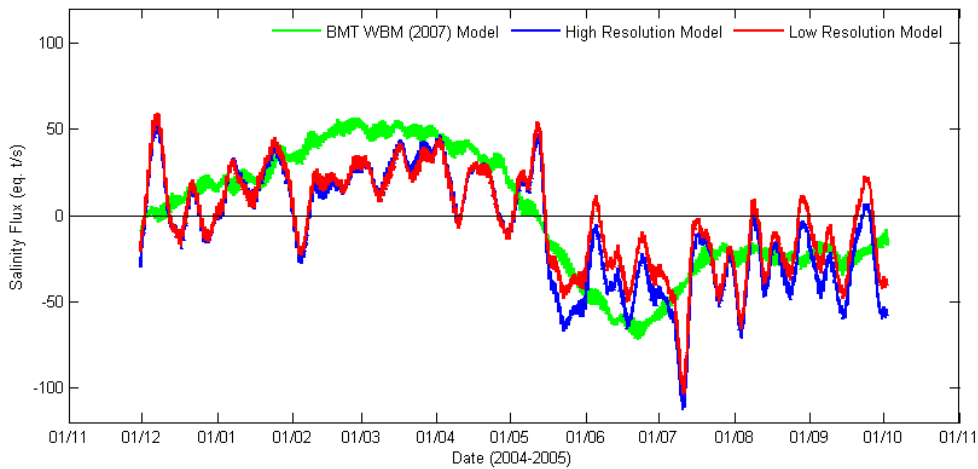


Figure 4-6 Salt fluxes obtained from the low and high resolution models

Table 4-1 Salt fluxes comparisons between high and low resolution model. Salinity values were assumed to be gL^{-1} .

Salt Flux Item	High Resolution 2004-2005	Low Resolution 2004-2005	Low Resolution 2004-2008 (Average)
	Gt an ⁻¹	Gt an ⁻¹	Gt an ⁻¹
Tidal Influx	+253	+261	+262
Tidal Eflux	-254	-261	-262
Other Inflows	+0	+0	+0

4.2.2 Salinity and Temperature Variation

Figure 4-7 and Figure 4-8 show salinity and temperature contrasted with field data collected in the 1980s (Nunes 1985) at different locations across Spencer Gulf (Port Augusta, Yatala Harbor Aquatic Reserve, Point Lowly, and Wallaroo). These data indicate that the model was able to reproduce the latitudinal trends and seasonal variations revealed in the measured data set. Salinities at Port Augusta were under predicted by the model. As the high resolution model successfully reproduced the full data range variation at Port Augusta, it is believed that the low resolution model smears out the strong salinity gradients observed in that part of the Gulf (Nunes 1985) as a result of decreased grid resolution and associated increased numerical dispersion.

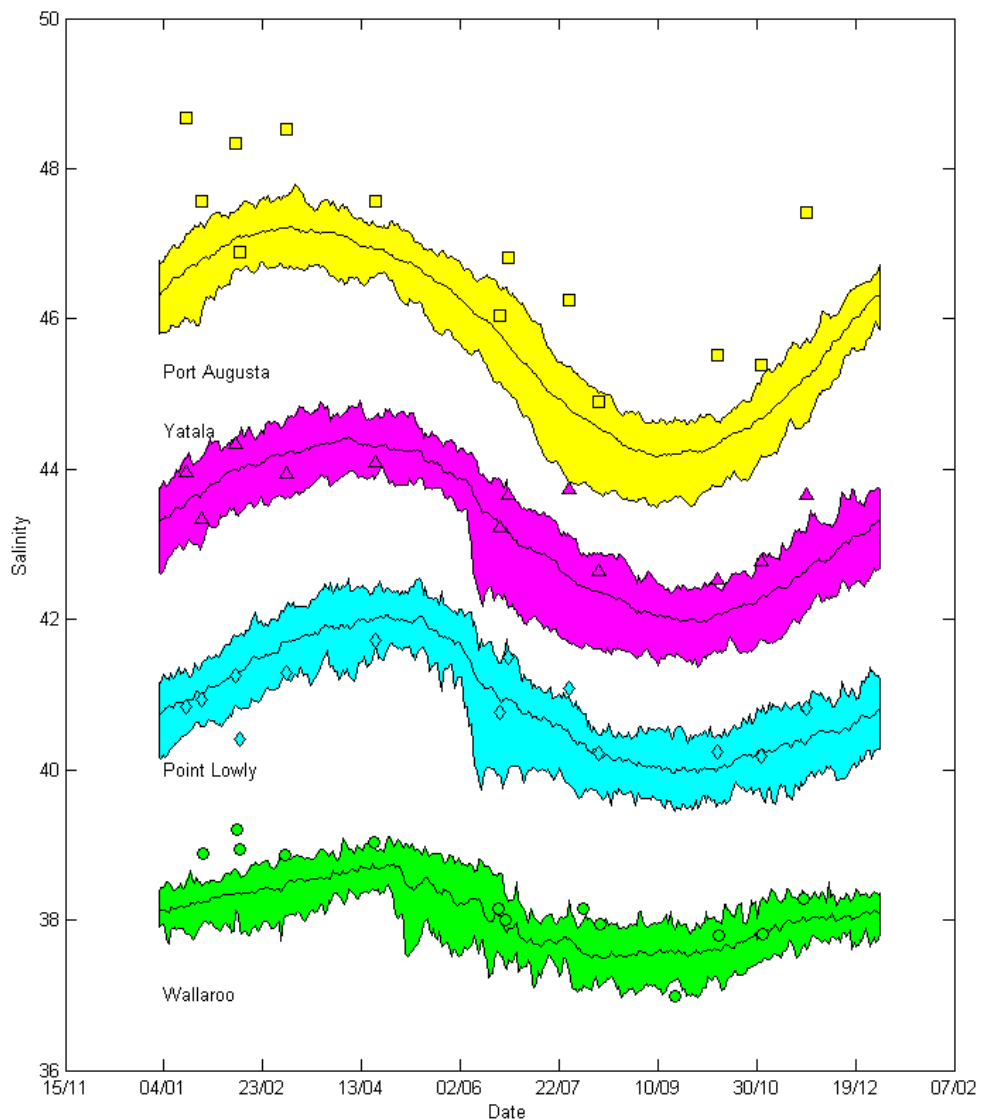


Figure 4-7 Modelled salinity evolution at different locations in the Gulf for the 2004-2008 period contrasted with field data from the 1980s (Nunes 1985). Coloured areas shows the data range evolution for each day of the year in the 2004-2008 period, the centre line shows the average for each day of the year in the 2004-2008 period, and the top and bottom lines show respectively the maximum and minimum for each day of the year in the 2004-2008 period. Field data is shown by the solid markers: circles for Wallaroo, diamonds for Point Lowly, triangles for Yatala Harbor, and squares for Port Augusta. Both modelled and field data at Port Augusta are uniformly and positively offset by 1.5 units (relative to actual values) and at Yatala Harbor by 1.0 unit. This has been done for clarity.

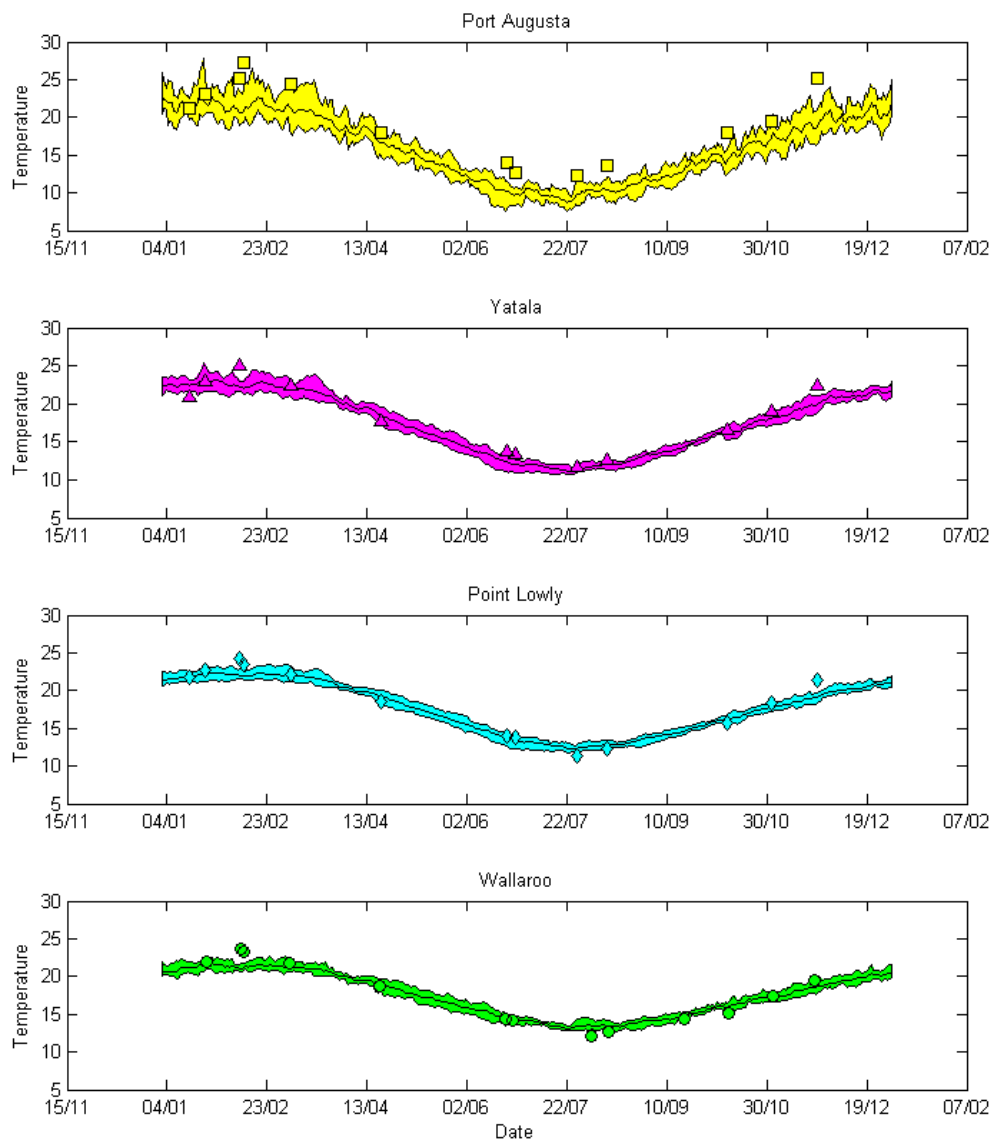


Figure 4-8 Modelled temperature evolution at different locations in the Gulf for the 2004-2008 period contrasted with field data from the 1980s (Nunes 1985). Same symbols as Figure 4-7.

4.2.3 Tidal Amplification and Modulation

The characteristics of the tides in Spencer Gulf were examined in detail during validation of the high resolution model, showing the adopted modelling framework was able to reproduce the major tidal features in Spencer Gulf:

- Tidal amplification of both diurnal and semi diurnal harmonics between Port Lincoln and Whyalla;
- Phase variation of these harmonics between Port Lincoln and Whyalla; and

- The relatively small semi-diurnal component associated with the (semi-diurnal) nodal point near Wallaroo.

Similarly to the comparisons presented in the Appendix H5.2 of the SEIS, the low resolution model simulation was contrasted to tidal data provided by Flinders Ports Corporation (FPC) at Port Lincoln, Wallaroo, and Whyalla. These comparisons were made in terms of harmonic analyses following the method described in Pawlowicz *et al.* (2002). For the harmonic analyses, the measured signal was re-sampled at the same model output resolution (3 hours) prior to the tidal decomposition. A seven-month period was used for Port Lincoln and a ten month period for the Wallaroo and Whyalla analyses. The resulting amplitude and phase of the main diurnal and semi-diurnal harmonics are presented in Table 4-2 and Table 4-3. Similarly to the high resolution model, the low resolution model did not extend into the local embayment at Port Lincoln. For this reason, the closest model point to Port Lincoln was selected to produce the comparisons. It is also noted that Port Lincoln was not used strictly to indicate model performance but instead to verify the validity of the tidal elevations used in the model boundary conditions and the model's ability to transform "deep ocean" boundary conditions to surface elevations representative of nearshore conditions.

As expected, the low resolution model presented the same tidal features of Spencer Gulf that were also reproduced by the high resolution model, particularly with respect to the general harmonic component phases (Table 4-3), tidal amplification between Wallaroo and Whyalla, and the minimal semi-diurnal tidal influence at Wallaroo (Table 4-2). In general, tidal range was slightly underpredicted in the low resolution model (Table 4-2), as expected from increased numerical dissipation associated with the lower grid resolution. This aspect is further illustrated in Figure 4-9 and Figure 4-10 where tidal elevations of the high and low resolution models are compared for Yatala Harbor, Point Lowly, and Wallaroo.

Table 4-2 Amplitude (m) of tide constituents obtained from harmonic analysis

Tidal Constituent	Port Lincoln (March to October 2005)*			Wallaroo			Whyalla		
	Field	HR Model	LR Model	Field	HR Model	LR Model	Field	HR Model	LR Model
S2	0.245	0.214	0.218	0.162	0.157	0.135	0.450	0.380	0.252
M2	0.228	0.175	0.214	0.164	0.139	0.135	0.425	0.341	0.265
K2	0.070	0.063	0.048	0.052	0.042	0.030	0.137	0.119	0.069
K1	0.234	0.196	0.228	0.338	0.318	0.285	0.433	0.438	0.367
O1	0.163	0.160	0.158	0.215	0.237	0.194	0.265	0.312	0.237
P1	0.075	0.056	0.066	0.099	0.085	0.081	0.123	0.112	0.097

* Not spatially coincident

Table 4-3 Phase (degrees) of tide constituents obtained from harmonic analysis

Tidal Constituent	Port Lincoln (March to October 2005)*			Wallaroo			Whyalla		
	Field	HR Model	LR Model	Field	HR Model	LR Model	Field	HR Model	LR Model
S2	83.5	80.3	88.3	186.1	172.3	166.4	243.4	251.9	233.4
M2	32.4	23.0	31.8	132.9	117.8	111.3	183.9	189.0	172.1
K2	83.0	78.5	86.1	184.1	167.1	164.9	239.3	248.9	234.1
K1	29.6	29.3	30.1	62.2	65.8	68.3	70.9	77.5	77.8
O1	1.0	0.8	2.5	32.7	34.5	36.0	41.4	45.8	44.9
P1	32.6	24.6	25.2	64.6	61.6	60.1	76.4	77.7	71.6

* Not spatially coincident

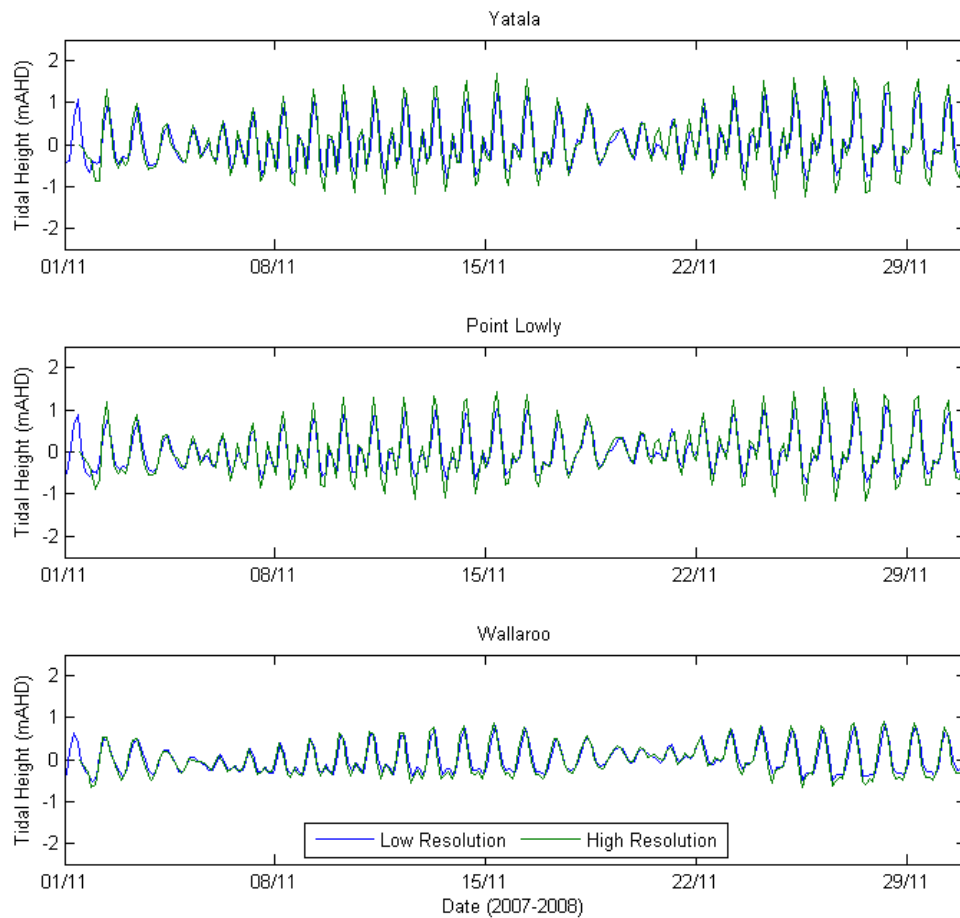


Figure 4-9 Comparison of tidal elevations obtained from the low and high resolution models November 2007. Timeseries appear 'pointed' due to the frequency of model outputs.

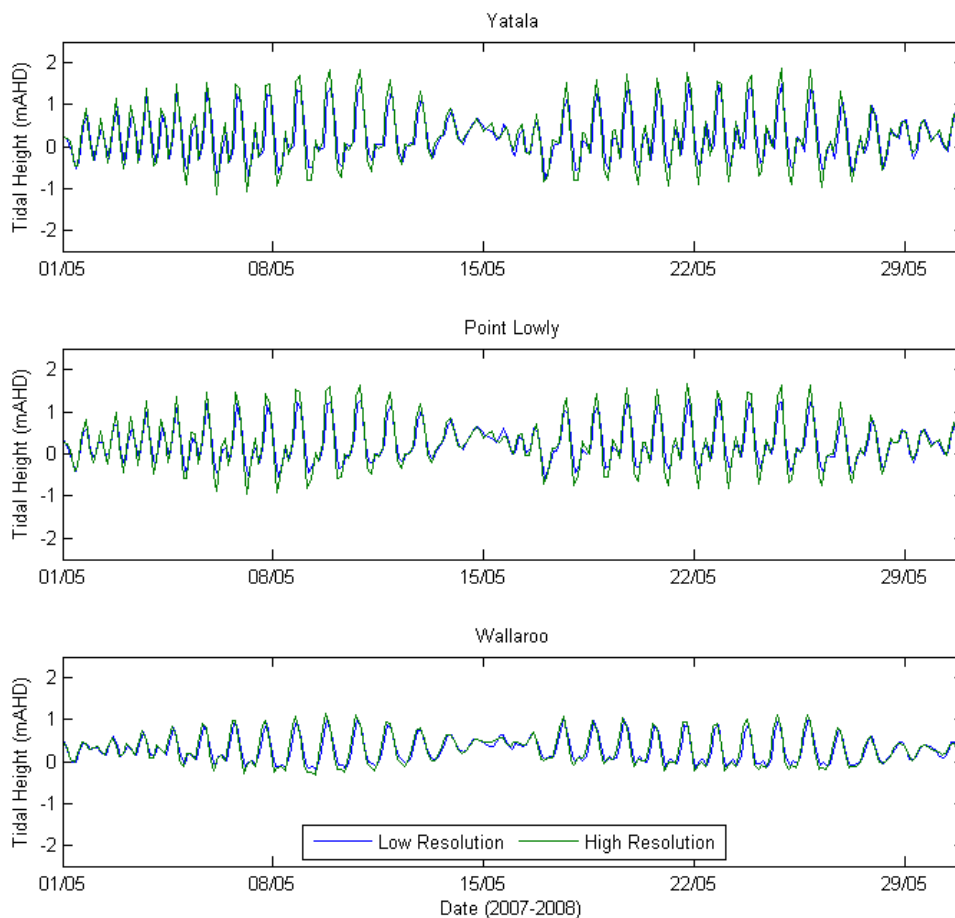


Figure 4-10 Comparison of tidal elevations obtained from the low and high resolution models in May 2008

4.3 Assessments

4.3.1 Simulations

Two simulations were executed using the low resolution model described above. These are referred to as 'B' and 'B+D' for baseline and baseline plus desalination, respectively. Details of these are provided in Table 4-4.

Table 4-4 Assumed proposed desalination plant discharges

Simulation Code	Period (Nov to Nov)	Intake Rate $m^3 s^{-1}$	Outfall Rate $m^3 s^{-1}$
B	2004-2072	0.00	0.00
B+D	2004-2072	6.5	3.6

4.3.2 Model Interrogation

Two methods of interrogating the model predictions were adopted, these being:

- 1 Timeseries extraction (primarily of salinity) at a suite of locations, namely (see Figure 4-11):
 - Northern Spencer Gulf:
 - Point Lowly;
 - Backy Point;
 - Blanche Harbor Aquatic Reserve;
 - Yatala Harbor Aquatic Reserve; and
 - Port Augusta.
 - Other:
 - Wallaroo;
 - Cowleds Landing Aquatic Reserve; and
 - Yarraville Shoals.
- 2 Spatially integrated (i.e. averaged) predictions across two distinct geographical areas, namely:
 - The entirety of Spencer Gulf; and
 - Northern Spencer Gulf, which encompassed the region north of 33.0° S.

These are presented separately below.

4.3.3 Results

4.3.3.1 Timeseries Results

Figure 4-12 and Figure 4-13 show the time evolution of seabed salinities at four of the locations in Northern Spencer Gulf and Wallaroo, over the entire simulation period. Figure 4-14 to Figure 4-16 present the same data but within selected time horizons. Note that different vertical salinity scales have been employed across the sites for ease of presentation. The figures show that both the seasonality of salinity signatures at each site, and the relativity of salinity magnitudes between sites (i.e. the north south salinity gradient), were not materially altered by the inclusion of the desalination discharge over the simulation period. The figures also suggest that the natural annual salt accumulation and discharge process continues to operate with the inclusion of the desalination discharge.

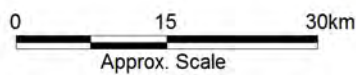


Title:
Timeseries extraction points

Figure:
4-11

Rev:
A

BMT WBM endeavours to ensure that the information provided in this map is correct at the time of publication. BMT WBM does not warrant, guarantee or make representations regarding the currency and accuracy of information contained in this map.



Filepath :

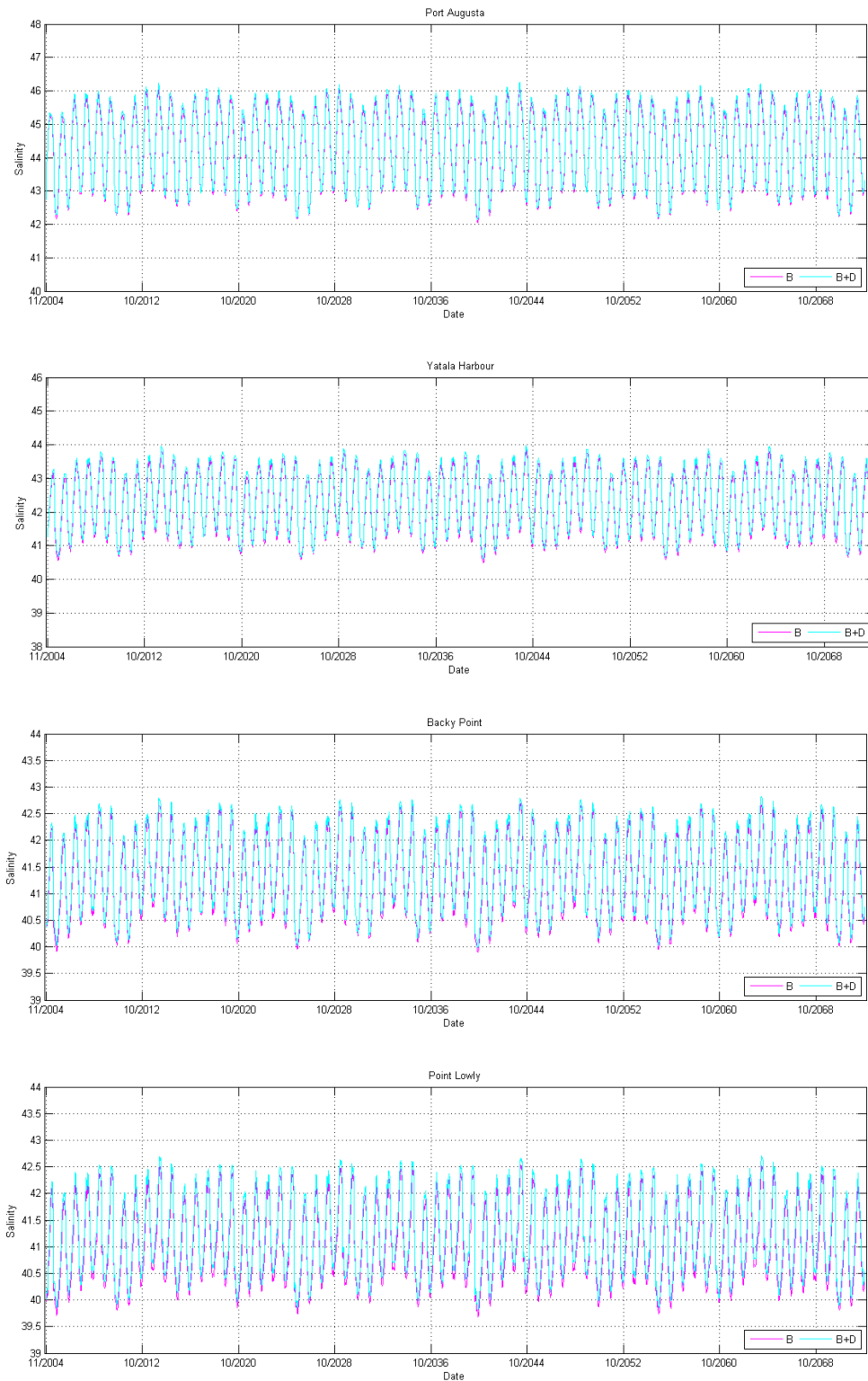


Figure 4-12 Modelled seabed salinities at Northern Spencer Gulf with (B+D) and without (B) the proposed desalination plant outfall discharge for the 2004 to 2072 period: Port Augusta (upper panel), Yatala Harbor Aquatic Reserve (centre upper panel), Backy Point (centre lower panel), and Point Lowly (lower panel).

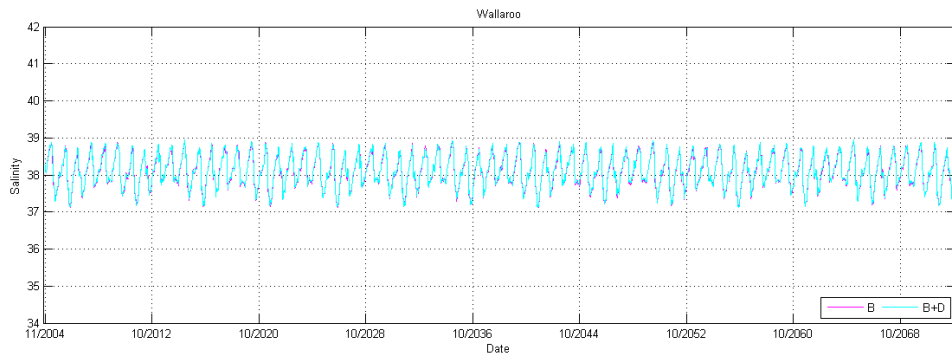


Figure 4-13 Modelled bottom salinities at Wallaroo with (B+D) and without (B) the proposed desalination plant outfall discharge for the 2004 to 2072 period.

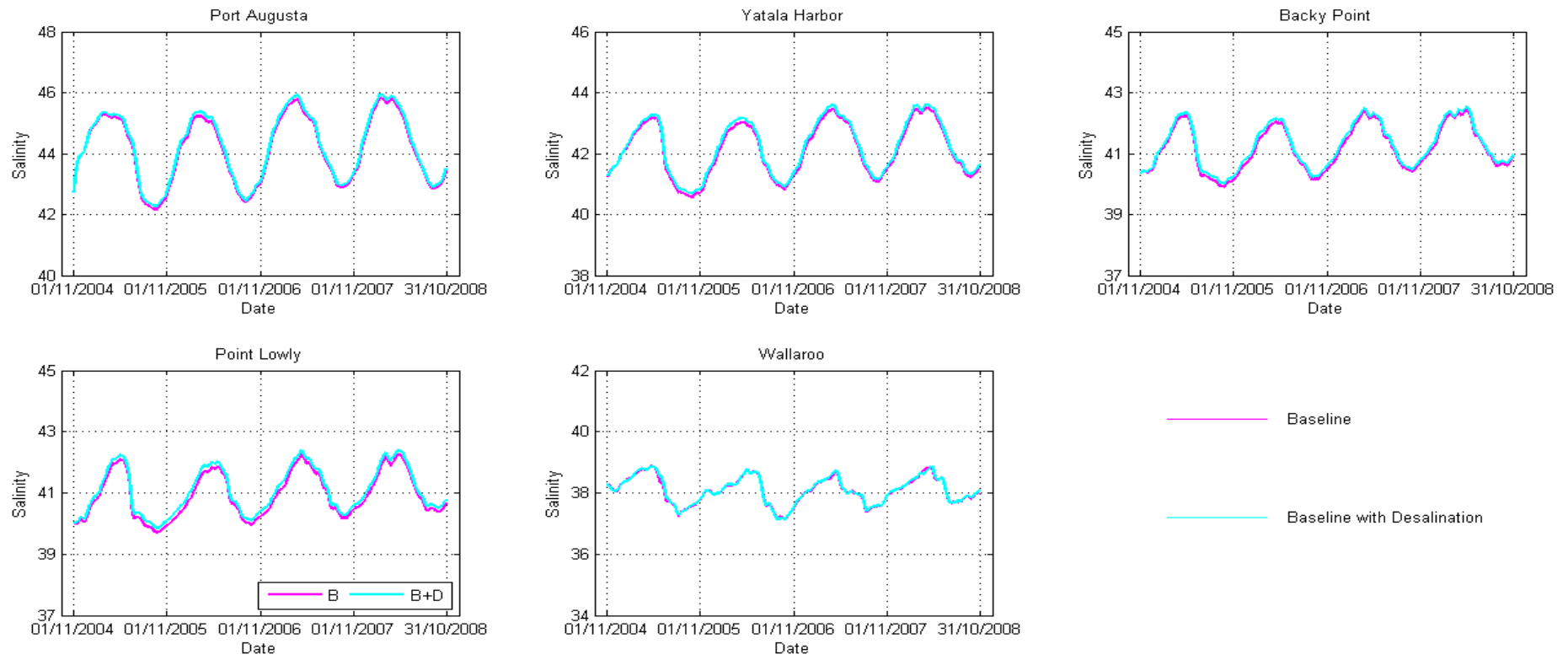


Figure 4-14 Modelled bottom salinities at Port Augusta, Yatala Harbor Aquatic Reserve, Backy Point, Point Lowly, and Wallaroo with (B+D) and without (B) the proposed desalination plant outfall discharge for the Nov 2004 to Nov 2008 period.

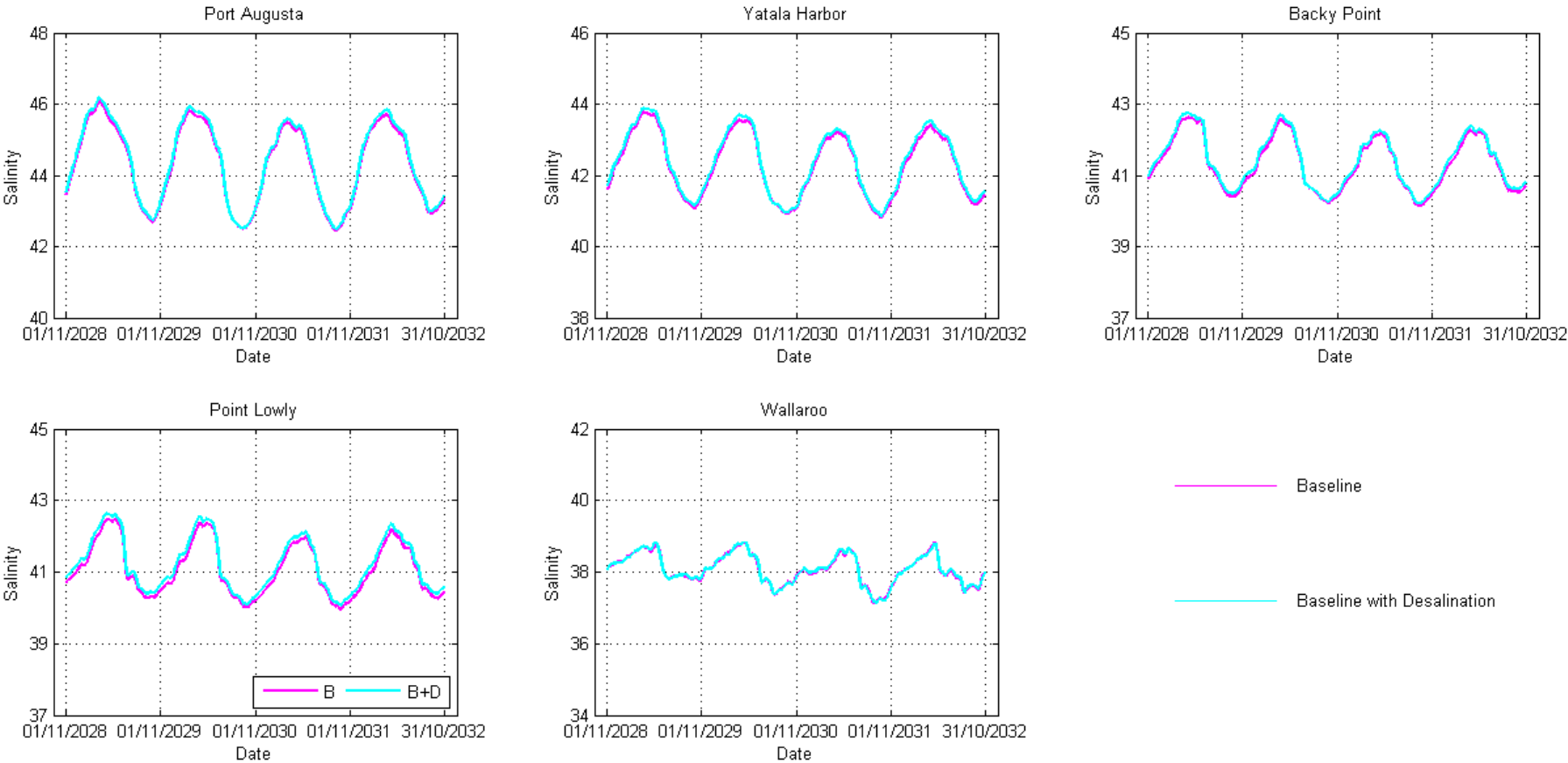


Figure 4-15 Modelled bottom salinities at Port Augusta, Yatala Harbor Aquatic Reserve, Backy Point, Point Lowly, and Wallaroo with (B+D) and without (B) the proposed desalination plant outfall discharge for the Nov 2028 to Nov 2032 period.

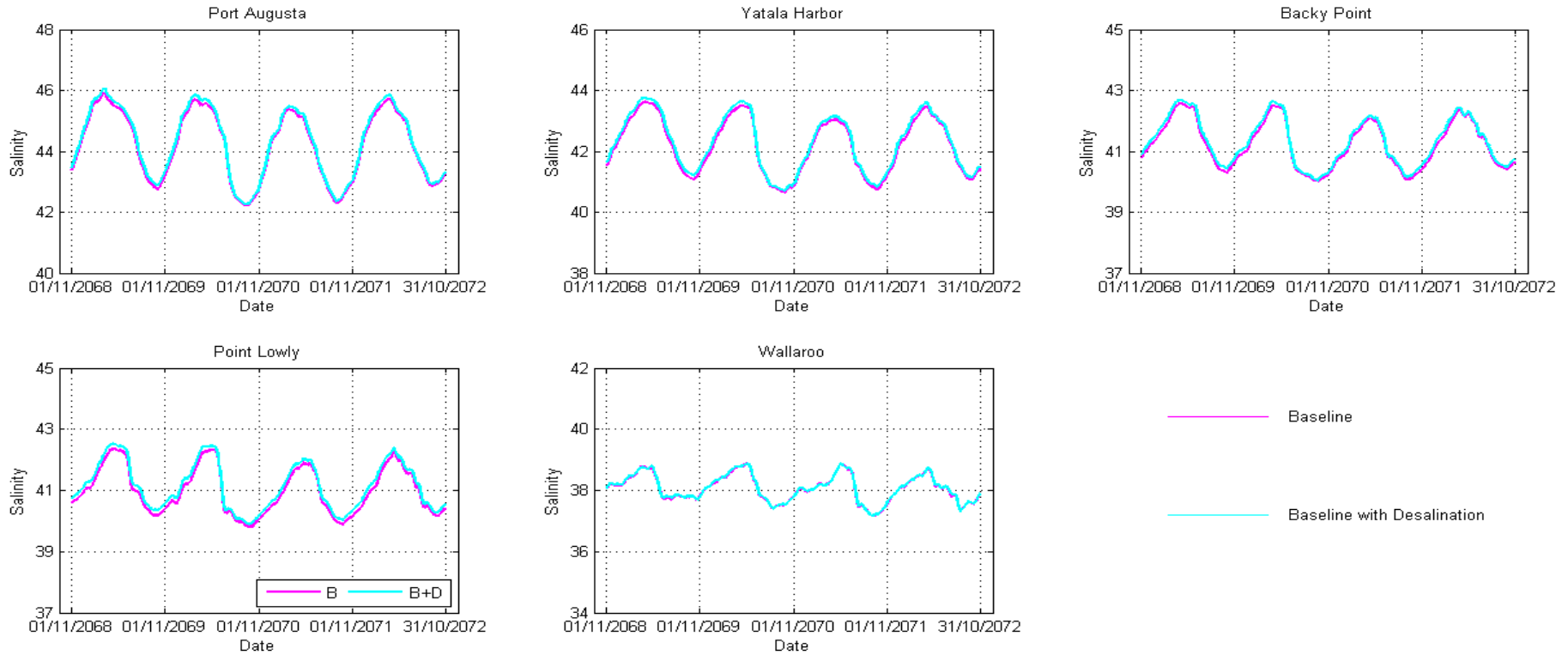


Figure 4-16 Modelled bottom salinities at Port Augusta, Yatala Harbor Aquatic Reserve, Backy Point, Point Lowly, and Wallaroo with (B+D) and without (B) the proposed desalination plant outfall discharge for the Nov 2068 to Nov 2072 period.

Long term bottom salinity changes were also calculated at all eight sites listed above (and shown in Figure 4-11), as well as the two integrated regions. These are presented in terms of differences between the 'B+D' and 'B' scenario salinity percentile distributions at each site. The percentage change with respect to the baseline (at each percentile within the distribution) was also computed.

The results are presented in Figure 4-17.

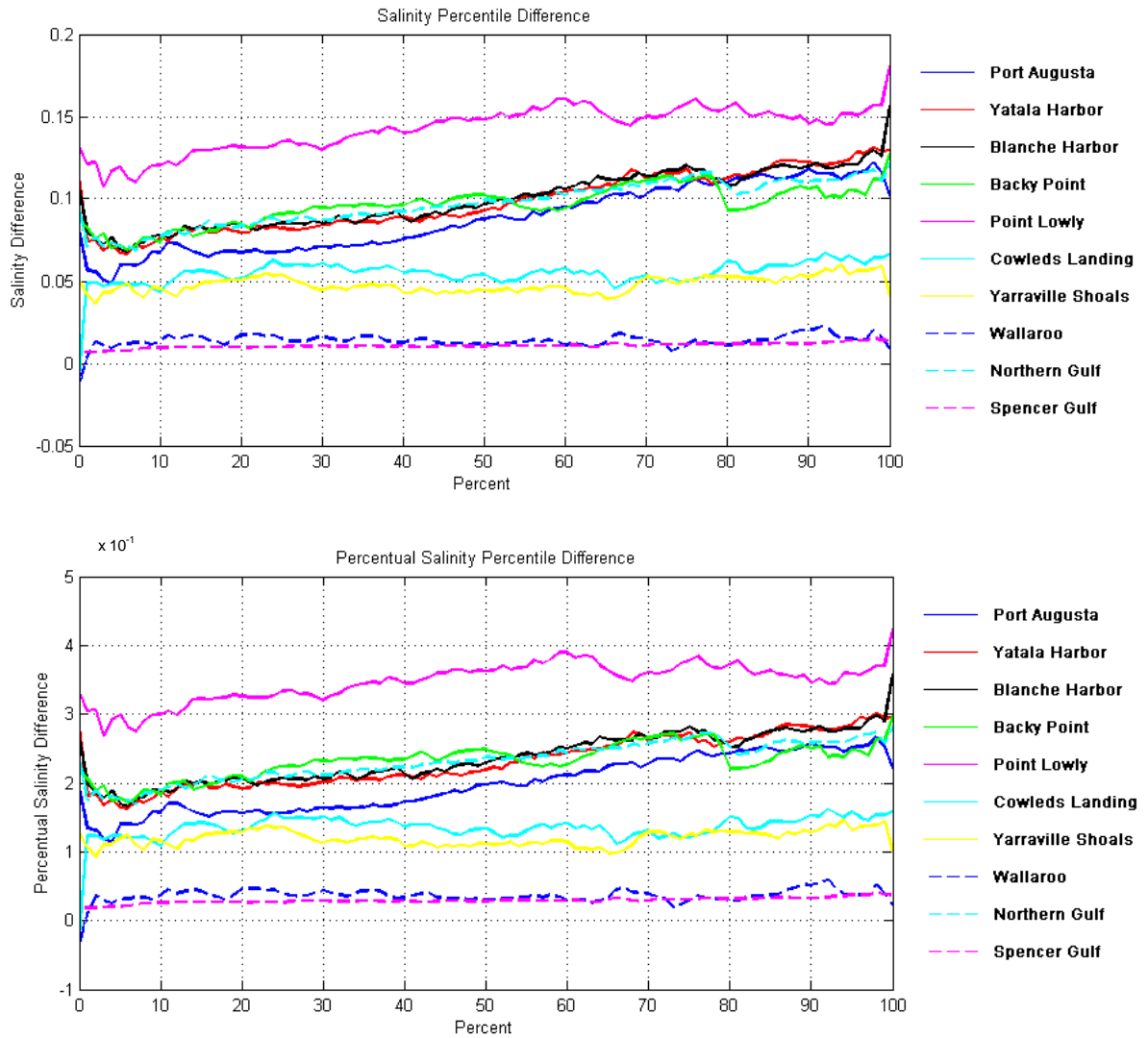


Figure 4-17 Salinity percentile differences (upper panel) and associated percentage difference with respect to the baseline (lower panel).

The results can be subdivided in four bands. The first band reflects local effects at Point Lowly, and corresponds to a salinity difference range of 0.10 to 0.16 (i.e. excluding the 100th percentile differences). Associated percentage changes are between 0.3% and 0.4% compared to the baseline salinities.

The second band shows the effects in the Northern Spencer Gulf. For this band the salinity changes are 0.05 to 0.13 (excluding the 100th percentile changes). Associated percentage changes are between 0.1% and 0.3% compared to the baseline salinities.

The third band shows that the expected range of salinity changes south of Point Lowly (i.e. Cowleds Landing Reserve and Yarraville Shoals) is 0.05 to 0.06 and is much more stable over all percentiles. Associated percentage changes are between 0.1% and 0.2% compared to the baseline salinities.

The fourth band shows the results much further south and over the entire Spencer Gulf. This band presents a small salinity change in the range of 0.0 to 0.02, and this is also stable over all percentiles. These changes cannot be accurately measured by state of the art field instrumentation. Associated percentage changes are generally less than 0.15% of the baseline salinities.

These timeseries (and the corresponding surface salinity timeseries) were also post-processed to compute average bottom and top salinity differences between the two simulations (i.e. average (B+D) – average(B)) at each of the extraction locations. Results are presented in Table 4-5 (Northern Gulf) and Table 4-6 (southern sites). These differences did not materially increase between horizons and the largest differences were concentrated locally at Point Lowly, as expected. Differences generally decreased away from Point Lowly, such that at Wallaroo, for example, salinity differences were computed to be in the order of 0.01, which is less than typical measurement detection limits.

Table 4-5 Average salinity difference between simulations with and without the proposed desalination plant discharge at the five different locations in the Northern Spencer Gulf

Level	Period	Average Salinity Difference				
		Location				
		Point Lowly	Backy Point	Blanche Harbor Aquatic Reserve	Yatala Harbor Aquatic Reserve	Port Augusta
Bottom	2004-2072	0.14	0.10	0.10	0.10	0.09
	2004-2008	0.14	0.10	0.10	0.10	0.09
	2028-2032	0.14	0.09	0.09	0.09	0.08
	2068-2072	0.15	0.10	0.10	0.11	0.10
Surface	2004-2072	0.08	0.09	0.10	0.10	0.09
	2004-2008	0.08	0.10	0.10	0.10	0.09
	2028-2032	0.07	0.09	0.09	0.09	0.08
	2068-2072	0.09	0.10	0.10	0.11	0.10

Table 4-6 Average salinity difference between simulations with and without the proposed desalination plant discharge at the three different locations south of the Northern Spencer Gulf

Level	Period	Average Salinity Difference		
		Location		
		Wallaroo	Yarraville Shoals	Cowleds Landing Aquatic Reserve
Bottom	2004-2072	0.01	0.05	0.06
	2004-2008	0.02	0.05	0.05
	2028-2032	0.01	0.04	0.05
	2068-2072	0.01	0.05	0.07
Surface	2004-2072	0.01	0.04	0.06
	2004-2008	0.01	0.04	0.05
	2028-2032	0.01	0.03	0.05
	2068-2072	0.01	0.04	0.07

4.3.3.2 Spatially Integrated Results

The spatially integrated effects of the proposed desalination discharge on the Northern Gulf salinities are presented in Figure 4-18 (absolute salinity) and Figure 4-19 (salinity difference) over the entire simulation period. Figure 4-20 to Figure 4-22 re-present the data from Figure 4-18 but within the same selected time horizons as above.

In general, Figure 4-18 suggests the seasonality of spatially integrated salinity in the Northern Gulf was not materially disrupted by the proposed discharge, such that salt accumulation in summer months and salt ejection in winter persisted. The figure also shows that the brine discharge did not produce continuing salinity increases with time.

Figure 4-19 suggests that salinity differences were mostly bounded by 0.05 and 0.15. The occasional negative values always occurred during the salt ejection phase of the annual salinity cycle and may reflect slight temporal changes in the hydrodynamic regime as a result of the proposed desalination plant discharge. Importantly, these negative differences are not reflected in the lowest and highest salinities observed in the timeseries.

The above timeseries of integrated salinities were re-processed as cumulative distributions, and are presented in Figure 4-23 for the entire timeseries (2004 to 2072) and selected time horizons (2004 to 2008, 2028 to 2032 and 2068 to 2072).

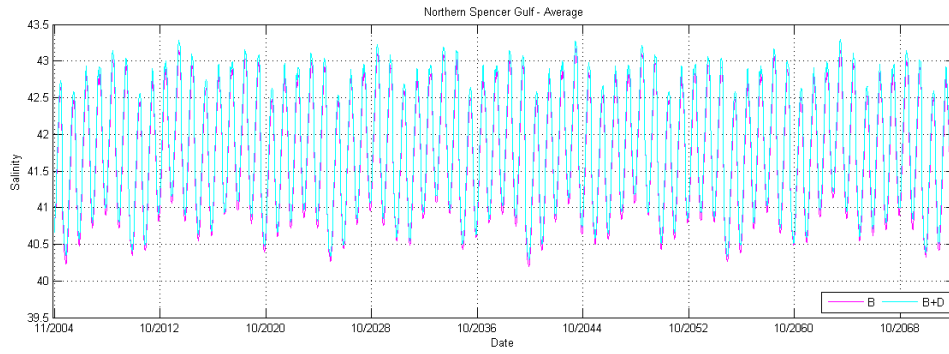


Figure 4-18 Modelled Northern Spencer Gulf averaged salinities with and without the proposed desalination plant outfall discharge for the 2004 to 2072 period

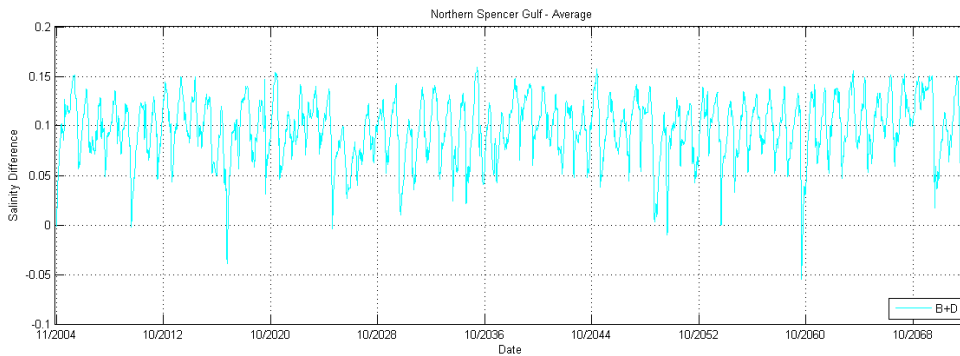


Figure 4-19 Modelled Northern Spencer Gulf averaged salinity differences between the simulations with and without the proposed desalination plant outfall discharge for the 2004 to 2072 period

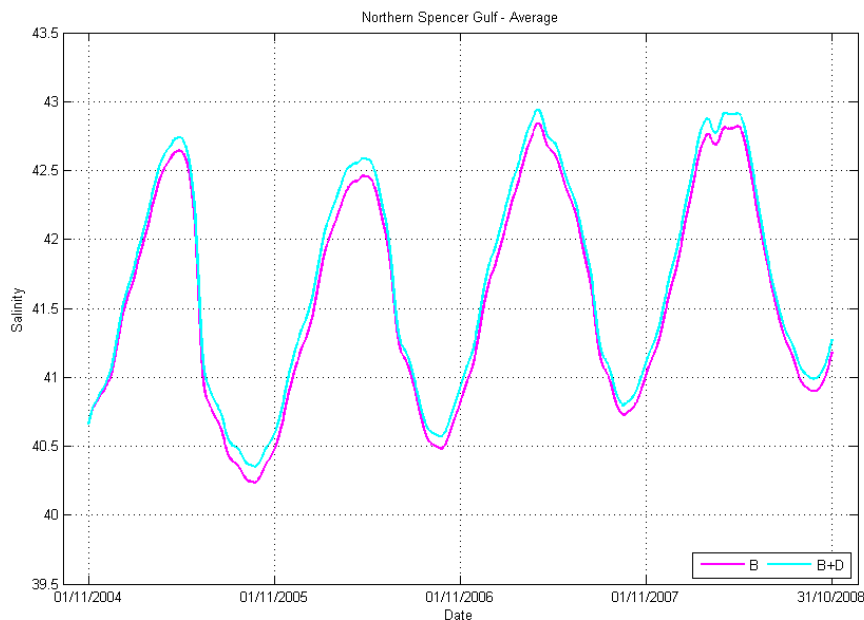


Figure 4-20 Modelled Northern Spencer Gulf averaged salinities with and without the proposed desalination plant outfall discharge for the 2004 to 2008 period

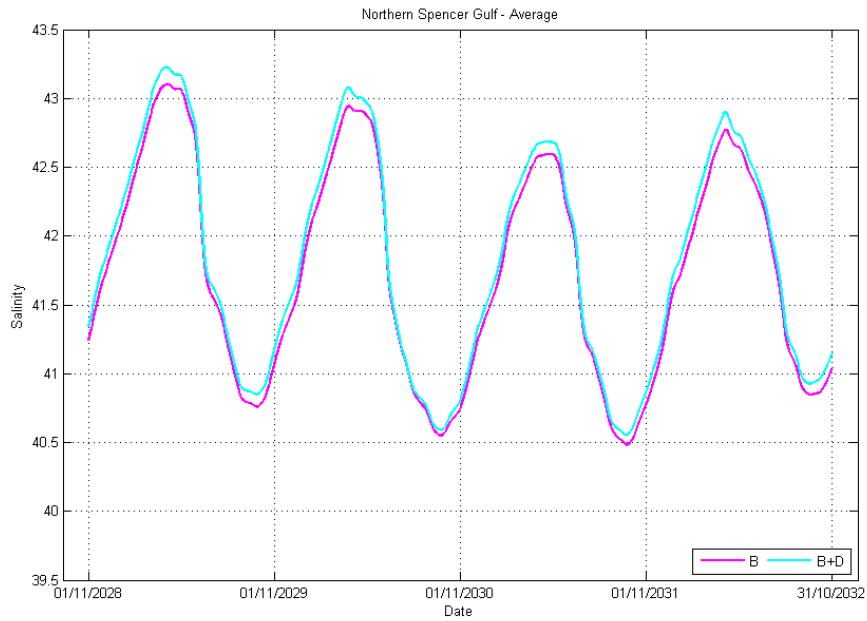


Figure 4-21 Modelled Northern Spencer Gulf averaged salinities with and without the proposed desalination plant outfall discharge for the 2028 to 2032 period

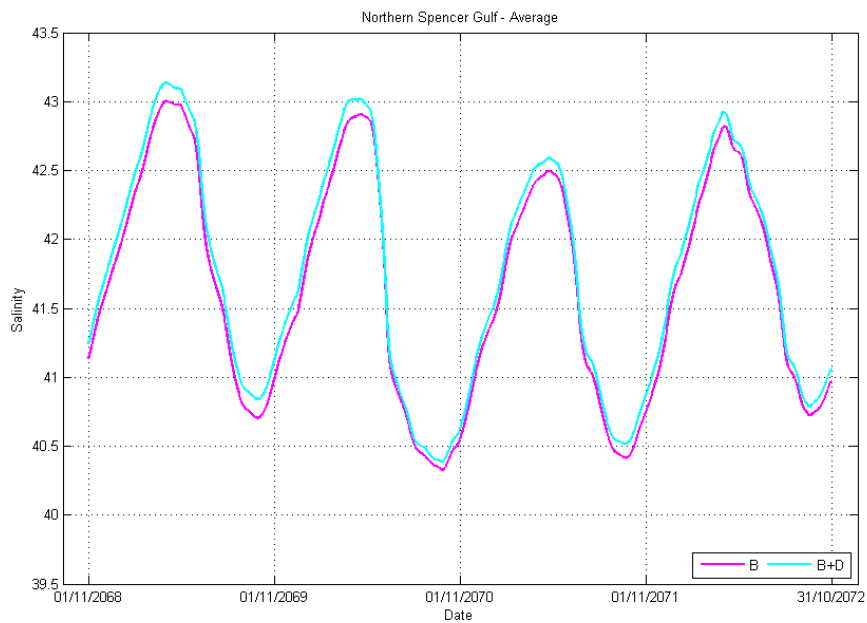


Figure 4-22 Modelled Northern Spencer Gulf averaged salinities with and without the proposed desalination plant outfall discharge for the 2068 to 2072 period

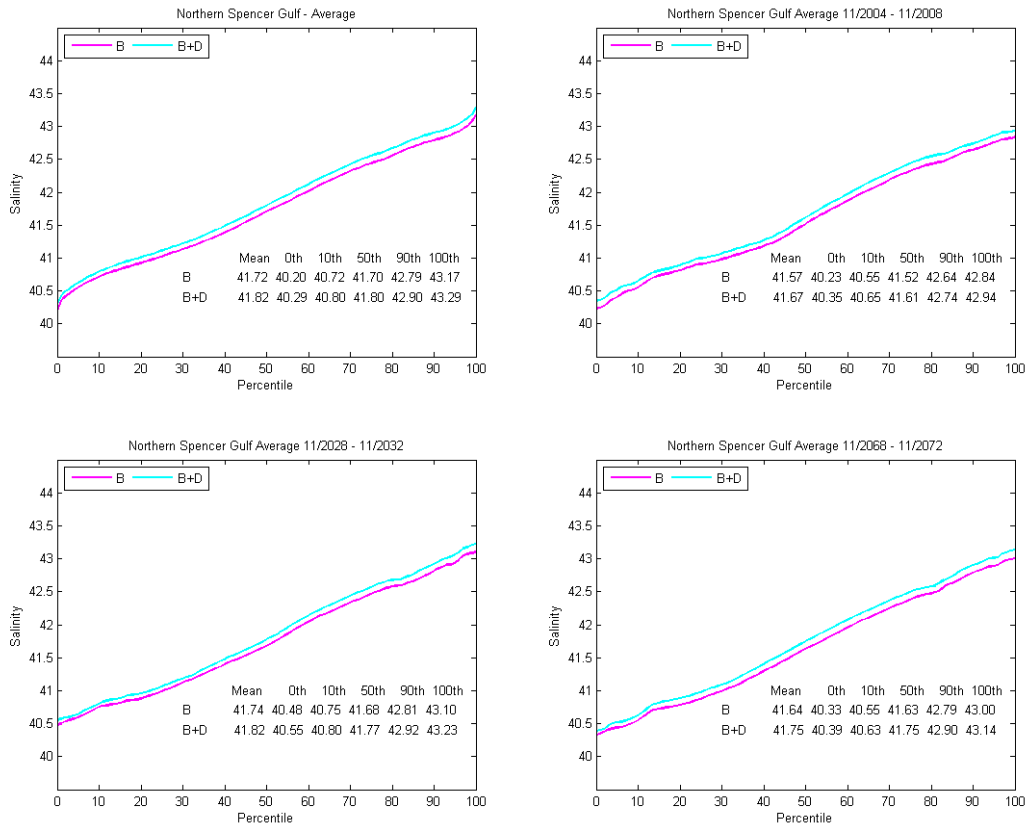


Figure 4-23 Modelled cumulative distributions of the Northern Spencer Gulf averaged salinities with and without the proposed desalination plant outfall discharge. Top left panel: 2004 to 2072 period; top right panel: 2004-2008 period; bottom left panel: 2028-2032 period; Bottom right panel: 2068-2072 period.

The top right panel in the figure (entire simulation) presents a relatively consistent picture of salinity increase across the range of percentiles, with this being approximately 0.1. Notwithstanding this, differences were always maintained between 0.05 and 0.14 for the means and any of the presented percentiles. Changes in the form and relativity of the distributions of the baseline and desalination simulations between time horizons are small, with no evidence to suggest increases in salinity differences between the two simulations with time.

Similar analyses were undertaken for the entire gulf data sets, and results are presented below. Specifically, Figure 4-24 provides timeseries of the gulf wide average salinities for both simulations (B and B+D) over the entire time period. Figure 4-25 to Figure 4-27 provide the same data within the previously selected time horizons, and Figure 4-28 presents the percentile analysis analogous to Figure 4-23.

Overall, the figures show that the effects of the proposed desalination discharge, as integrated over the entirety of Spencer Gulf were less pronounced than for Northern Spencer Gulf alone. For example, the difference in percentiles irrespective of period were always smaller than 0.02 (Figure 4-28, and therefore below the accuracy of state of the art instruments used to measure salinity in the field.

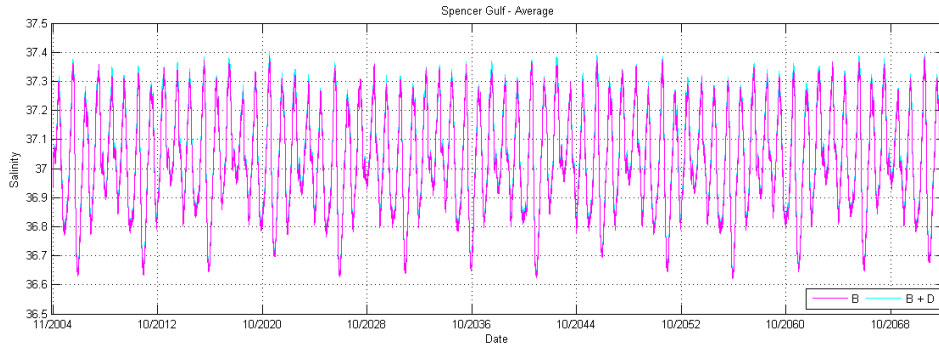


Figure 4-24 Modelled entire Spencer Gulf averaged salinities with and without the proposed desalination plant outfall discharge for the 2004 to 2072 period

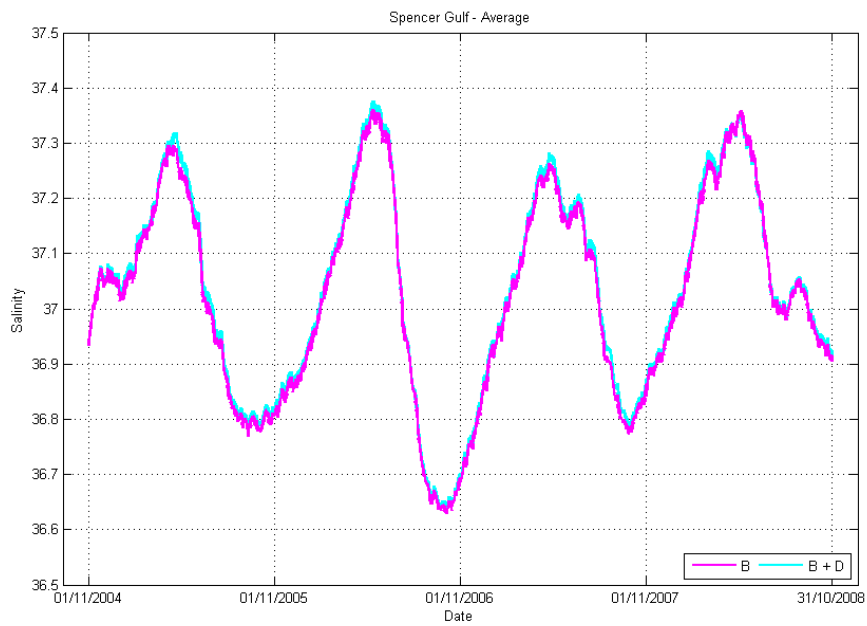


Figure 4-25 Modelled entire Spencer Gulf averaged salinities with and without the proposed desalination plant outfall discharge for the 2004 to 2008 period

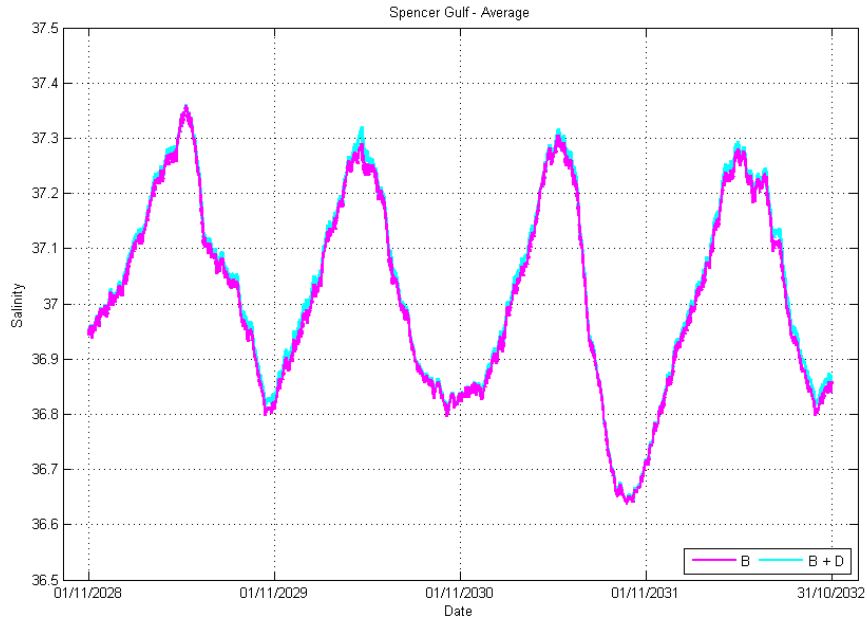


Figure 4-26 Modelled entire Spencer Gulf averaged salinities with and without the proposed desalination plant outfall discharge for the 2028 to 2032 period

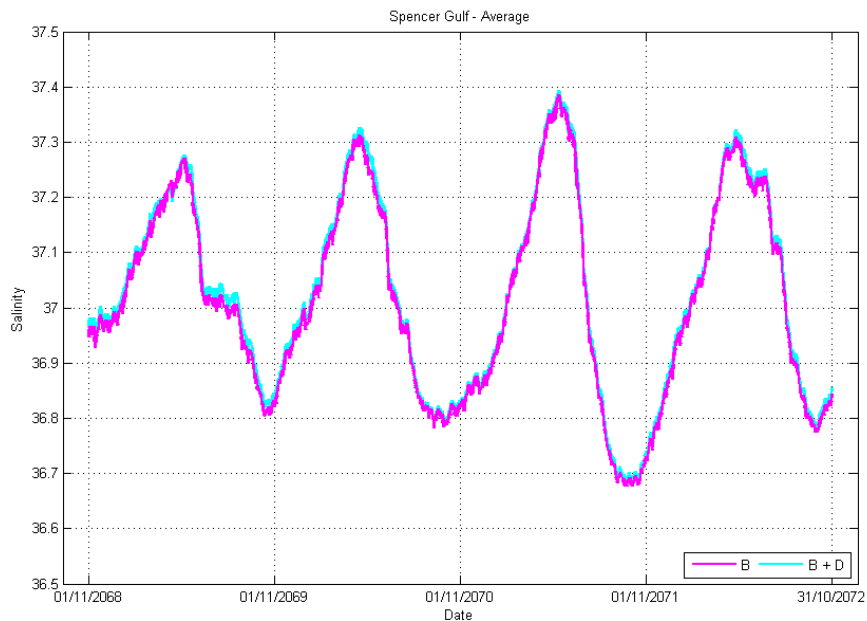


Figure 4-27 Modelled entire Spencer Gulf averaged salinities with and without the proposed desalination plant outfall discharge for the 2068 to 2072 period

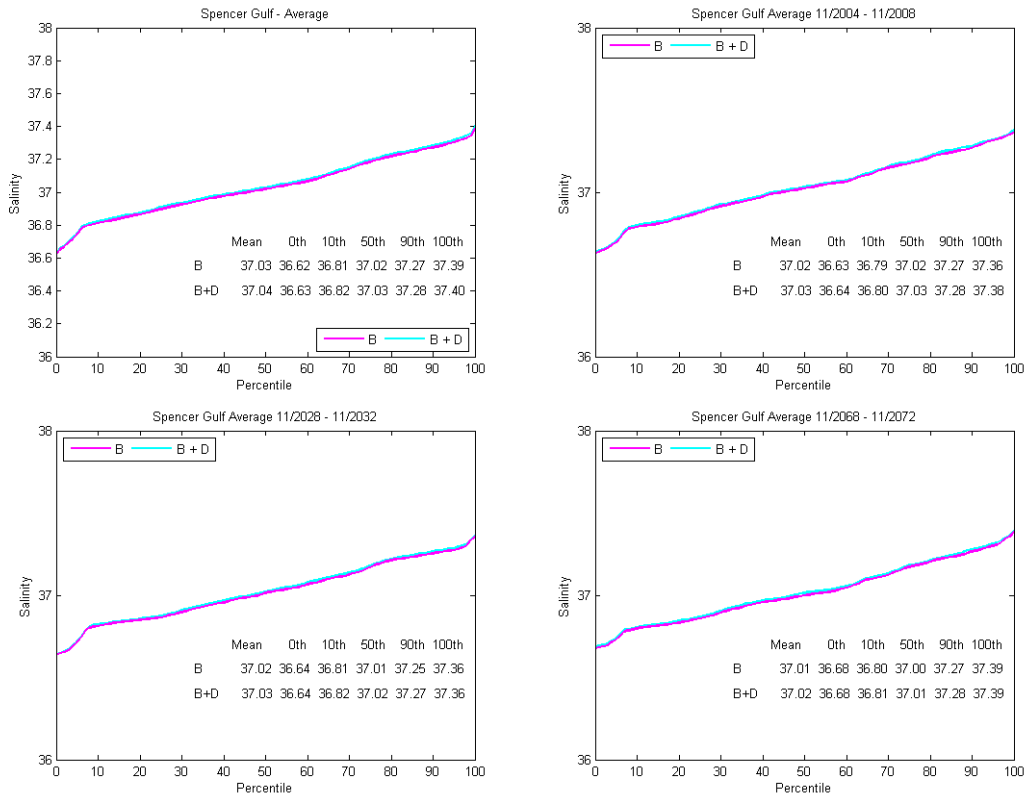


Figure 4-28 Modelled cumulative distributions of the entire Spencer Gulf averaged salinities with and without the proposed desalination plant outfall discharge. Top left panel: 2004 to 2072 period; top right panel: 2004-2008 period; bottom left panel: 2028-2032 period; Bottom right panel: 2068-2072 period.

To support the above analyses, the ratios of total salt masses in the Northern and entire gulf domains, for both runs B and B+D were computed. Results are presented in Figure 4-29. The results clearly reflect the relative size of the two areas (i.e. the ratios are small), and the associated salt mass ratio, estimated to vary between 1.06% and 1.2% depends on the season. The salt ratio decreases considerably over winter and presents similar ratios between the scenarios at these times. The largest difference of salinity ratios between the B and B+D simulations regularly coincided with the salt accumulation phase (summer) in the Northern Spencer Gulf.

Tracer released with the desalination discharge (at the appropriately diluted concentrations as per the CFD lookup tables) was also used to compute the ratio of brine (not total salt) mass in the Northern and entire gulfs. The results are provided in Figure 4-30 and show that the ratio stabilises after approximately two years and remains around 10% and 20% over the entire simulation period, with relative accumulation of tracer brine in the Northern Gulf over summer and subsequent reduction of the ratio during winter.

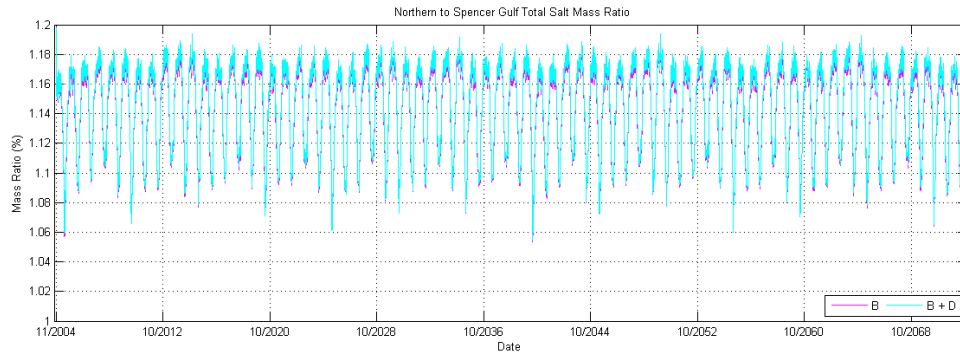


Figure 4-29 Modelled Northern Spencer to entire Spencer Gulf salt mass ratio with and without the proposed desalination plant outfall discharge for the 2004 to 2072 period

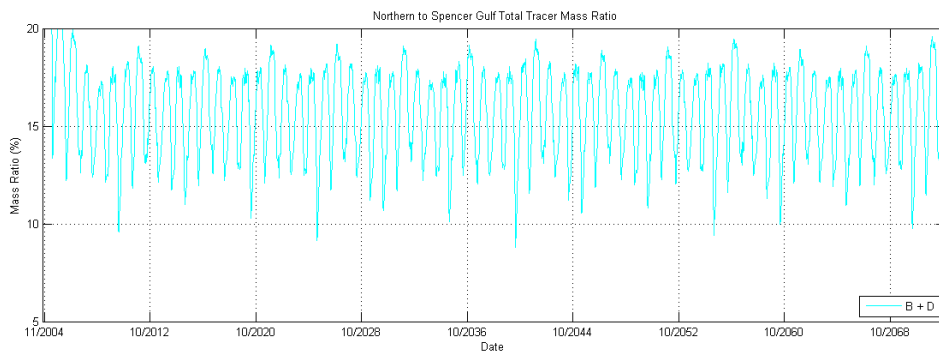


Figure 4-30 Ratio of brine tracer between Northern and entire Spencer Gulf areas

Finally, Table 4-7 shows the magnitude of the annual salt fluxes from the different sources within Spencer Gulf for both simulations. The table shows that the desalination plant intake and outfall balance each other in terms of salt mass (as expected) and that the salt fluxes imposed by the desalination plant are about 0.0033% of tidal salt fluxes.

Table 4-7 Simulated salt fluxes with and without the effect of the proposed desalination plant. Salinity values were assumed to be gL⁻¹.

Salt Flux Item	B: 2004-2008 (Average)	B: 2004-2072 (Average)	B+D: 2004-2008 (Average)	B+D: 2004-2072 (Average)
	Gt an ⁻¹	Gt an ⁻¹	Gt an ⁻¹	Gt an ⁻¹
Tidal Influx	+262	+261	+261	+261
Tidal Eflux	-262	-261	-261	-261
Desal. Return	0.00	0.00	+0.01	+0.01
Desal. Intake	0.00	0.00	-0.01	-0.01
Other Inflows	+0.00	+0.00	+0.00	+0.00

5 CLIMATE CHANGE SIMULATIONS

In order to assess the long term behaviour of the proposed return water discharge within the context of climate change, further low resolution model simulations were undertaken where climate forcing was progressively altered over time to reflect climate change conditions. Again, the influence of these changes was examined in terms of gulf wide and long term trends, consistent with the focus of the model validation exercise and previous data presentation.

5.1 Model Schematisation

With the exception of boundary condition data, the same model configuration described in Section 4 was used for the assessments presented in this section.

5.2 Climate Change Parameterisation

The methodology employed to capture the influence of climate change on the model boundary condition forcing was externally peer-reviewed before and after its implementation, and is described below.

5.2.1 Overview

In general, the assessment presented herein assumes conditions consistent with the Special Report on Emissions Scenarios (SRES) A1F1 storyline (IPCC 2007). This A1F1 storyline reflects the following scenario:

“A future world of very rapid economic growth, a global population that peaks in mid-century and declines thereafter, and the rapid introduction of new and more efficient technologies, but with a reliance on fossil intensive energy”.

This scenario is the most conservative of all considered, does not assume CO₂ stabilization scenarios and imposes the largest increased atmospheric CO₂ concentrations, global temperature increase, and sea level rise (IPCC 2007). This is consistent with recent Australian-context projections (Steffen 2009).

In order to support application of this qualitative storyline (which is cast partly in terms of CO₂ emissions) to the current study, quantitative results reported in Suppiah *et al.* (2006) and CSIRO (2007) were used to translate CO₂ conditions to meteorological forcing modulations. Specifically, Suppiah *et al.* (2006) provided projections for air temperature, rainfall and sea surface temperature variations, and CSIRO (2007) provided the remaining projections, with the exception of longwave radiation, which was derived in terms of cloud cover and projected temperatures (i.e. partially reliant on the projections of Suppiah *et al.* 2006).

5.2.2 Meteorological Forcing Modulation

The spatially variant meteorological forcing data applied to the high and low resolution models was used as the basis for developing modulated boundary conditions to drive the climate change simulations. These data span 2004 to 2008 and were chosen as they represent the most reliable and

highest resolution data available for Spencer Gulf. The ways in which these data were adapted to incorporate the projections of Suppiah *et al.* (2006) and CSIRO (2007) for the respective climate timeseries are described below.

5.2.2.1 Air Temperature and Rainfall

The projections of climate change of Suppiah *et al.* (2006) were used to construct air temperature and rainfall data used to force the low resolution hydrodynamic model under climate change scenarios.

In order to derive a link between CO₂ projections and meteorological changes for all IPCC (2007) storylines (which did not differ from those considered by IPCC, 2001), Suppiah *et al.* (2006) provided projections within the South Australian context for future air temperature and rainfall changes based on predictions of 13 Global Climate Models (GCMs) that were deemed to perform satisfactorily. These projections were then summarised for different seasons and climatic regions in South Australia for different future time horizons (i.e. 2030 and 2070) with respect to the thirty year period centred on 1990. The present study adopted the air temperature and rainfall projections presented by Suppiah *et al.* (2006) as related to the A1F1 storyline.

Since our forcing data was centred around 2006, it was important to quantify the proportion of the above projections provided by Suppiah *et al.* (2006) that occur between 1990 (the Suppiah *et al.* (2006) point of origin) and the centre of our data set, i.e. 2006. This information was necessary so as to appropriately apply the Suppiah *et al.* (2006) projections used in the current modelling study from 2004 onwards.

In order to undertake this, air temperature data for the period from 1974 to 2008 and covering Spencer Gulf was sourced from the IPCC Data Distribution Center (DDC). This is known as HadCRUTv3 data and is provided as monthly means on a 5 by 5 degree grid worldwide. These data are based on land and sea measurements, and the method for deriving the gridded data from measurements is described by Jones *et al.* (1999).

As a preliminary step, the high resolution air temperature data used in the current modelling study was compared to the 2004 to 2008 HadCRUTv3 air temperature data to ensure consistency between the data sets. To do so, the high resolution data was spatially and temporally averaged to match the HadCRUTv3 data, which comprises monthly average data at a 5 degree grid resolution. The resultant data comparison is shown in Figure 5-1 (monthly averaged data) and Figure 5-2 (seasonally averaged data). Seasonal averages were computed for both data sets as this unit of time was adopted by Suppiah *et al.* (2006) for projection definition. The HadCRUTv3 data was sourced from the area shown in Figure 5-3.

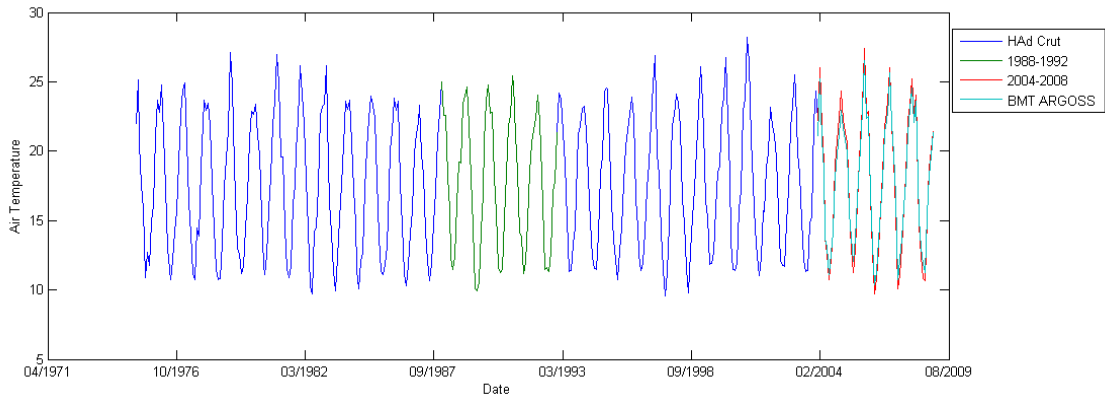


Figure 5-1 Comparison of monthly-averaged air temperatures between IPCC DDC HadCRUTv3 data with the Spencer Gulf WRF model data sets

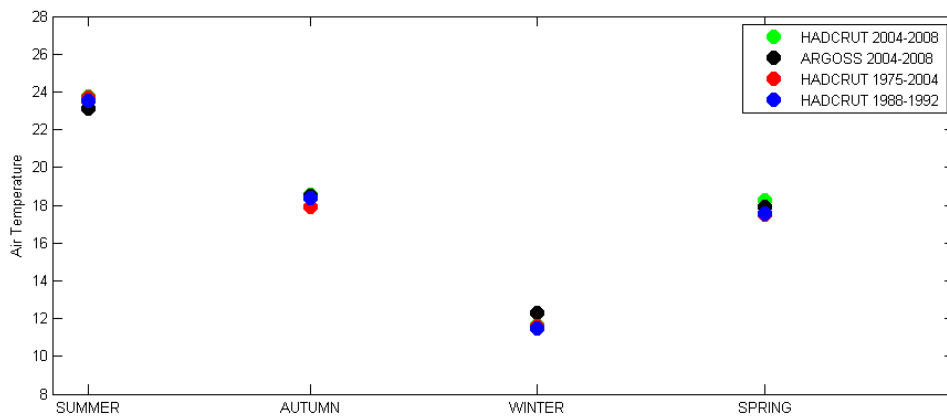
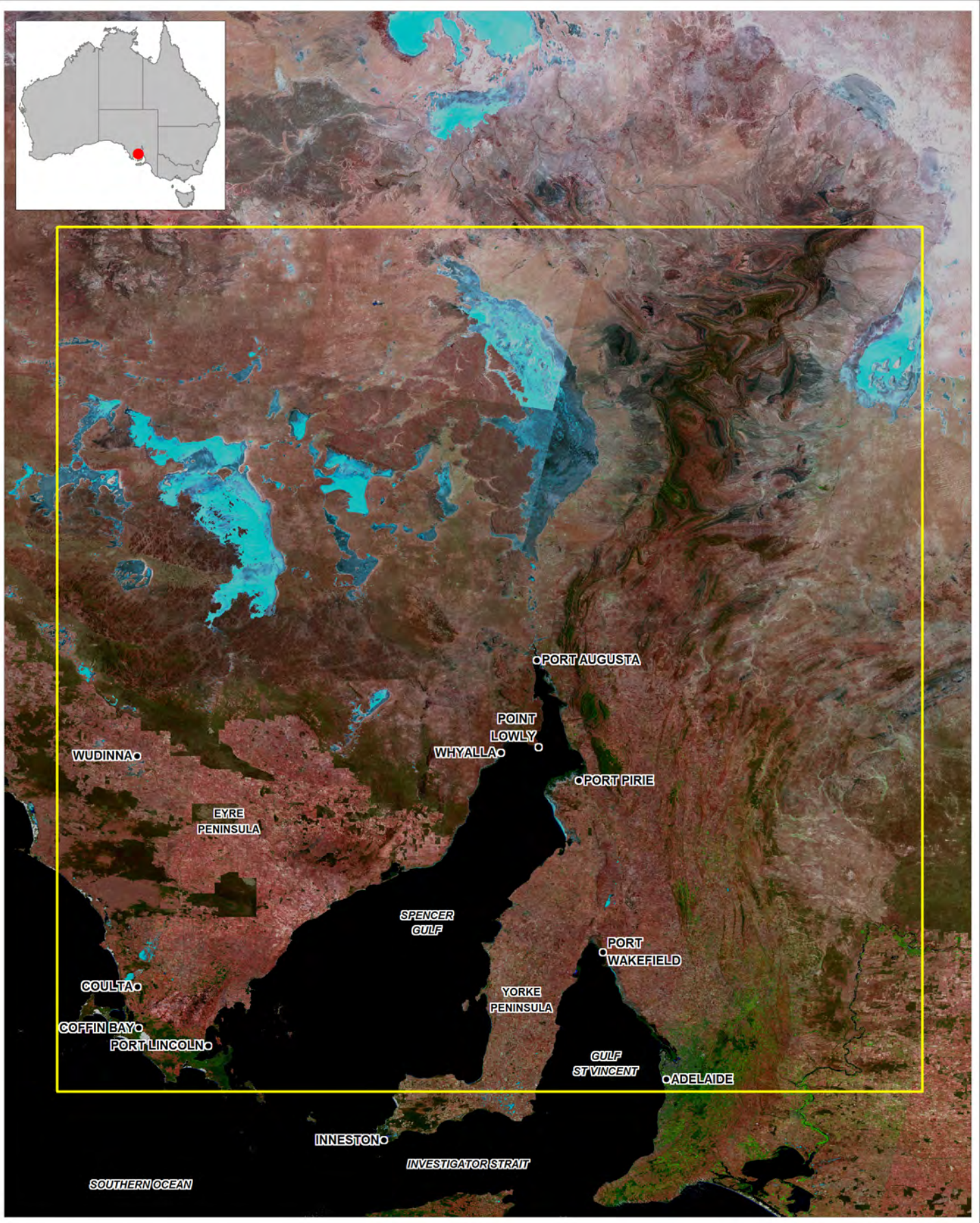
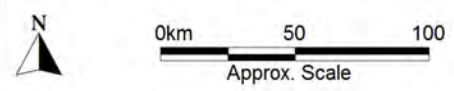


Figure 5-2 Comparison of seasonal averages between IPCC DDC HadCRUTv3 data with the Spencer Gulf WRF model data sets



<p>Title: Spatial coverage of the IPCC DDC HadCRUTv3 and WRF model data to produce the climate change forcing</p>	<p>Figure: 5-3</p>	<p>Rev: A</p>
--	-------------------------------	--------------------------

BMT WBM endeavours to ensure that the information provided in this map is correct at the time of publication. BMT WBM does not warrant, guarantee or make representations regarding the currency and accuracy of information contained in this map.



Filepath :

Despite the differences in temporal and spatial nature of the air temperature data sets presented above it can be seen that the high resolution meteorological data used to date and the HadCRUTv3 data are consistent and present an equivalent evolution for the period 2004-2008 (i.e. both reflect the same features of the same climatic area). In addition, Figure 5-1 demonstrates that the annual ranges in air temperature captured by the high resolution meteorological data are representative of those characterising the antecedent 30 year period, centred on 1990. As such, the high resolution data provide a robust starting point for applying climatic variations to the low resolution model.

Following this successful comparison, the Suppiah *et al.* (2006) projections for Eyre Peninsula and Northern & Yorke NRM regions were adjusted to be applied from 2004 onwards. Details of the methodology to affect this adjustment (as applied to air temperature) are as follows:

- 1 The seasonal air temperature variation for the future time horizons (2030 and 2070) given by Suppiah *et al.* (2006) was added to the correspondingly averaged IPCC DDC data (30-year centred in 1990), and these sums formed the seasonal averages at the respective future time horizons;
- 2 The differences between the seasonal air temperature averages at the future time horizons and the Spencer Gulf 2004-2008 seasonal air temperature averages were calculated, providing the rate of increase to apply from the period centred on 2006;
- 3 A linear increase between the 2004-2008 (centred 2006) and the 2028-2032 (centred 2030) time horizons seasonal averages was assumed preserving the increase in 5-year seasonal averages required to achieve the projections of Suppiah *et al.* (2006);
- 4 Step 3 was repeated for the period from 2028-2032 (centred 2030) to 2068-2072 (centred 2070);
- 5 The first year of the 2004-2008 air temperature data was appended to the end of the initial 5 year period to form a new 5-year baseline starting at 2005 (i.e., 2005-2009 centred 2007);
- 6 An initial guess of a multiplication factor for each season was applied to all the spatially distributed air temperature boundary conditions. These were then spatially and temporally averaged to match the HadCRUTv3 resolution and a new 5 year average computed;
- 7 This average was computed iteratively until it matched the desired variation across the period, as extracted from the Suppiah *et al.* (2006) projections; and
- 8 Steps 4 to 7 were repeated until a timeseries for the complete 2004-2072 air temperature data forcing was produced.

Daily rainfall data, as sourced from BoM SILO database, was also modified using the rolling average technique above, but with the Suppiah *et al.* (2006) projections for rainfall considered.

5.2.2.2 Other Meteorological Data

The above procedure described for air temperature was also applied for all other meteorological variables (with the exception to incoming long wave radiation). The difference in these other applications was that the changes imposed were based on projections of the Climate Change in Australia report (CSIRO 2007). Linear changes between 1990 and 2030 and between 2030 and 2070 were assumed, appropriately accounting for the difference in time origin.

5.2.2.3 Longwave Radiation

Projected changes for long wave radiation were not available. Changes for longwave radiation were thus imposed by considering the effects of changes in air temperature alone (i.e. assuming greenhouse gases effects in the resulting radiation were already taken into account in the temperature change). The approach used assumed a relationship between cloud cover (C), air temperature (T_a), and long wave radiation (R_l).

$$R_l = (1 + 0.17C^2)C_\varepsilon T_a^6 \quad (1)$$

Where C_ε is a constant (Swinbank 1963). Re-arranging (1) gives

$$C^2 = \frac{1}{0.17} \left(\frac{R_l}{C_\varepsilon T_a^6} - 1 \right) \quad (2)$$

A cloud cover timeseries for each surface boundary condition set was estimated from the 2004-2008 high resolution incoming long wave radiation and air temperature and successively appended to form a cloud cover timeseries between 2004 and 2072. The prognostic air temperatures were then substituted into equation (1) to compute the change in incoming longwave radiation due to air temperature change alone.

5.2.3 Open Boundary Forcing Modulation

The effects of climate change on the model open boundaries were accounted for in the mean sea level, and sea surface temperatures. No changes were imposed on oceanic salinities and water temperatures below the surface.

The applied sea level rise follows the projection in the Climate Change in Australia report (CSIRO 2007) that defines a 0.59 m mean sea level by 2100 from the 1990 baseline. In order to apply these changes the following approach was used:

- Harmonic analysis was performed on the surface elevation data between 2004 and 2008;
- Tidal elevations were reconstructed from the harmonic analysis for the period 2004 to 2008 and 2004 to 2072;
- Residuals between the surface elevation data and the reconstructed tides were calculated for the period between 2004 and 2008, and successively appended to the 2004-2008 timeseries to form a residual timeseries between 2004 and 2072;
- The final water surface elevation timeseries for the baseline simulation was constructed from adding the residuals timeseries to the reconstructed tidal elevations; and
- The final water surface elevation timeseries for the climate change simulation was constructed by adding the assumed sea level rise to the baseline timeseries.

Sea surface temperatures assumed half of the increase imposed on air temperatures. This assumption was based on reported trends since 1950 of sea surface temperature rises in comparison to land based stations in South Australia (Suppiah *et al.* 2006).

5.2.4 Summary

A summary of the changes imposed at each of the future horizons, seasons and variables for all boundary forcing data sets is presented in Table 5-1 and Table 5-2. Figure 5-4 to Figure 5-11 present example boundary forcing timeseries as applied in the climate change simulations. Baseline data is also included. It is noted that the adjustments described above apply to all boundary condition sets shown in Figure 4-3.

Table 5-1 Climate change parameters for Horizon 2030

Data Type	Seasonal Variation wrt 1990				Seasonal Variation wrt 2006				Source
	Sum	Aut	Win	Spr	Sum	Aut	Win	Spr	
Temperature (°C)	1.4	1.2	1.2	1.4	1.34	0.58	1.16	0.63	Suppiah <i>et al.</i> (2006)
Rainfall (%)	-9	-10	-12	-20	-26	+22	+7.4	+2.6	Suppiah <i>et al.</i> (2006)
Wind Speed (%)	7.5	3.5	3.5	3.5	4.5	2.1	2.1	2.1	CSIRO (2007)
Relative Humidity (%)	-1.5	-1.5	-2.5	-2.0	-0.9	-0.9	-1.5	-1.2	CSIRO (2007)
Solar Radiation (%)	0.0	1.0	3.5	1.5	0.0	0.6	2.1	0.9	CSIRO (2007)
Long Wave Radiation	Computed from air temperature and assumed baseline cloud cover								Derived
Mean Sea Level Rise (m)	Assumed linear 0.59 m increase from 1990 to 2100								CSIRO (2007)
Sea Surface Temperature (°C)	Assumed half of air temperature increase								Suppiah <i>et al.</i> (2006)
Sea Surface Salinity	Not changed								N/A

Table 5-2 Climate change parameters for Horizon 2070

Data Type	Seasonal Variation wrt 1990				Seasonal Variation wrt 2006				Source
	Sum	Aut	Win	Spr	Sum	Aut	Win	Spr	
Temperature (°C)	4.3	3.8	3.8	4.1	4.24	3.18	3.76	3.33	Suppiah <i>et al.</i> (2006)
Rainfall (%)	-25	-30	-35	-60	-39	-5.2	-21	-49	Suppiah <i>et al.</i> (2006)
Wind Speed (%)	15	10	5	12.5	12	8	4	10	CSIRO (2007)
Relative Humidity (%)	-2.5	-3.0	-3.5	-3.5	-2.0	-2.4	-2.8	-2.8	CSIRO (2007)
Solar Radiation (%)	3.5	3.5	10	3.5	2.8	2.8	8.0	2.8	CSIRO (2007)
Long Wave Radiation	Computed from air temperature and assumed baseline cloud cover								Derived
Mean Sea Level Rise (m)	Assumed linear 0.59 m increase from 1990 to 2100								CSIRO (2007)
Sea Surface Temperature (°C)	Assumed half of air temperature increase								Suppiah <i>et al.</i> (2006)
Sea Surface Salinity	Not changed								N/A

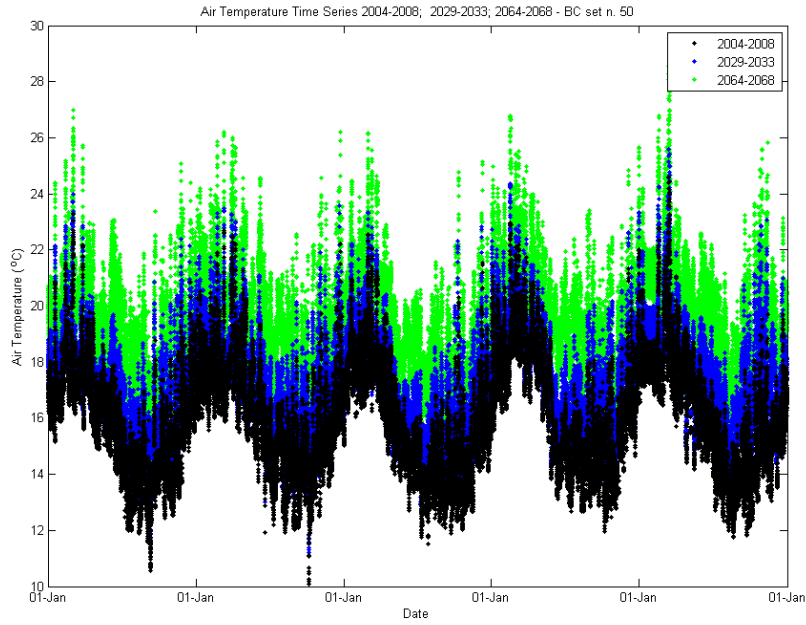


Figure 5-4 Example of air temperature and associated imposed climate change at different time horizons: boundary condition set n. 50

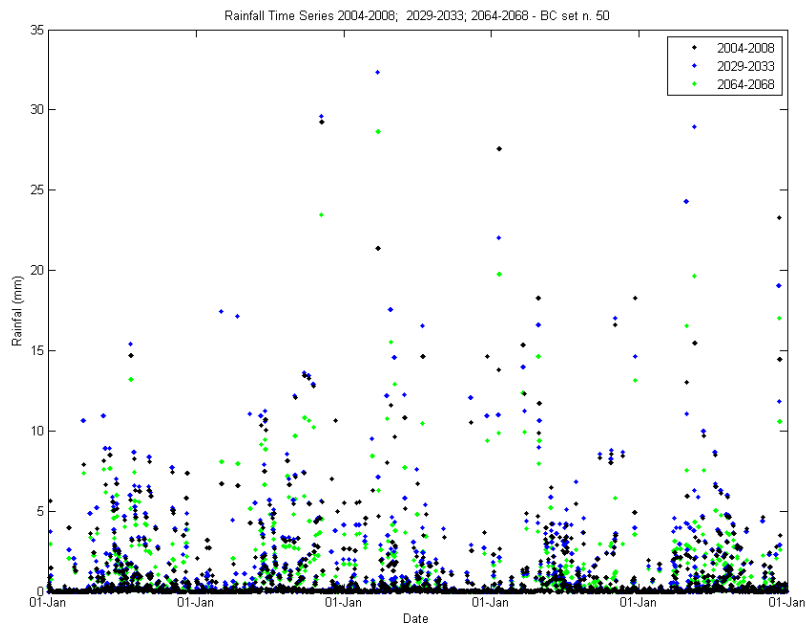


Figure 5-5 Example of air temperature and associated imposed climate change at different time horizons: boundary condition set n. 50

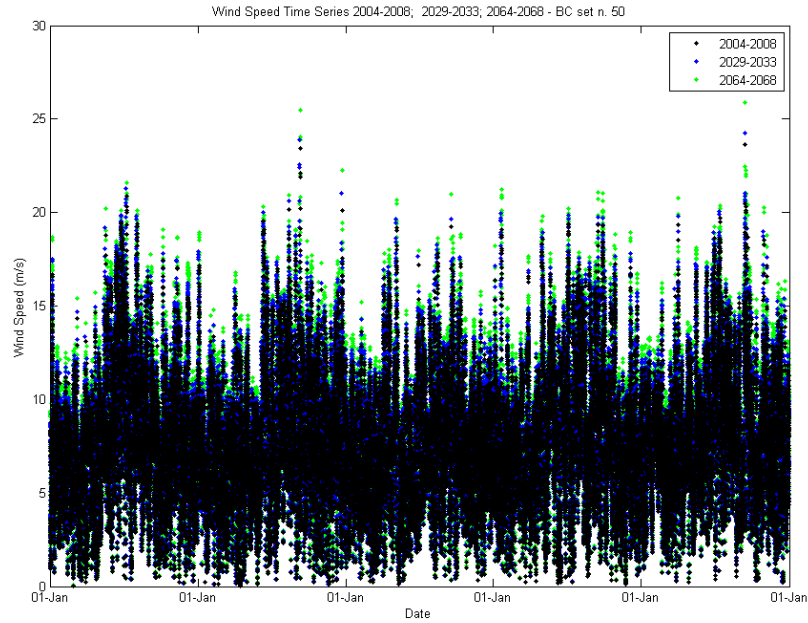


Figure 5-6 Example of wind speed and associated imposed climate change at different time horizons: boundary condition set n. 50

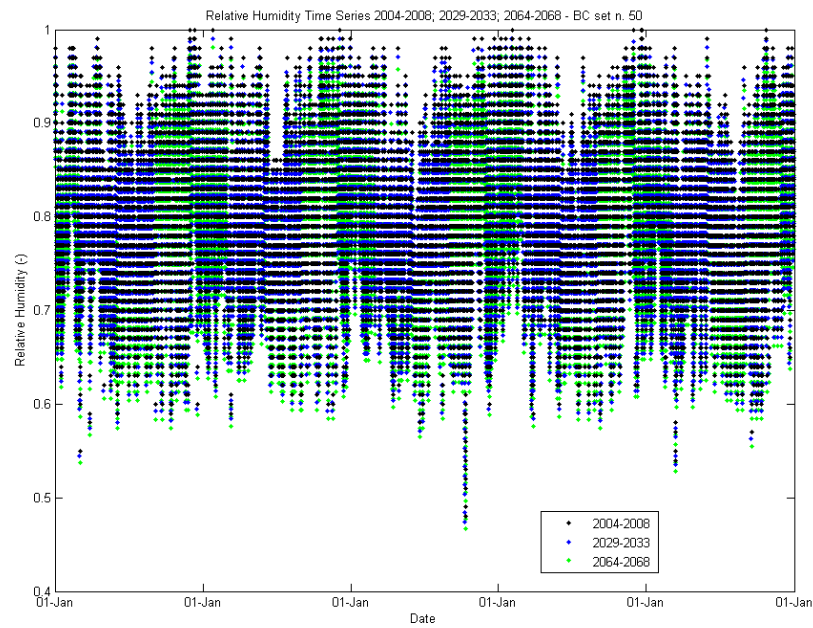


Figure 5-7 Example of relative humidity and associated imposed climate change at different time horizons: boundary condition set n. 50

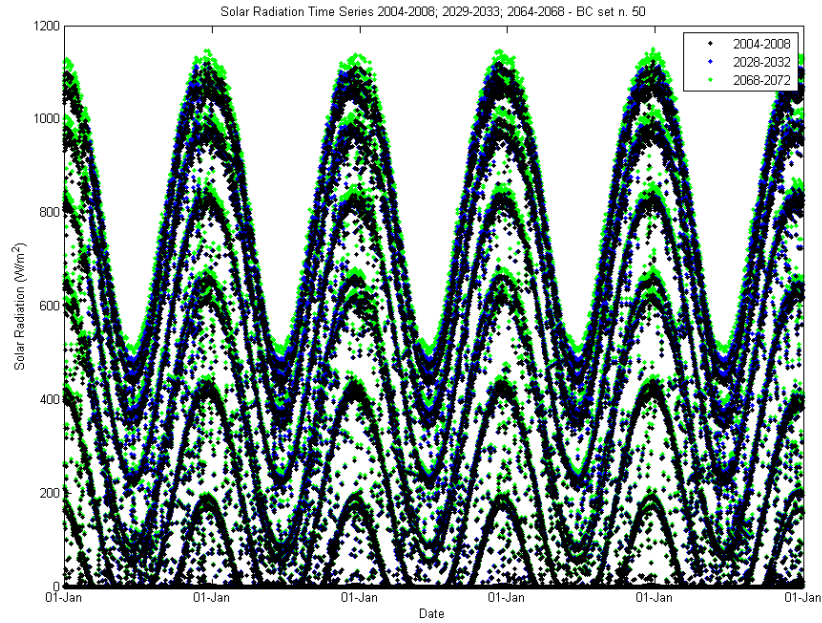


Figure 5-8 Example of solar radiation and associated imposed climate change at different time horizons: boundary condition set n. 50

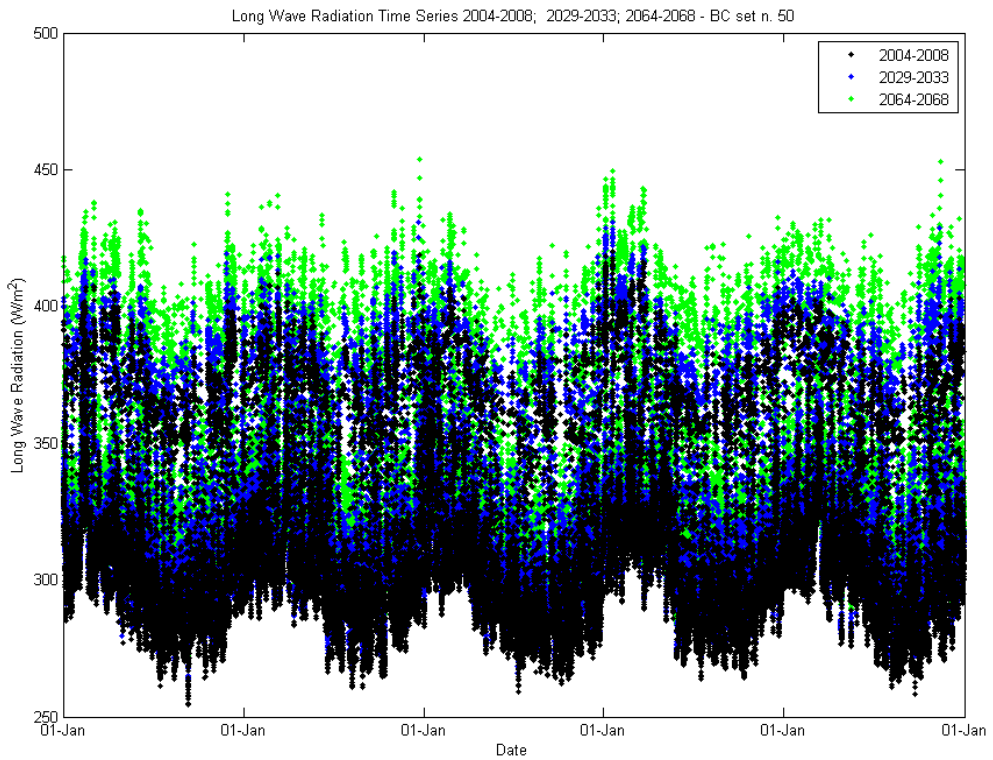


Figure 5-9 Example of long wave radiation and associated imposed climate change at different time horizons: boundary condition set n. 50

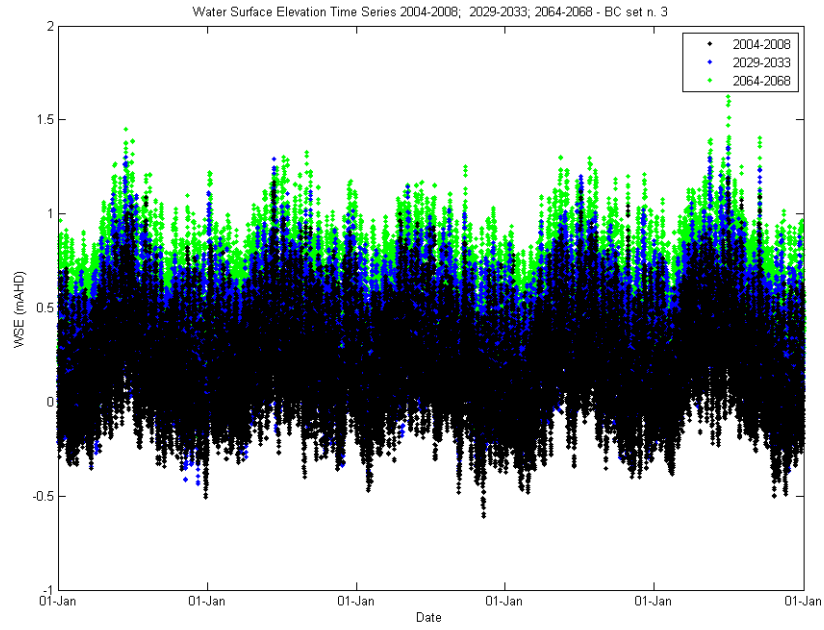


Figure 5-10 Example of water surface elevations and associated imposed climate change at different time horizons: boundary condition set n. 3

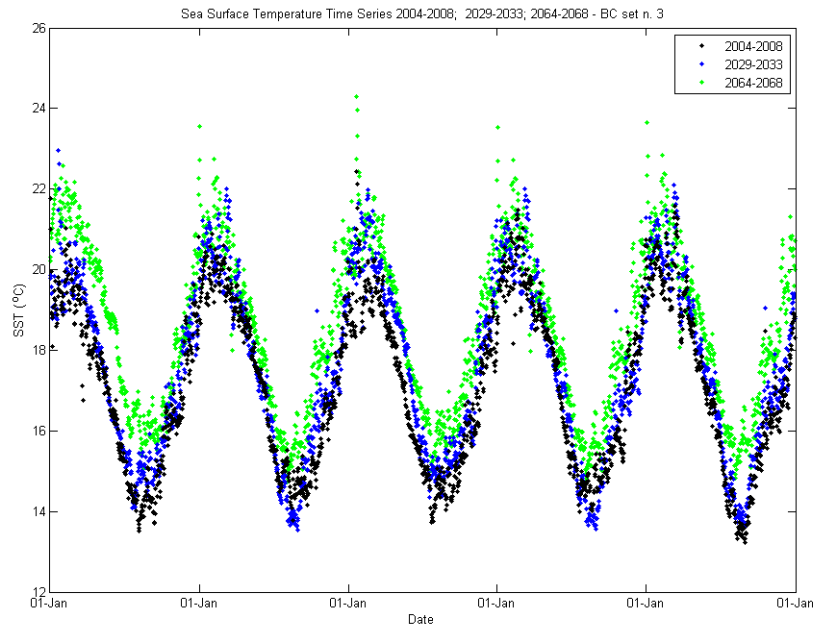


Figure 5-11 Example of sea surface temperature and associated imposed climate change at different time horizons: boundary condition set n. 3

5.3 Simulations

Similarly to the simulations presented in Section 4 above, two simulation sets for the period between 2004 and 2072 were performed, accounting for climate change scenarios with and without the proposed desalination plant discharges. Again, for the scenario accounting for the proposed desalination plant discharge, yearly average discharge rates were assumed throughout the simulation. The characteristics of the proposed desalination plant discharge are summarised in Table 5-3.

Table 5-3 Assumed proposed desalination plant discharges in the simulations

Simulation Code	Period (Nov to Nov)	Intake Rate m^3s^{-1}	Outfall Rate m^3s^{-1}
B+C	2004-2072	0.00	0.00
B+C+D	2004-2072	6.5	3.6

5.4 Results

Similarly to the spatially integrated predictions presented in Section 4, the climate change scenario results were assessed for two different areas representing the Northern Spencer Gulf and the entire Spencer Gulf. Results presented here include those without climate change applied (as repeated from Section 4), and as such, allow for comparison of the relative effects imposed by climate change, desalination and both combined.

Figure 5-12 shows timeseries of the evolution of Northern Spencer Gulf average salinities from simulations B (baseline), B+D (baseline and desalination), B+C (baseline plus climate change) and B+C+D (baseline plus desalination and climate change) over the entire simulation period. Figure 5-13 to Figure 5-15 present the same data over selected time horizons. The figures demonstrate that the seasonality of the salinity signature in all simulations was not disrupted, out to the 2070 time horizon (see Nunes-Vaz *et al.* 1990, SEIS Appendix H5.2).

The figures show, however, that average salinities in the Northern Gulf increased considerably over time due to climate change, particularly between the 2030 and 2070 time horizons. This increase is illustrated in Figure 5-16, where the timeseries displayed in Figure 5-14 and Figure 5-15 were compiled into a day-of-the-year average. The definition of “day-of-the-year average” for the 2028 to 2032 period for the baseline model (for example) is as follows:

- The daily baseline simulation outputs for 1 November for each year between 2028 and 2031 were collated and the average between these four data sets was computed;
- The process was repeated for all subsequent days involving the period between 2 November 2028 and 31 October 2032; and
- A timeseries was then obtained by collating these average values (i.e. 1 November, 2 November, and 31 October).

The same definition and process was applied to all simulations over this period and the 2070 centred time horizon.

The figures show that the peak day-of-year value for the baseline (B) Northern Gulf salinities were 42.8 in both horizons (pink line), while the climate change simulations were 43.2 and 43.9 for the

2068 and 2072 horizons, respectively (black lines). The raw timeseries of the single year that presented the highest salinity of all years involved in the day-of-the year averaging process (hereafter defined as “peak year”) is also presented in Figure 5-16, which shows maximum peak salinities in the 2030 and 2070 horizons equal to 43.4 and 44.2, respectively.

These salinity increases under the climate change scenarios are due to increased evaporation resulting from the modulated atmospheric forcing. This increased evaporation (note evaporation is negative as it represents an outward flux from the model perspective) is shown as a difference with respect to the baseline (simulation B) for the two future horizons in Figure 5-17 and Figure 5-18 (i.e. $(B+C) - B$). The climate-driven salinity increases $(B+C)$ are greater than those due to desalination alone $(B+D)$.

Similarly to the scenarios without climate change, the additional effects of the brine discharge within the climate change scenario $(B+D+C)$, compared to $B+C$ did not show continuously increasing salinities with time. This is illustrated in the cumulative distributions presented in Figure 5-19 for the entire timeseries (2004 to 2072) and percentiles for past (2004 to 2008) and future time horizons (2028 to 2032 and 2068 to 2072). Specifically, the red $(B+C+D)$ and black $(B+C)$ curves do not significantly diverge across time horizons.

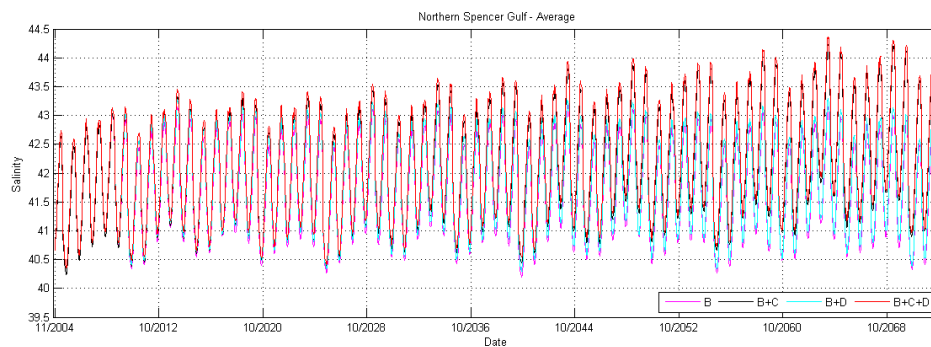


Figure 5-12 Modelled Northern Spencer Gulf averaged salinities for different climate scenarios and with and without the proposed desalination plant outfall discharge for the 2004 to 2072 period

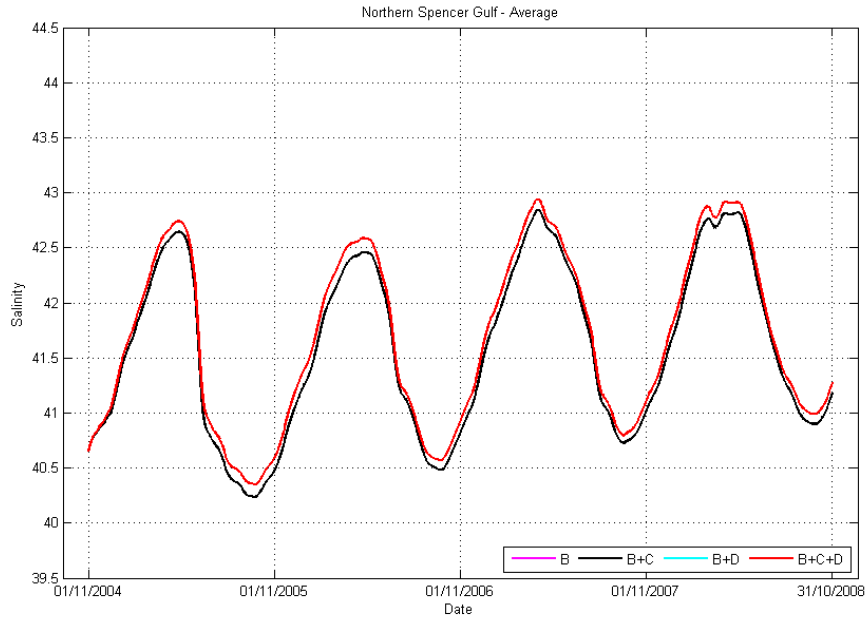


Figure 5-13 Modelled Northern Spencer Gulf averaged salinities for different climate scenarios and with and without the proposed desalination plant outfall discharge for the 2004 to 2008 period

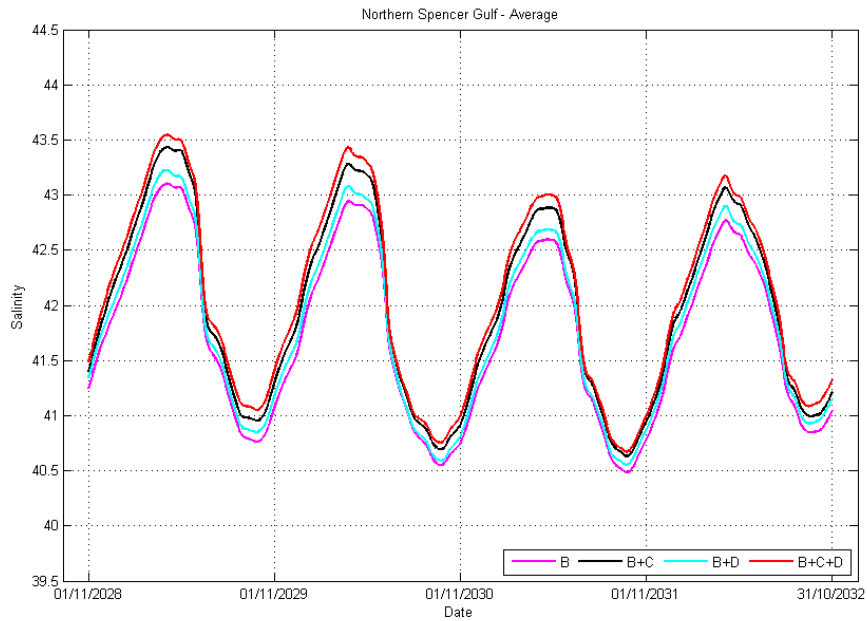


Figure 5-14 Modelled Northern Spencer Gulf averaged salinities for different climate scenarios and with and without the proposed desalination plant outfall discharge for the 2028 to 2032 period

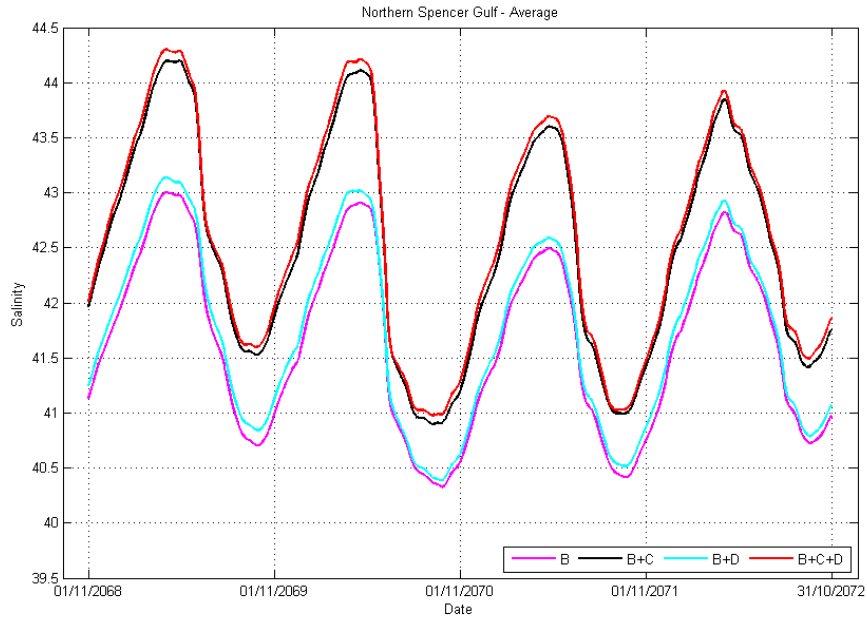


Figure 5-15 Modelled Northern Spencer Gulf averaged salinities for different climate scenarios and with and without the proposed desalination plant outfall discharge for the 2068 to 2072 period

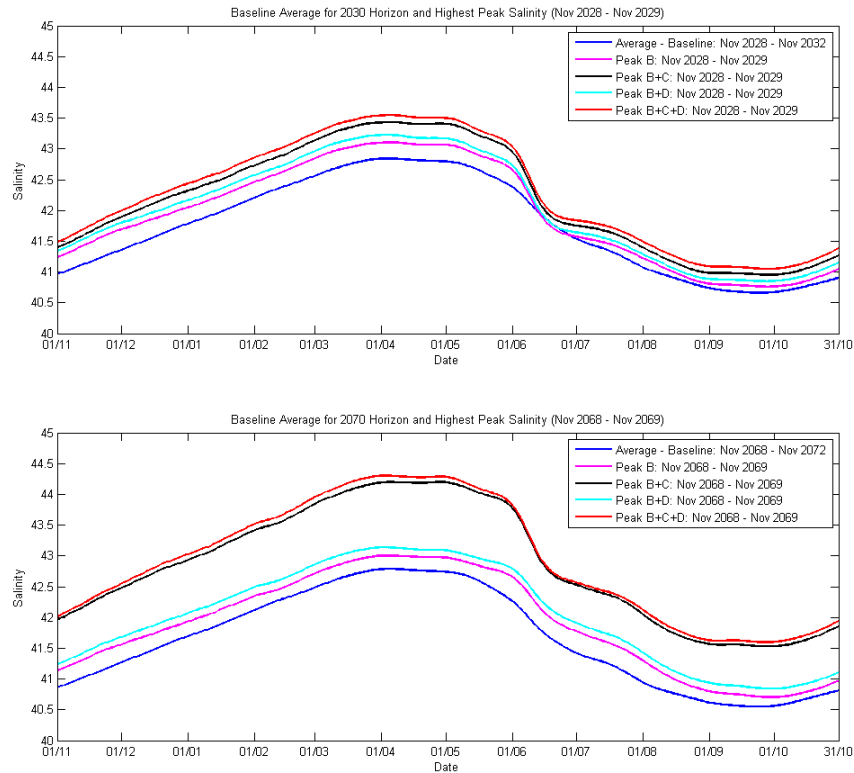


Figure 5-16 Modelled baseline-averaged and peak-year Northern Spencer Gulf average salinities for the 2028 to 2032 (upper panel) and 2068 to 2072 (lower panel) periods

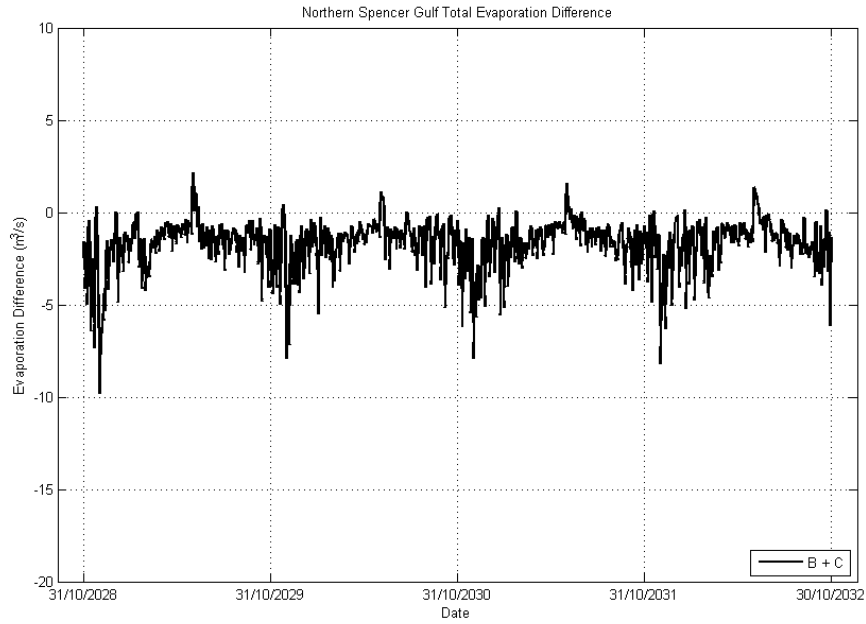


Figure 5-17 Difference of evaporation rates between climate change and baseline simulations for modelled Northern Spencer Gulf for the 2028 to 2032 period. The evaporation flux used to compute these differences assumes a negative sign indicating a flux out of the Gulf.

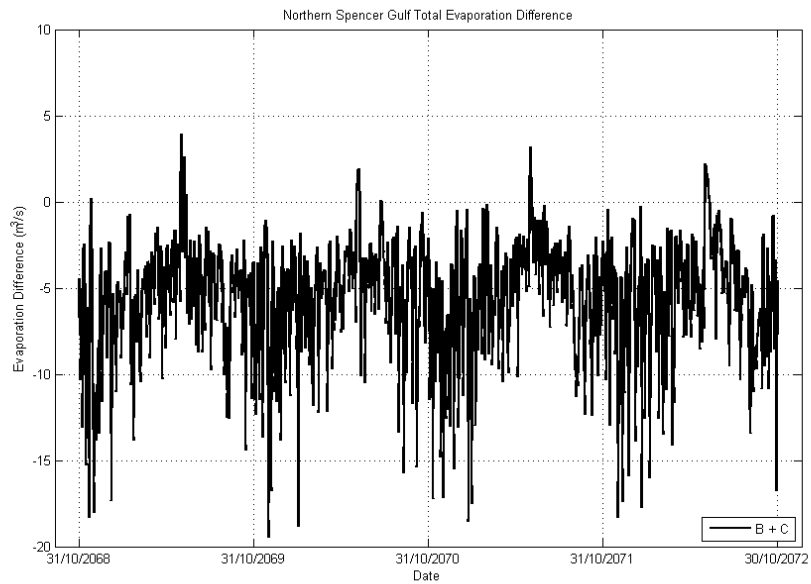


Figure 5-18 Difference of evaporation rates between climate change and baseline simulations for modelled Northern Spencer Gulf for the 2068 to 2072 period. The evaporation flux used to compute these differences assumes a negative sign indicating a flux out of the Gulf.

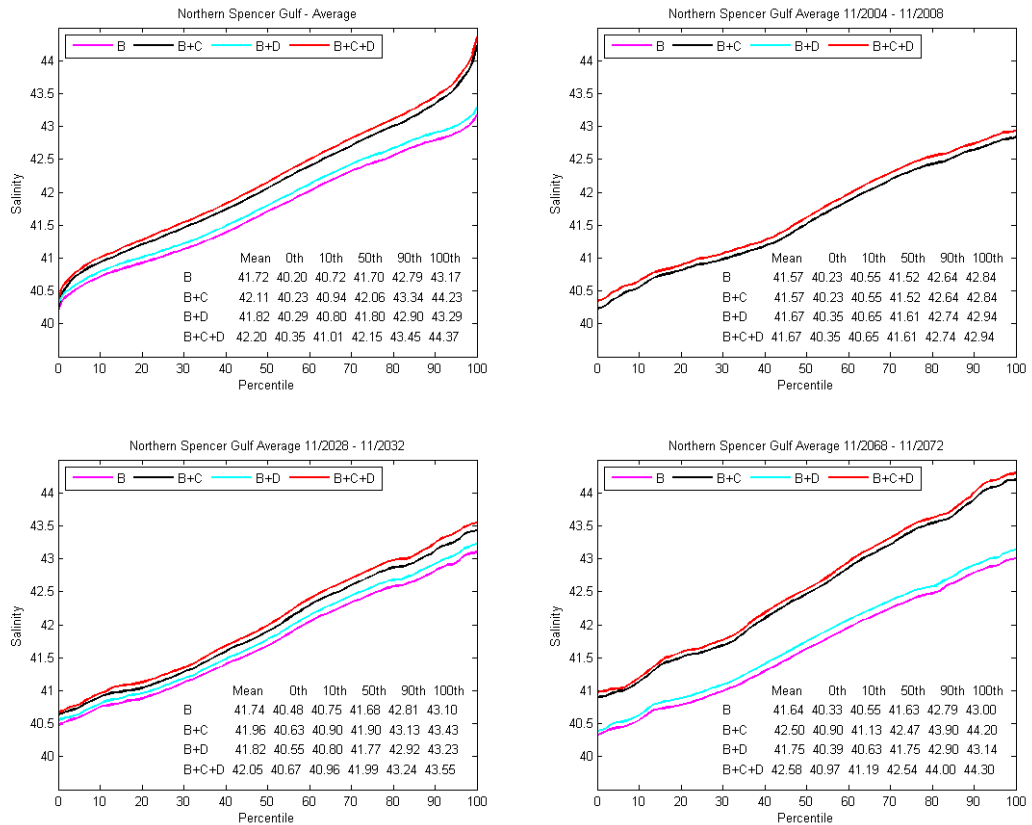


Figure 5-19 Modelled cumulative distributions of the Northern Spencer Gulf averaged salinities for different climate scenarios, and with and without the proposed desalination plant outfall discharge. Top left panel: 2004 to 2072 period; top right panel: 2004-2008 period; bottom left panel: 2028-2032 period; Bottom right panel: 2068-2072 period.

The figures for the entire gulf corresponding to those already presented for the Northern Gulf are presented below. The figures show that for the entire gulf the effects of climate change dominate the effects of the proposed desalination plant discharge (Figure 5-20 to Figure 5-23). For example, the cumulative distributions of modelled average Spencer Gulf salinities show that by the 2070 horizon, the effects of climate change would result in an average Spencer Gulf salinity increase of between 0.30 and 0.53, whilst the effects of the desalination plant increase the average Gulf salinity by 0.01.

Finally, modelled water balances presented in Table 5-4 show that on average the difference between desalination plant extraction and return corresponds to less than 0.3% of the difference between evaporation and rainfall over Spencer Gulf. Resulting salt balances are also presented in Table 5-5.

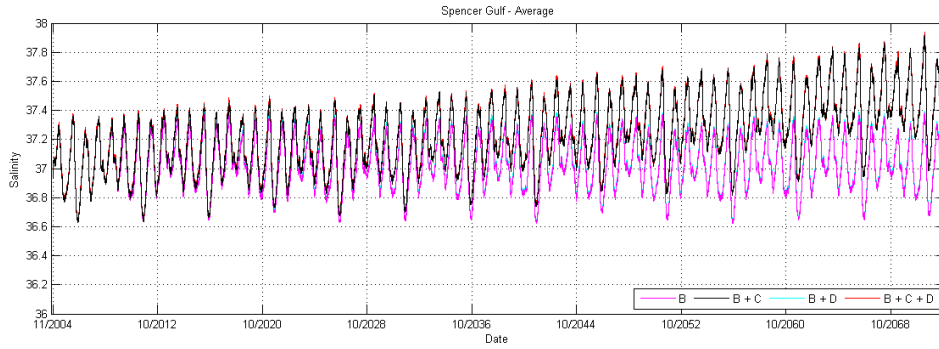


Figure 5-20 Modelled Spencer Gulf averaged salinities for different climate scenarios and with and without the proposed desalination plant outfall discharge for the 2004 to 2072 period

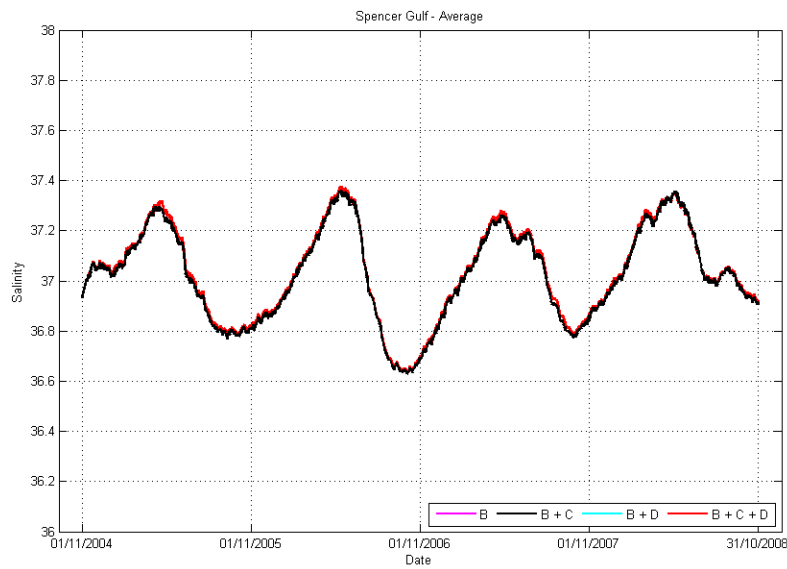


Figure 5-21 Modelled Spencer Gulf averaged salinities for different climate scenarios and with and without the proposed desalination plant outfall discharge for the 2004 to 2008 period

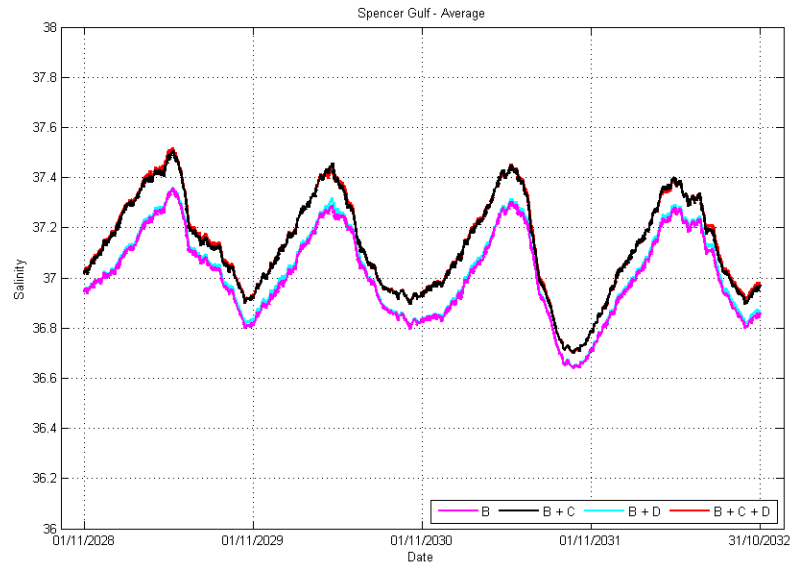


Figure 5-22 Modelled Spencer Gulf averaged salinities for different climate scenarios and with and without the proposed desalination plant outfall discharge for the 2028 to 2032 period

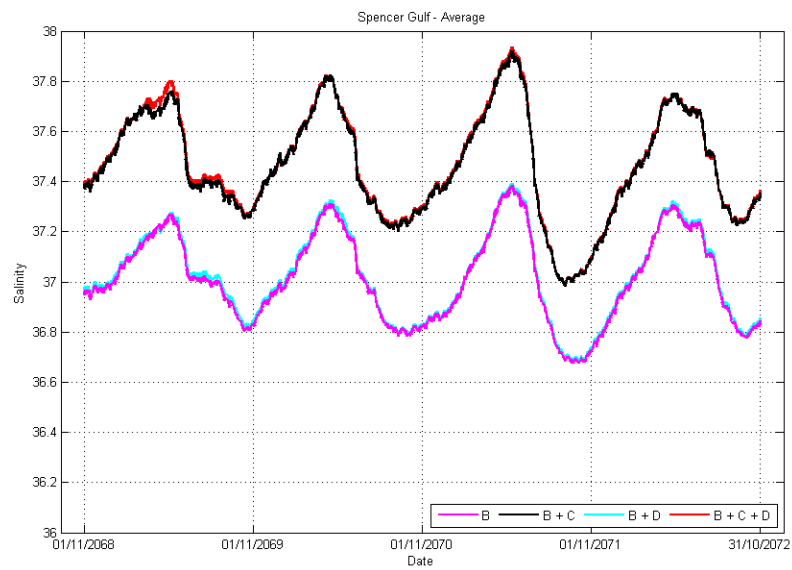


Figure 5-23 Modelled Northern Spencer Gulf averaged salinities for different climate scenarios and with and without the proposed desalination plant outfall discharge for the 2068 to 2072 period

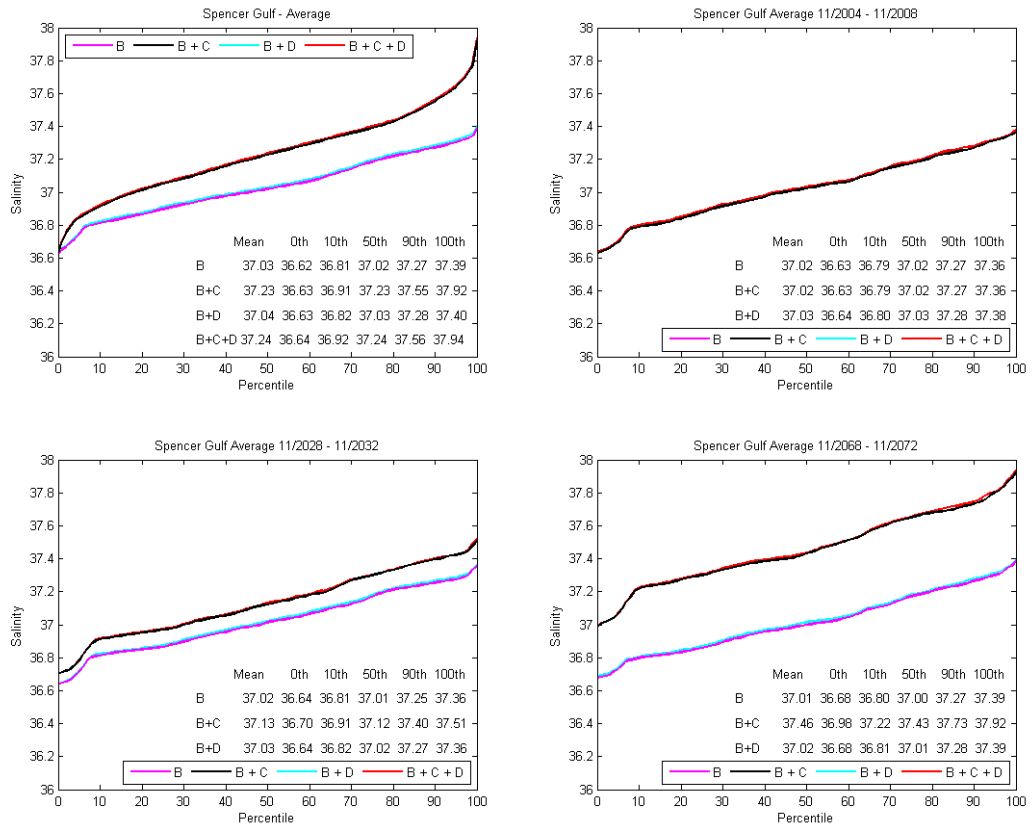


Figure 5-24 Modelled cumulative distributions of the Spencer Gulf averaged salinities for different climate scenarios, and with and without the proposed desalination plant outfall discharge. Top left panel: 2004 to 2072 period; top right panel: 2004-2008 period; bottom left panel: 2028-2032 period; Bottom right panel: 2068-2072 period.

Table 5-4 Simulated water balance with and without the effect of the proposed desalination plant

Salt Flux Item	B: 2004-2072 (Average)	B+D: 2004-2072 (Average)	B+C: 2004-2072 (Average)	B+C+D: 2004-2072 (Average)
	Gl an ⁻¹	Gl an ⁻¹	Gl an ⁻¹	Gl an ⁻¹
Tidal Influx	+7,280,000	+7,270,000	+7,270,000	+7,260,000
Tidal Eflux	-7,260,000	-7,250,000	-7,250,000	-7,250,000
Desal. Return	0.00	+113	0.00	+113
Desal. Intake	0.00	-205	0.00	-205
Evaporation	-30,160	-30,180	-31,430	-31,430
Rainfall	+6,920	+6,920	+6,860	+6,860
Other Inflows	+5	+5	+5	+5

Table 5-5 Simulated salt fluxes with and without the effect of the proposed desalination plant and with and without the effect of climate change. Salinity values were assumed to be gL^{-1} .

Salt Flux Item	B: 2004-2072 (Average)	B+C: 2004-2072 (Average)	B+D: 2004-2072 (Average)	B+C+D: 2004-2072 (Average)
	Gt an^{-1}	Gt an^{-1}	Gt an^{-1}	Gt an^{-1}
Tidal Influx	+262	+262	+261	+261
Tidal Eflux	-262	-262	-261	-261
Desal. Return	0.00	0.00	+0.01	+0.01
Desal. Intake	0.00	0.00	-0.01	-0.01
Other Inflows	+0.00	+0.00	+0.00	+0.00

6 DISSOLVED OXYGEN SIMULATIONS

In order to assess the likely dissolved oxygen dynamics associated with the proposed SEIS diffuser design, the high resolution ELCOM model (as presented in Appendix H5.2 of the SEIS) was augmented to include direct simulation of dissolved oxygen via activation of the water quality model CAEDYM (Computational Aquatic Ecosystem Dynamics Model).

CAEDYM is a process-based model of the major biogeochemical processes influencing water quality. It optionally models inorganic particles, oxygen, organic and inorganic nutrients (C, N, P and Si), multiple phytoplankton and zooplankton groups, fish and bacteria. Recent developments also include optional modules for benthic organisms (e.g. clams, macroalgae), pathogens and microbial indicator organisms, and a generic geochemical module capable of simulating pH, aqueous speciation (including metals), precipitation/dissolution reactions and sediment diagenesis. CAEDYM has been applied to a variety of aquatic systems including wetlands, lakes/reservoirs, rivers, estuaries and the coastal ocean (<http://www.cwr.uwa.edu.au/software1/models/caedym/caedym.php>). Specifically, ELCOM-CAEDYM (as used in this study) has been applied in the Australian context to this same matter of investigating dissolved oxygen dynamics in the vicinity of brine return water discharges (Okely *et al.*, 2006) so its use in this regard is established.

6.1 Model Setup

The high resolution ELCOM model was used to simulate dissolved oxygen dynamics in the vicinity of the diffuser. Individual setup elements are described below.

6.1.1 Simulation Period

A simulation period was selected for this analysis so as to capture the potential worst case scenario in terms of local dissolved oxygen dynamics. Specifically, the period was selected to coincide with the small amplitude neap tides (dodge tides) that occur each year in May. The period selected was as follows:

- 06/05/2008 12:00 to 16/05/2008 3:00.

Within this period was a dodge tide, and the smallest tidal elevation changes within this dodge tide was the following one day period:

- 14/05/2008 03:13 to 15/05/2008 03:13; (tidal range approximately 0.38 metres over the day).

This period is presented in Figure 6-1, and was used for data extraction purposes.

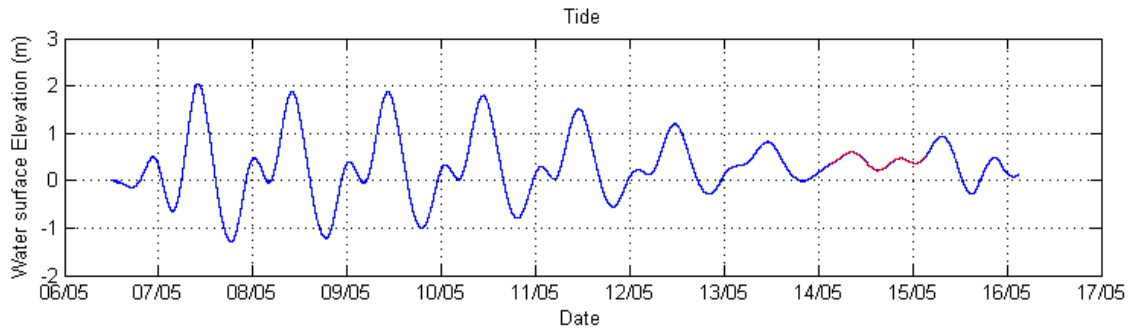


Figure 6-1 Autumn dodge tide at Point Lowly (central day shown in red)

6.1.2 Initial Conditions

6.1.2.1 Salinity

The simulation described here was hot-started in terms of the specification of the initial salinity field. Specifically, this field was set by interrogating the low resolution model at the autumn ELCOM-CAEDYM starting time, with the interrogated low resolution model having been run over a preceding multi-annual period. Depth averaged (spatially variant) low resolution salinity was extracted and interpolated to the high resolution model domain to provide the initial salinity field. This approach ensured that the initialisation of the high resolution simulation captured the spatial salinity variations characterising the Gulf during autumn. No evidence for initial transients resulting from this interpolation was observed.

6.1.2.2 Temperature

The simulation was initialised for water temperature using the same technique as for salinity.

6.1.2.3 Dissolved Oxygen

The initial dissolved oxygen field was set using the data presented in Johnson (1981). These data include measurements of water column dissolved oxygen at several locations (including Pt Lowly), depths and seasons throughout Spencer Gulf, and span the years 1975 to 1978. The data from Pt Lowly was analysed in terms of observed percent saturation dissolved oxygen and are shown in Figure 6-2. The horizontal axis is a 'day of year', and this was selected to facilitate identification of any seasonal trends. The figure shows that in general, the waters around Pt Lowly are very well oxygenated, with the minimum observed percentage saturation being approximately 92%.

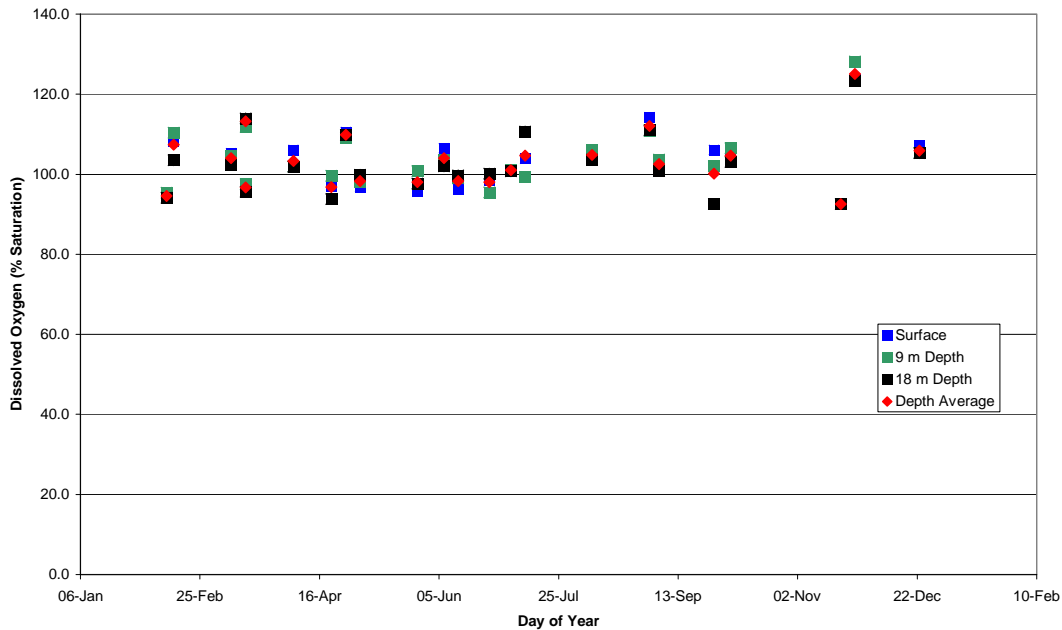


Figure 6-2 Johnson (1981) dissolved oxygen (percentage saturation) measurements at Pt Lowly

In order to adopt a conservative approach in the ELCOM-CAEDYM simulations, a background percentage saturation of 92% (the lowest observed value) was selected. Once this saturation value had been selected, the dissolved oxygen concentrations in mgL^{-1} were computed from the initial salinity and temperature fields described above, and used to initialise ELCOM-CAEDYM.

6.1.2.4 Model Spin Up

In addition to initialising the high resolution model with the salinity, temperature and dissolved oxygen fields as described above, the full high resolution ELCOM-CAEDYM model was also spun up for approximately one (1) week preceding the dodge tide of interest. This spin up allowed for the localised behaviour of the return water plume to be established in three dimensions.

6.1.3 Boundary Conditions

6.1.3.1 Return Water

The quality of the return water entering the ELCOM-CAEDYM model (as a mixed quantity) was set using extracted timeseries from a previously computed temporally coincident base case (no return water) high resolution simulation. Specifically, the depth average temperature, salinity and dissolved oxygen concentrations above the diffuser location in this base case were extracted and combined with the return water in a dynamically varying ratio set by the CFD study and the background tidal velocities. This used the same methodology as described in Section 3.6.4, so is not repeated here. The assumed raw (i.e. at diffuser nozzle) return water quality was provided by BHP Billiton and was:

- Salinity: 75 gL^{-1} ;
- Temperature: Ambient at the intake site, plus 1 degree Celsius (this also varied dynamically according to the simulated temperature at the intake site in each season);

- 100% saturation dissolved oxygen at the given temperature and salinity; and
- Maximum flow rate ($4.3 \text{ m}^3\text{s}^{-1}$).

Depth average information was used firstly to be consistent with the previously adopted methodology, but also to capture the fact that the discharge plume, on exit from the diffuser, mixes with a large fraction of the water column.

6.1.3.2 Atmospheric Forcing

The same atmospheric forcing data used in the high resolution simulations was applied to the ELCOM-CAEDYM simulations. Full water column – atmosphere interaction was allowed. In order, however, to establish ‘worst case’ wind conditions, wind speeds were set to zero for a two day period commencing one day prior to the nominated extraction period shown in red in Figure 6-1. This reduced wind mixing of the water column and hence supply of atmospheric oxygen to depth. It is noted that turning off the wind field in this instance has been a deliberate decision to promote simulation of worst case conditions, and is not a reflection of a simplifying model assumption.

6.1.4 CAEDYM Configuration

CAEDYM was configured to simulate the following oxygen dynamics:

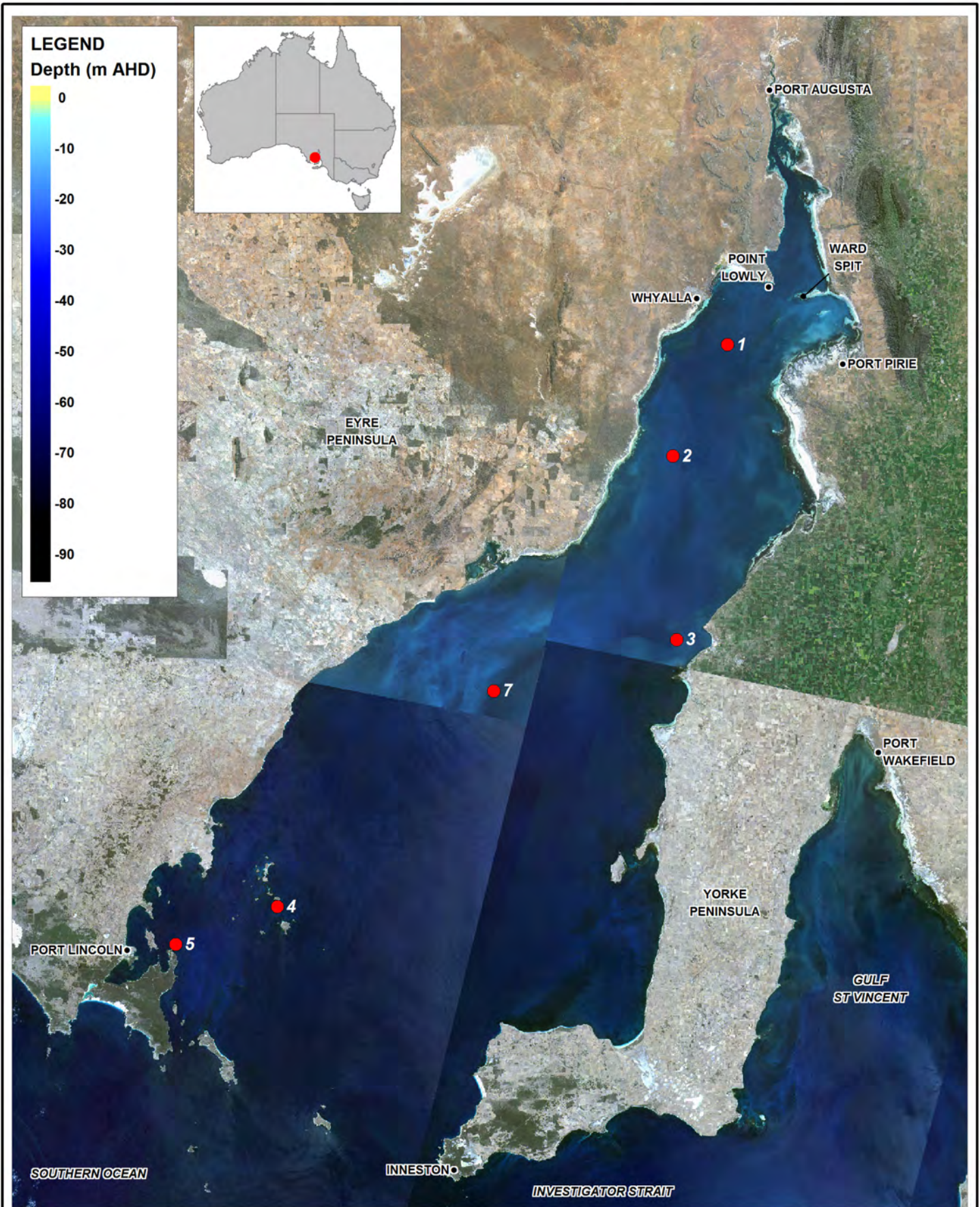
- Atmospheric exchange; and
- Sediment oxygen demand (SOD).

Atmospheric exchange in CAEDYM is based on the model of Wanninkhof (1992) and the flux equation of Riley and Skirrow (1974). A simple static sediment oxygen demand (SOD) model is employed within CAEDYM that uses a Michaelis-Menton function given by

$$SOD = SOD_{MAX} \left(\frac{DO}{K_{SOD} + DO} \right)$$

where SOD_{MAX} is the maximum demand, K_{SOD} is a half saturation constant and DO is the overlying dissolved oxygen concentration.

Lauer (2005) was used to set the value of SOD_{MAX} within the ELCOM-CAEDYM simulations. Lauer (2005) sampled SOD at 6 locations within Spencer Gulf (Figure 6-3) across several seasons. No measurements were made directly off Pt Lowly, however the site closest (Western Shoal) showed little seasonal variation in SOD, with typical values around 0.3 to $0.4 \text{ gm}^{-2}\text{day}^{-1}$ (as converted from Lauer 2005, Figure 5-7). Despite this, other sites throughout the Gulf exhibited much larger SOD. As such, and with the overall intent to be conservative, the maximum SOD observed by Lauer (2005) at sites within the main body of the Gulf, and across all seasons, was adopted for the current simulations. The adopted SOD was thus set at $0.921 \text{ gm}^{-2}\text{day}^{-1}$. The half saturation constant (K_{SOD}) was set to 0.5.

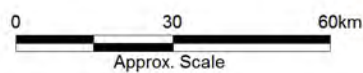


Title:
**Lauer (2005) SOD sampling sites
(estimated from Lauer (2005) Figure 5.1)**

Figure:
6-3

Rev:
A

BMT WBM endeavours to ensure that the information provided in this map is correct at the time of publication. BMT WBM does not warrant, guarantee or make representations regarding the currency and accuracy of information contained in this map.



Filepath :

This ELCOM-CAEDYM setup was reviewed by CWR staff to ensure accuracy and consistency in the application of CAEDYM with other contextually relevant Australian studies.

6.2 Model Execution

Two simulations were executed as follows:

- Autumn without return water discharge (the previously described base case); and
- Autumn with return water discharge.

Comparison of these allowed for the assessment of the return water discharge on local dissolved oxygen dynamics.

6.3 Results

The following results are presented in the subsequent sections:

- 1 Bottom sheet dissolved oxygen. These sheets show a snapshot of bottom layer predicted dissolved oxygen concentrations at the end of the red dodge tide period shown in Figure 6-1, with base case (no return water discharge) and brine discharge results co-presented to facilitate comparison;
- 2 Mid depth sheet dissolved oxygen. These sheets show a snapshot of mid depth layer predicted dissolved oxygen concentrations at the same time as above, again with base case (no return water discharge) and brine discharge results co-presented;
- 3 Vertical profiles of dissolved oxygen. These profiles span the entire simulation period for both base case and discharge scenarios, and are located 100 and 500 metres northeast and southwest of the diffuser, perpendicular to its alignment. Difference contours (i.e. desalination case subtract base case) of these curtains are also provided; and
- 4 Vertical curtain of dissolved oxygen. This curtain shows a snapshot of dissolved oxygen near the end of the one day dodge tide period (as defined above), with base case (no return water discharge) and brine discharge results presented in parallel to facilitate comparison. The curtain runs over a distance of approximately 1800 metres directly perpendicular to the alignment of the proposed diffuser. The diffuser outlet is at approximately 1200 metres along the curtain.

All results are presented as milligrams per litre (mgL^{-1}) of dissolved oxygen. This is to allow reference to the water quality objectives (WQOs) provided by DEH (2006), which uses these units. Specifically, DEH (2006) states that the WQO for dissolved oxygen (albeit varying from zone to zone) is greater than 6.5 mgL^{-1} (DEH, 2006. Appendix A).

6.3.1 Bottom Sheets

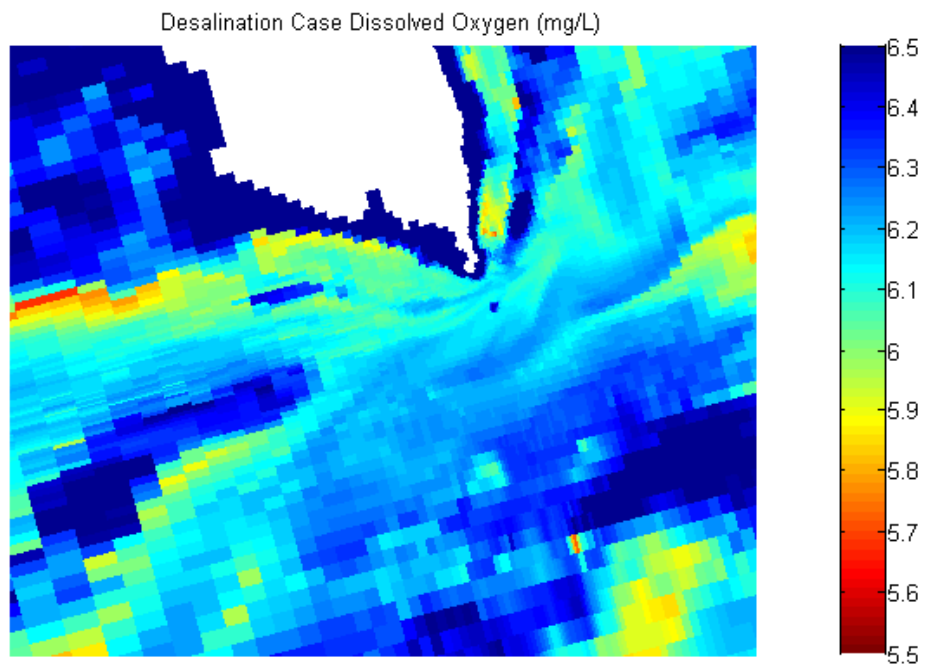
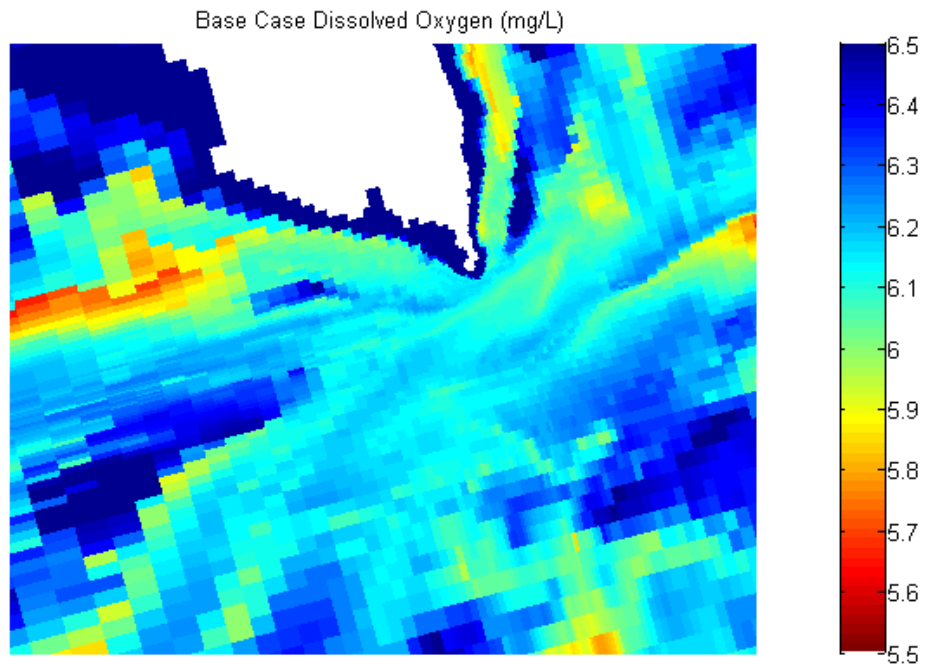


Figure 6-4 Bottom layer dissolved oxygen (mgL^{-1}) at the end of the dodge period

6.3.2 Mid Depth Sheets

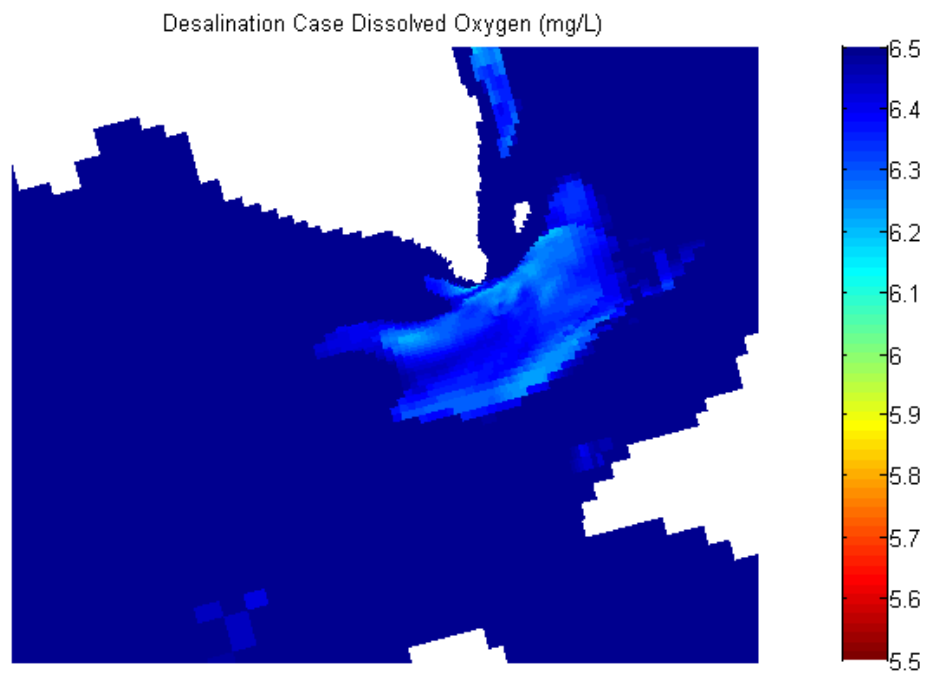
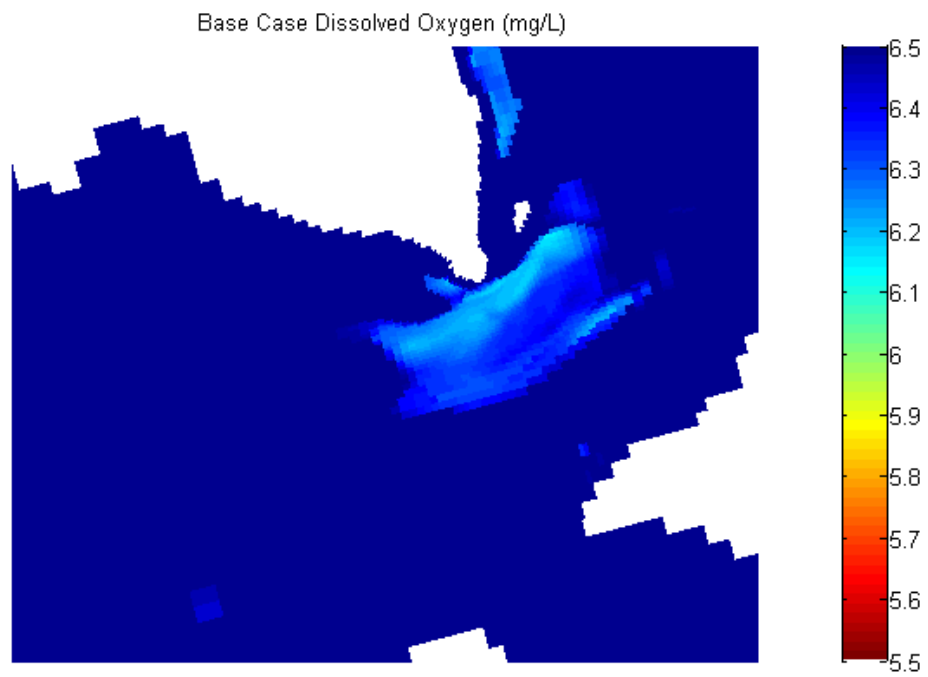


Figure 6-5 Mid depth dissolved oxygen (mgL^{-1}) at the end of the dodge period

6.3.3 Profiles

6.3.3.1 100 Metres Northeast

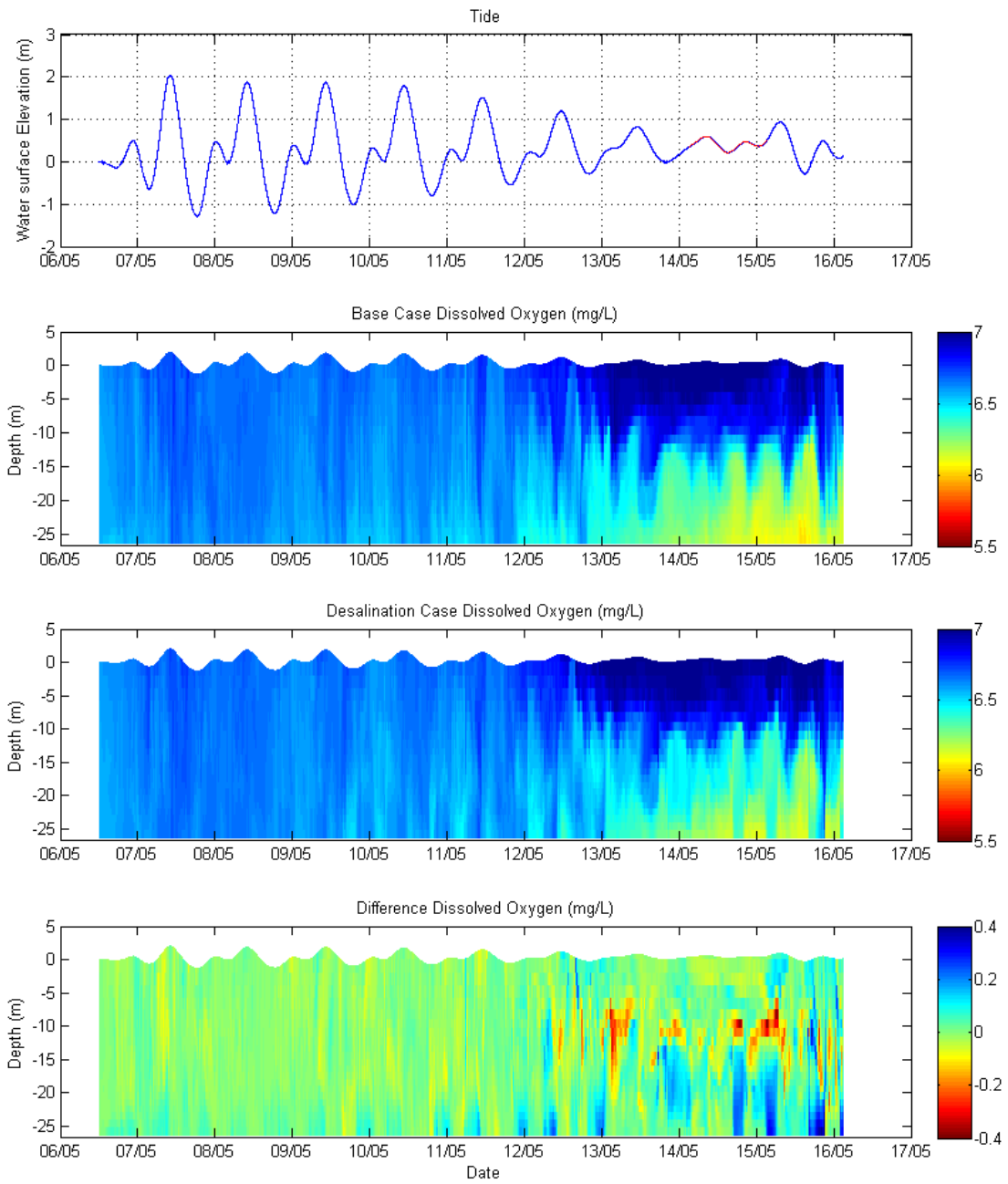


Figure 6-6 Profile dissolved oxygen (mgL⁻¹) - 100 metres northeast

6.3.3.2 100 Metres Southwest

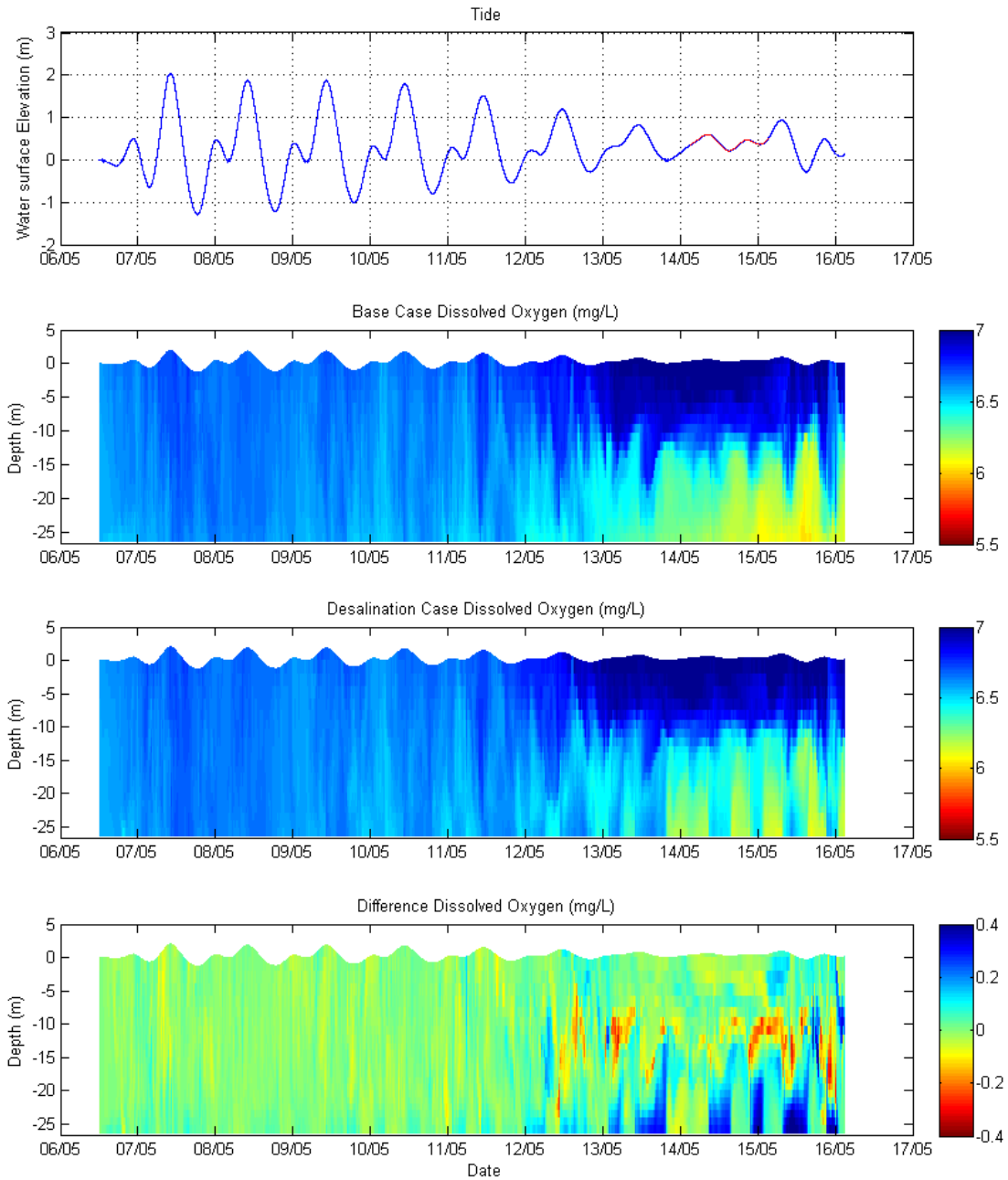


Figure 6-7 Profile dissolved oxygen (mgL⁻¹) - 100 metres southwest

6.3.3.3 500 Metres Northeast

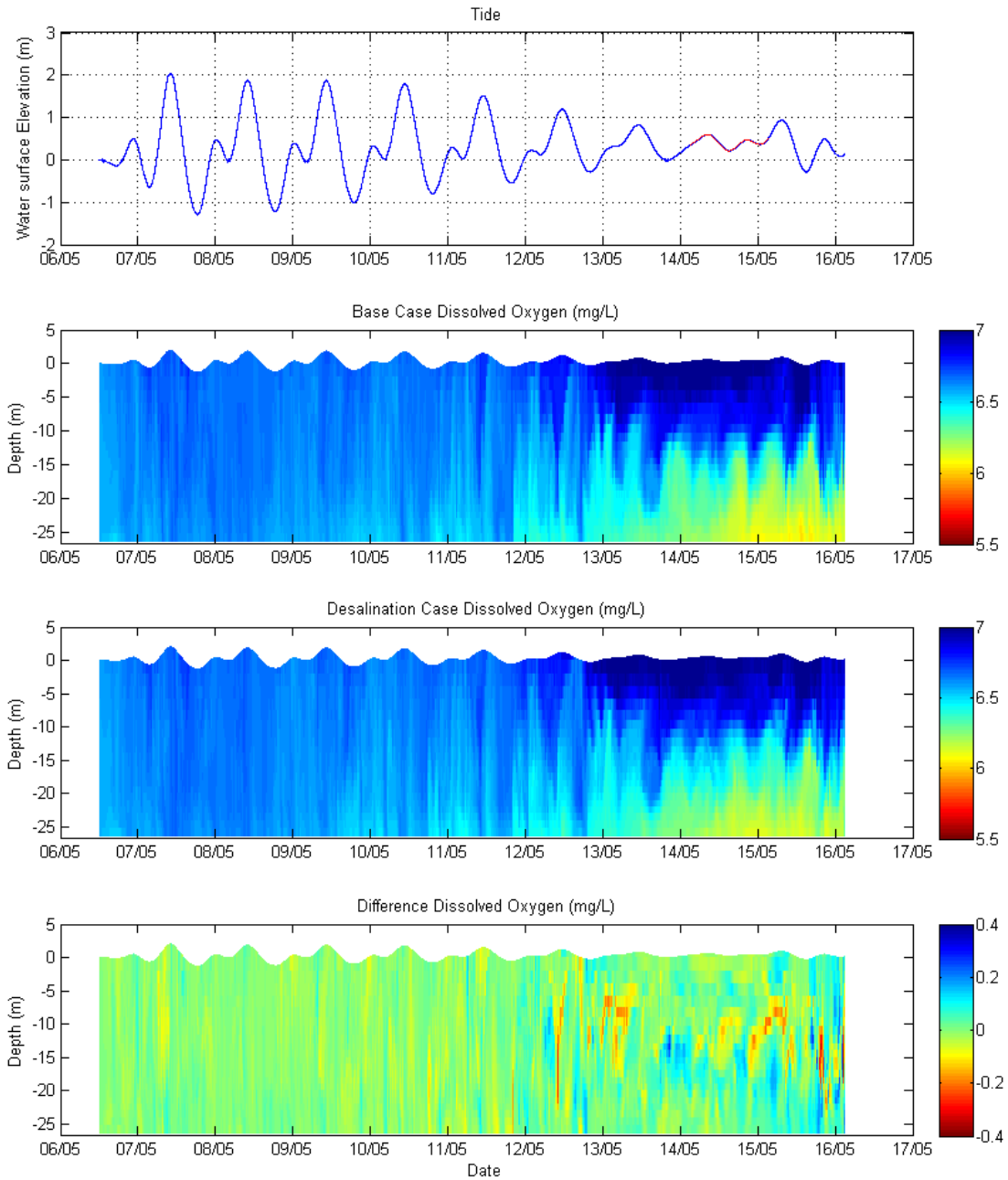


Figure 6-8 Profile dissolved oxygen (mgL⁻¹) - 500 metres northeast

6.3.3.4 500 Metres Southwest

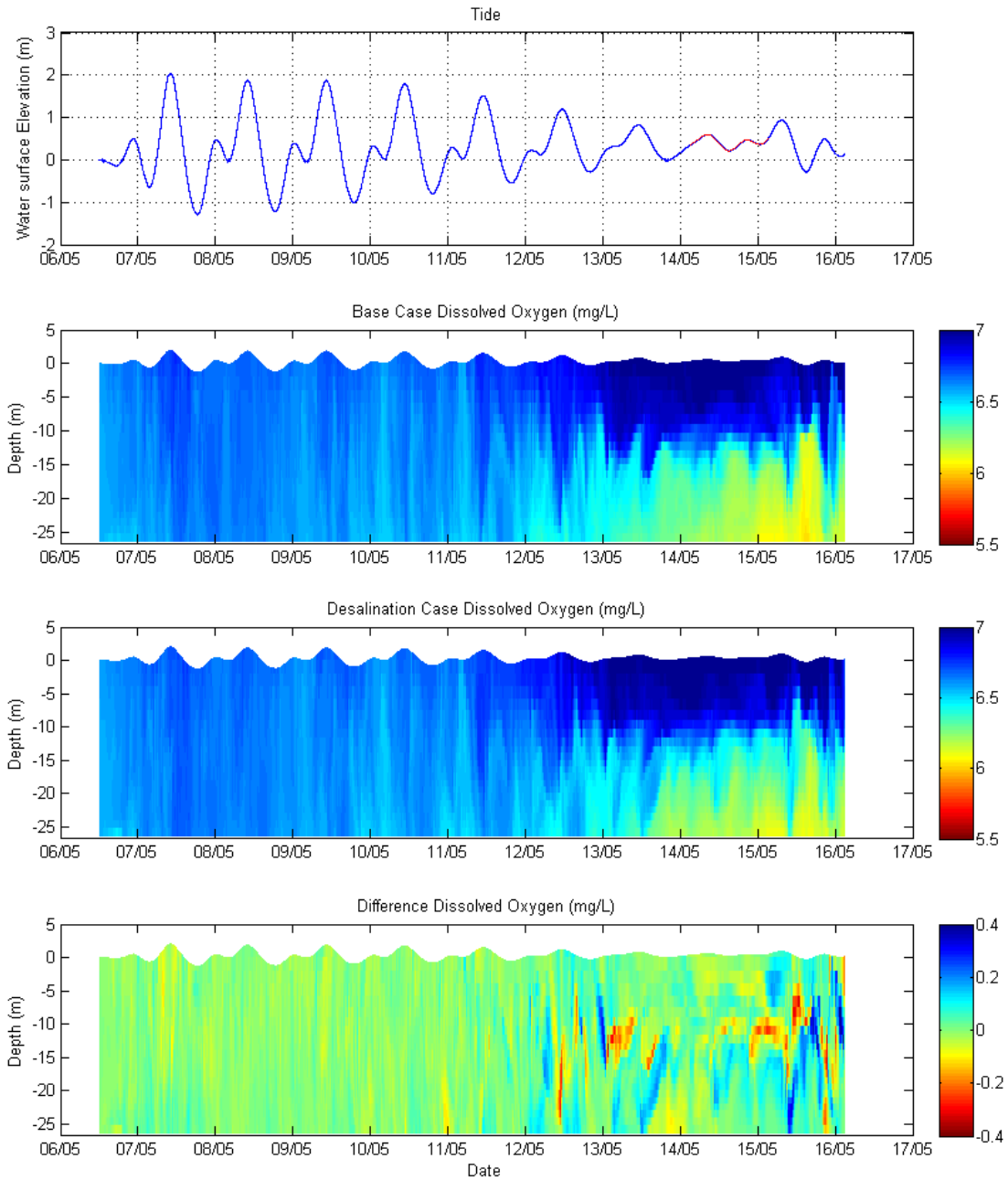


Figure 6-9 Profile dissolved oxygen (mgL⁻¹) - 500 metres southwest

6.3.4 Curtain

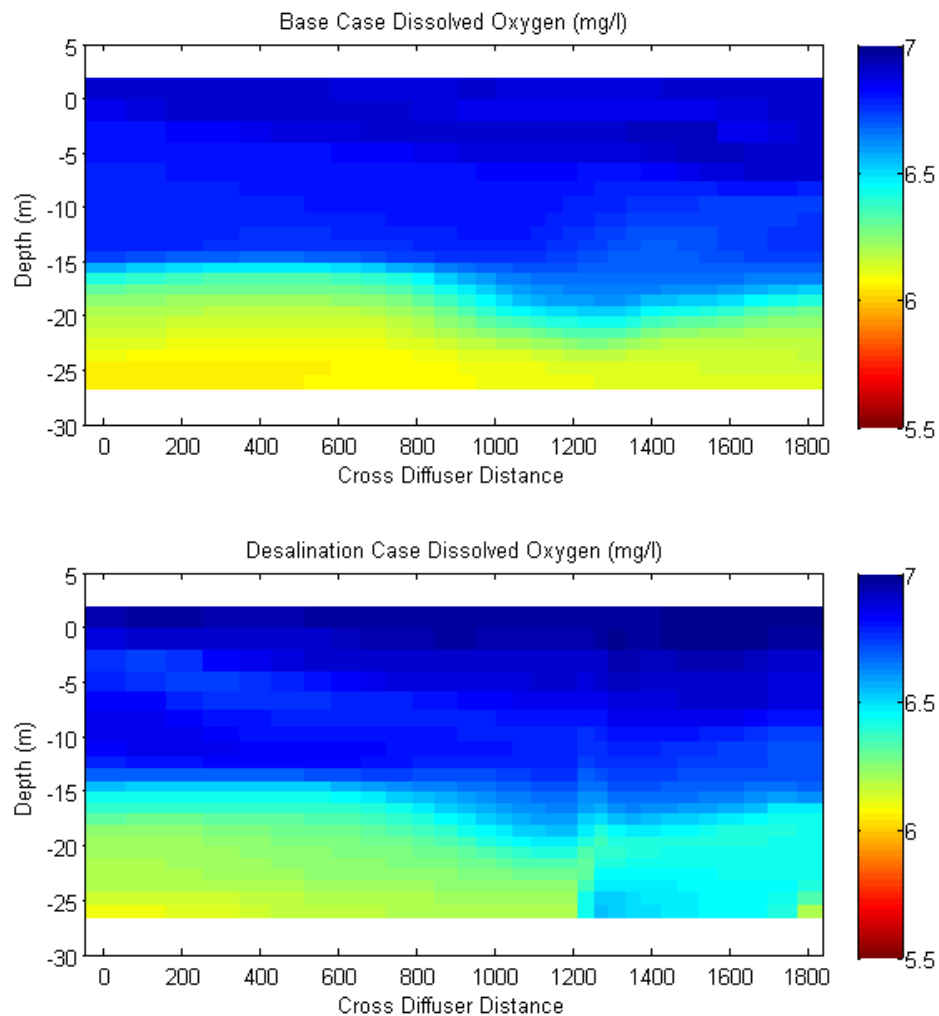


Figure 6-10 Transverse curtain dissolved oxygen (mgL^{-1}) at the end of the dodge period as tides commence. The diffuser is at approximately 1200 metres.

The model predicts that some vertical stratification of dissolved oxygen may develop over the wind-free dodge period in the natural (base case) conditions, so that at times the dissolved oxygen concentrations may drop below the nominated WQO at depth. There is, however, no evidence in the model results to suggest that significant additional deoxygenation of bottom waters occurs during the simulated period as a result of the desalination discharge, i.e. over and above predicted natural conditions. This appears to be the case even with the adoption of the conservative assumption that the greatest sediment oxygen demand measured in Lauer (2005) for sites in the main section of Spencer Gulf operates throughout the entire model domain. In some cases the model shows that the brine discharge acts as an effective conduit for delivery of well-oxygenated mid-depth waters to the bed, thus occasionally increasing dissolved oxygen at depth, as evidenced, for example, in the profile timeseries contours presented in Figure 6-9.

7 UPWELLING POTENTIAL

The potential for upwelling has been examined here using the upgraded modelling tools developed as part of the SEIS process, and this analysis is described below. It is noted that this analysis is very much exploratory and investigative, and that the first part of the analysis (scenario 1 below) was motivated by an attempt to replicate, in part, modelling provided as part of a public submission to the DEIS.

7.1 Background

The process of upwelling is well established in the literature (recently, Shintani *et al.*, 2010). The basic principle of upwelling is that wind blowing in one direction on the surface of a water body can induce a return current in the opposite direction at depth. In a stratified water body, wind action can thus induce thermocline (or pycnocline) tilt and result in delivery of bottom waters to the surface at the upwind end of the domain. This process of causing deep waters to move upwards under the action of a surface wind is known as upwelling.

More quantitatively, Thompson and Imberger (1980) and Imberger and Hamblin (1982) considered a lake (as an example of where upwelling might occur) as a two layer rectangular basin and developed the concept of the Wedderburn number, W

$$W = \frac{g' h_1^2}{u_*^2 L} \quad (1)$$

where $g' = g(\rho_2 - \rho_1) \rho_1^{-1}$ is the reduced gravity where ρ_1 and ρ_2 are the upper and lower layer densities, respectively, h_1 is the upper layer thickness at rest condition, u_* is the water-side shear velocity, and L is the length of the rectangular basin. Specifically, it was shown that the magnitude of upwelling scales inversely with this dimensionless parameter, or that as g' increases, the propensity for upwelling decreases for a given wind shear.

Notwithstanding the above, the intent of this report is not to review or explain this process in detail, but rather to investigate its applicability to the case of return water discharge upwelling to shallow water at Pt Lowly. The reader is referred to Shintani *et al.* (2010) and included references for a mathematical description of the dynamics of upwelling.

In order to undertake this investigation, a suite of numerical simulations has been executed using the high resolution model, or a derivative. The analysis approach was such as to graduate from describing a relatively simplistic setting through to simulating a representation of real world conditions. As such, the following simulations are presented:

- 1 A two-dimensional (i.e. vertically and longitudinally resolved but laterally constrained – a vertical slice model) simulation;
- 2 A three-dimensional version of 1, with the lateral constraint removed so that water can flow into and out of the model through its sides, but maintaining the vertical slice geometry. This is referred to as the quasi three-dimensional model;

- 3 A fully three dimensional model (i.e. using real bathymetry) with a range of wind forcing regimes but no tidal forcing (i.e. completely perpetually slack water); and
- 4 A fully three dimensional model with tidal forcing turned on and the autumn dodge tide described in Section 6.1.1 simulated, with (to allow comparison) a wind forcing selected from 3 applied instead of the actual wind forcing.

All simulations and their results are described below.

7.2 Two-Dimensional Model

The first model applied here is that of a vertical slice two-dimensional domain.

7.2.1 Model Domain

To affect this simulation, the high resolution ELCOM model described above and elsewhere was truncated to cover a transect that (approximately) spanned Spencer Gulf from Port Bonython to the eastern shore. The location of this transect is shown in Figure 7-1.

To do so, three dimensional bathymetry was excised from the entire high resolution ELCOM model domain outside a narrow band of five rows of cells set along the alignment shown in Figure 7-1. This is the equivalent of placing solid 'walls' on each side of the alignment. The vertical slice bathymetry is presented in Figure 7-2 and Figure 7-3.

7.2.2 Vertical Resolution

In order to allow resolution of any upwelling processes, the previously described high resolution ELCOM model was augmented to include a vertical resolution of 20 cm at all depths throughout the domain.

7.2.3 Timestep

To complement the above increase in vertical resolution, the timestep in this simulation was reduced to 5 seconds.

7.2.4 Longitudinal Resolution

The model resolution 'along' the slice from Port Bonython to the eastern shore of Spencer Gulf varies from 40 metres to several hundred metres, reflecting the overall (complete) high resolution model domain. Importantly, the region of 40 metre resolution covers the steep slope westward of the deep basin (see Figure 7-2). This, in combination with the 0.2 metre vertical layer thicknesses, provided high resolution in the area where upwelling potential is to be investigated.

The vertical slice is five cells 'wide' (approximately 600 metres) so that any influence of the solid side walls in terms of viscous drag is minimised. The domain is approximately 20 kilometres 'long', and despite being laterally constrained, the bathymetry is real within the section of the slice. The short sides (i.e. at Port Bonython and the eastern shore) are also closed and are set to land. This created a closed box on all sides.



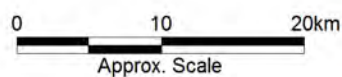
Image ©2009 Google™
Data SIO, NOAA, U.S. Navy,
NGA, GEBCO
Image © 2010 DigitalGlobe
Image NASA
Image © 2010 Cnes/Spot Image

Title:
Plan location of two-dimensional model

Figure:
7-1

Rev:
A

BMT WBM endeavours to ensure that the information provided in this map is correct at the time of publication. BMT WBM does not warrant, guarantee or make representations regarding the currency and accuracy of information contained in this map.



Filepath :

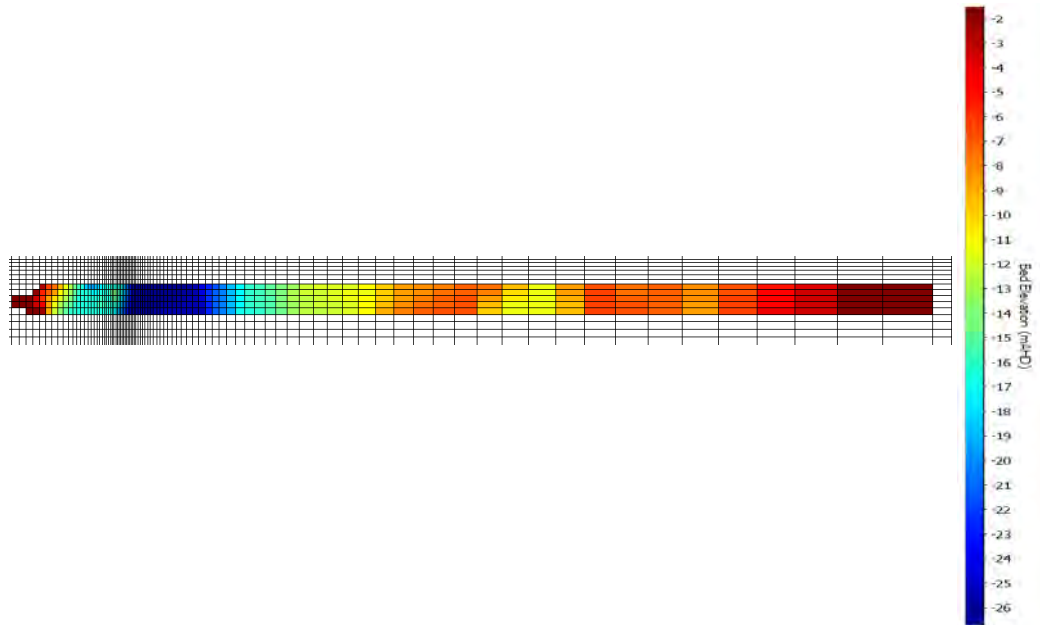


Figure 7-2 Two-dimensional model bathymetry – plan view. The left hand end is not ‘square’ as it encompasses a small (shallow) beach area just to the south of Point Lowly. The figure shows model grid lines to illustrate the high resolution region around the area of upwelling potential.

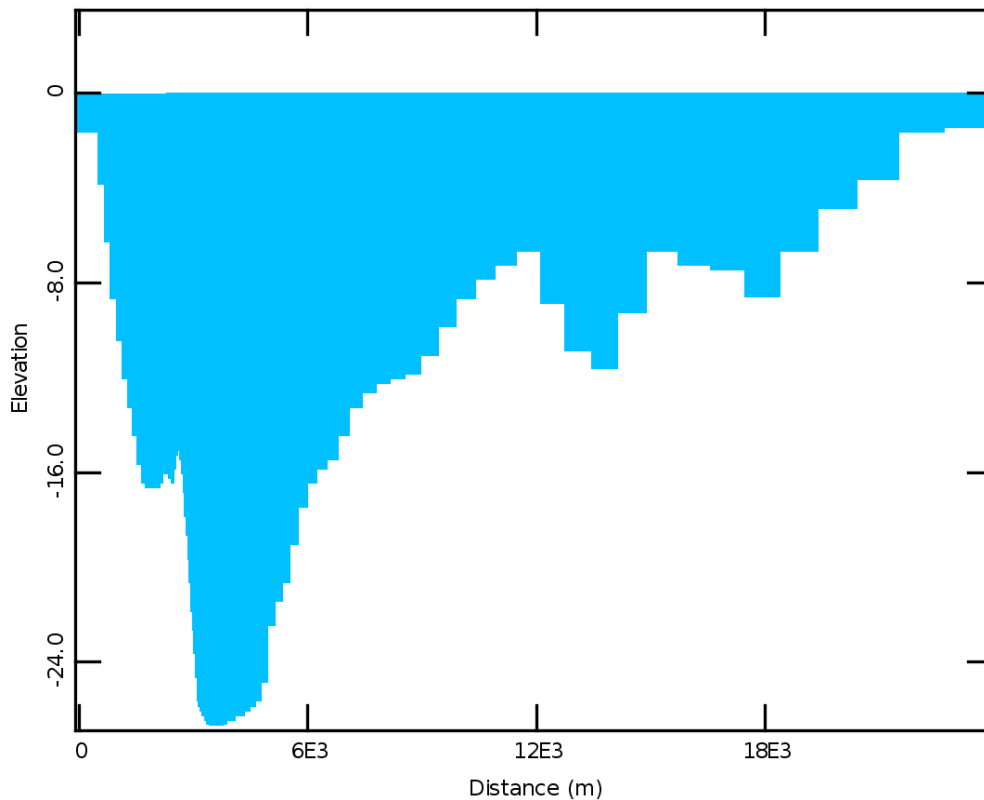


Figure 7-3 Two-dimensional model bathymetry – profile view

7.2.5 Initial Condition

The initial condition in salinity was set as a linear increase from ambient to a 1.52 gL^{-1} anomaly at the bed, over the bottom 5 metres. Ambient was assumed to be 43 gL^{-1} . As such, this linear salinity field provides a maximum salinity at the bottom of 44.52 gL^{-1} , which is the result of a 20:1 dilution of 75 gL^{-1} brine. This dilution does not represent the dilutions attained in this SEIS overall study (see Section 3.6.4.2, where worst case dilutions are 43:1). Temperature was set to a uniform value of 20 C.

7.2.6 Wind Forcing

The wind direction in the ELCOM model was set to be parallel to the model orientation in Figure 7-1, i.e. blowing along the longitudinal axis of the model from Port Bonython to the eastern shore. The wind speed was set to a constant at 15 ms^{-1} , applied as a step function from 0 ms^{-1} .

7.2.7 Tidal Forcing

The two-dimensional nature of this model precludes application of tidal flows perpendicular to the plane of the model. As such, tidal currents are effectively shut off in this simulation.

7.2.8 Simulation Period

The ELCOM model was executed for 2 days under the above forcing.

7.2.9 Results

The two figures following present salinity colour contours of the vertical slice model overlain with velocity vectors at just after initialisation (referred to as zero hours) and 6 hours into the simulation. The top panel in each is a vertical curtain running from Port Bonython to the eastern shore (left to right), and the panels under that in each figure are horizontal surface and bottom salinities (with velocity arrows), respectively, also running from Port Bonython (left hand side) to the eastern shore (right hand side). Salinity colour contours have been truncated at 43.4 gL^{-1} (i.e. all salinities above this value appear the same colour of red) in the figures to allow visualisation of upwelling. As such, the red colour in the salt initialisation figure does represent salt at 45 gL^{-1} , despite appearing the colour tagged as 43.4 gL^{-1} in the colourbar. Arrows are plotted on a regular grid which is (for the top panel in each figure below) at a much coarser spatial resolution than the model resolution, especially in the vicinity of the steep slope to the west of the brine injection location. This has been done for clarity of presentation.

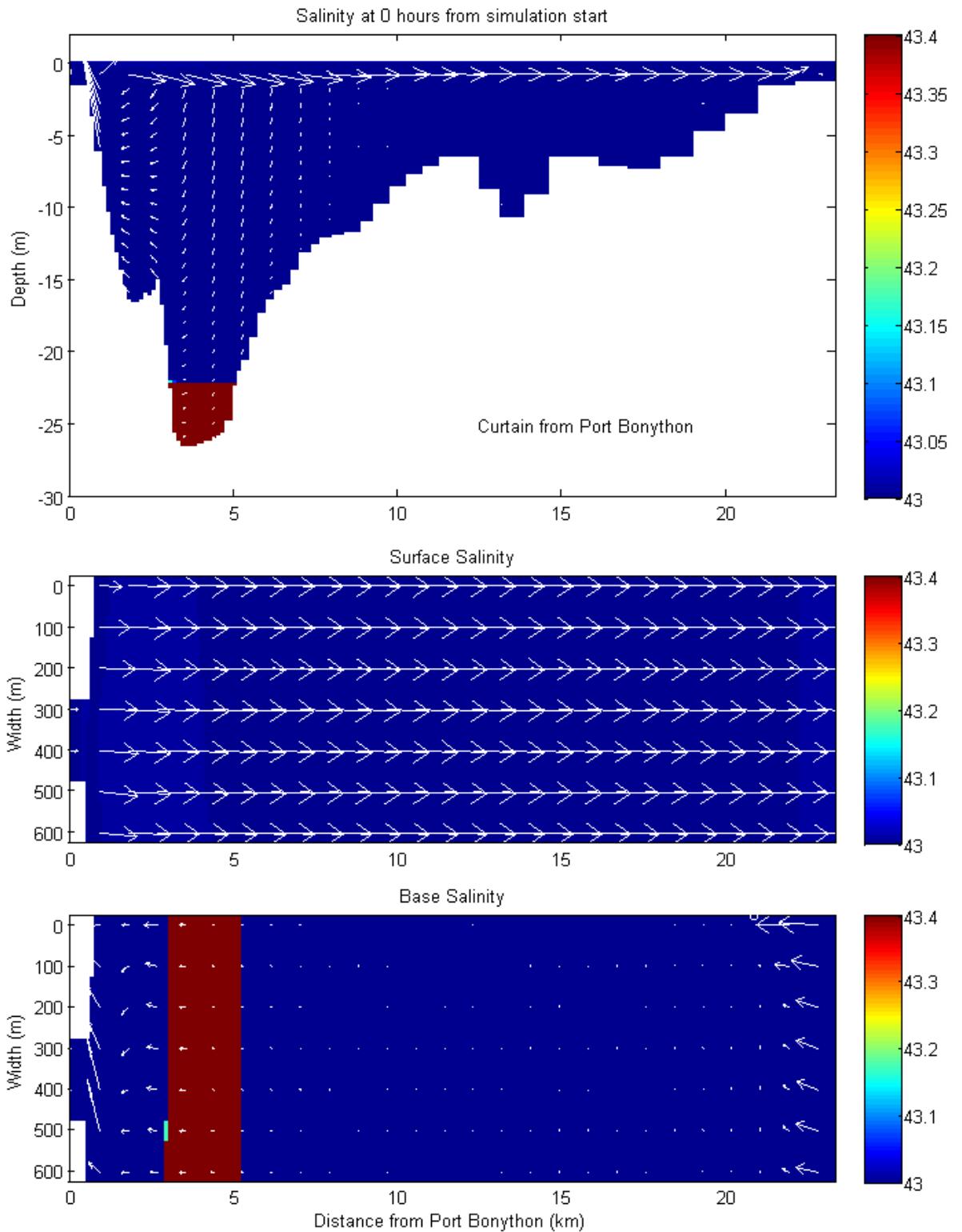


Figure 7-4 Salinity and velocities immediately following initialisation. As for all subsequent figures, velocity arrows in the top panel are plotted at a much coarser spatial resolution than the model resolution.

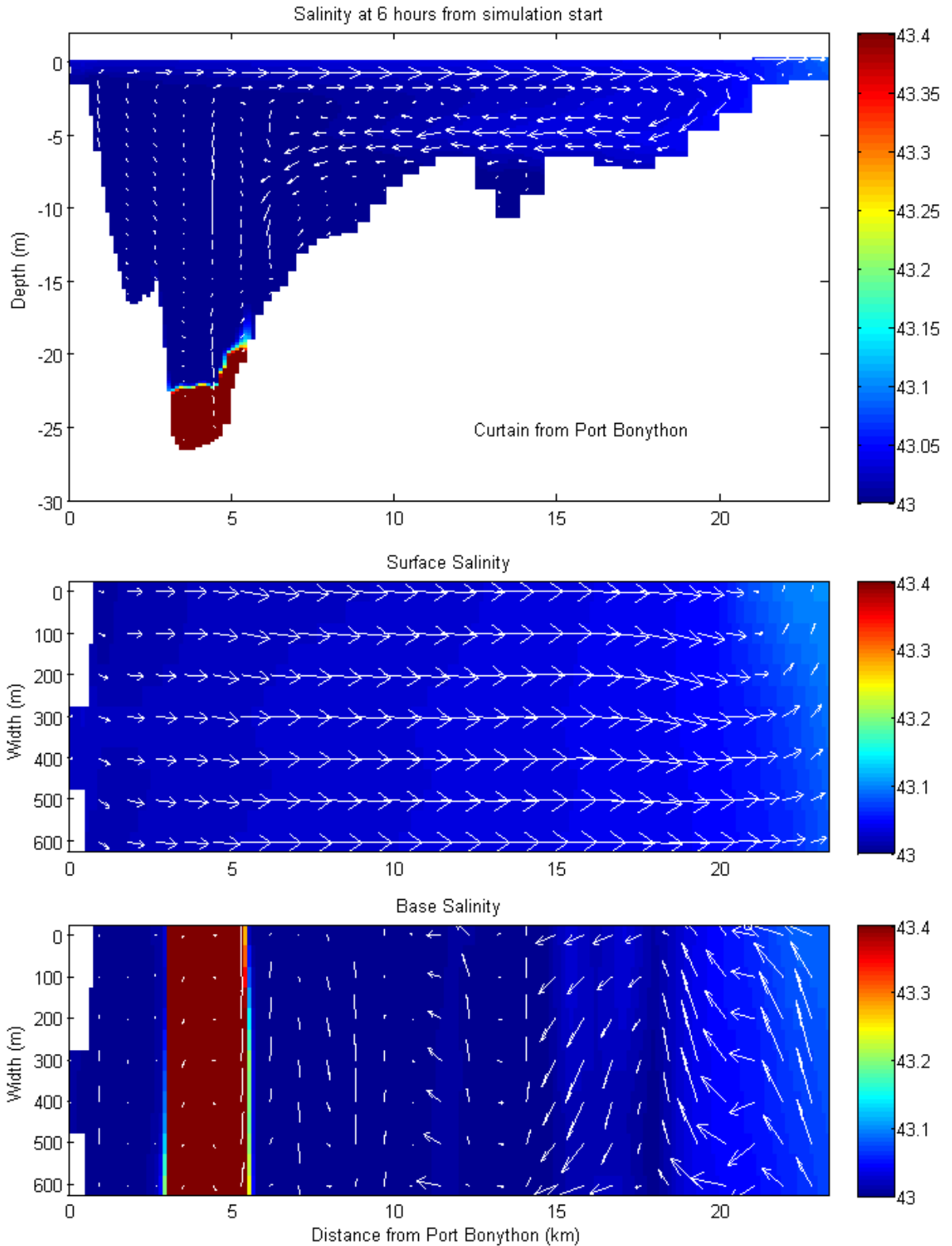


Figure 7-5 Salinity and velocities 6 hours following initialisation

The figures demonstrate that after 6 hours the two-dimensional model predicts that an upwelling circulation has developed, with surface and bottom waters travelling in opposite directions. The brine pool in the model also appears to feel the influence of this circulation. It is noted that, despite this

perturbation, ELCOM is clearly able to maintain a sharp interface at the top side of the pool (ELCOM's ability to maintain sharp constituent gradients was described in detail in the DEIS). Figure 7-6 presents the same data, but at 27.3 hours from initialisation.

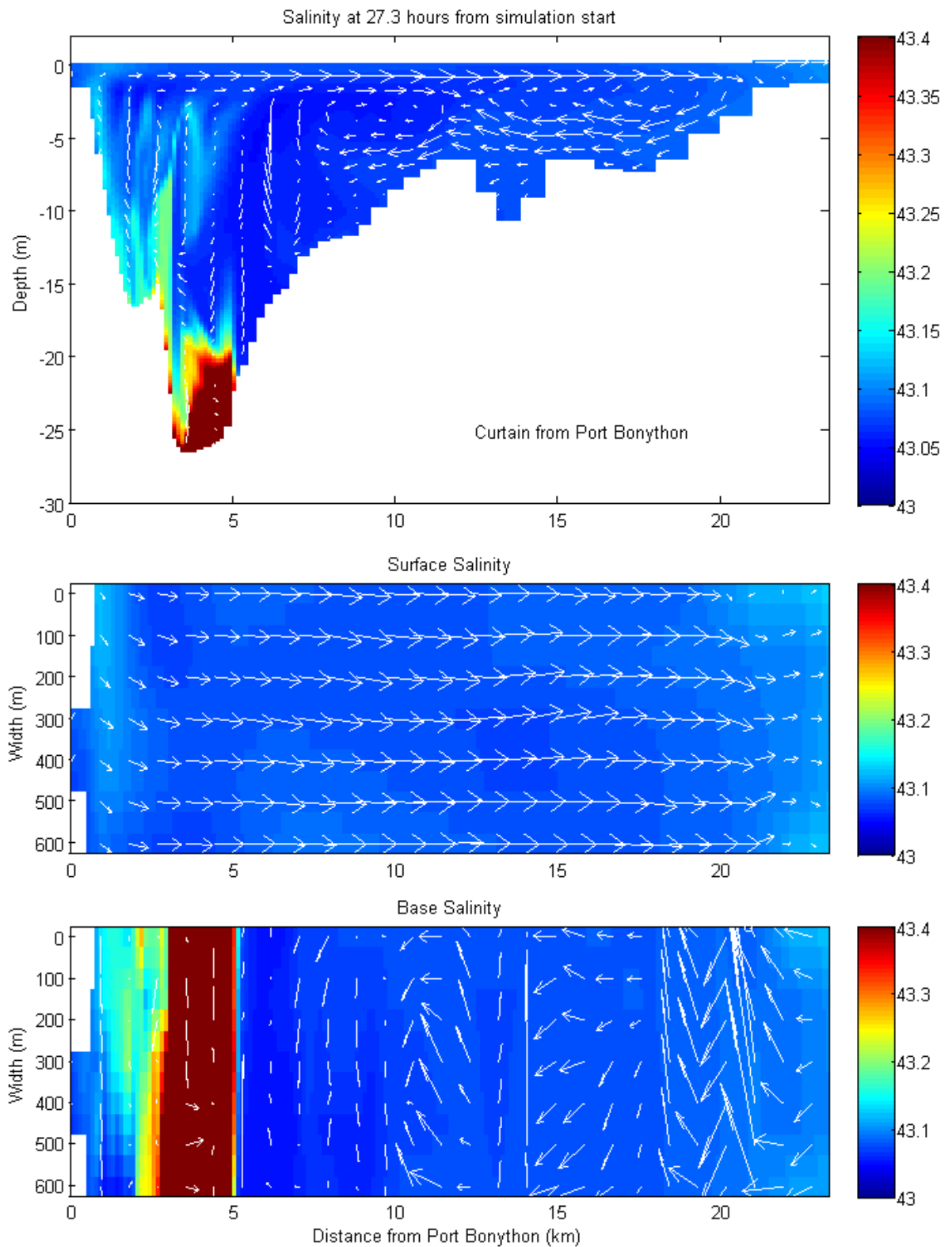


Figure 7-6 Salinity and velocities 27.3 hours following initialisation

The figure shows that the brine pool, in this simulation, has a propensity to be advected upwards and towards Port Bonython as a result of the circulation generated within the model. There is also some evidence for vertical mixing in response to the perturbation of the brine pool, as expected. Nonetheless, this mixed water, once evacuated from its initial location, is also advected towards the Port Bonython shoreline as it is entrained in the upwelling circulation.

The slightly higher salinities at eastern shore of the model (which are due to evaporative effects resulting from application of full meteorological forcing data to the model) also reveal the action of the upwelling circulation in that salt is transported at depth towards the left hand end of the model.

To demonstrate the persistence of the circulation and its influence on the brine pool, the same simulation after two days is provided in Figure 7-7. The figure shows that the pool has been largely evacuated from its initial condition, with a clear signature of upwelling motion along the very steep western slope. Some mixing is also evident, as expected given the energetic and persistent wind forcing. The evaporation generated salt inflow from the eastern shore has penetrated almost 15 km into the model under the influence of the upwelling return circulation, as shown by the spatial matching of the colour contours and arrows at bed level on the right hand side of the top pane of Figure 7-7.

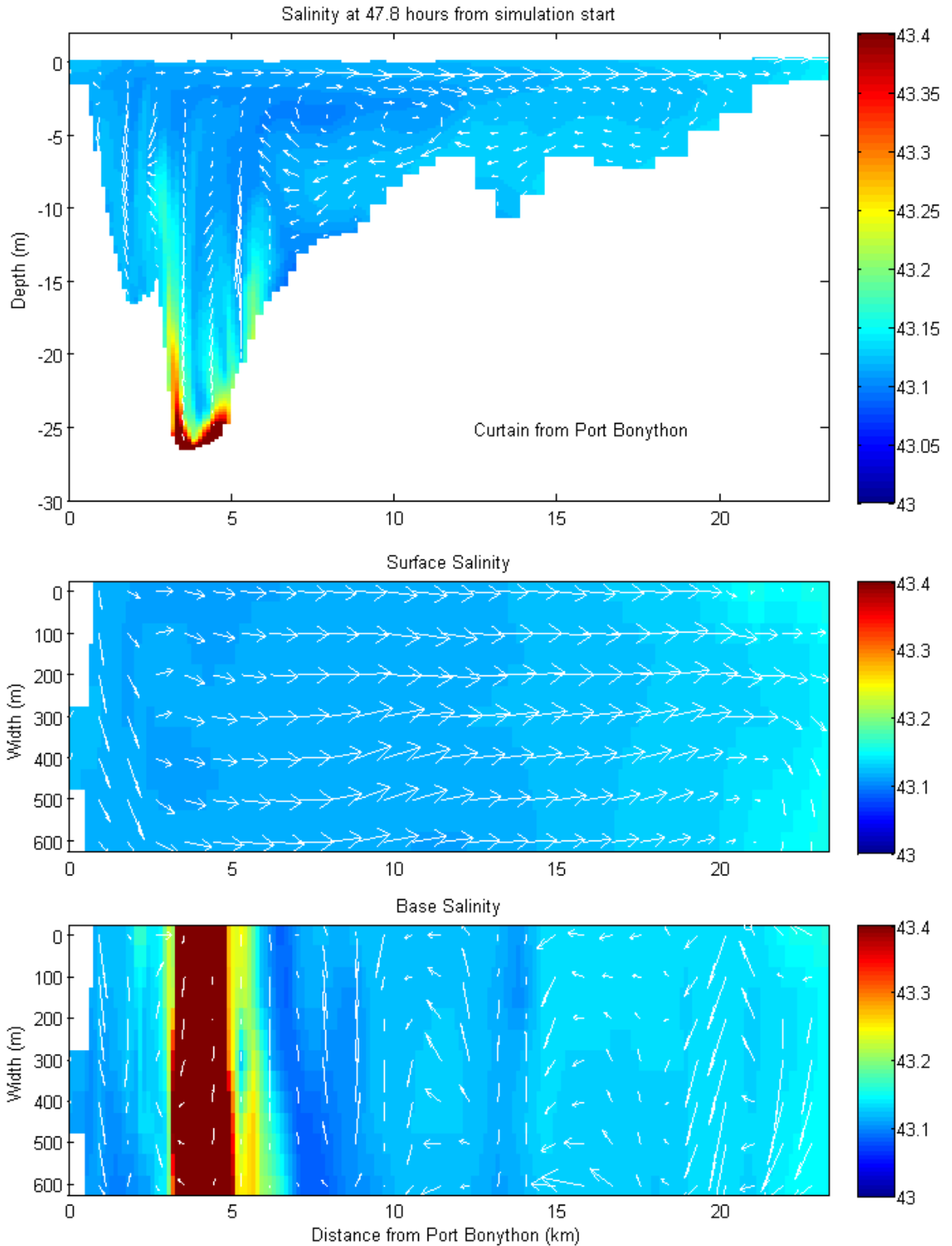


Figure 7-7 Salinity and velocities 47.8 hours following initialisation

Notwithstanding this result, it was felt important to investigate any potential role played by the solid side walls (within the two dimensional model schematisation), in particular with regards to upwelling tendencies and circulations. Such investigation is provided below.

7.3 Quasi Three-Dimensional Model

In order to progress the investigation of the likely potential for upwelling at Point Lowly, the model described in Section 7.2 was rerun unchanged, but with the laterally bounding side walls removed to allow water to travel in and out of the domain as required (i.e. in a direction perpendicular to the page).

7.3.1 Results

Figure 7-8 presents the salinity colour contours of the quasi three-dimensional vertical slice model overlain with velocity vectors at 6 hours into the simulation to allow direct comparison with Figure 7-5. The panels within the figure and contouring are the same as presented above, again noting the difference in spatial resolution of the arrows and model grid.

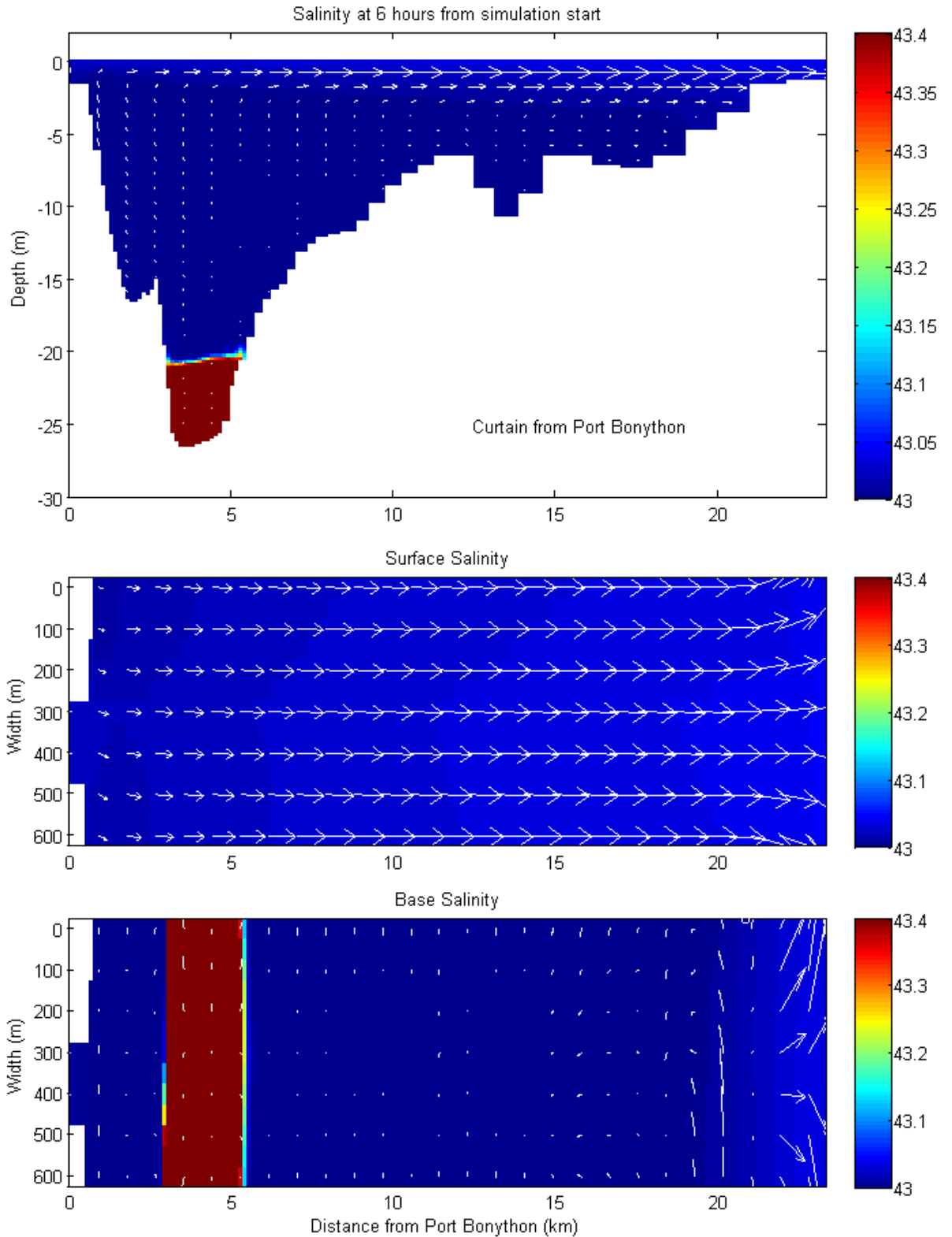


Figure 7-8 Salinity and velocities immediately following initialisation

The figure demonstrates that after 6 hours the quasi three-dimensional model predicts an absence of an upwelling circulation, and little disturbance of the brine pool off Point Lowly. This is most likely because, after being advected eastwards under the action of surface wind forcing, surface water

parcels appear to preferentially flow laterally out of the model on reaching the eastern shore. These outflows are evident in the second and third panes in Figure 7-8. For reasons of mass conservation, these outflows are balanced by inflows across the open wall boundaries, and these inflows may be responsible for the very small velocities evident in the upper left hand portion of the upper pane in Figure 7-8.

In order to better contrast the results from this and the two dimensional model, Figure 7-9 presents the developed curtain velocity profiles for both the quasi-three dimensional and two dimensional models after 1.5 days of simulation. Velocity magnitude is colour contoured, with the same sparse presentation of velocity vectors. The figure shows that the return underflow (i.e. a signature of the operation of upwelling) is more evident in the two dimensional simulation than the quasi-three dimensional model.

Following completion of the previous two simulations, it was felt that using a fully three dimensional model to assist with further exploration of upwelling potential at Point Lowly was appropriate. The following section describes the associated works.

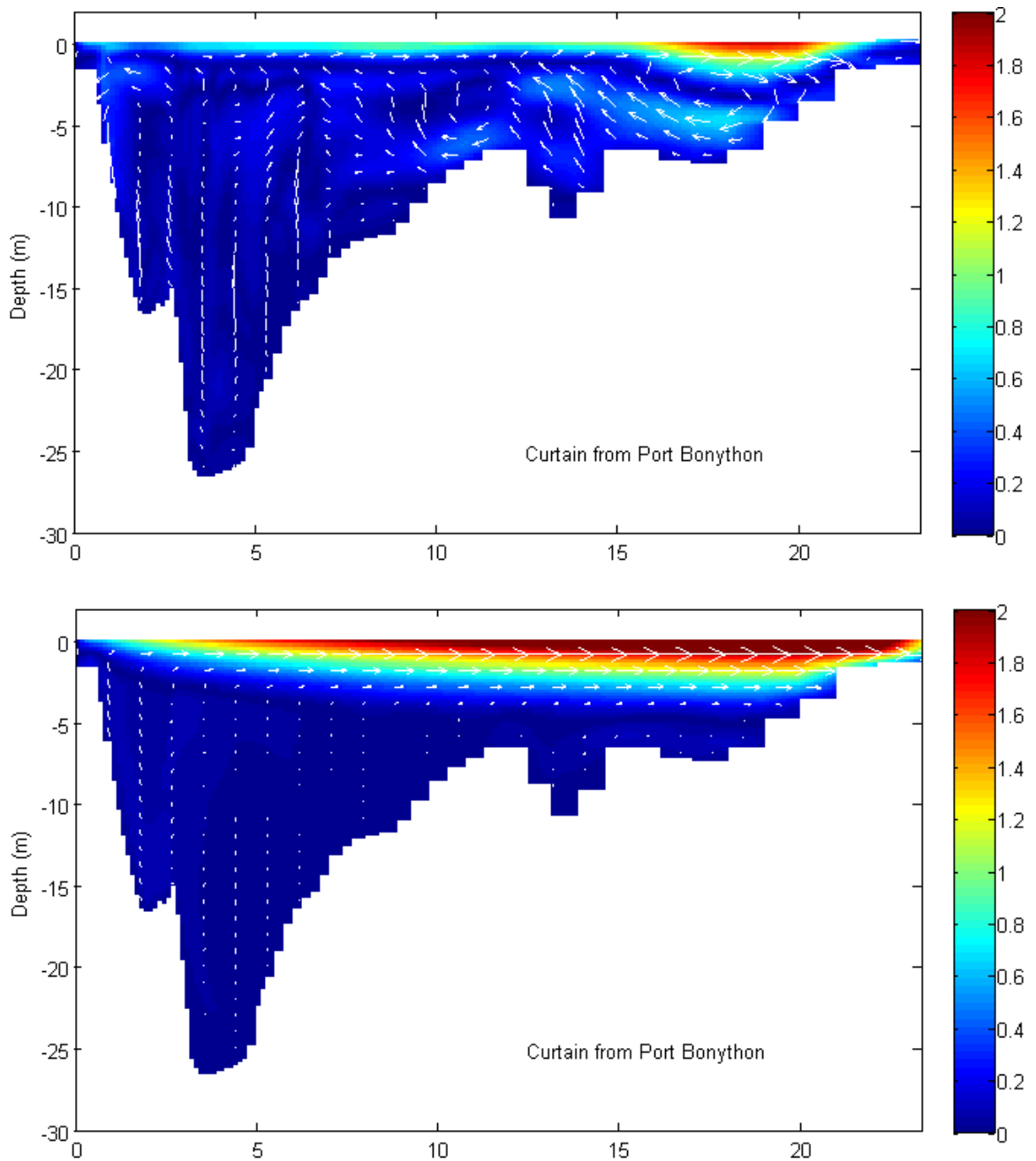


Figure 7-9 Comparison of 2D (upper) and quasi-3D (lower) model predictions after 1.5 days simulation. Velocities are ms^{-1}

7.4 Fully Three-Dimensional Model

The high resolution model described previously was used to further investigate the potential for upwelling at Point Lowly across a suite of wind forcing regimes. The model setup and scenarios are described below.

7.4.1 Model Domain

The entire high resolution model domain described previously was used in these simulations.

7.4.2 Vertical Resolution

In order to reduce the influence of numerical dispersion on potential upwelling processes, the vertical resolution of the high resolution model was increased such that all layers between approximately -24 and -12 metres were set to be 0.5 metres thick.

7.4.3 Longitudinal Resolution

The entire extents of Spencer Gulf were simulated. It is noted that this domain provides the highest lateral resolution in and around the site of potential upwelling.

7.4.4 Initial Condition

As an improvement on the previous assumptions regarding the vertical distribution of brine, this suite of simulations included a representation of a brine discharge into an initially uniform salinity condition. The initial background salinity was assumed to be uniformly 43 gL^{-1} , and the inflow set to a constant 44.52 gL^{-1} , corresponding to a dilution of 20:1 for a brine salinity of 75 gL^{-1} in the selected ambient conditions. It is noted that this dilution is conservative in that it is worse than any predictions from the CFD simulations of the current study's production runs. The brine discharge was allowed to enter the model for a two day period where all tides and winds were turned off, and the model interrogated over the third day when winds were turned on. Brine discharge also continued into the third day.

7.4.5 Wind Forcing

Three wind forcing scenarios were applied, as winds coming from the following directions:

- Westerly;
- Northerly; and
- North-Westerly.

The wind forcing for the above scenarios was set to reflect realistic wind conditions where possible. To do so, the wind records used in the high resolution model were interrogated at Point Lowly to find a period where a westerly wind reached approximately 15 ms^{-1} over one day. The period identified is shown in Figure 7-10.

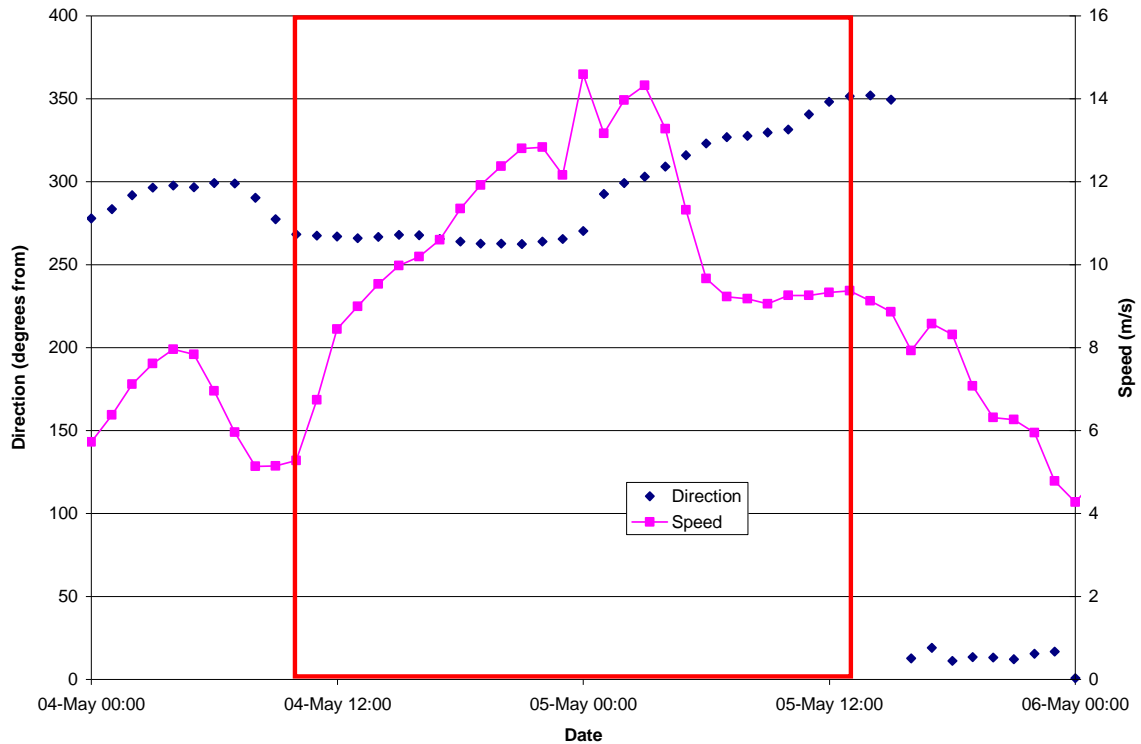


Figure 7-10 Westerly wind period (red box)

The evolution of wind speed (and direction) up to this threshold was also applied. The wind speeds were kept the same for the other two scenarios, with the wind directions changed manually to suit. Wind was spatially applied as a subset of the baseline high resolution model, with three points within the domain covering the current model. Specifically, the data from Point Lowly (shown above) was applied locally, and two other representative fields applied to the north and south (i.e. sites 4, 9 and 27 in Figure 4-3).

7.4.6 Tidal Forcing

Water surface elevations at the boundary near Port Lincoln were set to a constant value, effectively eliminating tidal action from these simulations.

7.4.7 Simulation Period

Each ELCOM model was executed for a 2 day warm up period (with no tides or winds applied) to allow the brine discharge to pool. The respective wind data set was then applied for the third day. Brine discharge was continued throughout the entire simulation.

7.4.8 Results

Each scenario's results are presented below, at times of 0, 6, 12, 18 and 24 hours into the third day. Each time presents three colour panels of dilution:

- A bottom sheet;

- A curtain running from the tip of Point Lowly (left hand side) in a south easterly direction towards Ward Spit (right hand side); and
- A zoom of the above curtain to 1500 metres offshore from Point Lowly to show the results in detail in the area of potential upwelling.

The maximum dilution presented is 85:1. Greater dilutions appear as a uniform red colour and are not differentiated.

7.4.8.1 Westerly Wind

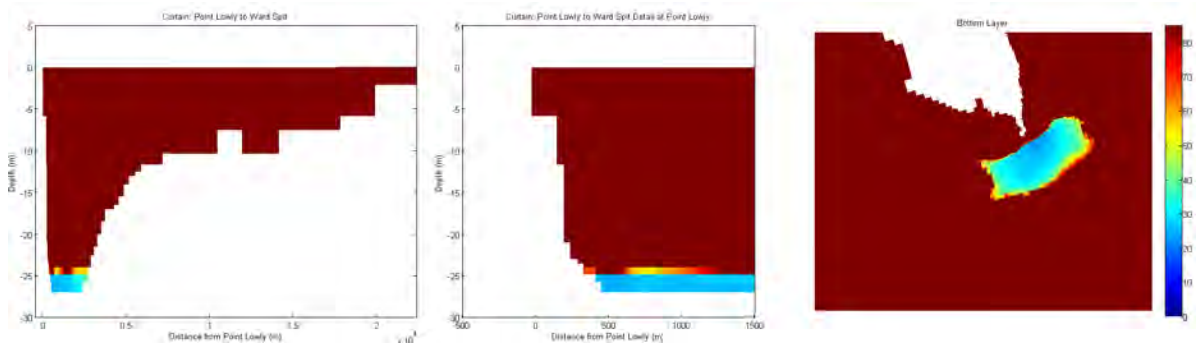


Figure 7-11 Dilution at 0 hours from wind commencement

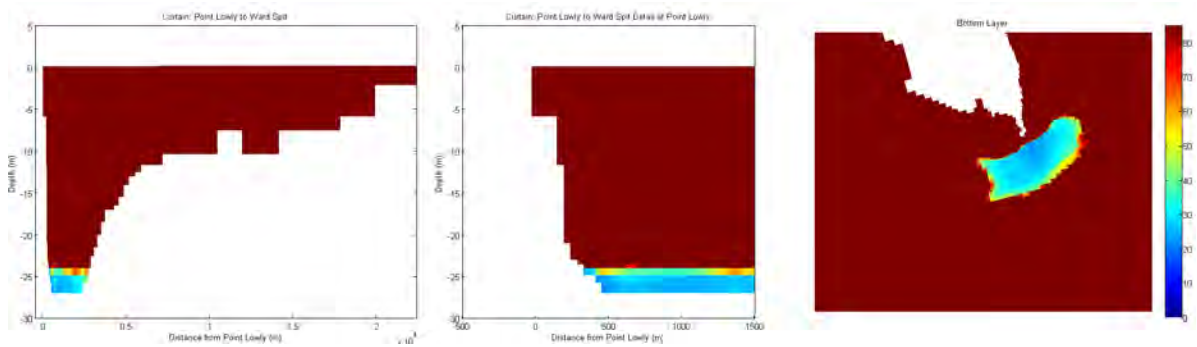


Figure 7-12 Dilution at 6 hours from wind commencement

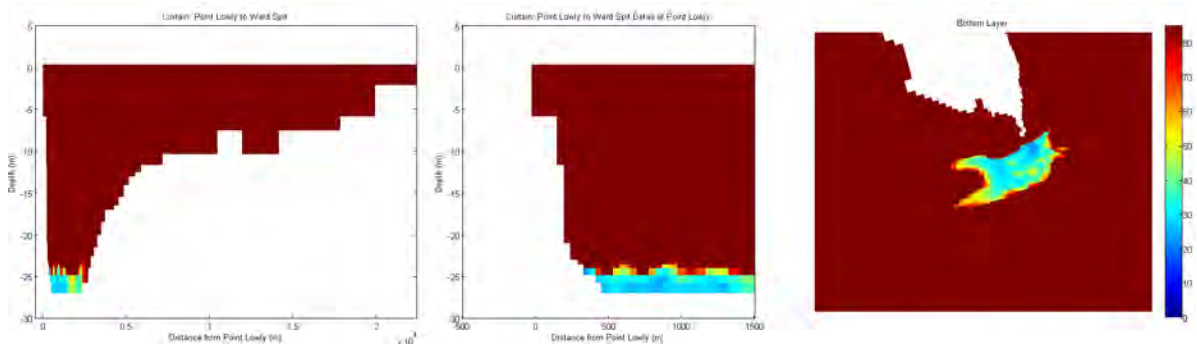


Figure 7-13 Dilution at 12 hours from wind commencement

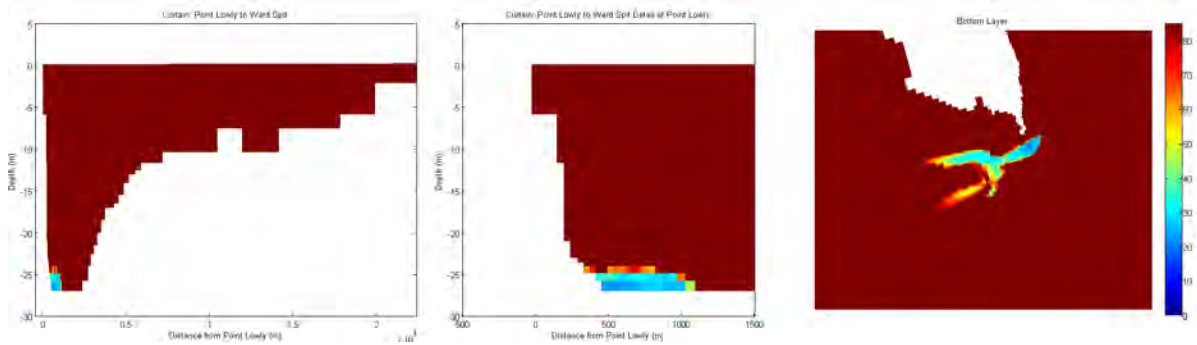


Figure 7-14 Dilution at 18 hours from wind commencement

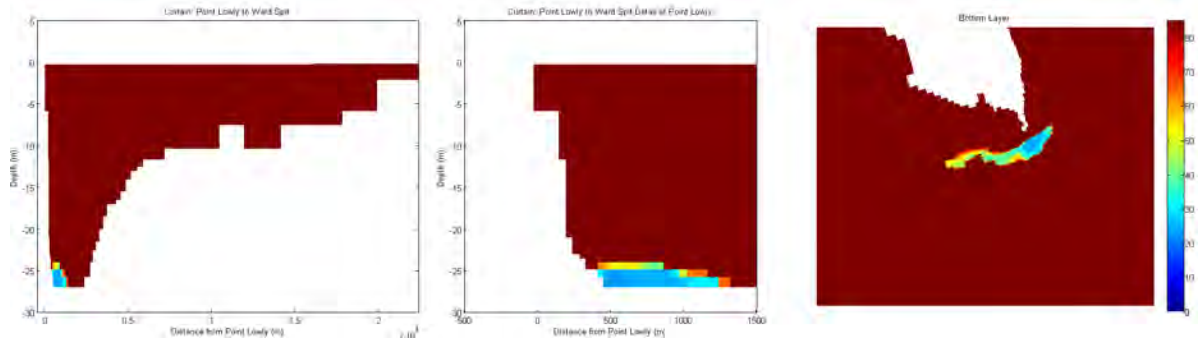


Figure 7-15 Dilution at 24 hours from wind commencement

7.4.8.2 Northerly Wind

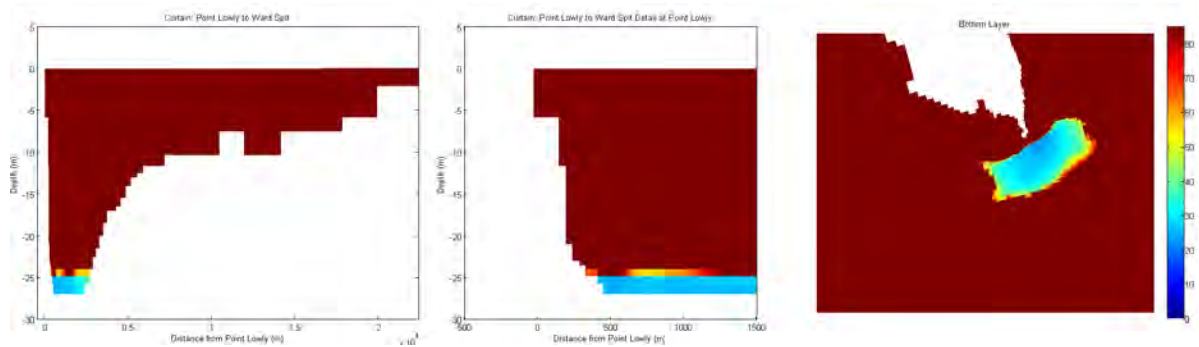


Figure 7-16 Dilution at 0 hours from wind commencement

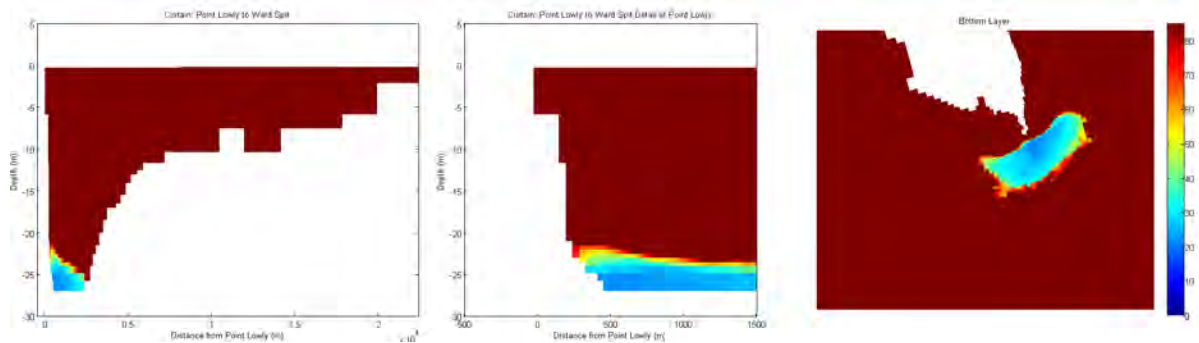


Figure 7-17 Dilution at 6 hours from wind commencement

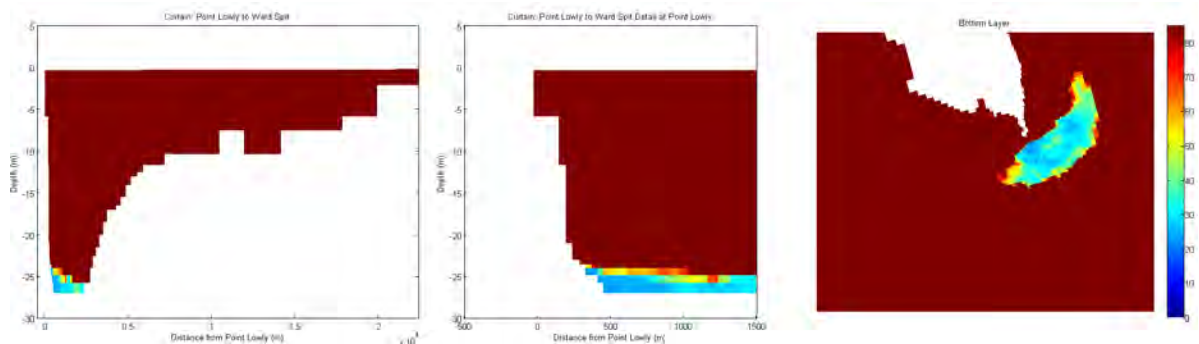


Figure 7-18 Dilution at 12 hours from wind commencement

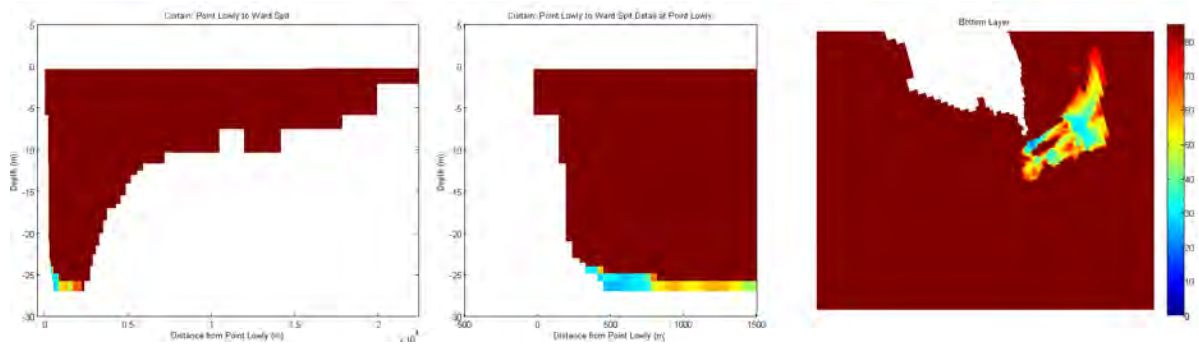


Figure 7-19 Dilution at 18 hours from wind commencement

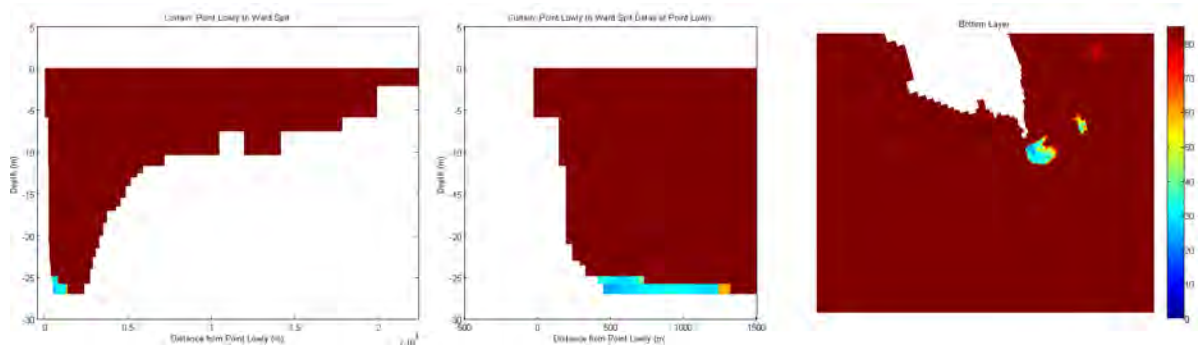


Figure 7-20 Dilution at 24 hours from wind commencement

7.4.8.3 North Westerly Wind

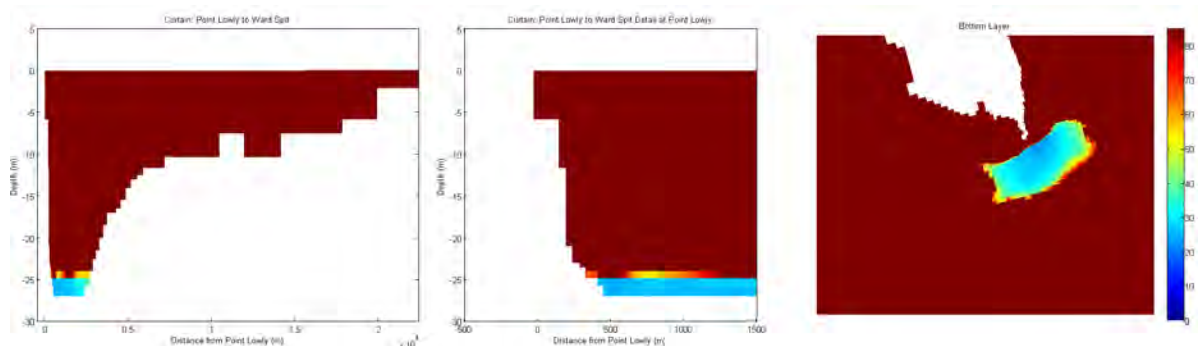


Figure 7-21 Dilution at 0 hours from wind commencement

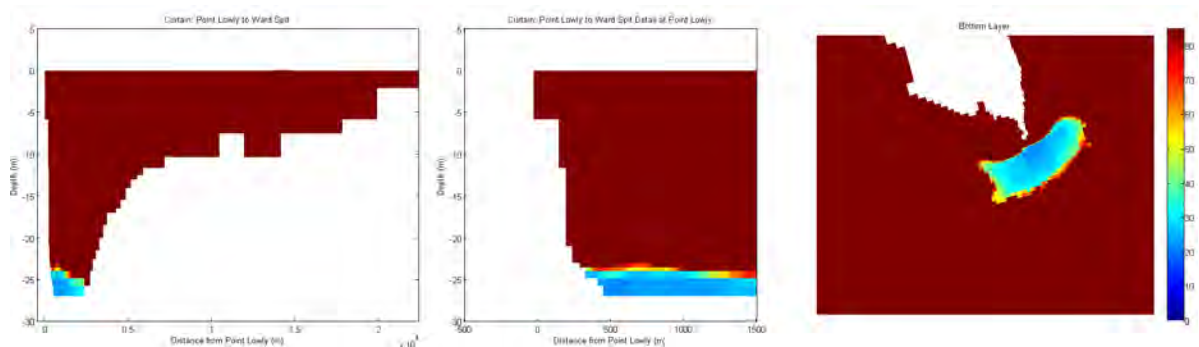


Figure 7-22 Dilution at 6 hours from wind commencement

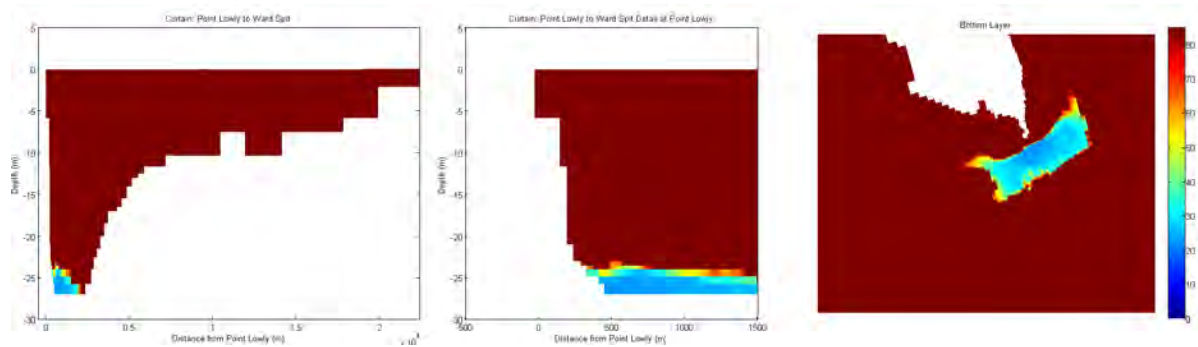


Figure 7-23 Dilution at 12 hours from wind commencement

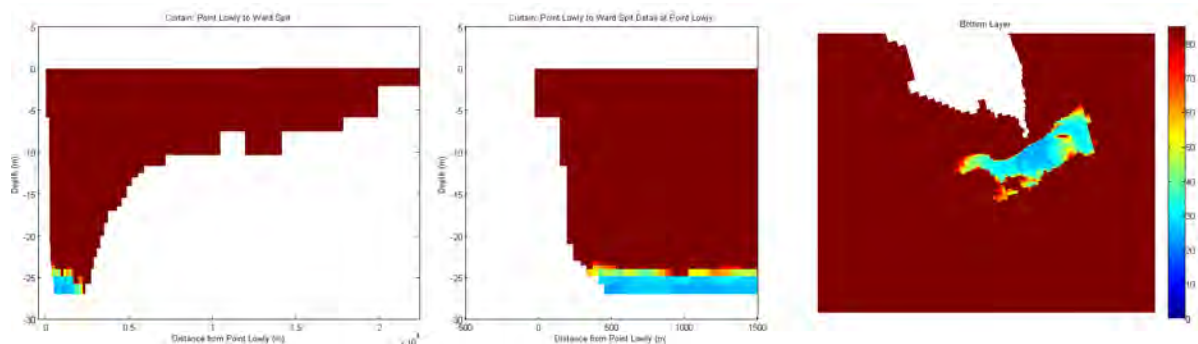


Figure 7-24 Dilution at 18 hours from wind commencement

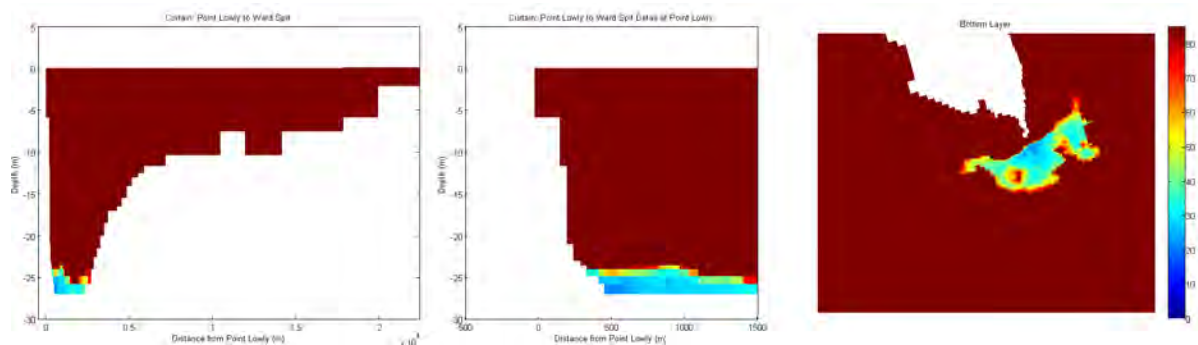


Figure 7-25 Dilution at 24 hours from wind commencement

The figures show that there is little propensity for upwelling to deliver brine to the shallow areas surrounding Point Lowly in the fully three dimensional domain over the periods simulated. Rather than flowing into the shallow areas of Point Lowly, the dense brine preferentially flows laterally away from the diffuser (at the same or similar depth to insertion) around Point Lowly to either the south (westerly wind), north (northerly wind) or both (north westerly wind) in the simulations considered here. As such, it appears that this lateral movement is a dynamically relevant wind-driven process by which brine leaves the diffuser site under the action of wind forcing.

Interestingly, the direction in which the brine pool appears to evacuate the site laterally is often broadly opposed to the surface wind direction, suggesting that the wind field may support generation of complex (and possibly return) flow fields in these tide-free simulations. Regardless of this however, the key result here is that in all simulations, the propensity of the brine pool is to evacuate in a lateral (to deep water), rather than onshore (to shallow water), direction.

The figures also suggest that limited vertical mixing occurs at the upper interface of the brine pool (as expected) as a result of wind induced turbulence. Having its origins in reservoir simulation applications, ELCOM is well suited to maintaining such sharp gradients with minimal interference from numerical diffusion - the ability of ELCOM to maintain sharp constituent and density gradients has been described in detail in Appendix O11.2 of the DEIS.

In summary, upwelling to shallow waters at biologically significant dilutions is not predicted in the period over which the three dimensional models were executed. Rather, the simulations suggest that brine preferentially flows laterally away from the site of injection, rather than inshore to the shallow areas.

To further investigate this result, however, the north westerly wind simulation was executed for a further three day period, directly following (and hot-started from) the period described above. This simulation was selected as it showed the least (although still not insignificant) propensity for evacuation of the brine pool over the original three day simulation period. The additional three day period was set to have a constant 14.32 ms⁻¹ north-westerly wind, with this speed being representative of peak speeds presented in Figure 7-10.

The contour plot layout used for Figure 7-11 to Figure 7-25 was again used to present these additional results as snapshots at 12 hour increments across the additional three day period. For consistency of presentation, figure captions refer to times since the commencement of the wind field at the start of day three in the original simulation – e.g. ‘36 hours from wind commencement’ presents predictions at one and a half days since wind was added to the model, which is half a day into the secondary simulation.

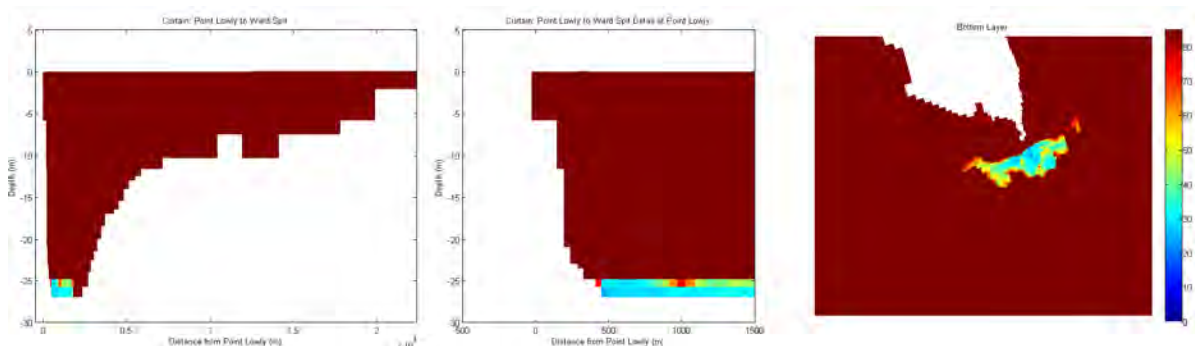


Figure 7-26 Dilution at 36 hours from wind commencement

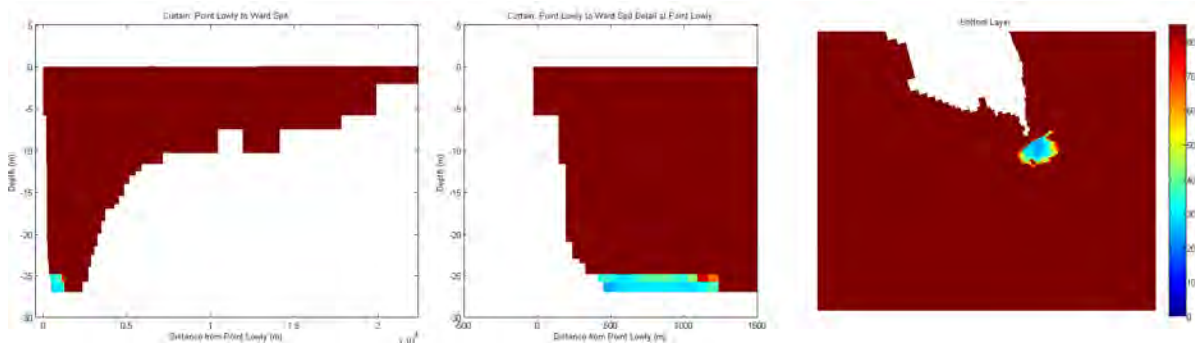


Figure 7-27 Dilution at 48 hours from wind commencement

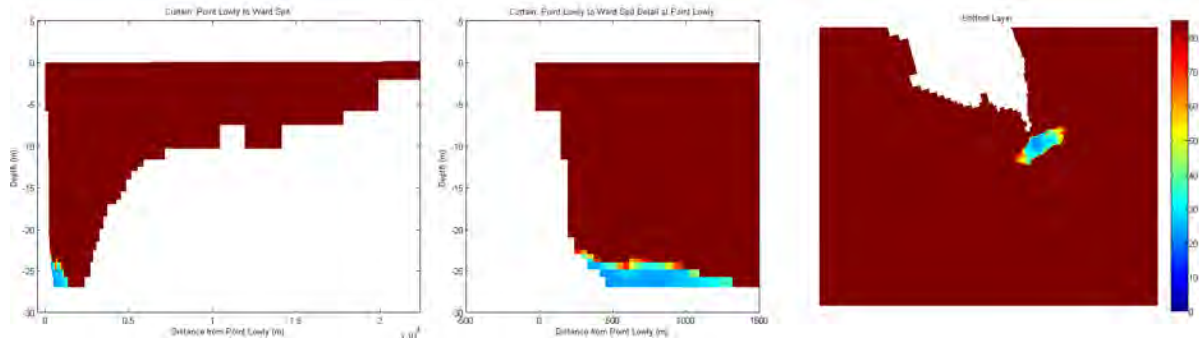


Figure 7-28 Dilution at 60 hours from wind commencement

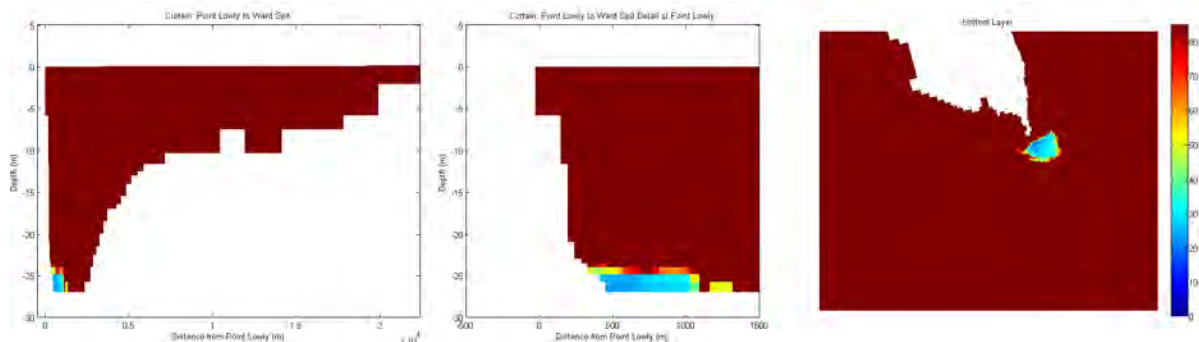


Figure 7-29 Dilution at 72 hours from wind commencement

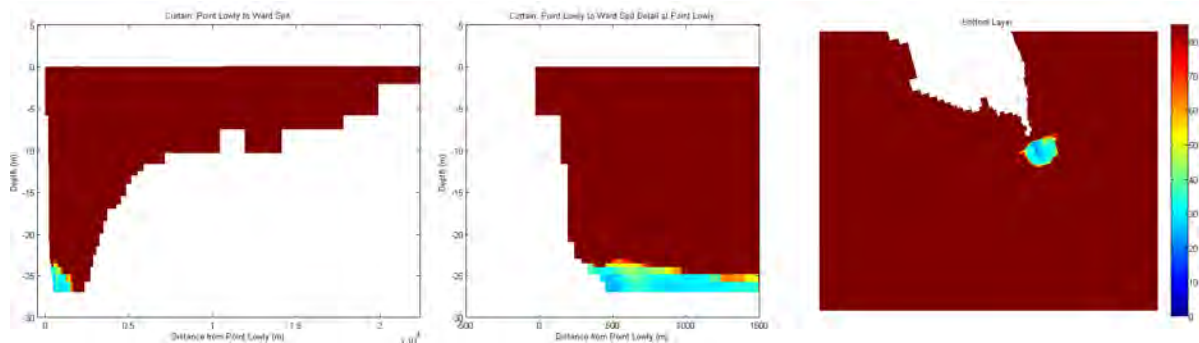


Figure 7-30 Dilution at 84 hours from wind commencement

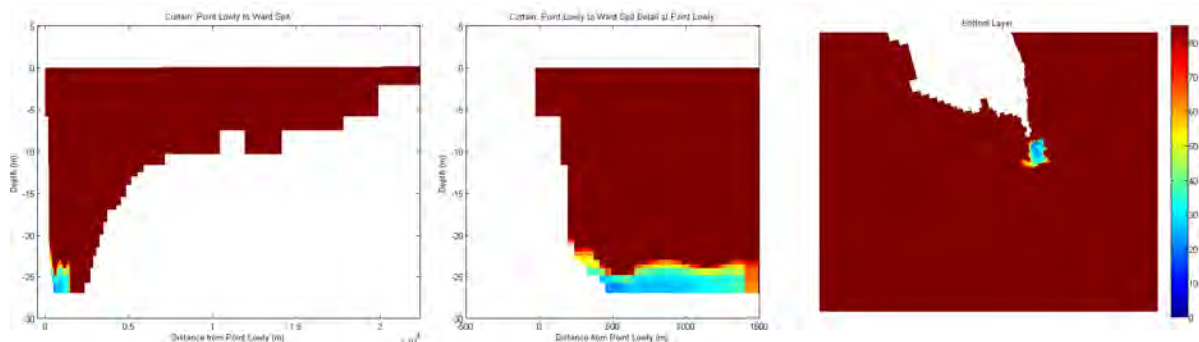


Figure 7-31 Dilution at 96 hours from wind commencement

The figures show that even under these conservative conditions (i.e. extended strong wind forcing and complete absence of tides) the model predicts no propensity for upwelling of brine to shallow areas, but rather a preference for lateral brine evacuation.

Given the above, it was felt that one further suite of simulations was required to fully explore this upwelling potential, that being a repeat of the simulations described above, but with tidal forcing added and the pre-dilution injection method described in Section 3.6.4 implemented. Such works are described below.

7.5 Fully Three Dimensional Model – Tides Active

In order to provide further context for upwelling potential at Point Lowly, the fully three dimensional model was rerun with tides applied, wind and diffuser flows (derived as described in Section 3.6). This is described below, and provides a rigorous tool for assessing upwelling potential at Point Lowly.

7.5.1 Model Domain

The entire high resolution model domain described previously was used in these simulations.

7.5.2 Vertical Resolution

In order to reduce the influence of numerical dispersion on potential upwelling processes, the vertical resolution of the high resolution model was increased such that all layers between approximately -24 and -12 metres were 0.5 metres thick.

7.5.3 Longitudinal Resolution

The entire extent of Spencer Gulf was simulated.

7.5.4 Initial Condition

As an improvement on the previous assumptions regarding the vertical distribution of brine, this simulation was initialised using results of the low resolution model after several years warmup. This allowed for a realistic initial salinity and temperature distribution across the depth and breadth of the domain.

The brine was introduced into the model using the same procedure described in Section 3.6, as applied to the optimised SEIS rosette. In other words, actual dilutions predicted by the CFD modelling were used to force this model, where background salinities (to mix with the brine) were sourced from a previous (desalination plant off) simulation.

7.5.5 Simulation Period

The period simulated was one week leading up to the dodge tide in May 2008 simulated as part of the dissolved oxygen study (see Section 6, Figure 6-1). The brine discharge was allowed to enter the warmed up model for a one week period where all tides and winds (as used in the high resolution model described in Section 3 over 2008) were turned on. The week period was selected as it provided a lead up to a dodge tide period, as shown previously. A one day window in the middle of

the dodge tide was selected for results extraction, again to maintain consistency with previous results presentation. This day period is shown in red below, for a tidal timeseries at Point Lowly. Brine discharge was continued throughout the entire simulation.

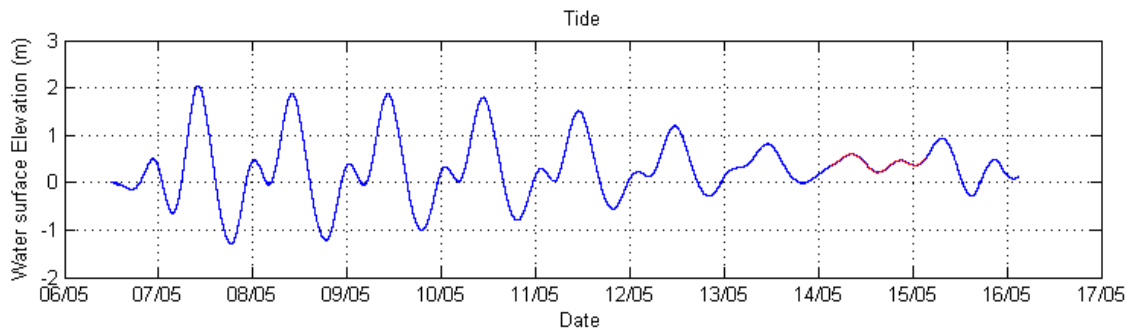


Figure 7-32 Autumn dodge tide at Pt Lowly (central day shown in red)

7.5.6 Wind Forcing

Actual wind fields for the period leading up to the dodge tide were applied to the simulation. During the one day period noted above in red, the same wind speed series shown in Figure 7-10 was applied to the model, and the wind direction (based on the results presented previously) was set to a constant north westerly direction.

7.5.7 Tidal Forcing

Water surface elevations at the boundary near Port Lincoln were set to be actual values for the week and dodge tide period shown above.

7.5.8 Results

Results are presented below in the same format as previously, namely at times of 0, 6, 12, 18 and 24 hours into the nominated dodge day. Each time presents three colour panels of dilution:

- A curtain running from the tip of Point Lowly (left hand side) in a south easterly direction towards Ward Spit (right hand side). This is not necessarily on the proposed diffuser alignment, but has been located to be coincident with shallow areas of interest;
- A zoom of the above curtain to 1500 metres offshore from Point Lowly to show the results in detail in the area of potential upwelling; and
- A bottom sheet.

To illustrate the results of this simulation, dilutions lower than 85:1 were contoured. All higher dilutions are uniformly presented as red.

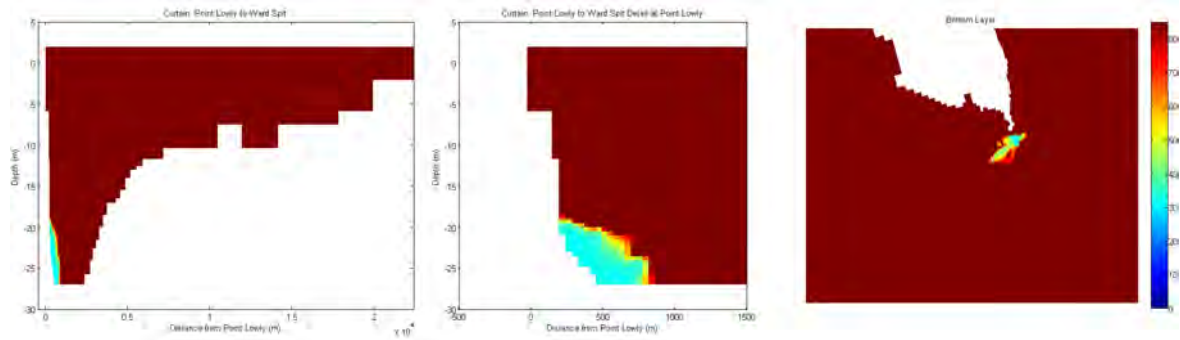


Figure 7-33 Dilution at 0 hours from wind commencement

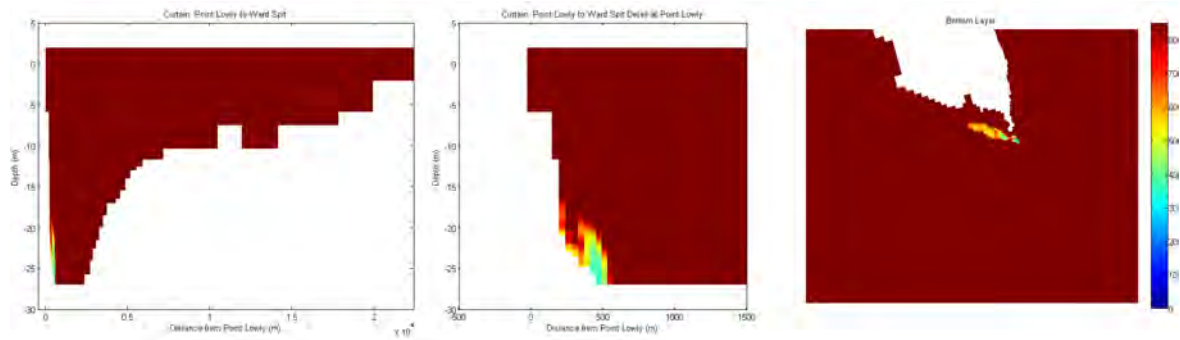


Figure 7-34 Dilution at 6 hours from wind commencement

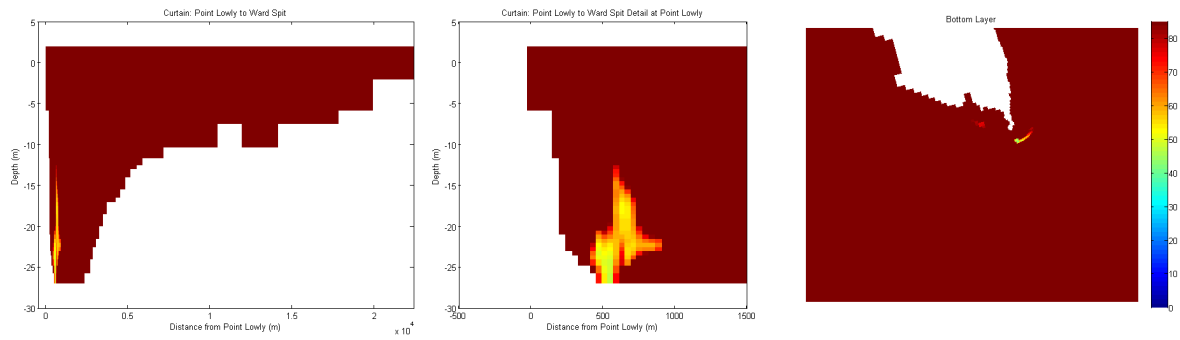


Figure 7-35 Dilution at 12 hours from wind commencement

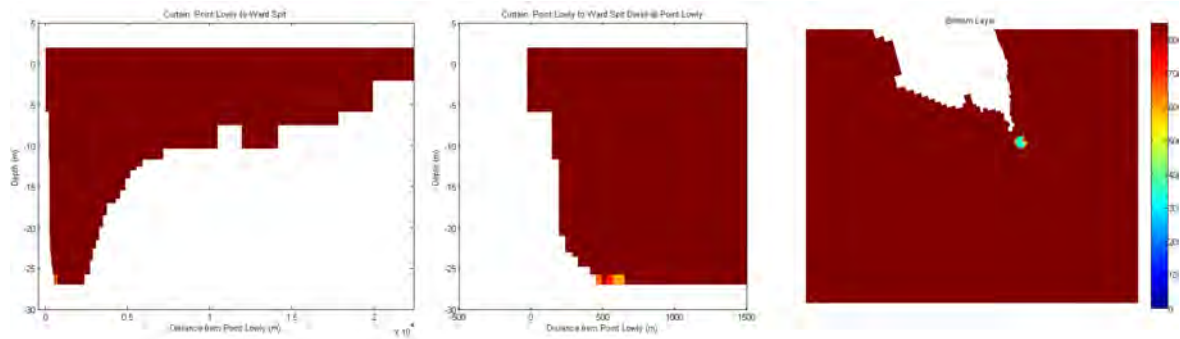


Figure 7-36 Dilution at 18 hours from wind commencement

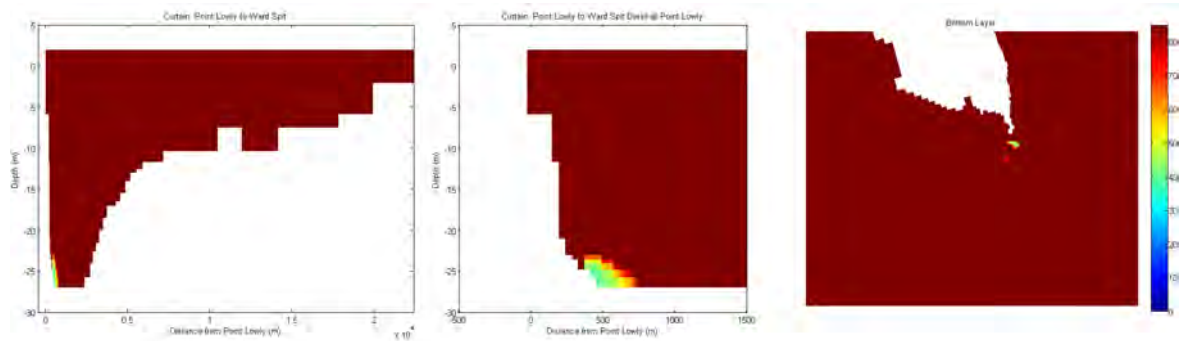


Figure 7-37 Dilution at 24 hours from wind commencement

The figures show little propensity for upwelling into the shallow areas surrounding Point Lowly to an extent that ecologically relevant dilutions approach areas of interest. It is noted that the initial (0 hour) curtain plot does not indicate the presence of upwelling as the north westerly wind has not commenced at that time. This is not to say that some return flow currents do not exist in the model (particularly in adjacent shallow areas, for example), but that if they do exist then they appear to have little influence on the brine pool at the diffuser discharge point in terms of evacuating it to shallow areas surrounding Point Lowly.

8 LARVAL ENTRAINMENT

The validated high resolution ELCOM model (as used for analyses in Section 3 of this report and described in detail in Appendix H5.2 of the SEIS) was employed to execute a suite of simulations examining the likely fate and distribution of larvae within Northern Spencer Gulf, including the likely potential for entrainment of larvae into the proposed desalination intake structure. This was achieved via use of the ELCOM drifter module with the addition of a vertical migration capability.

The larval and intake characteristics that were included in this modelling were specified by BHP Billiton. Spawning habitats included regionally distributed breeding populations that inhabit either the water column (e.g. anchovy) or the extensive soft-bottom habitat in Spencer Gulf (e.g. gobies), and localised habitats including the fringing coastal reef (e.g. Purple Urchin *Heliocidaris erythrogramma* and reef fish such as morwongs) and offshore sponge community near Point Lowly (e.g. sponges, ascidians and other filter feeding invertebrates). Initially, both pelagic and benthic spawning modes were considered, but pelagic spawning (with drifters initially positioned throughout the water column) was not further considered once it became apparent that dispersion of larvae across the water column was occurring for the benthic spawning mode.

Following execution of a suite of ELCOM simulations to describe the above, results were then post processed in a range of manners to encompass a number of scenarios that considered different larval and/or intake behaviours. Specifically, the various combinations of ELCOM simulations and post-processing scenarios enabled an understanding of the sensitivity of the percentage of entrained larvae to:

- The larval duration (referred to as expiry), i.e. the period during which larvae remained in the water column, after which their fate (mortality or settlement) is not relevant for the purpose of this modelling;
- A particular model of vertical migration (diurnal migration);
- Natural mortality (referred to as death);
- Early settlement (during larval lifespan);
- Avoidance of intake currents (as would be achievable by more mature fish larvae); and
- The height of the influence of the intake structure in the water column.

Entrainment into the Port Augusta power station cooling water inlets was also considered for one scenario. Details of the ELCOM model (other than the drifter configuration) are as previously described so are not repeated.

8.1 ELCOM Simulations

8.1.1 Simulation Suite

The particle tracking (numerical drifter) module within ELCOM was used to configure and execute a suite of four ELCOM simulations. Table 8-1 lists the suite of simulations executed and their corresponding target species.

Table 8-1 ELCOM simulations

Run Number	Target Species
1	Regionally distributed fish, e.g. Goby/grubfish – with vertical migration
2	Regionally distributed fish, e.g. Goby/grubfish – no vertical migration
3	Reef associated species - fish and invertebrates
4	Sponge bed associated species - invertebrates

8.1.2 Implementation of ELCOM Drifter Module

All simulations were configured to specify drifters as simple neutrally buoyant Lagrangian particles. That is, the drifters were allowed to be advected in all three spatial dimensions in response to hydrodynamic forcing only, with buoyancy effects turned off. The drifter module interpolates velocities from ELCOM cell centres to calculate advective velocities at precise (sub grid scale) drifter locations at each timestep. The exception to this was the implementation of vertical migration (see Section 8.1.6).

8.1.3 Simulation Durations

All simulations spanned 123 days. The exception was Run 4, which spanned 33 days. All simulations were warmed up for a three day period prior to drifter release, and commenced on 1st November 2007. This period captured the peak spawning period as identified during seasonal field surveys (advice from BHP Billiton's marine biology consultants).

8.1.4 Temporal Release Pattern

All simulations released drifters over their respective grids on a 7 hour cycle, with the exception of Run 4, which employed a 2.3 hour release period. These periods were deliberately chosen to not be evenly divisible into the local typical tidal period or 24 hour day. For example, Runs 1 and 2 released drifters for 93.6 days, starting from day 3 of the 123. These release arrangements thus had drifters being initiated when the remaining simulation time was less than the larval duration. As such, some drifters were still active (i.e. not entrained, settled, dead or expired) at the conclusion of the simulation.

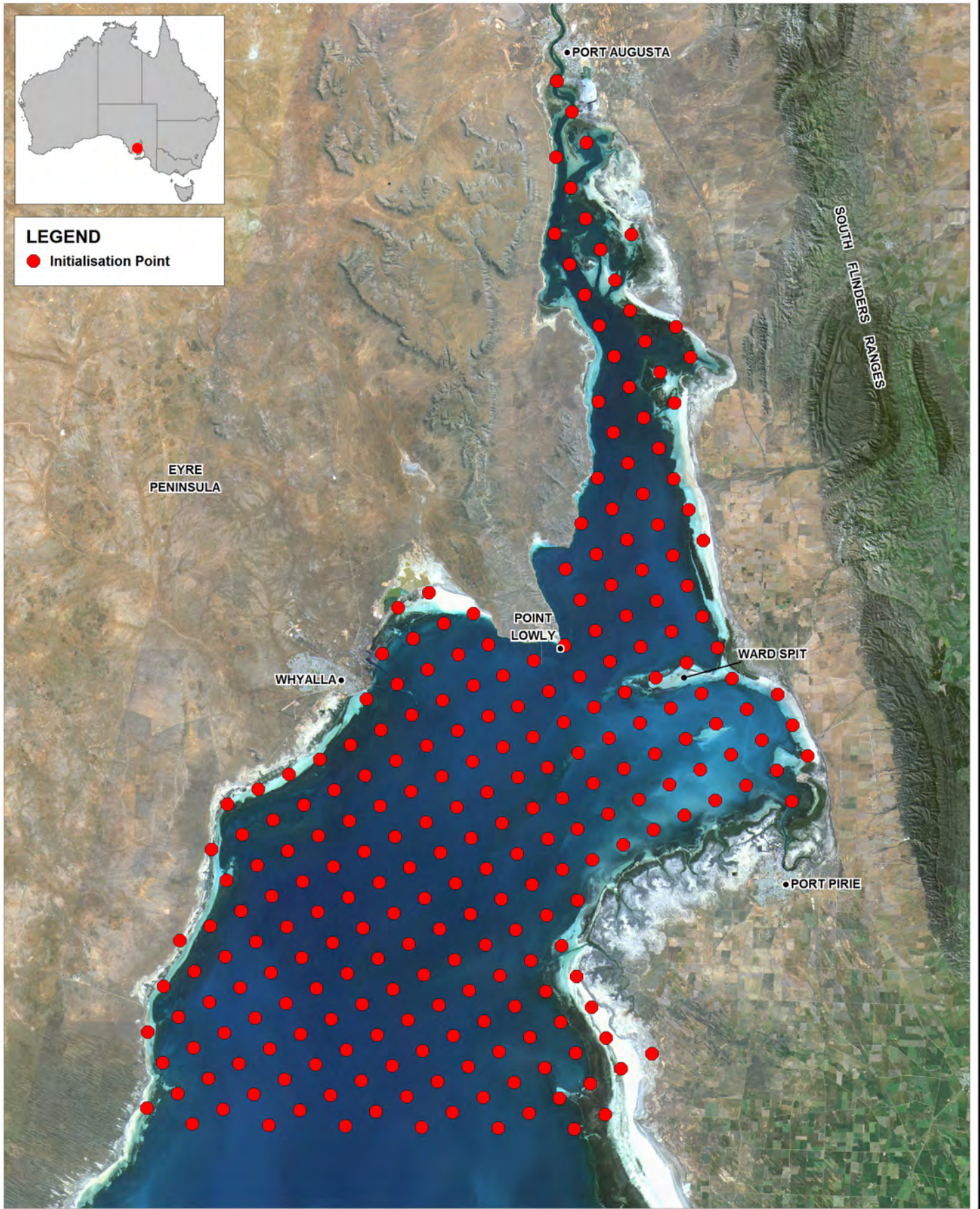
8.1.5 Spatial Release Pattern

In all simulations, drifters were initialised on a regular grid for each of the four simulations and the overall shape of the grid was tailored to suit known spawning grounds as part of post processing. The tailored initialisation of each simulation is shown in Figure 8-1 to Figure 8-3. All four simulations included multiple releases of drifters from these grids throughout each simulation. That is, drifters were released at the intervals described above from every point shown in the figures, for each simulation. Every drifter released from each point had a unique identifier to facilitate targeted post processing.



LEGEND

● Initialisation Point

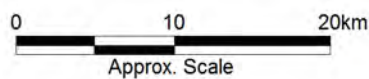


Title:
Drifter initialisation: runs 1 and 2

Figure:
8-1

Rev:
A

BMT WBM endeavours to ensure that the information provided in this map is correct at the time of publication. BMT WBM does not warrant, guarantee or make representations regarding the currency and accuracy of information contained in this map.



Filepath :



LEGEND

● Initialisation Point



Image ©2009 Google™
Data SIO, NOAA, U.S. Navy,
NGA, GEBCO
Image © 2010 DigitalGlobe
Image NASA
Image © 2010 Cnes/Spot Image

Title:
Drifter initialisation: run 3

Figure:
8-2

Rev:
A

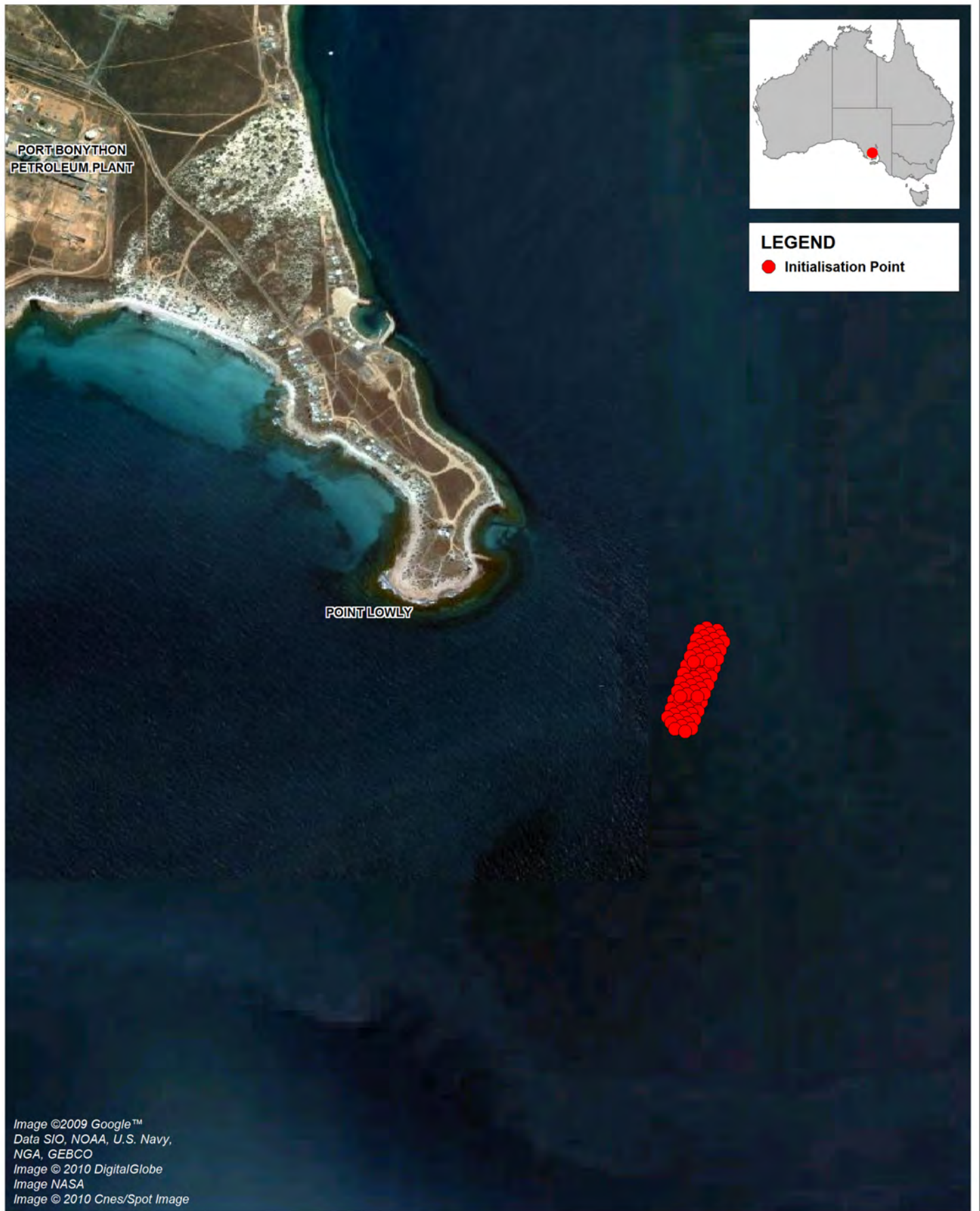
BMT WBM endeavours to ensure that the information provided in this map is correct at the time of publication. BMT WBM does not warrant, guarantee or make representations regarding the currency and accuracy of information contained in this map.



0 1.5 3km
Approx. Scale



Filepath :

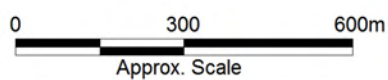


Title:
Drifter initialisation: run 4

Figure:
8-3

Rev:
A

BMT WBM endeavours to ensure that the information provided in this map is correct at the time of publication. BMT WBM does not warrant, guarantee or make representations regarding the currency and accuracy of information contained in this map.



Filepath :

8.1.6 Vertical Migration

It is noted that some larvae have the ability to move through the water column and as such influence their entrainment potential if entrainment is assumed to occur only across a limited vertical extent. Such vertical migration also influences the lateral transport of the larvae as they are subjected to a range of (vertically varying) lateral velocity fields as they migrate. Given the range of species and combinations of potential migration behaviour, it was elected to focus on simulating only diurnal daylight driven migration. This was simulated for Run 1. Specifically, ELCOM was upgraded to allow for user specification of upwards and downwards drifter migration within two periods each day. This migration overrode hydrodynamic forcing to the extent that it influenced drifter velocity and the relative vertical position (near bed or near surface at the end of a migration window) during periods of vertical migration.

Run 1 utilised this vertical migration, and for this simulation, the following migration pattern was implemented:

- At sunrise: larvae descended at a rate of 1 cms^{-1} ; and
- At sunset: larvae ascended at a rate of 1 cms^{-1} .

Migration ceased when larvae neared the bottom or surface, respectively. This feature was coded into the ELCOM model by the Centre for Water Research specifically for this study.

8.1.7 Larvae Counts

Each drifter was assigned a larvae count of 1000 (in post processing) to allow for probabilistic transformation of larvae as a fraction of the count of a single drifter. This assignment, combined with the above release grids, simulation durations and release periods resulted in release of 79,000,000 larvae for Runs 1 and 2, 24,000,000 larvae for Run 3 and 21,840,000 larvae for Run 4.

8.1.8 Outputs

Each ELCOM simulation produced the following for each drifter at each model output timestep (where the output timestep was always 5,400 seconds, i.e. data was saved every 225, 24 second, simulation timesteps):

- Timestamp;
- Longitude;
- Latitude;
- Model x and y local coordinate positions;
- Elevation (metres AHD);
- Depth (below water surface);
- Water surface elevation (m AHD); and
- Drifter speed (and velocity in all Cartesian directions).

For example, this resulted in the generation of just less than 2 billion data points for each of Runs 1 and 2.

8.2 Post Processing Techniques

The four simulations described above were submitted to a range of post processing analyses to investigate the likely behaviour of larvae with respect to the proposed desalination plant intake and the broader region. The post processing tools were constructed in Matlab specifically for this study. Matlab was configured to:

- Read the processed ELCOM (netcdf) output files;
- Employ user defined parameters to calculate derived quantities; and
- Export both numerical and GIS data sets.

The larval duration was specified at post-processing time. For the regional spawners, a duration of 30 days was chosen to reflect the larval duration of the more abundant larvae recorded during field surveys (advice from BHP Billiton's marine biology consultants). The larval duration chosen for the sponge community spawners was 7 days, reflecting the dominance of filter feeding sessile invertebrates, many of which have short larval durations measured in hours (CEE 2008). Larval durations of both 7 and 30 days were applied for reef spawners, which include a range of fish and invertebrate species. This also provided a sensitivity test for the larval duration parameter.

In addition, allowance for the following larvae related processes was made in the post processing tools:

- Natural mortality (other than expiry at the end of larval duration);
- Early settlement (prior to end of larval duration) - over specified habitats, from a specified depth after a specified time; and
- Avoidance (swimming).

Not all were used for all simulations.

8.2.1 ELCOM Inputs

All data listed in Section 8.1.8 were used in varying ways during post processing.

8.2.2 User Defined Parameters

User defined parameters that were able to be altered in the post processing were (albeit with not all being used at all times):

- Area over which larvae release is to occur (as a GIS polygon). This allowed for the rectangular grid release functionality of ELCOM to be tailored to the areas shown in Figure 8-1 to Figure 8-3;
- Method of assignment of larvae to drifters (allowing either a fixed or random number of larvae to be assigned to each drifter). The random method was coded but not used, so all data presented below had a fixed number of larvae assigned to each drifter;

- Number of larvae per drifter for fixed cases (always 1000) or the multiplier of a random number between 0 and 1 for the random method (not used);
- Larval duration (maximum lifespan of an individual larva in days);
- Area over which entrainment from the proposed desalination plant intake may occur (as a GIS polygon);
- Lower bound of height off the bed for which entrainment can occur;
- Upper bound of height off the bed for which entrainment can occur. Together with the previous input, this defined a vertical bandwidth for potential entrainment;
- Area over which larval settling is to occur (as a GIS polygon);
- Maximum height off the bed for which settling is allowed;
- Percentage of larvae that settle per day for any given drifter if it enters the polygon above at the correct height off the bed;
- Minimum number of days to settling;
- Probability of entrainment occurring if a drifter enters the above polygon at the correct height off the bed (to allow for some avoidance behaviour); and
- Percentage mortality of larvae associated with any given drifter within a day.

Other inputs such as model bathymetry and intake volumetric flow rate were also required to compute various results. Processing of each drifter ceased when all larvae associated with it either expired, settled or were entrained.

The full suite of scenarios (as defined by these inputs) for each model runs is provided in Table 8-2 to Table 8-5. One thousand larvae were always assigned to each drifter.

Table 8-2 Run 1 post processing (regional spawners - vertical migration)

	Scenario
Parameter	1
Description	Regional spawners, vertical migration
Larval Duration	30 days
Settling Area	N/A
Maximum Settling Height	N/A
Settling Percentage	0
Minimum Days to Settling	N/A
Entrainment Area	Figure 8-4
Lower Entrainment Height	u/c ¹
Upper Entrainment Height	u/c
Probability of Entrainment	1
Percentage Mortality	0

¹ u/c = unconstrained in the vertical

Table 8-3 Run 2 post processing (regional spawners – no vertical migration)

Parameter	Scenario		
	1	2	3
Description	Vertically constrained intake at Point Lowly	Unconstrained intake at Point Lowly	Unconstrained intake at Port Augusta
Larval Duration	30 days	30 days	30 days
Settling Area	N/A	N/A	N/A
Maximum Settling Height	N/A	N/A	N/A
Settling Percentage	0	0	0
Minimum Days to Settling	N/A	N/A	N/A
Entrainment Area	Figure 8-4	Figure 8-4	Figure 8-5
Lower Entrainment Height	2 m	u/c	u/c
Upper Entrainment Height	5 m	u/c	u/c
Probability of Entrainment	1	1	0.135
Percentage Mortality	0	0	0

The intent of Scenario 3 was to understand the likely larval entrainment characteristics of the Port Augusta power station, and also to use it as a point of comparison for predictions of entrainment at Point Lowly.

Table 8-4 Run 3 post processing (reef spawners)

Parameter	Scenario					
	1	2	3	4	5	6
Description	7 day larval duration	30 day larval duration	Natural mortality	Early settlement	Avoidance	Vertically constrained intake
Larval Duration	7 days	30 days	30 days	30 days	30 days	30 days
Settling Area	N/A	N/A	N/A	Figure 8-2	N/A	N/A
Maximum Settling Height	N/A	N/A	N/A	10 m	N/A	N/A
Settling Percentage	0	0	0	10%	0	0
Minimum Days to Settling	N/A	N/A	N/A	7	N/A	N/A
Entrainment Area	Figure 8-4	Figure 8-4	Figure 8-4	Figure 8-4	Figure 8-4	Figure 8-4
Lower Entrainment Height	u/c	u/c	u/c	u/c	u/c	2
Upper Entrainment Height	u/c	u/c	u/c	u/c	u/c	5
Probability of Entrainment	1	1	1	1	0.9	1
Percentage Mortality	0	0	10%	0	0	0

Table 8-5 Run 4 post processing (sponge community spawners)

Parameter	Scenario	
	1	2
Description	Vertically constrained intake	Vertically unconstrained intake
Assignment method	Fixed	Fixed
Larvae per drifter	1000	1000
Larval Duration	7 days	7 days
Settling Area	N/A	N/A
Maximum Settling Height	N/A	N/A
Settling Percentage	0	0
Minimum Days to Settling	N/A	N/A
Entrainment Area	Figure 8-4	Figure 8-4
Lower Entrainment Height	2 m	u/c
Upper Entrainment Height	5 m	u/c
Probability of Entrainment	1	1
Percentage Mortality	0	0

An important part of the post processing technique was the temporal and spatial interpolation of drifter tracks. This interpolation was required to increase the spatial resolution of processed drifter track so that if a track passed through an intake zone (polygon) without being captured by an ELCOM model output point, it was still entrained. Specifically, a uniform application of interpolation timestep was applied for all runs and scenarios to ensure consistency of interpretation, where the timestep was computed using the entrainment volume (as defined by the entrainment polygon and depths and/or entrainment height parameters), and desalination plant extraction rate. This uniform interpolation timestep was approximately 88 seconds, reduced from an ELCOM output frequency of 5,400 seconds.

A flow chart of all scenarios and their inter-relation is provided in Figure 8-6.



LEGEND



-  Intake Area
-  Intake Alignment

Image ©2009 Google™
Data SIO, NOAA, U.S. Navy,
NGA, GEBCO
Image © 2010 DigitalGlobe
Image NASA
Image © 2010 Cnes/Spot Image

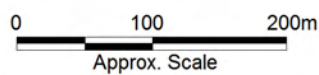


Title:
Intake polygon A: Point Lowly

Figure:
8-4

Rev:
A


BMT WBM endeavours to ensure that the information provided in this map is correct at the time of publication. BMT WBM does not warrant, guarantee or make representations regarding the currency and accuracy of information contained in this map.



Filepath :



LEGEND

 Intake Area

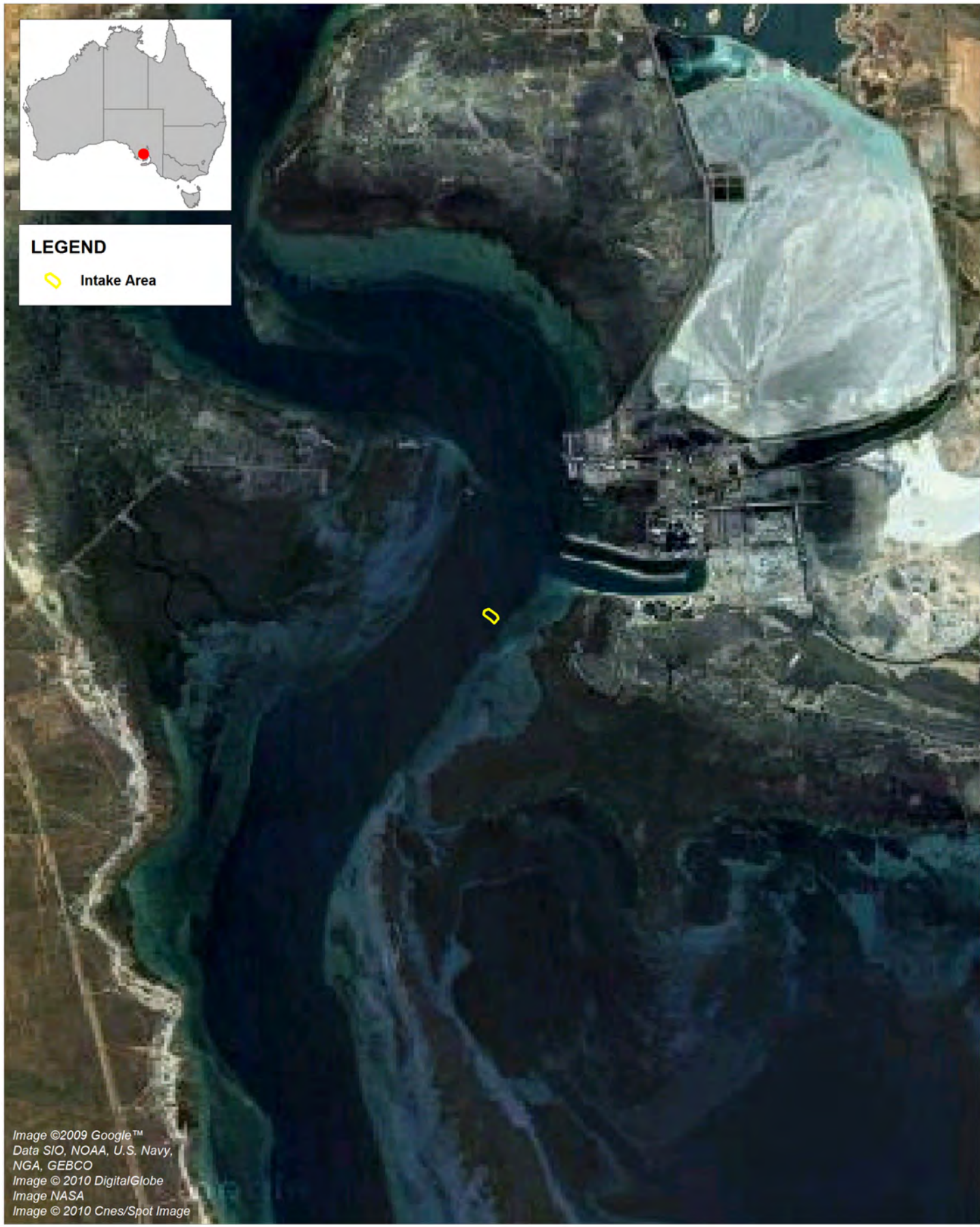


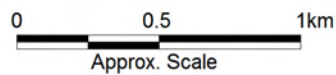
Image ©2009 Google™
Data SIO, NOAA, U.S. Navy,
NGA, GEBCO
Image © 2010 DigitalGlobe
Image NASA
Image © 2010 Cnes/Spot Image

Title:
Intake polygon B: Port Augusta

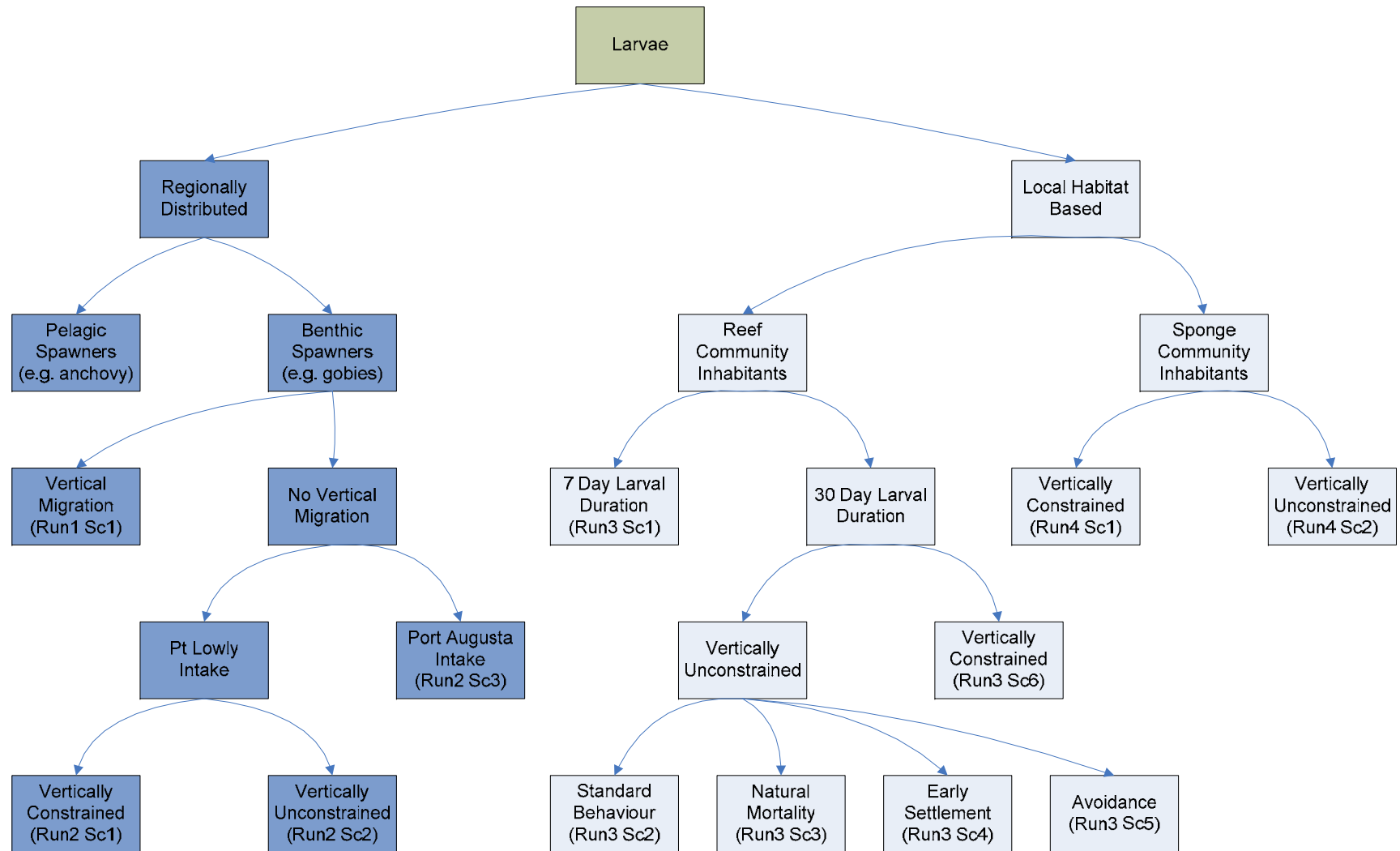
Figure:
8-5

Rev:
A

BMT WBM endeavours to ensure that the information provided in this map is correct at the time of publication. BMT WBM does not warrant, guarantee or make representations regarding the currency and accuracy of information contained in this map.



Filepath :



Note: unless otherwise specified:
 1) "Constrained" and "Unconstrained" refer to selection of entrainment depths
 2) All intakes at Point Lowly
 3) All larval durations 30 days
 4) Vertical migration not enabled
 5) Entrainment not vertically constrained

Figure 8-6 Runs and scenarios summary

8.2.3 Outputs

A range of outputs were produced from each scenario/model run via the post processing tools as follows.

8.2.3.1 GIS Data

Larval Pathways

For each timestep and each larva within a drifter, the drifter location was used to map a pseudo residence time to a user-defined two dimensional spatial array (on a regular grid) of latitudes and longitudes. That is, if a given drifter occupied an x-y location (or longitude, latitude) at any given time, then the nearest point in the user defined array was located, and its attribute increased by a value equal to the drifter interpolated timestep multiplied by the number of larvae associated with that drifter at that time. The process of mapping 'residence times' to the regular array was repeated for all drifters and all timesteps, provided the larvae associated with any given drifter were not completely removed via entrainment, settlement or mortality. More specifically, the following approach was adopted:

- At initialisation, the user sets the extents and resolution of a map of regularly spaced points across the model domain. These points are the continual accumulators of 'residence time';
- Create the spatial grid of points;
- Begin post processing, noting the latitude and longitude of every drifter at every interpolated timestep. It is noted that these positions are not related to the ELCOM grid size and can be any value within and across ELCOM cell centres. This is achieved by virtue of the fact that the ELCOM velocity field is spatially interpolated for the purposes of drifter trajectory computation. This allows fine resolution of drifter position (the same applies to the vertical) and removes grid dependence of the analysis. The ELCOM outputs were again interpolated in space and time as described above;
- Cycle through drifters, and at every output timestep find the closest user defined point (from above) to the drifter location and add a value of: (the output timestep) x (the number of particles associated with that drifter at that time) to that user defined point;
- Repeat for all following timesteps to the end of the larvae life; and
- Move to the next drifter and repeat, with 'times' effectively accumulating at each user defined latitude and longitude point as the analysis proceeds.

The result of the above is a spatial map of 'higher' and 'lower' residence times, which are an effective integration of all larvae locations over all times. One interpretation of these maps is that areas of 'higher' residence time correspond to locations where larvae either accumulate, or regularly traverse back and forth – i.e. areas where there is a higher likelihood of larvae being found.

In short, these maps do not present a physical quantity, but rather show a spatial plot of the likely relative distribution of larvae within the Gulf as predicted by this suite of numerical investigations – large values indicate accumulation and a higher likelihood of encountering larvae at any given time,

and low values indicate infrequent larvae visits or traverses and a relatively lower likelihood of encountering larvae.

All simulations had a user defined grid spacing for the residence times of 0.001 degrees, which is approximately 93 metres at Point Lowly.

Initialisation Points of Entrained Larvae

The locations from which entrained drifters were initialised were also recorded and the percentage of drifters entrained from each point computed. These were plotted as maps.

8.2.3.2 Numerical Data

Overall Entrainment Percentage

A range of single number outputs were also produced by the post processing tools. These are:

- Total number of larvae simulated;
- Number of entrained larvae;
- Percentage larvae entrained;
- Percentage of larvae died through mortality other than expiration at end of life; and
- Percentage larvae settled.

8.3 Results

8.3.1 GIS Data

8.3.1.1 Larval Pathway Maps

Larval pathway maps for the runs and scenarios below are shown in the following figures:

- Run 1, scenario 1 (regional spawners, vertical migration);
- Run 2, scenario 1 (regional spawners, no vertical migration);
- Run 2, scenario 1, zoomed around proposed intake site;
- Run 3, scenario 1 (reef spawners, 7-day larval duration);
- Run 3, scenario 2 (reef spawners, 30-day larval duration); and
- Run 4, scenario 1 (sponge community spawners).

Values are presented as the logarithms of the computed values. Importantly, values are relative only within a given pathway map, and not necessarily between maps where different numbers of larvae were released. That is, values presented in Runs 1 and 2 maps are broadly comparable with each other, but not with values from Runs 3 and 4, and values presented Runs 3 and 4 are also not comparable. Also note that larval pathways maps for Run 3 scenarios were similar such that only two (scenarios 1 and 2) are presented for illustration.



LEGEND

\log_{10} (Integrated Time)

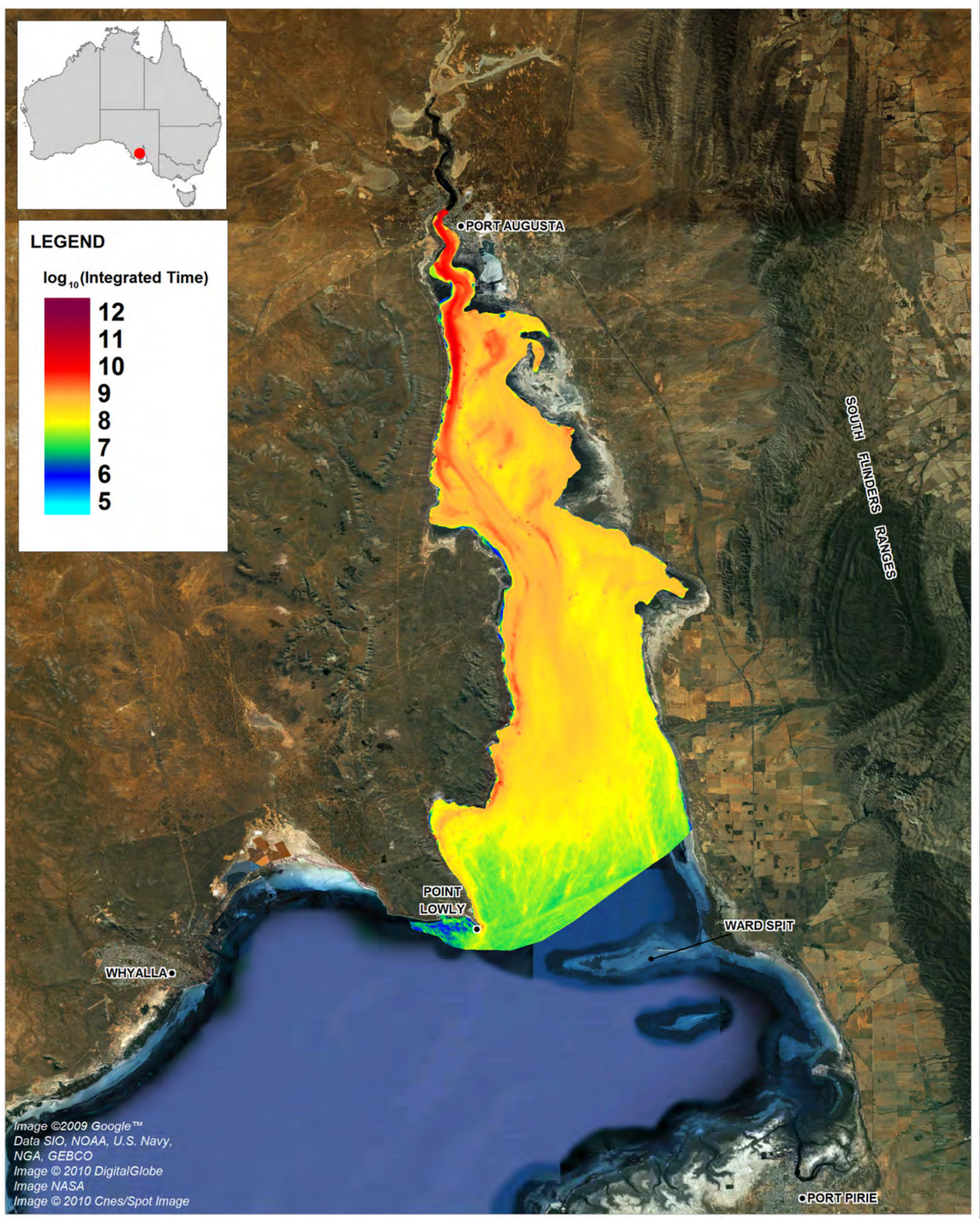
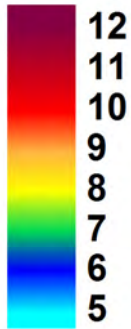


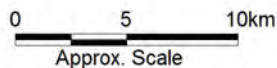
Image ©2009 Google™
 Data SIO, NOAA, U.S. Navy,
 NGA, GEBCO
 Image © 2010 DigitalGlobe
 Image NASA
 Image © 2010 Cnes/Spot Image

Title:
Larval Pathway Map: Run 1, Scenario 1

Figure:
8-7

Rev:
A

BMT WBM endeavours to ensure that the information provided in this map is correct at the time of publication. BMT WBM does not warrant, guarantee or make representations regarding the currency and accuracy of information contained in this map.



BMT WBM

www.bmtwbm.com.au

Filepath :



LEGEND

\log_{10} (Integrated Time)

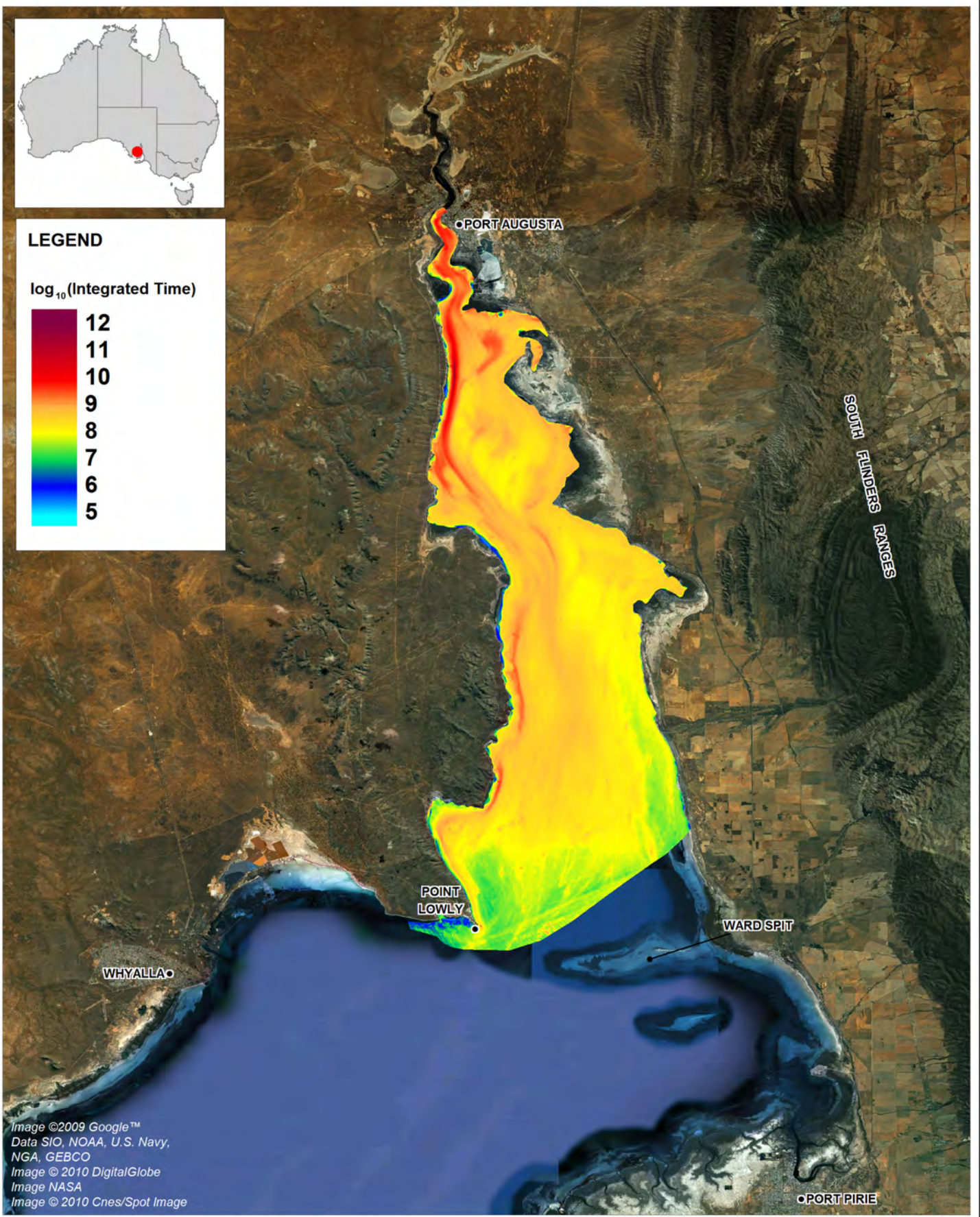
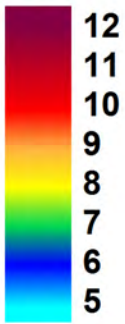


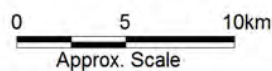
Image ©2009 Google™
 Data SIO, NOAA, U.S. Navy,
 NGA, GEBCO
 Image © 2010 DigitalGlobe
 Image NASA
 Image © 2010 Cnes/Spot Image

Title:
Larval Pathway Map: Run 2, Scenario 1

Figure:
8-8

Rev:
A

BMT WBM endeavours to ensure that the information provided in this map is correct at the time of publication. BMT WBM does not warrant, guarantee or make representations regarding the currency and accuracy of information contained in this map.



Filepath :

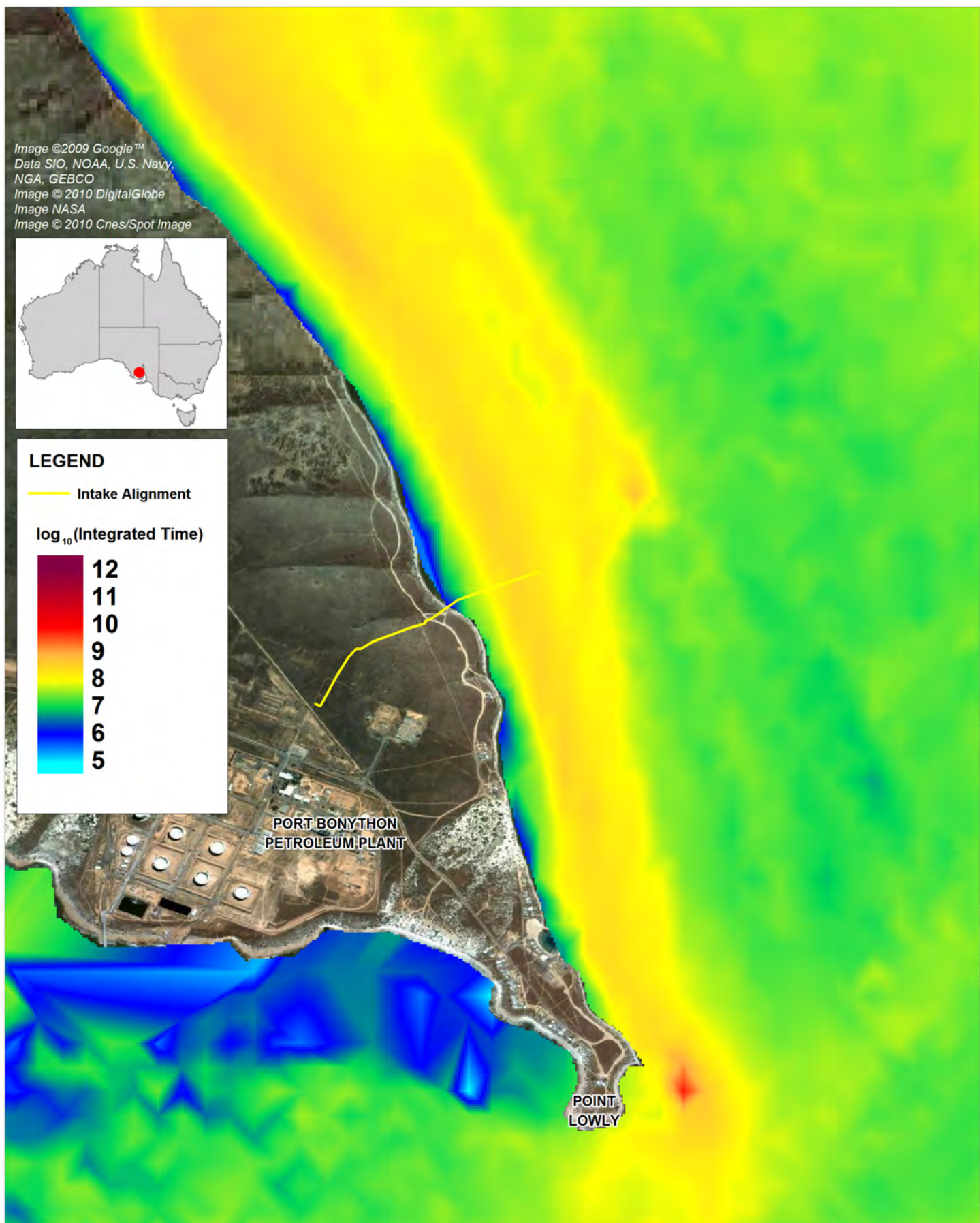
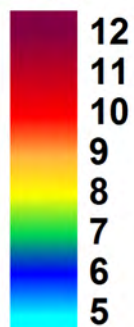
Image ©2009 Google™
 Data SIO, NOAA, U.S. Navy,
 NGA, GEBCO
 Image © 2010 DigitalGlobe
 Image NASA
 Image © 2010 Cnes/Spot Image



LEGEND

— Intake Alignment

\log_{10} (Integrated Time)

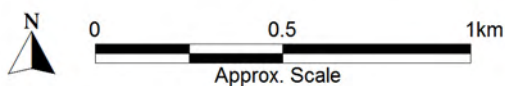


Title:
Larval Pathway Map: Run 2, Scenario 1, Intake Zoom

Figure:
8-9

Rev:
A

BMT WBM endeavours to ensure that the information provided in this map is correct at the time of publication. BMT WBM does not warrant, guarantee or make representations regarding the currency and accuracy of information contained in this map.



Filepath :



LEGEND

\log_{10} (Integrated Time)

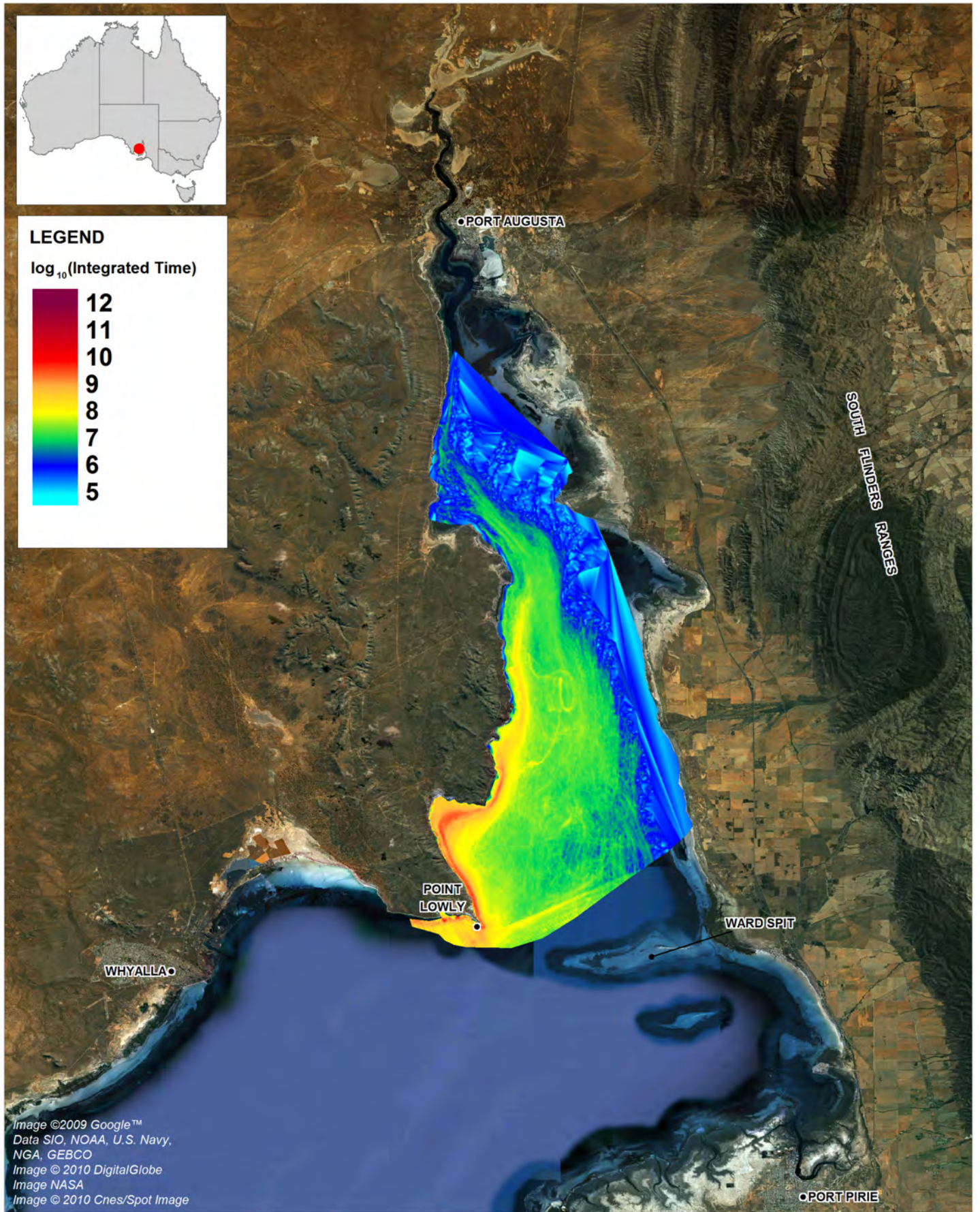
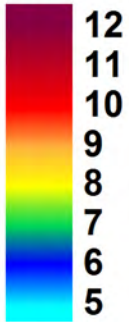


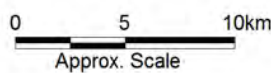
Image ©2009 Google™
 Data SIO, NOAA, U.S. Navy,
 NGA, GEBCO
 Image © 2010 DigitalGlobe
 Image NASA
 Image © 2010 Cnes/Spot Image

Title:
Larval Pathway Map: Run 3, Scenario 1

Figure:
8-10

Rev:
A

BMT WBM endeavours to ensure that the information provided in this map is correct at the time of publication. BMT WBM does not warrant, guarantee or make representations regarding the currency and accuracy of information contained in this map.



Filepath :



LEGEND

\log_{10} (Integrated Time)

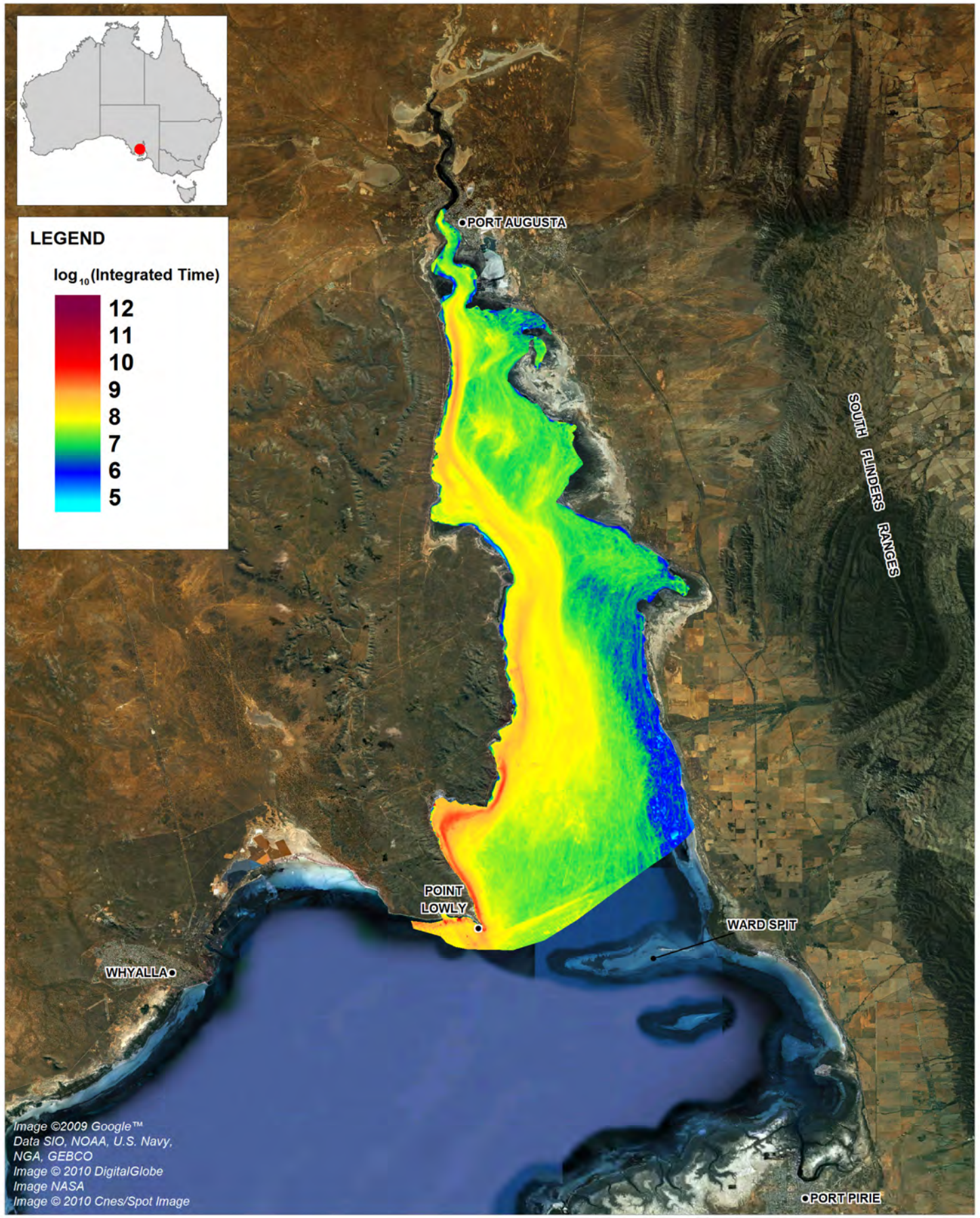
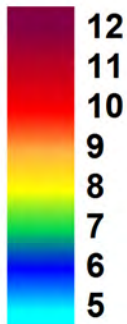


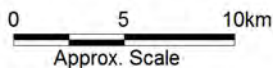
Image ©2009 Google™
 Data SIO, NOAA, U.S. Navy,
 NGA, GEBCO
 Image © 2010 DigitalGlobe
 Image NASA
 Image © 2010 Cnes/Spot Image

Title:
Larval Pathway Map: Run 3, Scenario 2

Figure:
8-11

Rev:
A

BMT WBM endeavours to ensure that the information provided in this map is correct at the time of publication. BMT WBM does not warrant, guarantee or make representations regarding the currency and accuracy of information contained in this map.



Filepath :



LEGEND

\log_{10} (Integrated Time)

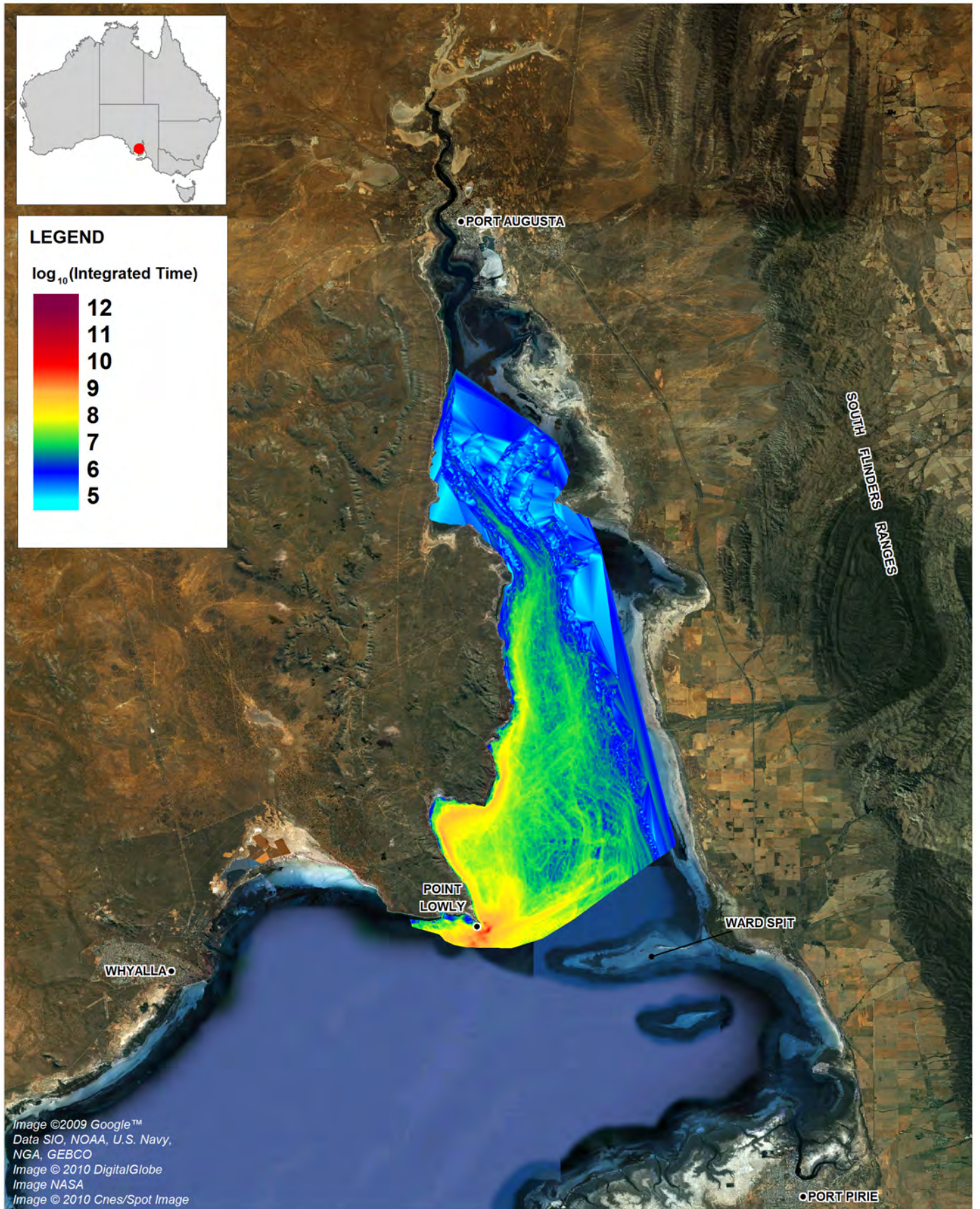
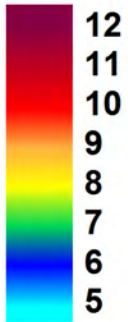


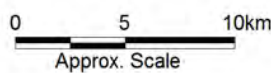
Image ©2009 Google™
 Data SIO, NOAA, U.S. Navy,
 NGA, GEBCO
 Image © 2010 DigitalGlobe
 Image NASA
 Image © 2010 Cnes/Spot Image

Title:
Larval Pathway Map: Run 4, Scenario 1

Figure:
8-12

Rev:
A

BMT WBM endeavours to ensure that the information provided in this map is correct at the time of publication. BMT WBM does not warrant, guarantee or make representations regarding the currency and accuracy of information contained in this map.



Filepath :

The figures show several key trends. Specifically the models predict:

- Aggregation or accumulation of larvae in and around northern Fitzgerald Bay. This is consistent with field observations (advice from BHP Billiton's marine biology consultants);
- A relatively frequently visited larval travel path along the coastline north from Point Lowly (for quite some distance), generally (but not always) inshore of the proposed intake infrastructure;
- Larval pathways very much favour deep channels rather than shallow areas, with the exception of the pathway along the western shore of the Gulf; and
- Predictions from Runs 1 and 2 (regional spawners) show generally higher residence times in the upper northern gulf than around Point Lowly, despite their uniform initialisation. This is consistent with field observations (Bruce and Short, 1992).

There is most likely to be some sensitivity of the above results to the spatial initialisation (both in form and distribution) of the numerical drifters. This was investigated to some extent in this study where three different spatial distributions (and densities) of initialisations were selected. Despite these differences in initialisation, the resultant pathway maps across all runs demonstrated similar features, with the most obvious similarity being the preference for travel along the shoreline north of Point Lowly and accumulation in northern Fitzgerald Bay.

8.3.1.2 Initial Locations of Entrained Larvae

The initial location of all entrained particles was also recorded within the post processing tool. These data were used to generate maps of the point of origin of entrained larvae. Each non-zero entrainment initialisation point was also colour coded to the percentage of larvae leaving that point that were entrained (as such not all percentages reported should sum to 100%). These maps are shown below for:

- Run 2 scenario 2 (regional spawners, unconstrained intake at Point Lowly);
- Run 2 scenario 3 (regional spawners, unconstrained intake at Port Augusta);
- Run 3 scenario 2 (reef spawners, 30 day larval duration); and
- Run 4 scenario 2 (sponge community spawners, vertically unconstrained intake).



LEGEND

Percentage Entrained

- 0.0 to 1.0
- 1.0 to 2.0
- 2.0 to 3.0
- 3.0 to 4.0
- 4.0 to 5.0
- 5.0 to 6.0
- 6.0 to 7.0
- 7.0 to 10.0
- > 10.0

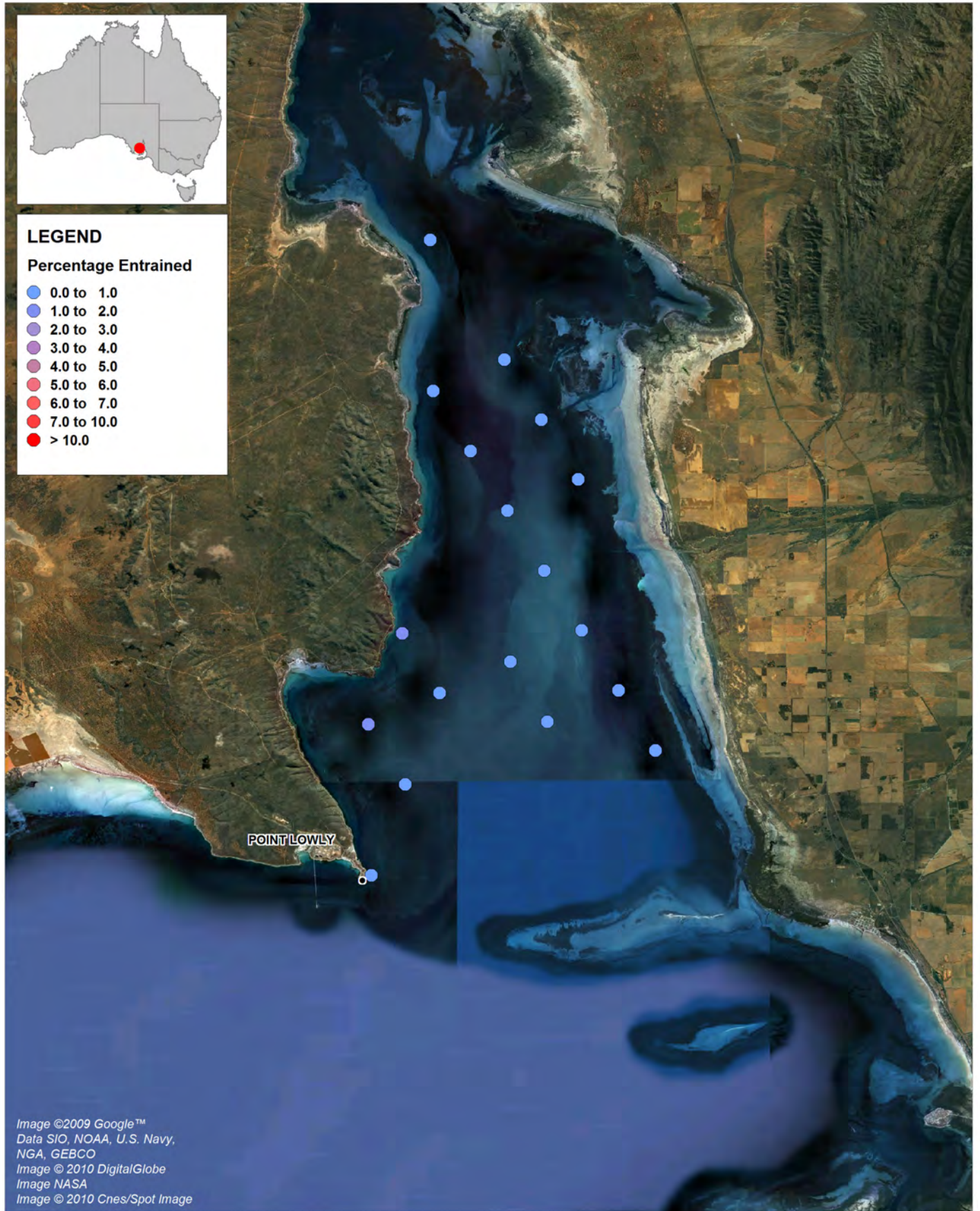


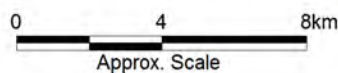
Image ©2009 Google™
 Data SIO, NOAA, U.S. Navy,
 NGA, GEBCO
 Image © 2010 DigitalGlobe
 Image NASA
 Image © 2010 Cnes/Spot Image

Title:
**Percentage entrained: run 2, scenario 2
 (regional spawners, unconstrained intake at Point Lowly)**

Figure:
8-13

Rev:
A

BMT WBM endeavours to ensure that the information provided in this map is correct at the time of publication. BMT WBM does not warrant, guarantee or make representations regarding the currency and accuracy of information contained in this map.



Filepath :



PORT AUGUSTA

LEGEND

Percentage Entrained

- 0.0 to 1.0
- 1.0 to 2.0
- 2.0 to 3.0
- 3.0 to 4.0
- 4.0 to 5.0
- 5.0 to 6.0
- 6.0 to 7.0
- 7.0 to 10.0
- > 10.0

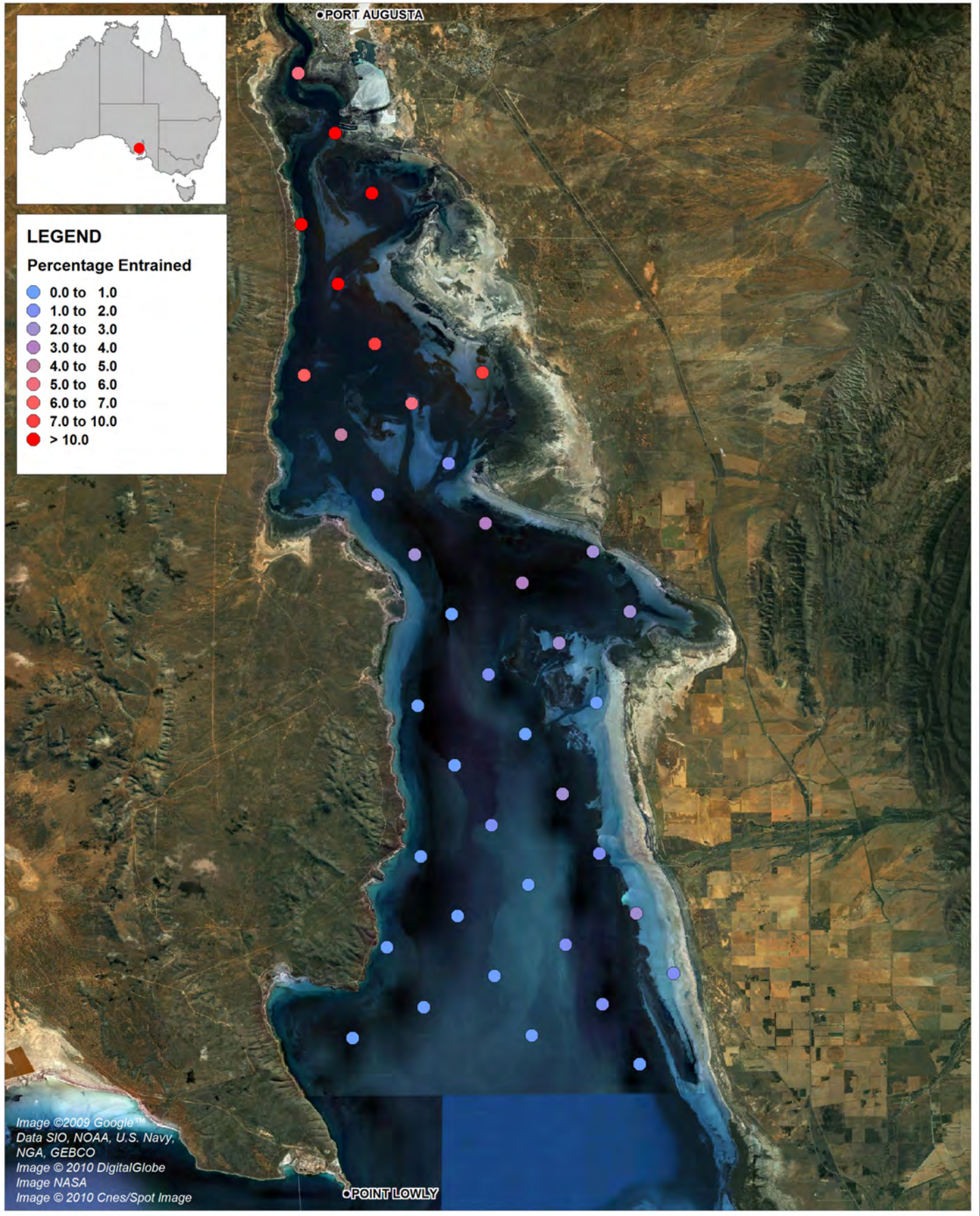


Image ©2009 Google™
 Data SIO, NOAA, U.S. Navy,
 NGA, GEBCO
 Image © 2010 DigitalGlobe
 Image NASA
 Image © 2010 Cnes/Spot Image

POINT LOWLY

Title:

**Percentage entrained: run 2, scenario 3
 (regional spawners, unconstrained intake at Port Augusta)**

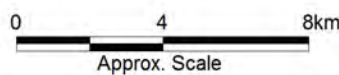
Figure:

8-14

Rev:

A

BMT WBM endeavours to ensure that the information provided in this map is correct at the time of publication. BMT WBM does not warrant, guarantee or make representations regarding the currency and accuracy of information contained in this map.



Filepath :



LEGEND

— Intake Alignment

Percentage Entrained

- 0.0 to 0.5
- 0.5 to 1.0
- 1.0 to 1.5
- 1.5 to 2.0
- 2.0 to 2.5
- 2.5 to 3.0
- 3.0 to 3.5
- 3.5 to 4.0
- 4.0 to 4.5
- 4.5 to 5.0

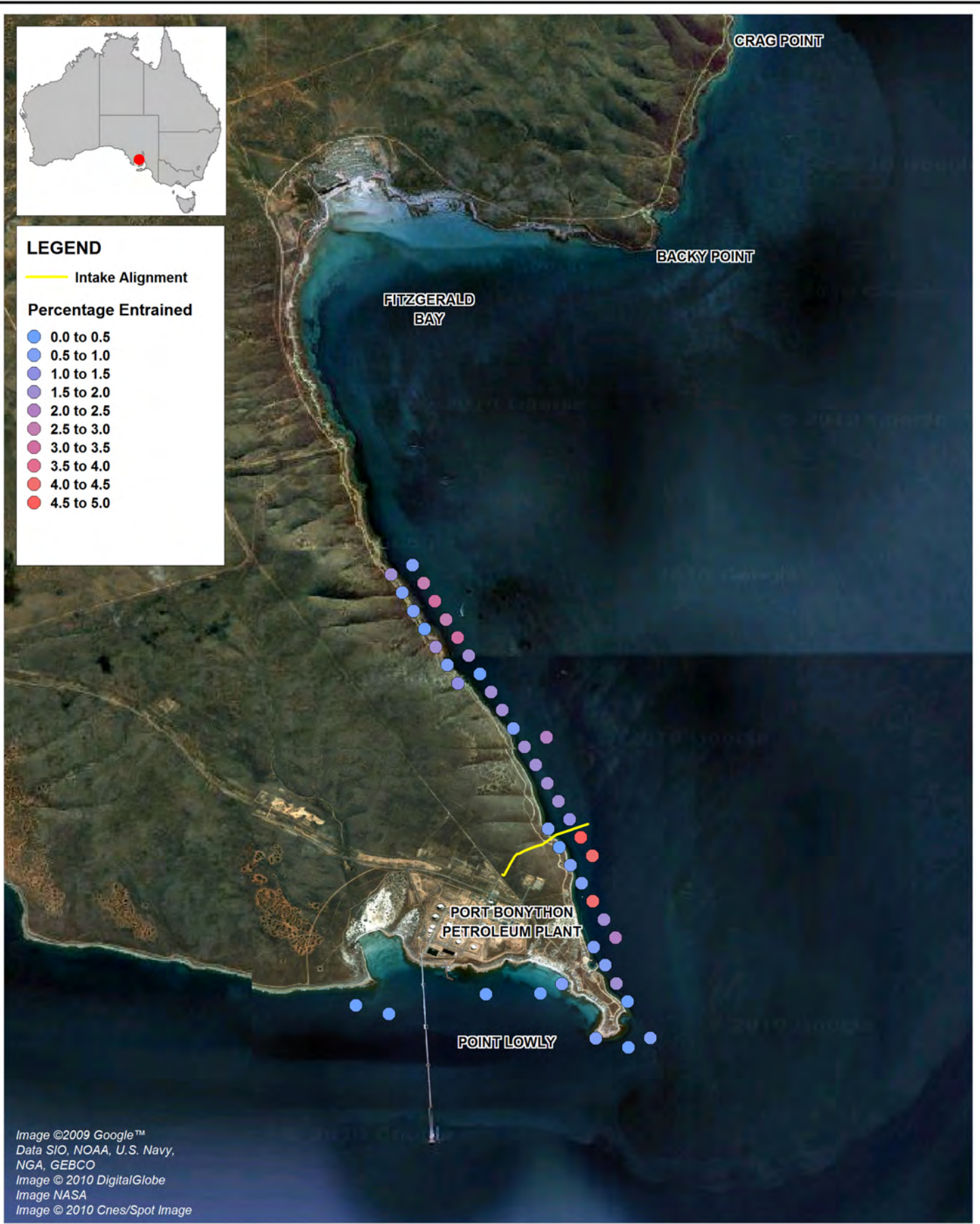


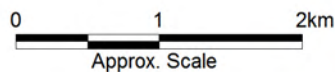
Image ©2009 Google™
 Data SIO, NOAA, U.S. Navy,
 NGA, GEBCO
 Image © 2010 DigitalGlobe
 Image NASA
 Image © 2010 Cnes/Spot Image

Title:
**Percentage entrained: run 3, scenario 2
 (reef spawners, 30 day larval duration)**

Figure:
8-15

Rev:
A

BMT WBM endeavours to ensure that the information provided in this map is correct at the time of publication. BMT WBM does not warrant, guarantee or make representations regarding the currency and accuracy of information contained in this map.



Filepath :



LEGEND

— Intake Alignment

Percentage Entrained

- 0.00 to 0.33
- 0.33 to 0.67
- 0.67 to 1.00



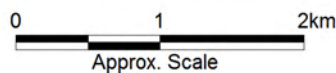
Image ©2009 Google™
 Data SIO, NOAA, U.S. Navy,
 NGA, GEBCO
 Image © 2010 DigitalGlobe
 Image NASA
 Image © 2010 Cnes/Spot Image

Title:
**Percentage entrained: run 4, scenario 2 (sponge
 community spawners, vertically unconstrained intake)**

Figure:
8-16

Rev:
A

BMT WBM endeavours to ensure that the information provided in this map is correct at the time of publication. BMT WBM does not warrant, guarantee or make representations regarding the currency and accuracy of information contained in this map.



Filepath :

8.3.2 Numerical Outputs

The following table presents the numerical results, where applicable, from the various runs and scenarios described above. 'Died' refers to additional mortality over and above simple expiry of larval duration (i.e. the latter was usually set to 7 or 30 days).

Table 8-6 Numerical results – run 1

	Scenario
	1
Description	Regional spawners – vertical migration
Total Larvae	7.9e+07
Number Entrained	11000
Percentage Entrained	0.014
Percentage Died	-
Percentage Settled	-

Table 8-7 Numerical results – run 2

	Scenario		
	1	2	3
Description	Vertically constrained intake at Point Lowly	Unconstrained intake at Point Lowly	Unconstrained intake at Port Augusta
Total Larvae	7.9e+07	7.9e+07	7.9e+07
Number Entrained	0	3.6e+04	2.22e+05
Percentage Entrained	0	0.05	0.28
Percentage Died	0	0	0
Percentage Settled	0	0	0

Table 8-8 Numerical results – run 3

	Scenario					
	1	2	3	4	5	6
Description	7 day larval duration	30 day larval duration	Natural mortality	Early settlement	Avoidance	Vertically constrained intake
Total Larvae	2.4e+07	2.4e+07	2.4e+07	2.4e+07	2.4e+07	2.4e+07
Number Entrained	1.72e+05	2.01e+05	1.65e+05	2.01e+05	1.82e+05	3.20e+04
Percentage Entrained	0.72	0.84	0.69	0.84	0.76	0.13
Percentage Died	0	0	94.37	0	0	0
Percentage Settled	0	0	0	1.28e-06	0	0

Table 8-9 Numerical results – run 4

	Scenario	
	1	2
Description	Vertically constrained intake	Vertically unconstrained intake
Total Larvae	2.184e+07	2.184e+07
Number Entrained	0	39000
Percentage Entrained	0	0.17
Percentage Died	0	0
Percentage Settled	0	0

The effect of vertical migration is shown in Table 8-6, where it can be seen that very few larvae (as a percentage of releases) would be entrained. These results can be directly compared to Scenario 2 of Run 2 (Table 8-7), where the only difference is the absence of vertical migration. Larvae entrainment when vertical migration was allowed was lower than without vertical migration. As a result, all other runs were performed without vertical migration as they produced a more conservative estimate of larval entrainment.

The numerical outputs presented for Run 3 scenarios (Table 8-8) show:

- Larval duration (Scenario 1) had a slight effect on the final number of entrained larvae in relation to the baseline (Scenario 2), as expected, given their initialisation was relatively near the intake;
- Mortality (Scenario 3) had the greatest impact on the final number of entrained larvae;

- Early settling (Scenario 4) did not produce substantial changes in entrained and expired larvae, as the turbulent environment allowed the particles to remain away from the seabed over considerable time; and
- Avoidance (Scenario 5), as expected, reduced the number of larvae entrained in relation to Scenario 2.

Constraining the entrainment level (Scenario 6) produced a change of entrained particles in relation to the baseline, as expected, such that unconstrained entrainment can therefore be seen as a conservative assumption on the number of entrained larvae.

Run 4 shows relatively little entrainment.

It is important to note that the models predict a relatively strong gradient in larval pathway residence time in the region proximate to the proposed intake location. This is particularly evident, for example, in Figure 8-9, where the intake is just seaward of a very strong gradient in larval pathway residence time. As such, the above numerical predictions need to be interpreted in the light of the presence of this gradient, and in particular, it is noted that slight changes in either the intake location or predicted larval pathways could result in material changes to the numerical predictions presented above.

As a final 'benchmarking' assessment, the entrainment percentages predicted above were compared to that expected by considering the relationship between the desalination plant intake volume over a thirty day period (i.e. one larval duration) and the volume of water initially occupied by a given drifter release. In the case of Run 2, the following apply:

- BHP Billiton 30 day intake volume = 19,500,000 m³; and
- Volume spanned by drifter initialisation = 28,025,000,000 m³.

Therefore, if all particles maintained a spatially uniform distribution and did not leave the initialisation region, then we would expect that 0.07% of larvae would be entrained, purely on a volumetric basis. This is consistent with the magnitude of predictions above for Run 2 (Table 8-7). Interestingly, Port Augusta (Run 2 Scenario 3) has a slightly higher modelled entrainment percentage than this (0.28%), and this is consistent with the data provided in larval pathways maps that show (non-uniform) accumulation in the upper reaches of the Gulf.

8.4 Summary

This section has examined the likely fate and transport of larvae released in Northern Spencer Gulf. It has provided assessment of:

- Likely larval accumulation zones and pathways;
- Likely entrainment characteristics under a range of larval property and intake configurations. In general, larval entrainment percentages were small, in absolute and comparative terms; and
- Benchmarking against hand calculations as required.

9 REFERENCES

- BHP Billiton (2009). *Olympic Dam Expansion – Draft Environmental Impact Statement 2009*.
- Bruce, B.D. and Short, D.A. (1992). *Observations on the distribution of larval fish in relation to a frontal zone at the mouth of Spencer Gulf, South Australia*. Proceedings of the Bureau of Rural Resources, Canberra No 15 - Larval Biology, Ed D.A Hancock, Australian Government Publishing Services, Canberra pp. 124-137.
- Cardno Lawson Treloar (2008). *Near field dilution and outfall hydraulics investigations – Adelaide desalination plant*. Report Prepared for Connell Wagner, 31 October 2008, LJ2738/R2479.
- CCE (2008). *Marine biology existing conditions and impact assessment*. Victorian Desalination Project Environmental Effects Statement.
- CSIRO (2007). *Climate change in Australia – technical report 2007*. Australian Government - Department of Climate Change.
- Department for Environment and Heritage (DEH) (2006). *Performance assessment system – for the draft Spencer Gulf marine plan*.
- DSE (2008). *Victorian desalination project environment effects statements, volume 2*.
- Hipsey, M.R., Antenucci, J.P. and Hamilton, D. (2009). *Computational aquatic ecosystem dynamics model: CAEDYM v3. v3.2 science manual (DRAFT)*.
- Imberger, J. and Hamblin, P. F. (1982). *Dynamics of lakes, reservoirs and cooling ponds*. Annual Review of Fluid Mechanics 14 153-187.
- IPCC (2001). *Climate change 2000: The science of climate change. Summary for policy makers and technical summary of working group*. Cambridge University Press.
- IPCC (2007). *General guidelines on the use of scenario data for climate impact and adaptation assessment*. Available from <http://www.ipcc-data.org/guidelines/index.html>
- Johnson, J.E. (1981). *Fisheries research paper number 3, Hydrological data for upper Spencer Gulf 1975 – 1978*. Department of Fisheries, South Australia, October 1981.
- Jones, P.D., New, M. and Parker, D.E. (1999). *Surface air temperatures and its changes over the past 150 years*. Reviews of Geophysics, **37**(2), 173-199.
- Kaempf, J., Brokensha, C. and Bolton, T. (2009). *Hindcasts of the fate of desalination brine in large inverse estuaries: Spencer Gulf and Gulf St Vincent, South Australia*. Desalination and Water Treatment, **2**(2009), 325-333.
- Lauer, P.R. (2005). *Benthic metabolism adjacent to southern bluefin tuna (Thunnus maccoyil) pontoons in South Australia*. PhD Thesis, School of Biological Sciences, Faculty of Science and Engineering, Flinders University of South Australia.

- Marti, C., Antenucci, J., Luketina, D., Okely, P. and Imberger, J. (2010). *Near field dilution characteristics of a negatively buoyant hypersaline jet generated by a desalination plant*. Journal of Hydraulic Engineering, in press 2010.
- Nunes, R.A. (1985). *Catalogue of data from a systematic programme of oceanographic measurements in Northern Spencer Gulf from 1982 to 1985*. Cruise Report No. 9. School of Earth Sciences, Flinders University of South Australia.
- Nunes-Vaz, R.A., Lennon, G.W. and D.G. Bowers (1990). *Physical behaviour of a large, negative or inverse estuary*. Cont. Shelf Res., **10**(3): 277-304.
- Okely, P., Yeates, P.S., Antenucci, J.P., Imberger, J. and Hipsey, M.R. (2006). *Modelling of the impact of the Perth seawater desalination plant discharge on dissolved oxygen in Cockburn Sound*. Centre for Water Research document WP2136PO.
- Okely, P., Antenucci, J.P., Yeates, P.S., Marti, C.L. and Imberger, J. (2007a). *Summary of investigations into the impact of the Perth seawater desalination plant discharge on Cockburn Sound*. Centre for Water Research document WP2160PO.
- Okely, P., Antenucci, J.P., Imberger, J. and Marti, C.L. (2007b). *Field investigations into the impact of the Perth seawater desalination plant discharge on Cockburn Sound*, Centre for Water Research document WP2150PO.
- Pawlowicz, R., Beardsley, B. and Lentz, S. (2002). *Classical tidal harmonic analysis including error estimates in MATLAB using T_TIDE*. Computers and Geosciences, 28(8): 929-937.
- Riley, J.P. and Skirrow, G. (1974). *Chemical Oceanography*. Academic Press, London.
- Roberts, P. J. W., and Toms, G. (1987). *Inclined dense jets in a flowing current*. Journal of Hydraulic Engineering., ASCE, 113(3), 323-341.
- Roberts, P. J. W., *et al.* (1997). *Mixing in inclined dense jets*. Journal of Hydraulic Engineering. ASCE, 123(8), 693-699.
- Roberts, P. J.W., Ferrier, A. and Daviero, G. (1997). *Mixing in Inclined Dense Jets*. Journal of Hydraulic Engineering, August 1997 pp95-108.
- SA Water (2008). *Proposed Adelaide Desalination Plant Environmental Impact Statement, Chapter 7*.
- SA Water (2009). *Proposed Adelaide Desalination Plant – Environmental Impact Statement. Response Document January 2009*.
- Shintani, T. de la Fuente, A., Nino, Y. and Imberger, J. (2010). *Generalizations of the Wedderburn number: Parameterizing upwelling in stratified lakes*. Limnology and Oceanography 55(3): 1377-1389.
- Steffen (2009). *Climate change 2009 faster change & more serious risks*. Australian Government - Department of Climate Change.

- Suppiah *et.al.* (2006). *Climate change under enhanced greenhouse conditions in South Australia*. South Australian Government.
- Swinbank, W.C. (1963). *Longwave radiation from clear skies*. Quarterly Journal of Royal Meteorological Society. 89: 339-348.
- Thompson, R. O. R. Y. and Imberger, J. (1980). *Response of a numerical model of a stratified lake to wind stress*. Proceedings of the International Symposium of Stratified Flows **2** 562-570.
- Wanninkhof, R. (1992). *Relationship between windspeed and gas exchange over the ocean*. J. Geophys. Res. (Oceans) **97(C5)**, pp. 7373-7382.



BMT WBM Brisbane Level 11, 490 Upper Edward Street Brisbane 4000
PO Box 203 Spring Hill QLD 4004
Tel +61 7 3831 6744 Fax +61 7 3832 3627
Email wbm@wbmpl.com.au
Web www.wbmpl.com.au

BMT WBM Denver 14 Inverness Drive East, #B132
Englewood Denver Colorado 80112 USA
Tel +1 303 792 9814 Fax +1 303 792 9742
Email wbm-denver@wbmpl.com.au
Web www.wbmpl.com.au

BMT WBM Mackay Suite 1, 138 Wood Street Mackay 4740
PO Box 4447 Mackay QLD 4740
Tel +61 7 4953 5144 Fax +61 7 4953 5132
Email wbm-mackay@wbmpl.com.au
Web www.wbmpl.com.au

BMT WBM Melbourne Level 5, 99 King Street Melbourne 3000
PO Box 604 Collins Street West VIC 8007
Tel +61 3 8620 6100 Fax +61 3 8620 6105
Email wbm-melbourne@wbmpl.com.au
Web www.wbmpl.com.au

BMT WBM Newcastle 126 Belford Street Broadmeadow 2292
PO Box 266 Broadmeadow NSW 2292
Tel +61 2 4940 8882 Fax +61 2 4940 8887
Email wbm-newcastle@wbmpl.com.au
Web www.wbmpl.com.au

BMT WBM Perth 1 Brodie Hall Drive Technology Park Bentley 6102
Tel +61 8 9328 2029 Fax +61 8 9486 7588
Email wbm-perth@wbmpl.com.au
Web www.wbmpl.com.au

BMT WBM Sydney Level 1, 256-258 Norton Street Leichhardt 2040
PO Box 194 Leichhardt NSW 2040
Tel +61 2 9713 4836 Fax +61 2 9713 4890
Email wbm-sydney@wbmpl.com.au
Web www.wbmpl.com.au

BMT WBM Vancouver 1190 Melville Street #700 Vancouver
British Columbia V6E 3W1 Canada
Tel +1 604 683 5777 Fax +1 604 608 3232
Email wbm-vancouver@wbmpl.com.au
Web www.wbmpl.com.au